ANL-7190

339
6-2-66

ANL-7190

Argonne National Laboratory

REACTOR ENGINEERING DIVISION ANNUAL REPORT

July 1, 1964 to June 30, 1965

DISCLAIMER

LEGAL NOTICE

This report was prepared as an account of Government sponsored work. Neither the United States, nor the Commission, nor any person acting on behalf of the Commission:

A. Makes any warranty or representation, expressed or implied, with respect to the accuracy, completeness, or usefulness of the information contained in this report, or that the use of any information, apparatus, method, or process disclosed in this report may not infringe privately owned rights; or

B. Assumes any liabilities with respect to the use of, or for damages resulting from the use of any information, apparatus, method, or process disclosed in this report.

As used in the above, "person acting on behalf of the Commission" includes any employee or contractor of the Commission, or employee of such contractor, to the extent that such employee or contractor of the Commission, or employee of such contractor prepares, disseminates, or provides access to, any information pursuant to his employment or contract with the Commission, or his employment with such contractor.

Printed in USA. Price $6.00 . Available from the Clearinghouse for Federal Scientific and Technical Information, National Bureau of Standards, U. S. Department of Commerce, Springfield, Virginia 22151

ANL-7190
Reactor Technology
(TID-4500)
AEC Research and
Development Report

ARGONNE NATIONAL LABORATORY
9700 South Cass Avenue
Argonne, Illinois 60439

REACTOR ENGINEERING DIVISION ANNUAL REPORT

July 1, 1964 to June 30, 1965

L. J. Koch, Division Director

March 1966

Operated by The University of Chicago
under
Contract W-31-109-eng-38
with the
U. S. Atomic Energy Commission

THIS PAGE

WAS INTENTIONALLY

LEFT BLANK

PREFACE

This first annual report published by the Reactor Engineering Division summarizes reactor project accomplishments and engineering research and developments in fiscal year 1965. To orient the reader, most descriptions are prefaced with background information about the nature of the work, the objectives, and prior progress.

In two instances, the narrative coverage extends beyond the fiscal cut-off date (June 30, 1965). On September 13, 1965, responsibility for the EBR-II Facility was formally transferred from the Reactor Engineering Division to the Idaho Division. Accordingly, the scope of Section 1.1 includes work performed up to the dedication and transfer date. In December, the FARET project was terminated by the U. S. Atomic Energy Commission. Thus Section 1.2 covers work to termination.

The Nuclear Rocket Program description is limited to declassified conceptual designs and results of supporting research and development. Detailed descriptions are reported in classified documents.

For those who wish to pursue certain subjects to greater depth, pertinent references are listed at the conclusion of most major sections. In addition, a complete list of publications, indexed to each section, is given in Section 8.

CONTRIBUTORS

R. P. Anderson
R. H. Armstrong
N. Balai
J. F. Bartusek (PE)[1]
C. R. Breden
N. Bulut (PE)[1]
T. R. Bump
J. P. Burelbach
R. D. Carlson
Y. W. Chang
I. Charak
J. J. Dickoon
T. W. Eckels (CEN)[2]
P. Elias
H. K. Fauske
E. C. Filewicz
S. H. Fistedis
J. R. Folkrod
L. W. Fromm
J. D. Geier
G. D. Giorgis
G. H. Golden
N. R. Grant
A. P. Grunwald
E. E. Hamer
A. H. Heineman
J. B. Heineman
B. M. Hoglund
R. E. Holtz
H. H. Hooker
C. Hsu
K. A. Hub
E. Hutter
A. R. Jamrog
M. J. Janicke
R. A. Jaross
W. J. Kann
I. Kliger
K. D. Kuczen
W. C. Lipinski
P. A. Lottes
D. E. Lutz
R. H. Lykken
J. F. Matousek
J. F. Marchaterre
A. Marchertas
E. L. Martinec
J. F. Mech
J. H. Monaweck
H. O. Monson
T. P. Mulcahey
J. A. Pardini
C. V. Pearson
M. Petrick
A. W. Pierce (RO)[3]
J. Poloncsik
G. F. Popper
R. R. Rohde
G. S. Rosenberg
D. Roy
H. L. Schmidt (PE)[1]
R. W. Seidensticker
O. S. Seim
W. R. Simmons
J. Simon (RC)[4]
R. M. Singer
R. C. Skaardal
A. Smaardyk
F. A. Smith
E. S. Sowa
R. P. Stein
H. C. Stevens (RO)[3]
T. E. Sullivan
J. H. Tessier
D. H. Thompson
W. Thompson (RC)[4]
D. Veith (PE)[1]
F. Verber
W. R. Ware
R. Weatherhead
J. T. Weills
E. A. Wimunc

---

[1]On loan from Plant Engineering Division.
[2]On loan from Chemical Engineering Division.
[3]On loan from Reactor Operations Division.
[4]On loan from Remote Control Division.

TABLE OF CONTENTS

Page

Section 1. REACTOR PROJECTS AND PROGRAMS

1.1 EXPERIMENTAL BREEDER REACTOR-II (EBR-II) 11

1.1.1 Summary 11

1.1.2 Approach-to-Power Program 13
1.1.2.1 Chronology 13
1.1.2.2 Fuel Surveillance 17
1.1.2.3 Failure of Oscillator Drive Mechanism 21
1.1.2.4 Electrical System and Instrument Air Safety Tests 26
1.1.2.5 Steam Generator Repair 28

1.1.3 Plant Improvements 30
1.1.3.1 Reactor Plant 30
1.1.3.2 Sodium-Boiler and Power Plant 32

1.1.4 Experimental Support 32
1.1.4.1 Material Surveillance Subassemblies 32
1.1.4.2 Mark-A and Mark-B Irradiation Test Subassemblies 34
1.1.4.3 Mark-II Oscillator System Design 37

1.2 FAST REACTOR TEST FACILITY (FARET) 40

1.2.1 Summary 40

1.2.2 Facility Description 43

1.2.3 Supporting Research, Design, and Development 45
1.2.3.1 Reactor Components 45
Reference Core I 46
Control Rod Drive Mechanisms 49
Reactor Vessel 51
Reactor Vessel Cover Handling System 54
1.2.3.2 Reactor-Related Tasks 55
Hydraulic Tests - Reactor Vessel 55
Hydraulic Tests - Core Subassemblies 56
Fuel Subassembly Sodium Flow Test Loop 58
In-Core Instrumentation - Thermocouples 59
In-Core Instrumentation - Flowmeters 60
In-Core Instrumentation Lead Connectors 62
1.2.3.3 In-Cell Fuel and Equipment Handling Systems 63
1.2.3.4 Preliminary Safety Analysis 74

TABLE OF CONTENTS

		Page
1.3	ARGONNE ADVANCED RESEARCH REACTOR (AARR)	77
1.3.1	Project History and Status	77
1.3.2	Conceptual Design	78
	1.3.2.1 Reactor Containment Building	79
	Structural Components and Services	79
	Reactor Components and Auxiliaries	80
	1.3.2.2 Laboratory and Office Building	84
	1.3.2.3 Storage and Mock-Up Building	85
	1.3.2.4 Equipment Building	85
1.3.3	Supporting Research, Design, and Development	86
	1.3.3.1 Preliminary Safety Analysis	86
	1.3.3.2 Mark-I Core Development	86
	Analytical and Experimental Heat Transfer	86
	Mechanical Design, Stress Analysis, and Hydraulics	89
	Fuel Material Fabrication	90
	Fuel Assembly Development	94
	Control Blade Material	95
	1.3.3.3 System Dynamics and Transient Analysis	96
	Process Control Analysis	96
	Transient Analysis and Safety Studies	97
	1.3.3.4 Component Design and Evaluation	100
	Reactor Vessel	100
	Experimental Facilities	102
1.4	EXPERIMENTAL BOILING WATER REACTOR (EBWR) - Plutonium Recycle Experiment	106
1.4.1	Summary	106
1.4.2	Plant Inspection, Modifications, and Maintenance	107
	1.4.2.1 Reactor Pressure Vessel	107
	1.4.2.2 Removal of Forced Circulation Tees	111
	1.4.2.3 Primary System Piping Welds	112
	1.4.2.4 Primary Purification System	112
	1.4.2.5 Feedwater Full-Flow Filters	113
	1.4.2.6 Retubing of Main and Recovery System Vent Condensers	113
	1.4.2.7 Containment Shell Main Air Lock Doors	113

TABLE OF CONTENTS

		Page
1.4.3	Supporting Research, Design, and Development	114
	1.4.3.1 Reference Core Design	114
	1.4.3.2 Plutonium Fuel Storage Rack	117
	1.4.3.3 Heat Transfer Characteristics and Hydrodynamics of Pu Recycle Core	118
	1.4.3.4 Reactor Kinetics	120
1.5	ARGONNE RESEARCH REACTOR (CP-5)	121
1.5.1	Stress Analysis of Vessel Coolant Distribution Plenum	121
1.6	ARGONNE NUCLEAR ROCKET PROGRAM	124
1.6.1	Objective and Scope	124
1.6.2	Reference Systems	124
1.6.3	System Analysis	127
	1.6.3.1 Steady-State Analysis	128
	1.6.3.2 System Dynamics Analysis	129
	1.6.3.3 Advanced Concepts Analysis	129
1.6.4	Fuel Element Development and Testing	131
	1.6.4.1 Steady-State Tests	131
	1.6.4.2 Thermal-Cycling Tests	132
	1.6.4.3 Rapid-Cooling Tests	132
1.6.5	Argonne Hydrogen Flow Facility	132
	1.6.5.1 Building D-311	133
	1.6.5.2 Hot Hydrogen Test Loops	133
	1.6.5.3 Prototype Heaters	137
	1.6.5.4 Loop-Heater Performance	138
1.6.6	Structural Mechanics	139
	1.6.6.1 Deformation Analysis of a Grid Plate Support Structure	139
	1.6.6.2 Possible Influences of Anisotropy on Plane Strain Thermal Stress Solutions	140
	1.6.6.3 Reduced-Scale Model Tests	140
	1.6.6.4 Vibration Exciter Facility	141
	1.6.6.5 Shell Stability Analysis	141
	1.6.6.6 Experimental Study of Shell Deformation and Stability	142

TABLE OF CONTENTS

		Page
	Section 2. FAST REACTOR RESEARCH AND DEVELOPMENT	
2.1	Advanced Systems and Concepts	143
	2.1.1 1000-MW(e) Metal-Fueled Fast Breeder Reactor Concept	143
	2.1.2 Engineering Design and Cost Study of Large Steam-Electric Generating Units	148
2.2	Materials and Components	149
	2.2.1 1200°F Materials and Component Evaluation Loop	150
	2.2.2 High-Temperature (1200°F) Sodium, Long-Term Environmental Test Loop	151
	2.2.3 Material Compatibility Test Facility	151
	2.2.4 1200°F Furnace - Tensile Testing Machine	152
	2.2.5 Sodium Vapor Trap Development	153
	2.2.6 Self-Seeking Sodium Level Probe	153
2.3	Sodium Quality Control	154
	2.3.1 Sodium Quality Measurement Loop	154
	2.3.2 Drybox Sodium Sampling Test Loop	155
	Section 3. LIQUID METAL HEAT TRANSFER RESEARCH PROGRAM	
3.1	Objectives	156
3.2	Two-Phase Adiabatic Flow of Sodium	156
3.3	Boiling Sodium Studies	159
	3.3.1 2100°F Boiling Sodium Test Facility	159
	3.3.2 Prototype Heater Development	162
3.4	Evaluation of Traditional Liquid-Metal Heat Transfer Design Computations	162
	3.4.1 Heat Transfer in Double-Pipe Heat Exchangers	163
	3.4.2 Temperatures in Reactor Coolant Channels	164
	Section 4. MAGNETOHYDRODYNAMICS	
4.1	Potential of Liquid-Metal MHD Cycles for Central Station Power Systems	167
	4.1.1 Efficiencies of Binary Cycles	167
	4.1.2 MHD Generator Tests	169

TABLE OF CONTENTS

		Page
	4.1.3 End Losses in MHD Generators	169
	4.1.4 Two-Phase Nozzle Studies	170
4.2	Condensing Injector Studies	171
4.3	Production of a-c Current from MHD Generators	172
4.4	Use of Electromagnetic Field to Control Liquid Metal Condensation Rates	173
4.5	Significance of Heat Transfer in MHD Generators	174
	Section 5. FAST REACTOR SAFETY RESEARCH AND DEVELOPMENT	
5.1	Sodium Expulsion Studies	176
5.2	Reactor Control and Stability	177
5.3	Digital Control of EBR-II	178
5.4	Fuel Meltdown Studies: TREAT Loops	178
	5.4.1 Experimental Facilities	179
5.5	A Critique on Current Assessment of Radiation Damage in Reactor Pressure Vessel Steels	184
5.6	Experiment vs. Analysis of Core Support Grid	186
	Section 6. STUDIES AND EVALUATIONS	
6.1	Use of High-Temperature Process Heat as Part of a Total Nuclear-Energy Source	189
	Section 7. EDUCATION - RESEARCH ACTIVITIES	
7.1	ANL-AMU Heat Transfer Program	193
	7.1.1 Frequency-Response Analysis of Steam Voids to Sinusoidal Power Modulation in a Thin-Walled Boiling Water Coolant Channel	193
	7.1.2 Heat Transfer Instabilities near the Thermodynamic Critical Point	195
	7.1.3 Flow Regimes and Transitions in Vertical Two-Phase Flow at Elevated Pressure	196

TABLE OF CONTENTS

		Page
7.1.4	Propagation of Density Disturbances in Air-Water Flow	197
7.1.5	Self-Sustained Hydrodynamic Oscillations in a Natural Circulation Two-Phase Flow Boiling Loop	198

Section 8. PUBLICATIONS

8.1	Methods of Reporting	201
8.2	Recap of Publications	201

Section 1

REACTOR PROJECTS AND PROGRAMS

1.1 EXPERIMENTAL BREEDER REACTOR-II (EBR-II)

1.1.1 Summary

During the year, EBR-II was successfully placed into operation at power levels up to 45 MW (thermal) and 15 MW (electrical). In the course of the approach to power, most of the principal design objectives were realized. Reactor performance, both thermal and neutronic, measured up to predictions. Extensive experience in operation and maintenance of large sodium systems and components in a nuclear power plant environment was obtained. In-core experimental irradiations of new fast reactor fuels - including high-burnup capsules of oxide, carbide, and metal fuels - were started.

Earlier, in the first half of 1964, the primary and secondary systems were coupled for the first time by connecting the intermediate heat exchanger to the secondary piping. Operation of the combined systems, including the steam system, to temperatures approaching 600°F followed. During this period, the reworked primary pumps were tested, a primary sodium cleanliness verification run completed, preliminary heat balances made, and controllability of the secondary pump at extremely low flow rates demonstrated. Near the end of these tests, a leak developed in the a-c electromagnetic secondary pump, necessitating its removal and (on site) repair. After reinstallation of the pump, the facility was ready for power operation.

The approach to power commenced on July 16, 1964. Reactor power was raised in steps from 0.5 to 1, 2, 3, 4, and 5 MW, and then to 10, 20, and 30 MW. Power and flow coefficients of reactivity were determined and transfer function measurements made concurrently.

A demonstration run at 30 MW was conducted August 13-17, with the turbine generator producing 7.5 MW(e). The reactor then was shut down for the first removal of fuel for inspection.

In October, reactor power was raised to 37.5 MW, with the generator producing 11.8 MW(e) and delivering 8.8 MW(e) to the NRTS network. At the end of this run, two control rod drives were found stuck. A four-month investigative and corrective program which followed traced the failure to a ball bushing in the oscillator assembly. This assembly had been temporarily installed in the reactor for transfer function measurements. While it was being removed from the system, a pin-hole leak was discovered in a tube-to-tubesheet weld in one of the eight evaporators of the steam generator. Repair and helium leak testing was accomplished within three weeks without removing the unit from the system.

In March, 1965, reactor power was increased to 45 MW, and the generator output to 15 MW. Thereafter, operation was continued at this power level, with shutdowns essentially only for inspection of fuel and insertion of experimental irradiation subassemblies.

On September 13, 1965, dedication ceremonies were held, and responsibility for the EBR-II Facility was formally transferred from the Reactor Engineering Division to the Idaho Division. Accordingly, the scope of this section has been extended to include work performed up to the dedication date.

At that time, fuel elements in the reactor had attained maximum burnup of almost 1.2 at-%. Examination of elements with up to 1.1 at-% burnup had revealed they were in good condition, with no change in external diameter or appearance. Of the more than 1400 regular driver fuel elements removed for inspection, none was found defective.

Throughout operation, the reactor was highly stable, readily controllable, and amenable to rapid fuel reloading. More than a hundred subassemblies were transferred successfully, including 20 or more with various degrees of burnup up to 1.0 at-% and higher. Many of the high-burnup subassemblies were removed from the primary tank to the reprocessing facility within 9 to 15 days after reactor shutdown - while still generating very substantial decay heat. These transfers firmly established the feasibility of the blind, or under-plug, fuel-handling scheme for sodium-cooled reactors.

Through the successful implementation of the approach-to-power program, the primary objective of EBR-II - demonstration of the engineering feasibility of this type of plant - was accomplished. In addition, use of EBR-II as a fast flux irradiation facility has been implemented: plutonium-bearing fuels of interest for advanced fast power breeders are being irradiated. Eight materials surveillance subassemblies, containing about two thousand specimens of diverse types, were also inserted in the reactor.

Modifications to the reactor are planned to enhance the effectiveness of the system for irradiation purposes. Fabrication has started on a modified driver fuel element designed to accommodate a larger number of experiments in the reactor (as well as to increase the achievable burnup of the driver fuel). Studies are underway on further changes in both core and blanket to permit still more experiments. Special subassemblies are being designed and fabricated to permit irradiation of test fuel elements in flowing sodium (present practice requires encapsulation), and to allow possible specimen reinsertion in the reactor.

1.1.2 Approach-to-Power Program

1.1.2.1 Chronology

Figures 1-1 and 1-2 summarize the thermal power levels and cumulative thermal energy attained throughout the period from July, 1964, to September, 1965. Notation is made on Fig. 1-1 of the major events which occurred during periods of reactor shutdown.

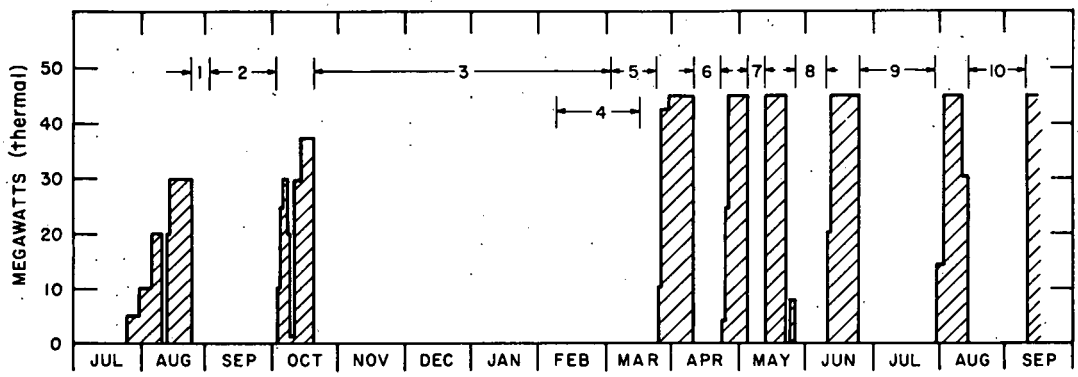

1. FUEL HANDLING
2. MAIN GRIPPER REPAIR
3. OSCILLATOR FAILURE INVESTIGATION AND FUEL HANDLING
4. EVAPORATOR LEAK REPAIR
5. ZERO POWER EXPERIMENTS
6. FUEL HANDLING AND CONTROL ROD GRIPPER REPAIR
7. FUEL HANDLING
8. FUEL HANDLING, CONTAINMENT TESTING, AND FUEL EXAMINATION
9. FUEL HANDLING AND FUEL EXAMINATION
10. FUEL HANDLING AND FUEL EXAMINATION

NOTE: MATERIALS SURVEILLANCE SUBASSEMBIES LOADED INTO REACTOR IN PERIOD 3; EXPERIMENTAL IRRADIATION SUBASSEMBLIES (FUEL) LOADED IN PERIODS 7, 9, AND 10.

Fig. 1-1. Graphical summary of thermal power output of EBR-II and major events during the period July, 1964 to September, 1965

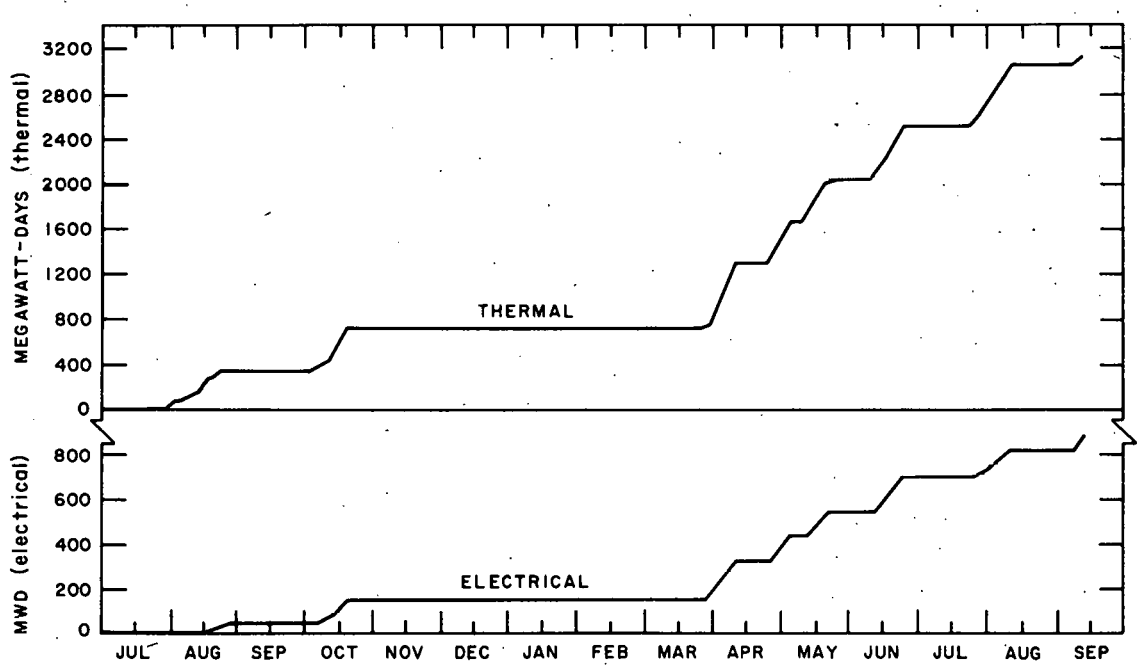

Fig. 1-2. Integrated thermal and electrical power output of EBR-II during the period July, 1964 to September, 1965

Through the first half of July, 1964, the plant was maintained in standby condition pending AEC approval for the start of power operation. This approval was received on July 16 and the reactor made critical on that day. During the remainder of the month, transfer function measurements were made at incremental power levels up to 10 MW, using two types of analyzing equipment: a null device and a cross-correlation integrating device. These measurements indicated that the reactor was producing no unexpected feedback properties. Power coefficient of reactivity was determined at levels up to 10 MW(t), with 100% primary flowrate. Flow coefficients were determined at 5 MW(t), with 100% and 74% flowrates. In addition, careful examinations were made of the subassembly sodium outlet temperatures at each incremental power or flow change. None of the tests revealed any unexpected results.

A gradual increase in reactor power continued in August with power operation at 10, 20, and 30 MW(t). Between August 13 and August 17, while the reactor was at 30 MW(t), the turbine-generator was placed on line and supplied an average output of 7.5 MW(e) to the NRTS grid system. Transfer function measurements, power and flow coefficient measurements, and heat balances were made at appropriate intervals. At each incremental increase of power, the primary flow rate was first established at 100% and reduced only after it was ascertained that no unpredicted changes in subassembly outlet temperatures or power coefficient had occurred. At 10 MW(t), the primary flow rates used were 100%, 74%, and 36%; at 20 MW(t), 100%, 74%, and 52%; and at 30 MW(t), 100% and 74%.

The reactor was shut down on August 23, after a cumulative thermal energy production of 343 megawatt-days, for the purpose of examining subassemblies, fuel elements, and fuel alloy pins as part of the fuel surveillance program. One core-type and one inner-blanket-type subassembly were removed to the Fuel Cycle Facility for this purpose.

Following these fuel-handling operations, the special oscillator rod used in the transfer function studies was to be replaced with a new rod. On September 2, during the insertion of the new rod, the main fuel gripper contacted the subassembly holddown device inside the primary tank and was damaged. Investigation showed that the contact had resulted from improper temperature distribution within, and consequent distortion of the gripper shaft. Further, that the temperature distribution was related to having maintained the shaft in the "up," cool, position for a prolonged period. A change in operating procedure was instituted to preclude recurrence of the incident. By October 3, the gripper had been removed, repaired, and reinstalled. In addition to the gripper work, other maintenance and modification work was done during the shutdown. This included repair of a damaged expansion-joint bellows in the desuperheated steam line to the condenser, and investigation of an apparent lubricating oil loss in the main primary pump drive motor bearings.

After preliminary power coefficient measurements at increments from 0 to 30 MW(t), and a short power run at 30 MW(t), the plant was operated at 37.5 MW(t), 11 MW(e) from October 13 to October 19. On the latter date a spurious scram occurred, after which it was found that two control rods (Nos. 7 and 9) had not dropped. A program of investigative and corrective action was then undertaken which eventually required four months to complete. Briefly, the difficulty was caused by a malfunction of the oscillator assembly which was temporarily installed for reactor kinetic studies.

Near the end of the oscillator corrective work, on February 7, 1965, a minor water leak in evaporator No. 702 was discovered. Although continued operation with the evaporator in this condition was possible, the decision was made to repair the leak immediately. A pinhole leak was located in a tube-to-tubesheet weld on the steam side tubesheet. This allowed water or steam to enter the air space between the steam and sodium tubesheets. (The evaporators are of the shell-and-tube type, with double-walled tubes and double tubesheets; the leak, therefore, was into the building atmosphere and not into the sodium.) Access for rewelding of the tube-to-tubesheet joint was accomplished by removing a section of the 10-in. riser immediately above the upper steam header. Thus the feasibility of repairing this kind of weld defect in evaporators of EBR-II design, without removing the evaporator from the system, was convincingly demonstrated.

On March 2, the reactor was brought critical. Various physics measurements and foil irradiations were made at "zero" power. Next, the secondary sodium system was refilled and, after a two-week delay for obtaining authorization, power operation was resumed. On March 27, a power level of 45 MW(t), 14 MW(e), was attained. Operation at this level continued until April 11, at which time the maximum reactor fuel burnup was approximately 0.5 at-%. The reactor then was shut down for the routine examination of fuel elements for irradiation damage.

During preparations for this fuel handling, two control rod drive grippers (Nos. 8 and 11) malfunctioned, making difficult the proper release of the rods from the drives. Both drives were removed from the primary tank. Inspection of drive No. 8 showed that one of the two small cam pieces necessary for gripper jaw operation had broken loose (remaining inside the mechanism). Drive No. 11 revealed burnishing of the cam pieces and a slight galling of the gripper sleeve. Both rods were replaced with spare units that were modified to eliminate such difficulty.

The reactor was operated at power from April 26 to May 21, with an 8-day shutdown (starting on May 4) for fuel surveillance. Subassemblies with a maximum burnup of ~0.8 at-% were transferred to the Fuel Cycle Facility for examination. Also during this shutdown period, the reactor was

run at zero power to check out the newly installed reactor kinetics monitoring equipment. This equipment employs stainless steel rod drop and trapezoidal reactivity insertion techniques.

An interesting experiment was run at this time to calibrate two experimental fission product monitoring devices used at EBR-II: a delayed-neutron monitor operating in a bypass stream of reactor outlet sodium, and a charged-wire fission gas monitor sampling primary blanket gas. The calibrations were performed by moving a bare fuel pin alternately into and out of the core while operating at 10 MW(t). The response of the monitor signals clearly indicated that both devices were capable of detecting fission product activity associated with a single unclad fuel pin. The time response of the delayed-neutron system was much faster than that of the charged-wire system.

The plant was shut down on May 26 for scheduled maintenance and leak-rate tests of the reactor containment system. The reactor was started again on June 10 and continued in operation until June 25, at which time an approximate maximum fuel burnup of 1.0 at-% had been attained.

Because the design burnup level now had been reached, a large number of subassemblies were removed for inspection. Minor difficulty was encountered with the large rotating plug during this fuel handling. This phenomenon, a tendency toward "sticking" of the plug during initial operation, has persisted and, despite investigation, is still unexplained. The plug is readily freed and remains free during the fuel handling operation without significantly affecting operations.

Sticking trouble also developed in starting one of the main primary pumps. In this instance, it was necessary to partially disassemble the drive motor and mechanically dislodge the pump shaft. The sticking was attributed to accumulation of sodium oxide in the running clearance between pump shaft and structure. An increase in the argon gas back-flow through this gap has since eliminated recurrence of such sticking.

The plant was maintained in standby condition until July 21 while awaiting results of fuel inspection at the 1.0 at-% maximum burnup level. Then the reactor was operated briefly at 10 MW(t) to facilitate physics measurements prior to attempting the next increment of burnup.

At that time, removal of additional subassemblies from the reactor became necessary. Fuel element inspection results had shown the regular elements at 1.0 at-% to be in excellent condition. A number of special elements, however, exhibited a very much higher fuel alloy swelling rate (up to 8 vol-%/at-% burnup, compared to a maximum of about 5 vol-%/at-% burnup for regular elements). These elements were identical to regular elements except that they had been especially accurately measured during

fabrication for better comparison with post-irradiation measurements. Apparently, some facet of the measuring technique or some unsuspected perturbation in the fabrication sequence affected the element performance adversely. (The specific cause has not been determined.) In consequence, all subassemblies (about ten) containing special fuel elements were removed as a precautionary measure.

The reactor was operated at 45 MW(t) from July 29 to August 12, when it was shut down after an attainment of about 1.1 at-% maximum burn-up. This was followed by incremental operation up to 45 MW(t) for physics measurements which ended on August 16. Routine removal of subassemblies for surveillance purposes was then again performed.

The No. 9 control rod drive shaft was removed from the primary tank on August 23 because of persistent sensing-rod sticking which interferred with normal gripper jaw operation. A replacement shaft was installed.

During a scheduled replacement of a safety rod, an operator's error resulted in destructive twisting of the rod top adapter (handling head) while inserting the rod in the reactor. Various inspections and checkouts were necessary before further fuel handling could proceed. No significant damage to fuel-handling equipment was sustained and no modifications were required.

The reactor was restarted on September 9 and operated at 45 MW(t) and 15 MW(e) through September 13. At this time, the responsibility for the EBR-II Reactor Facility was formally transferred from the Reactor Engineering Division to the Idaho Division.

1.1.2.2 Fuel Surveillance

A very cautious, conservative approach was exercised during this surveillance because of the experimental nature and unique design of the core fuel elements and subassemblies, and the demand for high thermal performance. Some aspects of the latter include (at full power): extremely high power density, up to 1230 kW/liter of core volume; high heat fluxes, to 929,000 Btu/(hr)(ft^2); and high temperatures: 1213°F (fuel alloy); 1100°F (clad); 1040°F (coolant). In addition, coolant flow orificing to match flow distribution with power distribution within the reactor was of critical importance. The fuel alloy employed, U-5% Fs, was "new." Scrammable control rods and safety rods bearing fuel with liquid sodium bond were also new. These and other conditions, all directed toward high reactor performance, necessitated a systematic, careful evaluation of core integrity throughout the initial power operation period. The program followed is described briefly below.

Figure 1-3 shows the configuration and principal dimensions of the EBR-II fuel element and subassembly (cluster of fuel elements).

At frequent intervals, as burnup of fuel progressed, the reactor was shut down and one or more selected subassemblies were removed from the reactor and placed in the storage basket. After a cooling period of nine days or more, they were removed to the Fuel Cycle Facility for disassembly and inspection. Normally, the following examinations were made:

Subassembly: visual examination; straightness check (go, no-go).

Fuel elements: visual examination; diameter check (go, no-go); Na bond inspection; Na height determination.

Fuel alloy pins: visual inspection; chemical analysis; diameter, length, and weight determination.

All 91 fuel elements of a subassembly (61 in the case of a control or safety rod) were visually inspected. Some 17-21 elements from each subassembly were given diameter, bond, and height checks. In each instance, about 10 elements were stripped for fuel alloy pin examinations.

Examination results from fuel elements at the lower burnups were used primarily to assure that no serious mismatch of flow and power existed, no surface deposition or flow blockages were being encountered, no vibration or wear effects were manifest, etc. After higher burnup levels were reached, the examination results were employed to assess irradiation damage per se and to indicate whether additional burnup increments could be attempted safely. In the latter case, it was deemed advisable to instigate a "stop and go" procedure for reactor operation. More specifically, as each additional increment of burnup was accrued, the reactor was shut down until inspection of subassemblies removed at that time justified attempting the next increment of burnup.

This conservative procedure necessarily reduced substantially the "plant factor." However, it added significantly to the safety of the initial operation and probably precluded some potential fuel element failures. The potential failures were not related to regular fuel elements, but to a small number of special elements which had been incorporated in selected subassemblies. These specials were identical to regular elements except for variations in the fabrication process to permit more thorough pre-irradiation measurements. Inspection of the special elements disclosed they were undergoing substantially greater irradiation damage than the regular elements. At 1 at-% burnup, all of the special elements had to be removed from the reactor. On the other hand, all regular fuel elements were still in excellent condition and capable of greater burnup.

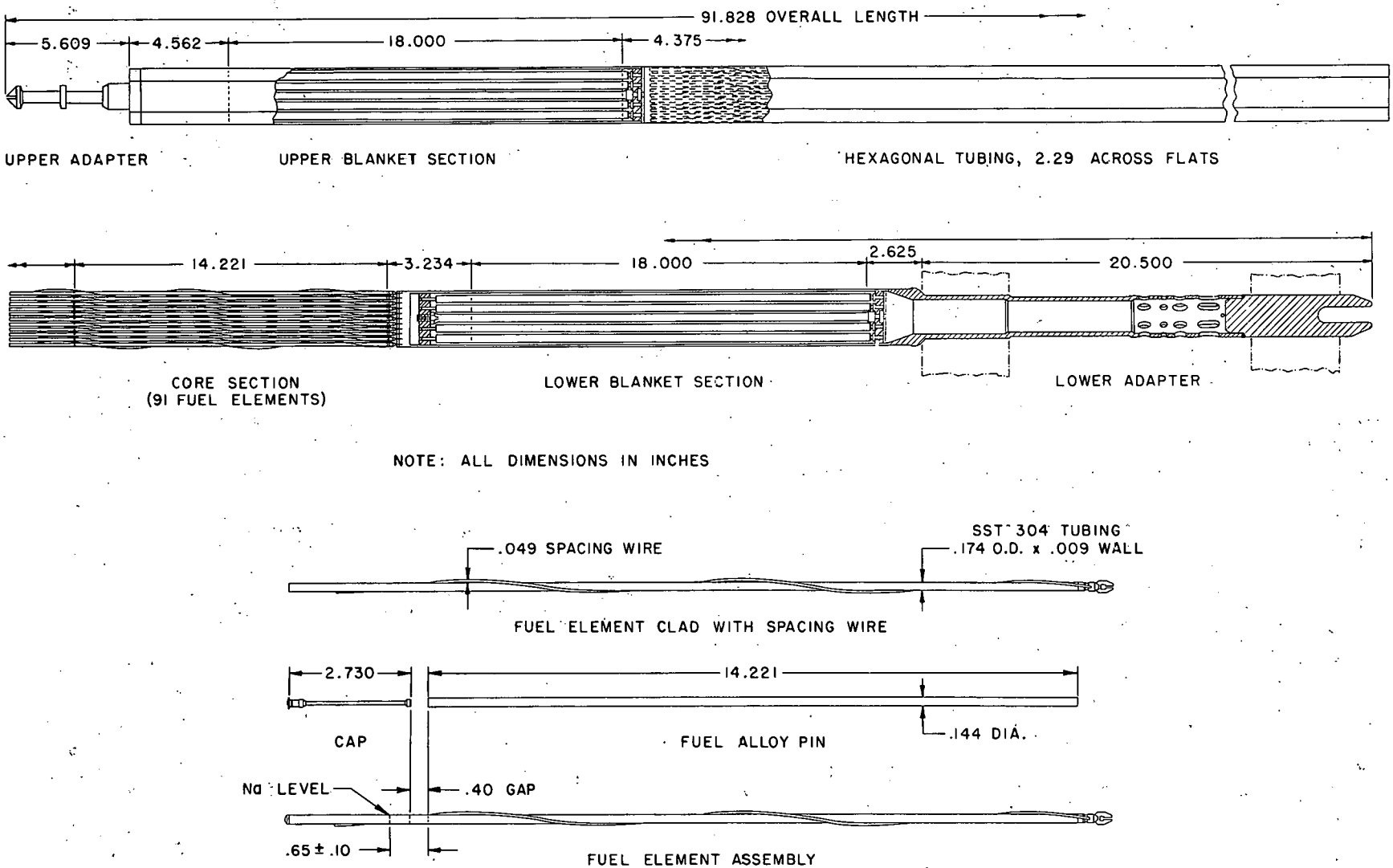

Fig. 1-3. EBR-II subassembly and fuel element

Except for the obvious benefit of visual examination, the most useful determination was that of the sodium height (distance from top of fuel alloy pin to sodium surface) within the element. As burnup proceeds, the volume of the fuel alloy increases, thereby displacing bond sodium and increasing the sodium surface height. As the height increases, the gas volume at the top of the element grows smaller and the gas pressure increases. Because maximum achievable burnup is limited by the maximum allowable pressure within the element, the sodium height is a valuable indicator as to whether additional burnup might be sustained safely. Additionally, the change in sodium height can be correlated, quantitatively, to the amount of swelling, or change in volume, experienced by the fuel alloy. Sodium height was measured by an eddy-current technique. Prior to these measurements, the elements were re-bonded to eliminate voids or bubbles which might have been introduced during post-irradiation handling or disassembly. If not removed, they could influence the height indication.

Because fuel alloy swelling is a function of temperature and burnup, and because both maximum and average fuel alloy temperatures within EBR-II elements vary with radial position in the reactor, subassemblies were selected for inspection from all the rows (1-6) of the reactor.

Most of the burnup data has been accrued at reactor operating conditions of 45 MW(t) power and full (100%) reactor flow. At this power level, fuel alloy temperatures ranged from about 720°F at inlet ends of all elements to about 1050°F at the highest temperature portions of the hottest elements. Similarly, clad temperatures ranged from about 710°F to 965°F.

Table 1-1. EBR-II Subassemblies Examined for Irradiation Damage

Reactor Megawatt-Days	Subassembly Number	From Reactor Row*	Maximum Local Burnup, at-%	Sodium Height, In. (at ~130°C)		
				Min.	Avg.	Max.
350	C115	2	.14	-	-	-
705	B304	6	.17	.71	.85	.97
705	L406	5 (CR)	.18	.73	.87	.98
705	C140	2	.27	.69	.83	.99
1285	C112	4	.43	.67	.90	1.16
1630	L413	5 (CR)	.46	.76	.96	1.06
1285	C143	2	.50	.84	.93	1.04
2010	C131	5	.57	.77	1.01	1.21
2500	B314	6	.5	.79	1.06	1.22
1630	C122	2	.63	.95	1.11	1.23
2500	L410	5 (CR)	.71	.95	1.17	1.37
2010	C103	2	.78	.92	1.13	1.26
2500	C141	4	.79	.92	1.15	1.44
2500	S601	3 (SR)	.89	1.07	1.29	1.59
2500	C145	2	.96	.99	1.35	1.54
2500	C138	1	.97	1.05	1.34	1.50
2910	S602	3 (SR)	1.02	1.19	1.35	1.68
2910	C136	3	1.06	1.30	1.59	1.77

*CR = control rod; SR = safety rod.

Table 1-1 shows the number, location (reactor row in which irradiated), and maximum local burnup (percent of heavy atoms) of the subassemblies inspected. Also given are the minimum, maximum, and average sodium heights observed in the elements of each subassembly. The average burnup in the highest burnup element of a subassembly is about 0.87 times the maximum local burnup shown. Moreover, the average burnup of all elements in a subassembly is roughly 0.81 times the maximum local burnup indicated (for subassemblies of row 4; somewhat higher in rows 1-3, and lower in rows 5-6).

Figure 1-4 shows volume-percent swelling of the fuel alloy versus maximum local burnup as calculated from change in sodium height. The upper curve is for the poorest performing element, the lower for the average element. The lower curve is based upon the average of the initial heights observed in a large number of (typical) elements, ~0.82 in. (at ~130°C); the upper curve is based on the maximum initial height observed, ~0.92 in. (at ~130°C). The latter curve may be somewhat optimistic, as there is no assurance that maximum sodium height after irradiation is necessarily associated with maximum initial height.

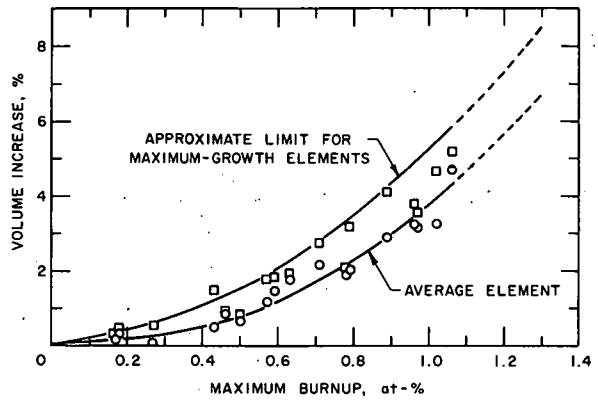

Fig. 1-4. Volume increase of fuel alloy as a function of burnup for EBR-II, Mark-I-type fuel element containing U-5% fissium alloy

Post-irradiation measurements of fuel alloy pin diameter (maxima and minima only) and length provided another check on fuel volume change, but this method is not considered as accurate as the use of sodium height change. Post-irradiation measurements of gas pressure in the space above the bond sodium were also made on a number of elements. As expected, there was no significant increase until high burnup levels were reached. For example, elements from subassembly C136, with maximum burnup of about 1.06 at-%, exhibited final pressures of 17-24 psia (at room temperature). By comparison, the pre-irradiation pressure was slightly less than one atmosphere.

In summary, core performance has been excellent. Subassembly performance was good in every respect: strength is adequate, straightness is no problem, chromium plating is fully retained, no evidence of any tendency to stick in the reactor grid has arisen, no evidence of deleterious deposits on fuel element surfaces or of any kind of flow blockage has been found, etc. All fuel elements examined were in good condition, with no change in external diameter or appearance. Of the more than 1400 regular driver fuel elements removed for inspection, none was found defective. The design burnup level (minimum of 1.0 at-% local burnup) has been attained and burnups at least to 1.2 at-% appear achievable.

1.1.2.3 Failure of Oscillator Drive Mechanism

This incident is described in detail because it illustrates the magnitude and complexity of blind manipulations and operations which can be performed to diagnose and correct equipment failures in sodium-cooled reactors.

On October 19, 1964, a spurious reactor scram occurred. At the time, the reactor was operating at 37.5 MW(t). Immediately thereafter it was learned that two of the eleven control rods (Nos. 7 and 9) had failed to scram. The oscillator drive mechanism was checked and also was found to be stuck. This drive occupies a position normally assigned to a control rod (No. 8). A program of investigation and corrective action was undertaken which eventually required four months to complete.

Site and Cause of the Sticking. At the start of the investigation, the immediate objectives were: (1) to determine the location of the sticking; and (2) to experiment with forcible movements of the shafts in hopes of identifying the general nature of the sticking.

There are twelve control rod positions, arranged in hexagonal configuration. Position Nos. 7 and 9 are located on either side of and immediately adjacent to the oscillator assembly position. The upper adapters of the control rods and oscillator rod connect to their respective drive shafts. The shafts extend upward, successively passing through the reactor upper plenum, reactor vessel cover, the bulk sodium over the reactor vessel, the rotating shield plug, and into the work area over the primary tank. The combined length of the control (or oscillator) rod and drive shaft is approximately 30 ft.

Thus, there are three general areas in which "sticking" possibly could occur: the portion of a control mechanism mounted on or extending through the rotating plug; the area of penetration of the reactor vessel cover by the drive shaft; and the control rod thimble assembly inside the reactor.

Control rod No. 7 was gradually worked down to the fully inserted position by alternate application of upward and downward forces ranging up to 700 lb. Further exercising of the shaft reduced the friction, but did not restore normal operation. Realizing that rotational movement would be required to thoroughly free the shaft, special tools were designed and their fabrication started. Meanwhile, by delatching the drive shaft and observing the free fall of control rod No. 7 through a sensing device, it was determined that the sticking was not associated with either the rod or its guide thimble. The drive shaft for control rod No. 9 then was freed similarly.

After delatching all control rods except No. 9 from their drive shafts, the reactor vessel cover was carefully raised about 1/8 in., while simultaneously observing the top ends of the drive shafts. The No. 7 shaft and the holddown tube of the oscillator mechanism (physically identical to a control rod drive shaft in the region of the reactor vessel cover), both rose while the other ten drive shafts remained stationary. This indicated clearly that the sticking was occurring in the penetrations of the reactor vessel cover. (See Fig. 1-5.)

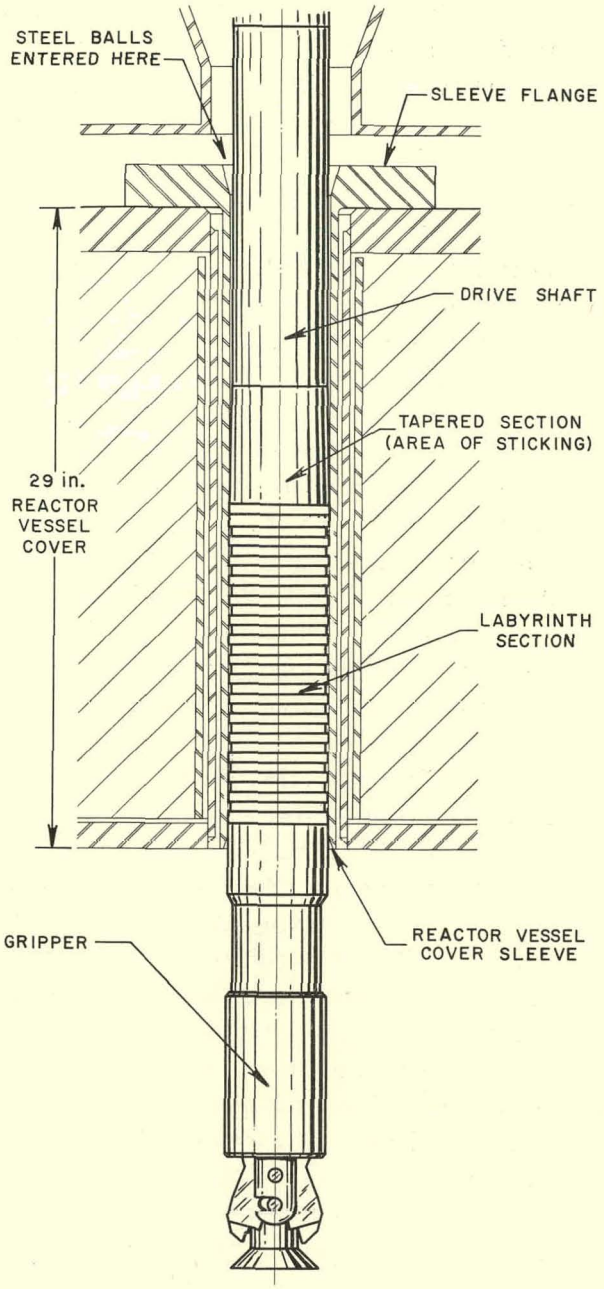

Fig. 1-5. Penetration of control rod drive shaft through reactor vessel. Steel balls from oscillator entered through guide funnel at top.

Attempts then were made to free the oscillator rod drive shaft and holddown tube. The drive shaft was loosened to the extent that it could be oscillated over a range of about 2 in.

By this time the special tools were available for rotation of the control rod No. 7 drive shaft. By using a combination of rotational and vertical movements the shaft was essentially completely freed.

Attention again was turned to freeing further the oscillator drive, but without success. It then was thought that restoration of reactor coolant flow might help, particularly if sodium oxide were the primary cause of sticking. After about an hour of pumping it was found that both No. 7 and 9 control rod drive shafts and the oscillator drive were stuck again. The decision was made to remove control rod drive No. 7 from the primary tank.

Removal of Control Rod Drives. Control rod drive No. 7 was removed into a shielded caisson. Inspection of the shaft through shielding windows showed clearly the cause of the sticking. Small steel balls had become lodged in the clearance annulus between the shaft and the Stellite sleeve liner of the reactor vessel cover penetration. Ten balls (or pieces) had adhered to the shaft in and above its labyrinth section and were recovered with it. These may be seen in Fig. 1-6. Score marks on the shaft are also apparent.

The presence of these 1/8-in.-diameter balls made it certain that one of the linear ball bushings in the oscillator drive assembly had failed and that the balls released had found their way to the top of the reactor vessel cover sleeves. (Balls of this diameter were employed inside the primary tank only in the oscillator bushings.)

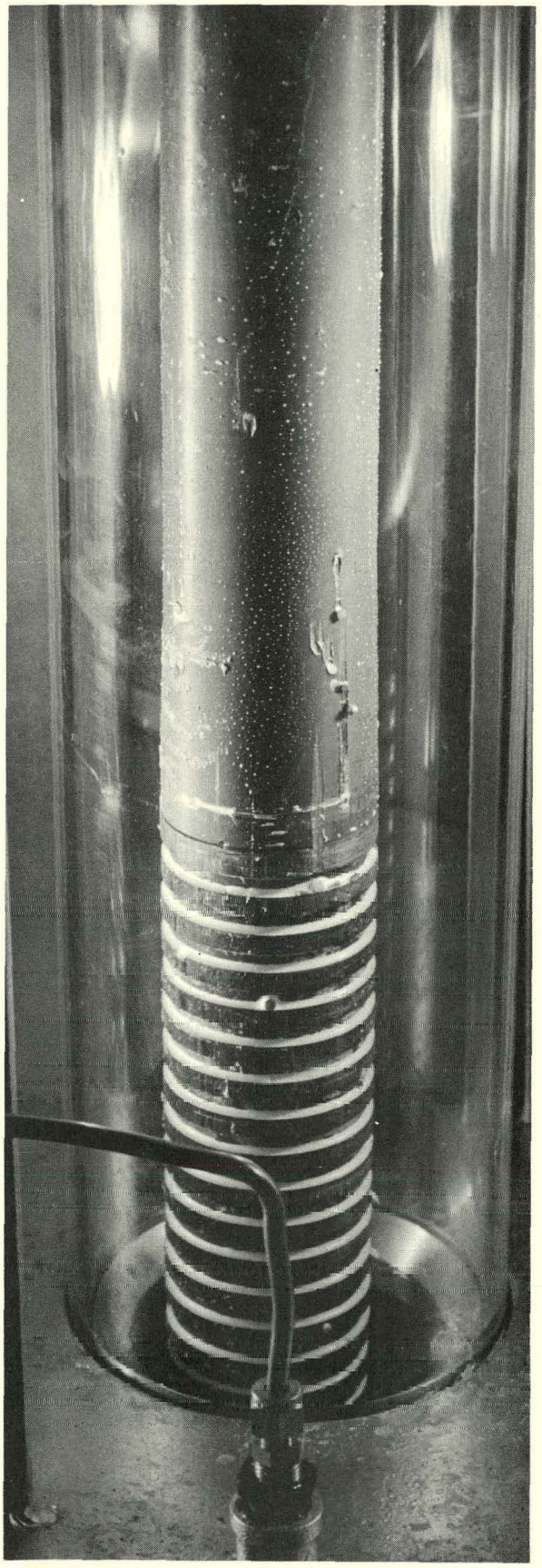

Fig. 1-6. Steel balls and scoring on No. 7 control rod drive shaft just above labyrinth section

The No. 9 control rod drive shaft then was removed from the primary tank. Inspection showed the same cause of sticking as in the case of No. 7.

Oscillator Assembly. The oscillator assembly consists of two principal parts: oscillator rod assembly and oscillator drive assembly. The oscillator rod assembly is positioned entirely inside the reactor. It consists of the oscillator rod, the oscillator thimble, and the (No. 8) control rod thimble. The oscillator rod reciprocates within the oscillator thimble which sits inside the control rod thimble. The control rod thimble, in turn, is supported in and locked to the reactor vessel grid.

The oscillator drive assembly consists of the oscillator drive shaft and a holddown tube. The drive shaft reciprocates inside the holddown tube (thus reciprocating the oscillator rod to which it latches). The holddown tube extends upward through the reactor vessel cover and the small rotating plug. Its lower end is designed to engage the top end of, and "hold down" the oscillator thimble.

Removal of the Oscillator Assembly. Three special tools had to be built before the oscillator drive assembly could be removed: one "feeler" tool, and two "ball catcher" tools. The "feeler" tool was used to sense separation of the oscillator drive shaft from the oscillator rod. To prevent the possible loss of additional balls from the oscillator during its removal, the two "catcher" tools could be inserted through the No. 7 and No. 9 sleeves and pantographed into position under No. 8 in such a way as to form a collector cup.

Initial attempts to remove the oscillator drive assembly from the reactor vessel cover were not successful. Use of a pull force of more than 5000 lb or use of a substantially different procedure seemed required. Forces of such magnitude were of serious concern. It was considered absolutely necessary to avoid damaging the reactor vessel cover sleeve, or rupturing the oscillator assembly in such location as to make it essentially inaccessible for subsequent removal attempts. Therefore, removal work was halted until a thorough study of the optimum procedure for removal (and of the maximum pull force which might be safely applied) could be completed. The next attempt to remove the drive assembly, using an upward force of about 2500 lb augmented by intermittent upward impact manually applied, was successful. Inspection of the holddown tube revealed six deep vertical grooves, just above the labyrinth, caused by steel balls jamming the holddown in a manner identical with control rod drives Nos. 7 and 9. No balls were recovered in the catcher tools.

Inspection of the oscillator drive revealed that the lower of the two ball bushings had disintegrated and all its balls were missing. It was evident that some of the balls released had been carried upward by sodium flow within the holddown tube to the single vent hole near the upper bushing. They then exited through this hole into the area above the reactor vessel cover sleeves and from there descended into the shaft-sleeve annuli.

An attempt was made to remove portions of the oscillator rod assembly. A tool was devised to be lowered through the No. 8 cover sleeve, lock into, and withdraw the oscillator thimble (containing the oscillator rod). The thimble could not be pulled out, however. It moved upward a short distance and became stuck. This made it apparent that some of the balls from the disintegrated bushing had entered the annulus between oscillator thimble and control rod thimble and had wedged the two together.

An effort next was made to recover any balls which might still be lying on top of the Stellite sleeve flange faces at positions Nos. 7, 8, and 9. Again, tools specifically designed for the purpose were fabricated. No balls were found.

Measurements of the relative vertical positions of the oscillator thimble and control rod thimble indicated that the reactor grid locking pin very probably was damaged. Consequently there was little hope of removing the oscillator rod assembly by lifting the control rod thimble (with the assembly inside it). Accordingly, it was felt that effort should be continued on attempting to pull the oscillator thimble free of the control rod thimble or to pull the oscillator rod free of the oscillator thimble. Again, it was considered absolutely necessary to conduct these removal attempts in such a way as to preclude rupturing of the assembly components or lessening the probability of success of subsequent removal steps. Therefore, removal work was suspended until a careful study of the best approach and of realistic limits on forces to be used could be completed.

As a result of the study, another tool was devised which enabled "holddown" of the oscillator thimble while pulling on the rod. But even with this tool, using a force of 1200 lb and impacting, only slight rod movement was obtained. It now was clear that the rod was firmly stuck in the thimble and that use of higher pull forces would be risky. Accordingly, it was decided to attempt removal of the entire assembly by lifting the control rod thimble, even though the evidence was strong that such an attempt would not prove successful.

Fuel handling then was carried out. Six fuel subassemblies immediately surrounding the No. 8 control rod thimble (containing the stuck oscillator rod and thimble) were replaced with scalloped, dummy subassemblies. These were needed to permit rotation of the thimble for unlocking. A tool was designed to be inserted through the auxiliary gripper sleeve of the reactor vessel cover, descend over the oscillator rod protruding from the oscillator thimble, and grasp the control rod thimble from the outside. After positioning the rotating plugs so that the auxiliary gripper sleeve was directly over the oscillator rod assembly, this tool was inserted and latched to the control rod thimble. With considerable difficulty, the thimble was rotated the required 60 degrees to unlock it from the grid locking bar. The thimble - with the entire oscillator rod assembly - then was readily pulled upward out of the reactor and primary tank into a shielded caisson. Examination of the reactor grid locking pin with special tools showed that no damage to the grid locking pin had been sustained.

The reactor was now in a condition in which all malfunctioning components had been removed. After reinstallation of the control rod drives, a series of checkouts were made to assure that the control rod and safety rod systems were operating satisfactorily. Final steps then were taken to restore the primary system to readiness for power operation. Subsequent operation confirmed that no significant permanent effects on the reactor had resulted from the incident.

1.1.2.4 Electrical System and Instrument Air Safety Tests

The design of the electrical power system of EBR-II employs an emergency power system for a number of critical loads throughout the plant. These loads include the Control Power System, the Annunciators, Emergency Lighting, Cooling Water Pumps, Shield and Thimble Cooling Systems, and others. This emergency power is provided by two diesel generators, a 100-kW unit and a 400-kW unit. The most vital loads, such as Shield and Thimble Cooling, are carried by the 100-kW unit and are backed up, in turn, by automatic switching to the 400-kW unit.

In order to test the performance of the diesel generators and the switchgear, as well as the response of the entire integrated electrical

system, an electrical power failure test was performed in June, 1964. This test simulated a power failure of the normal system, with the diesel generators assuming their designated emergency loads.

As one of the preliminary steps of this test, the 100-kW and 400-kW diesel generators were operated under their respective loads to check their capability and the interlocking arrangement. It was found that the 400-kW unit would not automatically assume the critical loads from the 100-kW unit in the event of failure of that unit. It was decided to conduct the electrical system test, using manual switchover for these loads.

The electrical failure test was initiated from a Plant Standby condition, with the primary bulk sodium temperature at approximately 590°F. This was done by opening the 13.8-kV feeders. Immediately thereafter, all critical loads were assumed by the emergency power system. In the Primary System, the primary pumps, primary tank immersion heater, rotating plug seal heaters, silicone pumps, and argon blowers were de-energized. In the Secondary System, the secondary sodium pump, recirculating pumps, Dowtherm pumps, and all heating circuits were de-energized. The Steam System suffered a loss of power to the condenser cooling water pumps, motor-driven condensate pump, and motor-driven feedwater pump. (Since the instrument air compressor is on emergency power, all control panels and most controls were not affected.)

All systems responded essentially as predicted. The Plant was orderly secured and brought back to the initial standby condition in approximately 3.5 hr.

Several minor improvements were made as a result of the test. The failure of the 400-kW unit to automatically pick up the critical loads of the 100-kW unit was investigated and corrected. A number of minor interlocks were found to malfunction and were repaired. It was also determined that better phone communication between switchgear centers and the control room was needed.

The instrument air safety test was intended to simulate the failure of the air compressors to operate for any of a number of possible reasons, e.g., drive motor breakdown, electrical switchgear failure, compressor bearing failure, etc.

The instrument air failure test was initiated by closing the main air supply valve, with the Plant in standby condition at 600°F. Since most controls are equipped with air accumulators, the Plant was slow in responding. The condensate system was isolated from the feedwater system, since the deaerator makeup valve closes upon loss of air. Steam bypass flow to condenser ceased along with the blowdown flow; therefore, the only makeup required by the steam drum was due to trap losses. Water stored in the deaerator was more than adequate to supply these losses.

Cooling water flow to the secondary system main pump and recirculating pumps also ceased. Since power to the main pump was shut off and power to the recirculating pumps was reduced, the temperature rise of the pumps' winding was acceptable.

The emergency air compressor in the Reactor Building assumed its load after the system air pressure slowly decreased to 71 psig. The fact that the compressor was cycling clearly indicated that it can adequately handle the emergency loads.

Here, again, the Plant behaved essentially as predicted. However, some minor inconsistencies with the predicted behavior were apparent. Unexpectedly, the startup feedwater pump remained in operation: its unloading valves were on plant air and not instrument air as supposed. Also, the steam header pressure gage and the feedwater valve position indicator were found to be inoperative with loss of instrument air.

In approximately 4 hr after initiation of the test, the Plant was successfully restored to the initial Standby condition.

1.1.2.5 Steam Generator Repair

The EBR-II steam generator consists of eight (8) evaporators coupled, through a steam drum, to two (2) superheaters. Both evaporators and superheaters are shell-and-tube heat exchangers, having 73 duplex tubes (1.438 in. O.D., 1.065 in. I.D.), welded into fixed double tubesheets at each end, an overall length of approximately 30 ft, and a shell diameter of 20 in. Sodium on the shell side flows countercurrent to the "water-steam" flow in the tubes. The dead air space between the double tubesheets can be viewed through inspection holes. The material of construction is low alloy carbon steel containing $2\frac{1}{4}\%$ chromium, 1% molybdenum. To provide for better heat transfer, the superheater tubes are cored to increase steam velocity. This is the only difference between the design of an evaporator and a superheater in EBR-II. Figure 1-7 shows a typical EBR-II evaporator.

On February 4, 1965, inspection of the air space between the upper tubesheets of evaporator EV-702 (located near the southwest corner of the Sodium-Boiler Plant) revealed a wet condition which strongly suggested a leak from the water side of the unit. This was confirmed by first thoroughly drying the wet region, and then pressurizing the water side to 2250 psig.

Since the leak was from the water side, the possibility of field repair was promising. The 10-in. riser from the evaporator to the steam drum was removed, thereby exposing the top surface of the steam tubesheet. To determine whether a failure occurred in a tube wall or a tube-to-tubesheet weld, each tube was fitted with a rubber stopper, and the dead air space between the tubesheets was pressurized with air. A leak was

readily detected in a tube-to-tubesheet weld with a solution of "Lek tec" and water. The precise location and shape of the defect was determined with a dye penetrant. Figure 1-8 shows the pinhole defect as a small dark spot near the end of the matchstick pointer. The hole was chased, by grinding, to a depth of approximately 3/32 in.

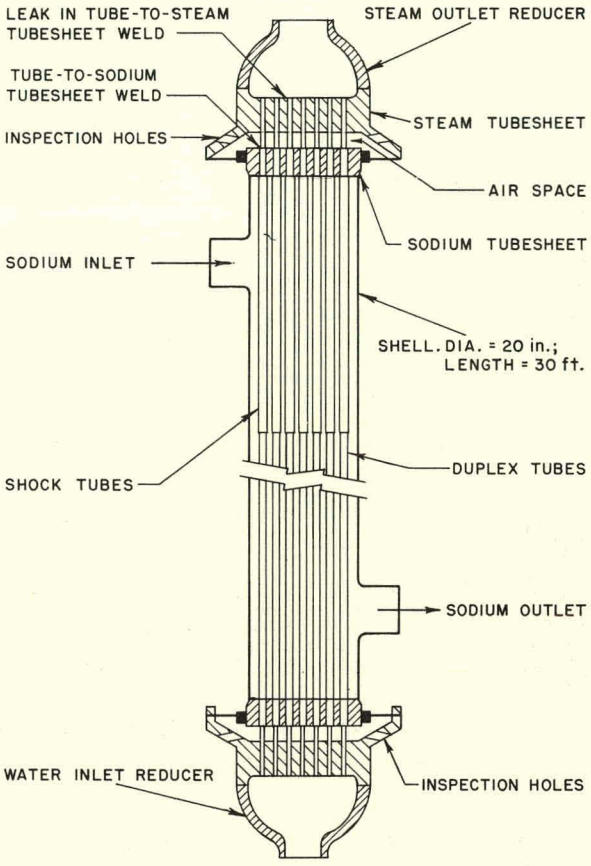

Fig. 1-7. EBR-II evaporator

After inspection, the leak was concluded to be a defect caused by gas inclusion during welding. A thin layer of weld metal covering the pinhole probably prevented detection by the final helium mass spectrometer test and also during initial operation. With slight amount of corrosion, the thin layer of weld metal was no longer effective and a leak developed.

Field repair was accomplished by manually welding over the ground area. The welding procedure consisted of the following:

(1) Preheat the tubesheet to 225°F.

(2) The gas tungsten-arc welding method was used. Argon was used as an inert gas, both for the tungsten electrode and as a backup-purge through the entire unit. A bare wire containing $1\frac{1}{4}\%$ chromium and 1% molybdenum was used as a filler.

(3) A post-weld heat treatment was made at 825°F by holding at temperature for one hour. The thermally-insulated tubesheet and head were then air cooled.

Photographs of the initial repair showed what appeared to be a crack. Although the defect in the photograph could not be seen when the repair was again inspected, a recheck with a dye penetrant did reveal a doubtful area. As a precautionary measure, this area was covered with weld metal even though a helium mass spectrometer leak test indicated no leak. Since the second "repair" was made in a region between the top of the weld and tube, neither pre-heat nor post-heat treatment was performed.

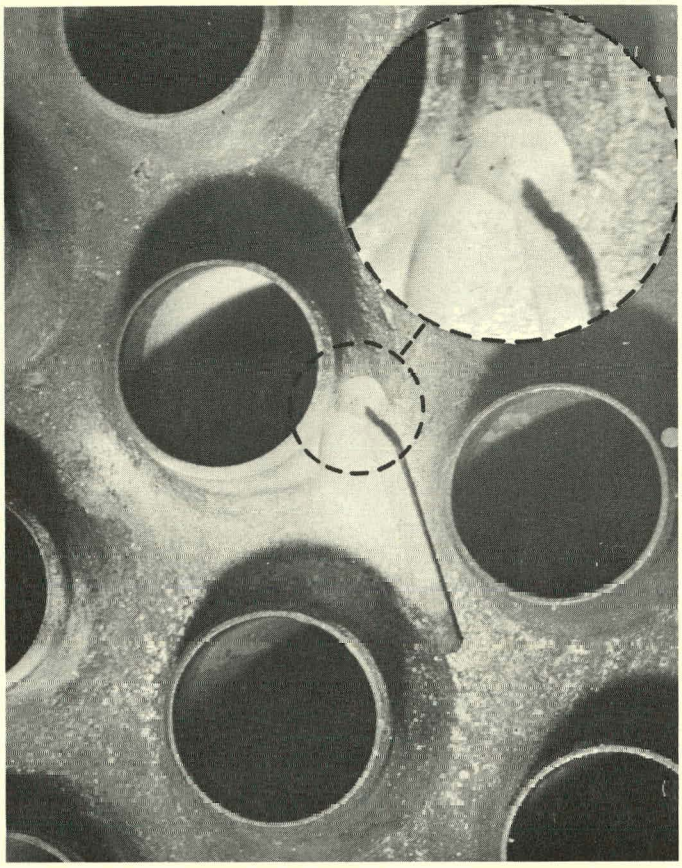

Fig. 1-8. Matchstick points to pinhole leak in EBR-II evaporator EV-702

Before the final helium mass spectrometer test, each tube-to-tubesheet weld was tested to ensure that fine particles were not concealing other potential leaks. This was accomplished by first plugging a tube with a rubber stopper, cupping the weld area, and then pressurizing the weld with air. Subsequent mass spectrometer test indicated "no leak" with the system operating at a sensitivity of approximately 4×10^{-10} cc/sec (helium) and at a pressure of 25 microns of mercury.

Following the repair of the evaporator, the riser was reinstalled. All welds were inspected with a dye penetrant and then radiographed. The system (evaporator and riser) was given a final hydrostatic test at 2250 psig.

Subsequent to this repair, the unit has been operated at pressure and temperature for more than 2000 hr, with no sign of leakage.

1.1.3 Plant Improvements

1.1.3.1 Reactor Plant

During the course of reactor operation, areas where improvements could be performed were determined and the necessary steps taken to effect their implementation. In the Reactor Plant, the principal area for improvements was in the fuel handling system; in particular, the Fuel Unloading Machine, Control Rod Gripper Jaws, and the Transfer Arm. Other improvements were concerned with the Auxiliary Gripper Plug and with pressure relief devices on the building containment vessel and the primary tank.

During the Approach-to-Power Program, until September 13, 1965, approximately 125 fuel handling operations were performed. These involved transfers of subassemblies either from the Interbuilding Coffin through the Fuel Unloading Machine onto the Transfer Arm in the Primary Tank or in

the reverse direction. Problems encountered during these operations were due principally to the presence of sodium in clearances between close-fitting, moving parts of the Fuel Unloading Machine (the gripper and gripper guide tube). If these surfaces are not kept free from sodium, the vertical travel of the gripper will be obstructed. It can be moved, but only with great force and at the risk of damaging parts of the drive mechanism. An improved gripper (Mark II) was designed, manufactured, tested, and installed in the Fuel Unloading Machine. This gripper features greater allowances for sodium which might adhere when it is operated above the level of sodium. In addition, a force-limiting mechanism was installed to prevent overstressing the drive mechanism should the gripper stick due to sodium accumulation.

On several occasions, the self-locking jaws of a Control Rod Gripper malfunctioned due to a weakness in the unlocking cam. This prevented proper disengagement of a control rod from its drive preparatory to transfer of the subassembly in the Primary Tank. Changes were made to improve the method of attachment to the Control Rod Drive Gripper.

The Transfer Arm Mechanism is a major component of the Fuel Handling System. It transports fuel subassemblies, while submerged in the primary tank sodium, between the Fuel Unloading Machine, the Storage Basket, and Reactor Loading Gripper Mechanism. In order to achieve greater reliability of the manually activated operations of the Transfer Arm Mechanism, several modifications were carried out. These resulted in an improved checkout sequence for the subassembly locking device and better provisions for supervision of these activities from the fuel handling control console.

The reactor vessel cover is provided with a penetration for an Auxiliary Fuel Handling Gripper. The penetration is normally plugged with a solid shaft for shielding purposes. This shield plug has been improved to provide indication of upward movement in the unlikely event of sticking between it and the reactor vessel cover. The reactor vessel cover is raised vertically for fuel handling. This movement would be automatically stopped should sticking occur.

Special, self-actuating pressure-relief devices were designed for the reactor containment building and for the primary tank. These devices will backup the existing building and tank pressure control systems. The reactor building device will operate, as necessary, to maintain a negative pressure within the building, without compromising containment integrity. It will relieve at -6 in. H_2O, and close at -2 in. H_2O. The primary tank pressure relief device is designed to operate only in the unlikely event of simultaneous failure of normal primary tank pressure control equipment and the onset of a severe pressure fluctuation in the primary tank. It will relieve the primary tank to the reactor building atmosphere if the tank pressure exceeds limits either above or below its normal pressure.

1.1.3.2 Sodium-Boiler and Power Plant

The secondary sodium system functioned well as the power level of the reactor was increased in the initial phases of the Approach-to-Power Program. Some difficulties were encountered in the secondary sodium pump control system, but did not seriously delay the program. Improvements were made by replacing the self-correcting feedback feature with a simple manual-type control for changing the flowrate. The feedback feature was unstable at very low voltages and unnecessary for stable operation at high voltages. This is due principally to the fact that the secondary flowrate is continuously under the direct manual control of an operator.

Performance of the steam system is best described as fair. Numerous minor difficulties were encountered and corrected. Almost all of the troubles related to conventional, commercial components. These included: early failure of blading on the steam turbine drive of the main feedwater pump; faulty operation of the feedwater control valves; poor performance of main header safety valves; and persistent mechanical troubles with the cooling tower.

1.1.4 Experimental Support

1.1.4.1 Material Surveillance Subassemblies

In order to maintain surveillance of the condition and behavior of the neutron shield graphite and of various metals typical of the components submerged in the primary sodium, a long-term materials irradiation test program was initiated for EBR-II. Ten material irradiation subassemblies have been fabricated for this purpose. Each subassembly will contain a wide variety of specimens for dimensional, physical property, and corrosion surveillance. A number of these subassemblies were placed in the reactor on March 1, 1965. They will be removed for analysis at intervals extending over the operating life of the EBR-II, thus providing increasing irradiation exposures.

Each subassembly consists basically of three sections as shown in Fig. 1-9. The upper section contains three graphite-filled cans that simulate those of the neutron shield surrounding the reactor vessel. These surveillance cans are necessarily smaller in cross section in order to fit into the subassemblies. Also, the can wall thickness has been scaled down to give approximately equivalent stresses under internal pressure. In each set, one can contains plain graphite, one contains borated graphite, and one contains half-plain and half-borated graphite. The first two types simulate the shield cans of "standard" configuration. Some of these cans, being positioned between reactor and nuclear detectors, require the thermalizing effect of plain graphite; others, utilized to reduce neutron flux, require the borated material. The third type is made up to simulate the loading in some

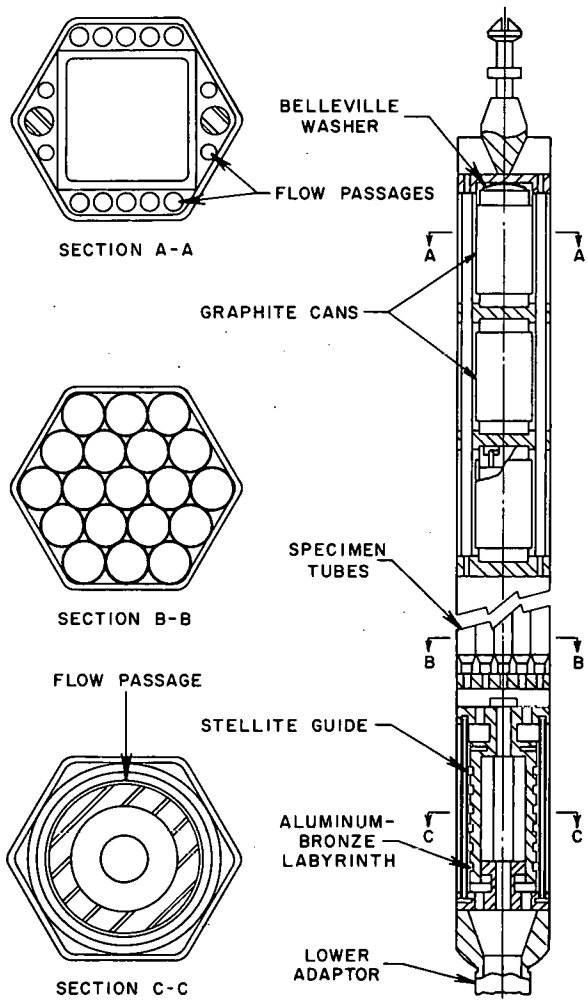

Fig. 1-9. Sectional views of EBR-II material surveillance subassembly

of the cans of "special" configuration which accommodate instrument thimbles or sodium lines or are located inside the reactor vessel cover. The cans have been manufactured and assembled using the same procedures and materials employed for those of the neutron shield. Before loading the cans into the surveillance subassemblies, complete micrometer measurements were made and recorded. After irradiation, analysis of the cans will include dimensional measurements, gas pressure measurement, and (possibly) gas analysis and graphite inspection.

The center section of the subassemblies contains nineteen, closely-packed tubes fastened to a grid at the bottom. The center tube contains four flux wires (one each of iron, titanium, nickel, and copper). The rest of the tubes contain two identical sets of metallic samples: one set of nine tubes exposing the samples to sodium coolant, the other set sealing the samples in helium.

Table 1-2 lists the fourteen metallic materials selected for testing in these subassemblies. They represent every component material in the primary sodium tank. Six types of samples were manufactured for various post-irradiation tests. Cylindrical samples of a fifteenth material (carbon steel) were furnished by another laboratory for hardness testing in the sealed tubes only. These samples also will be used to monitor dimensional stability and corrodibility.

Table 1-2. Surveillance Samples

Material	Type of Sample
Aluminum Bronze	Tensile, hardness
Haynes Stellite 6B	Hardness
Inconel X	Tensile, hardness, impact, springs
Type 420 Stainless Steel	Tensile, hardness
Tool Steel T-1	Tensile, hardness
Type 347 Stainless Steel	Hardness
Type 416 Stainless Steel	Hardness
Berylco 25	Hardness
Type 304 Stainless Steel with Boron	Hardness
Type 17-4 PH Stainless Steel	Tensile, hardness, impact
Type 304 Stainless Steel, Wrought	Tensile, hardness
Type 304 Stainless Steel, Welded	Tensile, bend test
Type 304 Stainless Steel, Special EBR-II	Tensile
Tantalum	Tensile, hardness
Carbon Steel (not ANL)	Tensile

The lower section contains an aluminum-bronze labyrinth and Stellite sleeve assembly similar (but reduced in size) to that used on the control rod drives where they pass through the

reactor vessel cover. Precise diametrical measurements were taken at three points on each land of the labyrinths and along eleven areas on the Stellite sleeve (opposite the lands). Upon removal from the reactor, these parts will be examined for changes in dimensions and effects of corrosion and erosion.

A total of 240 specimens will be available from each subassembly for these examinations, or more than two thousand specimens in all.

In order to expose the graphite cans to a neutron flux level equal to or greater than that seen by the majority of the graphite cans around the reactor vessel, the surveillance subassemblies will be positioned near the center of the outer blanket (twelfth row) in the reactor. Sodium flow through the subassemblies is slightly less than that in a standard outer blanket subassembly. Eight of the subassemblies were inserted in the reactor. The other two were placed in the storage basket to serve as controls. The storage basket is inside the primary tank, submerged in the same primary sodium (and at the same temperature) as the subassemblies in the reactor. The presently contemplated interval for removal of each subassembly from the reactor is 10,000 MWd. One control subassembly will be removed from the storage basket along with the fourth and the eighth subassemblies from the reactor.

1.1.4.2 Mark-A and Mark-B Irradiation Test Subassemblies

In order to gain maximum utilization of EBR-II as a fast flux fuel and materials irradiation facility, a program has been undertaken to provide a family of standardized experimental irradiation subassemblies to accommodate the wide variety of test samples and test conditions contemplated. Development of these subassemblies has been a continuing effort for many months, with a broad plan evolving in which several types of irradiation subassemblies have been, or are being, designed, tested, and placed into operation.

The first type, Mark-A, provides experimenters with a vehicle to irradiate nineteen samples simultaneously within one envelope at EBR-II neutron flux and temperature conditions. Encapsulation of the test samples is required. Coolant flows through an annular gap provided between the capsule and a shroud tube surrounding it. By means of an internal orifice, the total coolant flow rate for the subassembly can be varied to suit the test requirements. Several subassemblies of this design have been loaded into the reactor. One has completed its irradiation period, has been disassembled, and the capsules returned to the experimenter.

Through evaluation of the utilization of the Mark-A subassembly and discussions with experimenters, it became apparent that more flexibility was needed for future irradiation tests. Therefore, a Mark-B design is

being considered that will allow the loading of 61, 37, 19, or 7 samples, with or without encapsulation. This design utilizes helical spacer wires in place of shroud tubes, and provides for possible remote reassembly when the necessary ancillary equipment becomes available. The latter would enable successive irradiations of a given sample, with examination at the end of each period. Also, the proposed maximum sample length will be some 20 in. longer than in the Mark-A design. Preliminary plans also have been made for a Mark-C and, possibly, a Mark-D design. The former will allow coolant temperature rises higher than presently achievable by by-passing a portion of the coolant flow. The latter would accomplish the same and, in addition, would raise the coolant inlet temperature level by preheating.

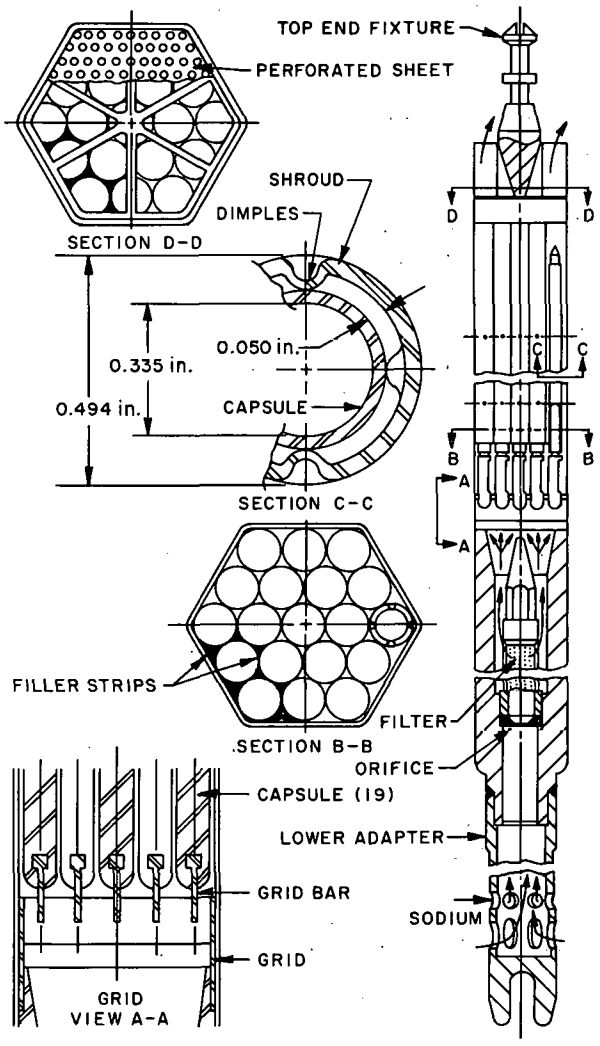

Fig. 1-10. Sectional views of Mark-A irradiation test subassembly

Additional details on Mark-A and Mark-B subassemblies are given below.

Mark-A. The design of the Mark-A subassembly is shown in Fig. 1-10. Maximum length of the capsules is about 40 in. Maximum sample length and diameter accommodatable are approximately 37 in. and 0.32 in., respectively. Each capsule slides into its own shroud tube, and is positioned by close-fitting dimples. The spaces between the shroud tubes are partially closed off with filler strips, so that essentially all of the coolant flow passes through the shroud tubes. As an added safety feature, a perforated sheet is welded to the bottom of the top end fixture. This sheet will retain any possible broken filler strips in the subassembly. Two different designs of lower adaptor are required: one for subassemblies destined for reactor rows 1-5, and the other for use in rows 6 and 7 (where the reactor grid holes are smaller).

A prototype of this design was manufactured to determine any fabrication or assembly problems, and to determine the pressure drop characteristics. Plots of flow rates vs. internal orifice diameter were obtained for the various reactor row positions. (See Fig. 1-11.)

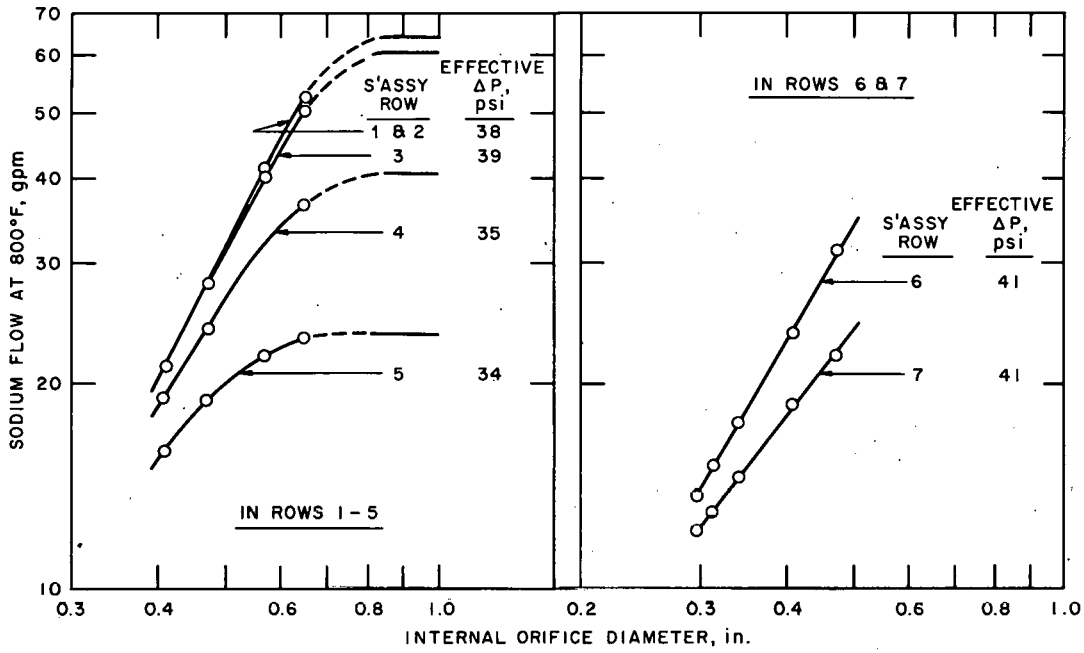

Fig. 1-11. Coolant flowrate as a function of internal orifice diameter in Mark-A irradiation test subassembly for the case of full reactor flow and nominal 67-subassembly reactor core

Sufficient hardware was purchased and/or fabricated for approximately thirty Mark-A subassemblies. Included was the tubing and tip material for the capsules, thereby assuring the uniformity of all material exposed to the reactor primary sodium. The capsule material is supplied to the experimenter on request.

The Idaho Division established a coordinating center to handle all requests for irradiations. Briefly, the procedure followed is:

(1) Experimenter obtains approval in principle from the Laboratory.

(2) Experimenter submits a description and hazard analysis.

(3) Experimenter prepares capsules.

(4) Capsules are submitted to Laboratory for non-destructive testing.

(5) Capsules are approved for loading based on (2) and (4) above.

(6) Capsules are loaded into subassembly.

(7) Subassembly is flow tested and loaded into reactor.

(8) Subassembly is irradiated per exposure requested.

(9) Subassembly is disassembled in Fuel Cycle Facility and capsules returned to experimenter.

Table 1-3. Mark-A Irradiation Subassemblies in EBR-II

Assembly No.	Reactor Position*	MWd Requested	Contents
XA01	Row 6 (C)	14,000	19 fuel
XG01	Row 4 (C)	400	6 fuel, 4 material, 9 shroud tubes blocked off
XG02	Row 7 (IB)	13,650	1 fuel, 18 dummy
XG03	Row 7 (IB)	19,450	2 fuel, 17 dummy
XG04	Row 7 (IB)	39,000	2 fuel, 17 dummy
XG05	Row 4 (C)	10,300	14 fuel, 5 material
XG06	Row 4 (C)	20,600	14 fuel, 5 material

*(C) = core; (IB) = inner blanket.

Seven of these subassemblies have been loaded into the reactor. Their respective positions, contents, and requested exposure are listed in Table 1-3.

Mark-B. This design was initiated to provide more flexibility for the experimenter and to facilitate the possibility of reinserting test elements in the reactor. The basic design features (Fig. 1-12) are similar to those of Mark-A, except that: (1) intercommunication of flow channels is effected by substitution of helical wire wrapping in place of dimpled shroud tubes; (2) allowable length of capsules (or samples) is increased; and (3) the inlet filter, no longer considered necessary, is eliminated. Four models are contemplated. The pertinent details are listed in Table 1-4.

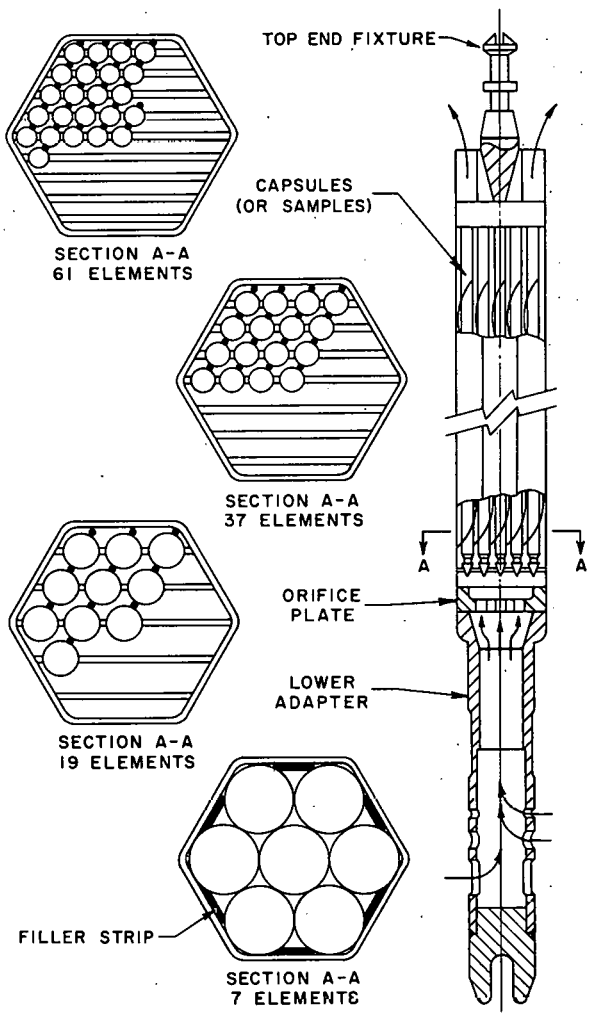

Fig. 1-12. Sectional views of Mark-B irradiation test subassembly

Table 1-4. Mark-B Irradiation Test Subassemblies

Type	No. of Capsules	Capsule O.D., in.
B-61	61	0.220
B-37	37	0.290
B-19	19	0.375
B-7	7	0.750

1.1.4.3 Mark-II Oscillator System Design

The new oscillator system will facilitate monitoring of reactor kinetics in EBR-II and allow greater flexibility in the acquisition of desired data. Need of the new system was occasioned by failure of the original oscillator as described earlier. Design is nearing completion, and fabrication of several components is underway.

The oscillator is a rotary device to be installed in place of a control drive (and rod). It is fully compatible with the fuel-handling system and will not cause any delay during the fuel handling starting and finishing sequences. The oscillator rod will be inserted or removed via

the existing fuel-handling gripper mechanism, transfer-arm mechanism, and fuel-unloading machine, and thus will not require any special tools or shielding coffins.

The oscillator rod, Fig. 1-13, consists of an outer tube containing four eccentrically located, cylindrical, inner tubes. The centers of the inner tubes are approximately 0.7 in. from the center of the outer tube. The latter can be rotated at speeds of 0.002 to 2.00 rps and, for a limited time, at higher speeds. Two of the inner tubes contain 75 gm of B_4C; they are connected to a gas-expansion chamber (volume = ~49 $in.^3$). This will permit about 1 at-% burnup of all boron atoms before increasing the internal pressure by four atmospheres, assuming 100% gas release. Subsequent oscillator rods can include minor modifications in B_4C loading, if desired.

The outer tube is topped by a quasi-standard fuel subassembly upper adapter; its bottom end connects to a sleeve bearing assembly that fits into a standard control rod thimble. The rod-bearing surfaces are made of Colmonoy No. 4 and Stellite 6B. The bearing assembly is anchored to the reactor support grid during oscillator operations, but is completely removable. No ball bearings are used in contact with sodium.

The oscillator drive connects to the upper adapter with a gripper similar to the control drive grippers. It has two flat areas on the gripper jaw teeth which bear against matching flats on the upper adapter and thus transmit the rotary motion. A 28-ft long rotating shaft assembly extends upward through the shield plug and through a pressurized packing seal. There, it connects to a variable-speed motor drive and gear assembly as well as to the sensing and jaw actuating devices. The rotating shaft is contained in a guide tube which extends from the top of the shield plug downward through the bulk sodium, the reactor vessel cover, and into the reactor vessel upper plenum. The guide tube houses four bearings spaced about 7 ft apart. Two of these bearings are submerged in sodium and are made of the same materials as the oscillator rod bearings. The other two bearings operate in the argon blanket region. They are made of Colmonoy No. 5 and Aluminum-Bronze, Ampco No. 22. All bearings are removable. The guide tube is suspended from a force-sensitive device that detects any significant friction during vertical travel of the reactor vessel cover.

The sensing, actuating, and driving devices are mounted on the control drive lifting platform and operate in air at room temperature. Appropriate control cables lead to the oscillator console in the control room.

Several component tests, as well as a short-term performance test of the complete oscillator in sodium, are planned before its installation in EBR-II.

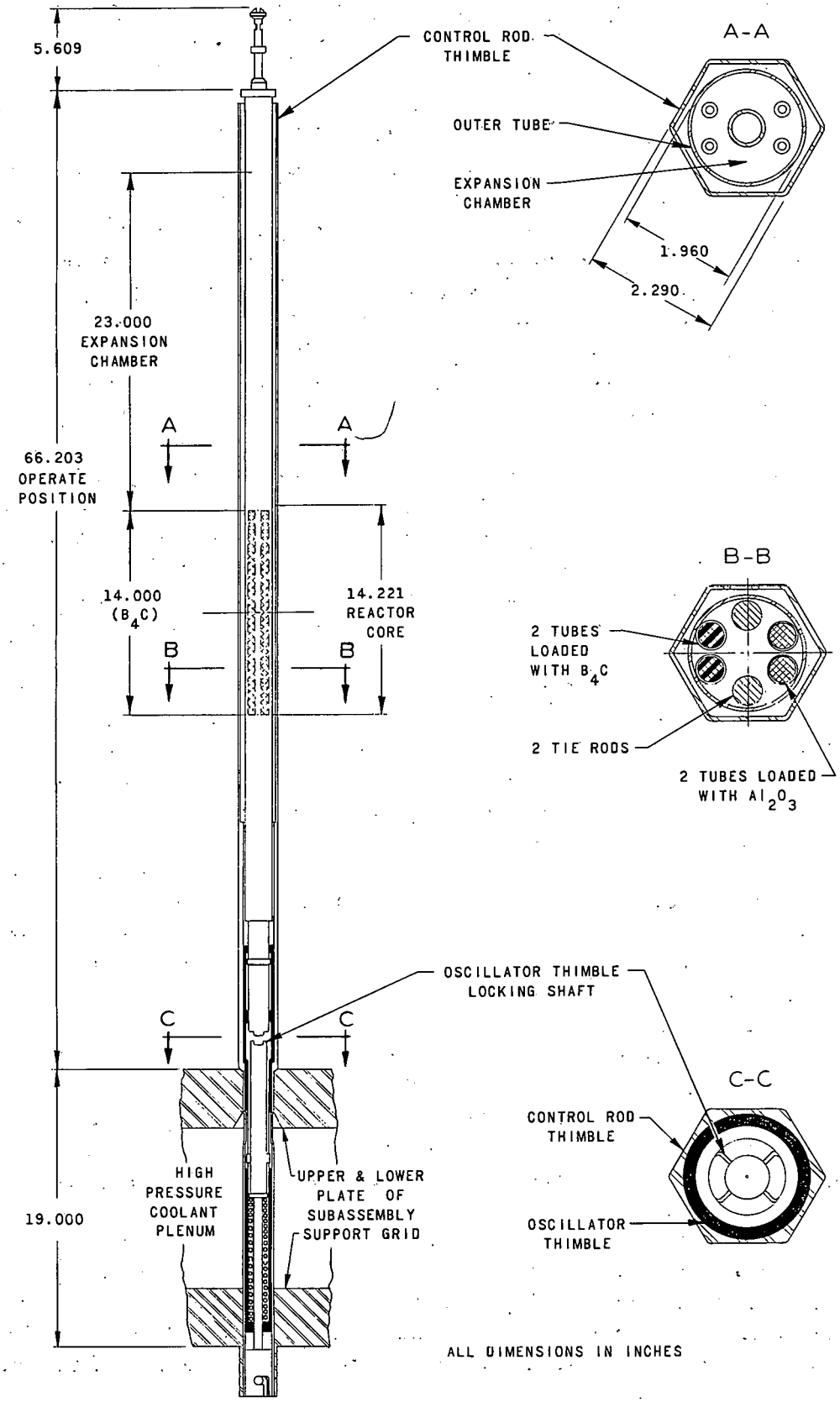

Fig. 1-13. EBR-II oscillator rod, Mark-II

1.2 FAST REACTOR TEST FACILITY (FARET)

1.2.1 Summary

The Fast Reactor Test Facility (FARET) Project was activated by the Laboratory in 1962, and authorized by Public Law 88-72 on July 22, 1963. The principal objective was to provide a facility for the performance testing of fuel for future, large, fast reactors. On December 2, 1965, the FARET Project was terminated by the Atomic Energy Commission as a result of a change in the Commission's program.

During the foregoing period, the Laboratory coordinated the facility design activities of the Architect-Engineer (Bechtel Corporation); carried out the research, design, and development of reactor components and related fuel-handling equipment; completed a safety analysis of the facility; and developed a tentative experimental program to be conducted in the reactor.[1-3*] In addition, the Laboratory coordinated the efforts of a Construction Manager (United Engineers and Constructors, Inc.) engaged by the Commission. This firm was responsible for procurement of principal plant components, with the exception of the reactor vessel and in-cell equipment. As shown in Table 1-5, the design and specifications were divided into nine procurement packages, according to types of work to be performed.

Table 1-5. Design Packages

No.	Title	Date Completed
I	Site Preparation	July 26, 1964
II	Reactor Vessel	August, 1964
III	Liquid Metal Heat Exchangers	April 15, 1965
IV	Liquid Metal Pumps	April 14, 1965
V	Control and Instrumentation	June 3, 1965
VI	Special Piping Materials and Valves	April 14, 1965
VII[a]	Liquid Metal Purification System	April 14, 1965
VIII	Specialty Steel	Cancelled
IX	Principal Design	June 3, 1965

[a]This package was later reorganized to include certain early procurement items.

A Program Evaluation and Review Technique (PERT) system was utilized to coordinate the various research, design, procurement, and construction activities. A comprehensive system of networks, showing interrelationship between tasks, was developed and kept up to date on a monthly basis.

A Preliminary Safety Analysis Report (PSAR) on the FARET facility was completed and reviewed by the Division of Reactor Development and Technology (DRDT), Division of Reactor Licensing (DRL), and the Advisory Committee for Reactor Safeguards (ACRS).[3] Subsequently, two major supplements and several minor submittals were prepared and a number of major review meetings were held.

Initially, the first experiment proposed for FARET was the investigation of Doppler broadening effects typical of large, fast, ceramic-fueled reactors. In February, 1965, the Laboratory decided to defer this experiment and to concentrate on fuels irradiation experiments. Particular

*Superscript numerals correspond to references listed at the end of each subsection throughout this report.

emphasis was placed upon the development of fuels performance data relevant to the Prototype Reactor in the AEC's Fast Reactor Development Program. New core arrangements were studied and a Reference Core I design and experimental program were established.[2]

A vendor (Babcock & Wilcox Co.) was selected for the design and fabrication of the reactor vessel. Preliminary design of the vessel was completed.

A preliminary design of the reactor vessel cover handling system also was completed. It utilizes a rather unique, large, flexible bellows. Tests on scaled-down bellows have been completed. The design of the prototype control drive mechanism has been completed. A variety of tests have been conducted to establish the feasibility and reliability of various subcomponents of this mechanism.

The design of the fuel-handling system and in-cell components has progressed to the prototype stage, with components in various stages of fabrication and procurement. Sub-components of the subassembly cut-off machine, such as the instrumentation lead severance device, are being fabricated. A laboratory mock-up has been completed for the investigation of in-cell handling operations.

A cell window design has been completed, based on Laboratory tests of large slabs of glass subjected to pressure, temperature, and impact. Specifications have been prepared for procurement of these units.

A large, 1200°F (sodium) Fuel Assembly Flow Test Loop was constructed. This loop will facilitate testing of subassemblies, in-core instrumentation, control drive mechanisms, and fuel-handling operations, in sodium and argon atmospheres similar to the anticipated reactor environment.

Thermocouples for the measurement of coolant and fuel temperatures are in various stages of development and evaluation.[4] Temperature-emf relationships for W-3% Re/W-25% Re thermocouples have been measured at temperatures up to 2800°C. Resistivity of alumina insulating material was investigated. In-pile tests were satisfactorily performed on sample couples in mixed-oxide fuel. These tests accumulated 940 hr of operation at fuel centerline temperatures up to 1345°C, and a fast integrated flux of 10^{19} nvt.

Some effort was devoted to the development of a flowmeter to measure the flow of sodium coolant through an individual subassembly. Three prototypes - turbine, electromagnetic, and thermal - are being fabricated for test purposes.

An important aspect of the instrumentation effort was the development of connectors that would operate satisfactorily in a sodium or sodium vapor environment at temperatures to 1200°F and would be reusable. Initial emphasis was on the development of an electrical connector to transmit electrical signals from in-core thermocouple sensors. A series of tests were performed in air, argon, and sodium environments. Encouraging results were obtained for slowly changing thermal conditions.

The following principal milestones show the overall progress of Project activities since 1962:

January, 1963	Publication of the Project Prospectus
April, 1963	Complete Preliminary Feasibility and Cost Study (in conjunction with Atomics International, Inc., and Shaw, Metz and Associates)
June, 1963	Start Title-I Design
July, 1963	Congressional Authorization (Public Law 88-72)
October, 1963	Complete Title-I Design Report
November, 1963	Start Title-II Design
April, 1964	Construction Manager Assigned
May, 1964	Complete Preliminary Safety Analysis Report
June, 1964	Complete Updated Cost Estimate
February, 1965	Complete Review of Check Cost Estimate
April, 1965	Select Reactor Vessel Vendor
June, 1965	Complete Interim Design Report
June, 1965	Complete Title-II Design
September, 1965	Complete Reference Core-I Design Report
November, 1965	Complete Preliminary Design of Reactor Vessel by Vendor
November, 1965	Complete PSAR Review by ACRS
December, 1965	Termination of Project

This section describes the work performed during fiscal 1965, and a portion of fiscal 1966 up to termination of the FARET Project in December, 1965. In the interests of completeness, work performed prior to fiscal 1965 is included in some instances.

1.2.2 Facility Description

The FARET facility, as designed, is a 50 MW(t), sodium-cooled fast reactor experimental facility to be located about 4000 feet southeast of the EBR-II in the East Area of the National Reactor Testing Station, in Idaho. The reactor mixed mean sodium outlet temperature range is 790°F-1150°F. Heat from the primary sodium system is transferred to a secondary sodium system from which heat is dissipated to the atmosphere in a sodium-to-air heat exchanger.

The facility (Fig. 1-14) consists mainly of a reactor building (87 ft wide, 172 ft long) of conventional construction and an attached support wing. The reactor building houses the containment structure. This structure consists of a steel and concrete cell (20 ft wide, 60 ft long, 37 ft high; 70 ft high over the annex) with walls ranging 3-5 ft thick above ground level, and a reactor vessel cavity and vault below ground level. Within this containment structure are located the reactor, essentially all radioactive liquid metal systems, and the fuel-handling services. With reference to Fig. 1-14, the reactor vessel (15), control drives (9) and fuel-handling equipment (10, 14) are located in the cell and cavity; the sodium coolant systems (18) are located in the vault.

The entire containment structure is designed for 30 psig pressure and for impact effects due to a nuclear incident.

The principal in-cell operations will be fuel handling and the servicing of experiments. The fuel-handling machine (10) is used to transport fresh subassemblies from the fuel transfer port, either directly to the reactor or to the fuel storage tank (14). It is also used to transfer fuel from the reactor either to the storage tank for cooling, or directly to the disassembly machine preparatory to shipment from the facility. Disassembly is limited to removal of structural material and shielding from the subassemblies; the fuel portions are left intact. The cut-off material (scrap) is deposited in transfer containers and removed from the cell via the fuel and equipment transfer tunnel (16).

The fuel-handling machine also will be used to plug and unplug instrument connectors at the top end of subassemblies.

The cell is designed such that essentially all fuel and related handling operations can be performed by remote control. Six shielding windows are provided for visual access. There are also five plugged openings for installation of additional windows. For maintenance or major adjustment, in-cell equipment can be removed either through the equipment port via the fuel transfer tunnel, or through the large roof opening at the south end of the cell.

1. BUILDING CRANE
2. STACK
3. VESSEL COVER HOIST
4. VESSEL COVER AND BELLOWS ASSEMBLY
5. SECONDARY SODIUM PUMP
6. HEATING AND VENTILATING EXHAUST
7. HEATING AND VENTILATING SUPPLY
8. CELL CRANE
9. CONTROL ROD DRIVES
10. FUEL HANDLING MACHINE
11. PRIMARY SODIUM PUMP
12. SODIUM TO AIR HEAT EXCHANGER
13. FUEL AND EQUIPMENT PORT
14. WET FUEL STORAGE TANK
15. REACTOR VESSEL
16. FUEL TRANSFER CASK
17. PERSONNEL ACCESS LOCK
18. PRIMARY HEAT EXCHANGER

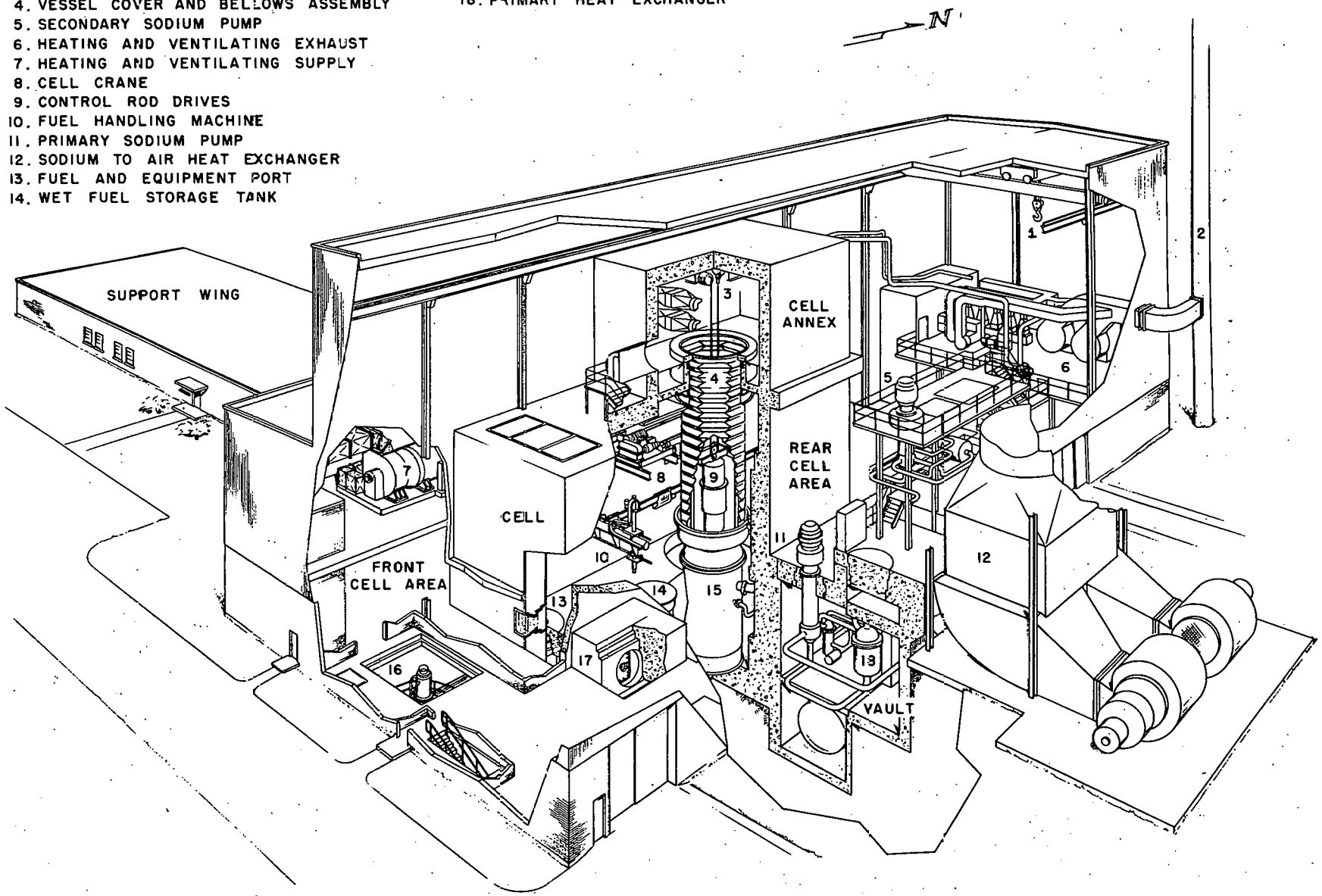

Fig. 1-14. Cutaway pictorial of reactor building and components

The cell structure at the north end over the reactor vessel extends upward to form a space (30 ft long, 24 ft wide, 25 ft high, inside), designated as the cell annex. A metal reinforced, fabric bellows installed between the annex and the reactor vessel cover provides a barrier between the cell and cell annex atmospheres. This arrangement permits access to the reactor vessel cover and control drive mechanisms when positioned in the cell, and, also while in a raised position, in an atmosphere separate from that of the cell.

The containment structure is provided with fixed and removable penetrations for personnel and equipment access; for power, control, and instrument wiring; and for various pipes and ducts. Personnel access is through locks in the rear cell area, environmental conditions permitting.

The support wing (144 ft long by 50 ft wide) is of conventional steel, concrete and masonry construction. The first floor contains the control room (immediately adjacent to the reactor building), administrative offices, and personnel facilities. The basement contains the boiler room, cable spreading room, the support wing ventilating system, and other minor utilities and services.

Outside the main building are located the secondary air-cooled heat exchangers for the main and auxiliary cooling systems, the 200 ft stack, and transformers and switchgear for the on-site electrical substation.

1.2.3 Supporting Research, Design, and Development

1.2.3.1 Reactor Components

These components include: (1) the first core; (2) the reactor vessel; (3) the reactor control system; and (4) the reactor vessel cover handling system.

The first core is comprised of a variety of test subassemblies, reflector subassemblies, control assemblies, and source assemblies. These are contained within the core structure which is located within the reactor vessel. The control drive mechanisms are located in, and are supported by, the reactor vessel cover. Preparatory to refueling, they are delatched from the control rods, the cover is remotely disconnected, and the cover and drive mechanisms are raised as a unit by the cover-handling system. This system is located above the vessel in the cell annex. A large flexible bellows between the cover and the floor of the cell annex provides environmental separation between the cell and cell annex atmospheres.

Reference Core I

The primary objective of experiments with the first core in FARET is to evaluate the performance of fast-reactor fuel elements typical of those to be used in a large, fast power reactor. The specific near-term objective is a fuel loading for the Prototype Reactor of the AEC Fast Reactor Development Program.[1] The Core I design operating conditions are planned to bracket the corresponding design specification of the prototype, with several of the different fuel-element designs tested under instrumented conditions.

More specifically, the Core I design will consist of carbide, metal, and oxide fuels in subassemblies driving each other and will test simultaneously ten different fuel-element designs with good statistics.[2] The Core I data are listed in Table 1-6. Tables 1-7 and 1-8 list the fuel element types, subassembly designs, and the tentative operating conditions.

Table 1-6. Core I Data

Entire core		**Radial reflector**	
Equivalent diameter, in.	17.5	Height, in.	80
Height, in.	18	Equivalent outside diameter, in.	42.3
Volume, liter	70	Radial thickness, in.	13.1
Subassemblies		**Radial reflector composition, vol-%**	
Mixed oxide	24	Stainless steel	82
Mixed carbide	16	Sodium	18
Pu-U alloy	8		
Special subassemblies	3	**Heat output, MW**	50
Control rods	12		
Radial reflector (including loops)	238	**Primary sodium temperature, °F**	
Total	301	To core	810
Configuration	Hexagonal	From core (nominal)	1050
Dimension across flats, in.	2.290		
Lattice spacing, in.	2.320	Primary sodium flow rate	
Tube-wall thickness, in.	0.040	Through core, gpm	6000
		Core pressure drop, psi	80
Control-rod composition, vol-%			
Boron carbide	55		
Stainless steel	20		
Sodium	25		

Table 1-7. Fuel-Element Data

Fuel Material	UO_2-15 wt-% PuO_2	UC-15 wt-% PuC	Metal[b]
Elements per subassembly	37	37	61
Fuel height, in.	18	18	18
Clad outside dia., in.	0.290	0.290	0.220
Clad thickness, in.	0.020	0.020[a]	0.016
Spacer wire dia., in.	0.057	0.057	0.052
Axial blanket height (each end), in.	6	6	6
Gas reservoir, in.	25	25	25
Element height, in.	55	55	55
Effective fuel density, %	80	80	70
Bond material	Helium	Helium	Sodium
Fuel U/Pu atom ratio	6/1	6/1	5/1
Fuel details	Coprecipitated; O/M 1.97-2.00	Single Phase; Solid Solution	-

[a] 0.015-in. C4 subassemblies. (See Table 1-8.)

[b] U-15 wt-% Pu-6.5 wt-% Ti; U-15 wt-% Pu-10 wt-% Zr. (See Table 1-9.)

Table 1-8. Subassembly Data

Fuel Material	Subassembly Designation	Fuel Type	Clad Material	No. of Subassemblies	No. of Instrumented Subassemblies	Maximum Linear Heat Flux (Design), kW/ft	Maximum Clad Temp., °F (°C)	Maximum Fuel Temp., °F (°C)	Burnups* at Removal, at-%	Maximum Clad Thermal Stress, psi	Coolant Velocity, fps
Oxide	01	Pellets	304	4	1	15	1250 (675)	3220 (1770)	5, 9, 12, 14	13,300	16
	02	Pellets	304	4	1	22	1290 (700)	4220 (2330)	5, 8, 10, 12	19,400	23
	03	Vipak	304	4	1	15	1250 (675)	1250 (1770)	5, 9, 12, 14	13,300	16
	04	Vipak	304	4	1	22	1290 (700)	4220 (2330)	5, 8, 10, 12	19,400	23
	05	Pellets	HSA	4	1	22	1340 (725)	4250 (2340)	5, 9, 12, 15	-	20
	06	Vipak	HSA	4	1	22	1340 (725)	4250 (2340)	5, 9, 12, 15	-	20
Carbide	C1	Pellets	304	4	1	15	1250 (675)	2030 (1110)	5, 9, 12, 14	13,300	16
	C2	Vipak	304	4	1	22	1290 (700)	2520 (1380)	5, 9, 12, 14	19,400	23
	C3	Pellets	HSA	4	1	29	1340 (725)	3050 (1680)	5, 9, 12, 15	-	30
	C4	Vipak	HSA	4	1	36	1340 (725)	3390 (1870)	5, 9, 12, 15	-	39
Metal	M1	U-Pu-Zr	HSA	4	1	14	1250 (675)	1580 (860)	5, 9, 12, 14	-	20
	M2	U-Pu-Ti	V-Ti	4	1	14	1250 (675)	1580 (860)	5, 9, 12, 14	-	20
Advanced	C4S	-	-	3	3						
				51	15						

NOTES: 1. Vipak means "vibratory compacted"; HSA means "high-strength alloy," not necessarily the same for oxide as for carbide, etc.

2. Coolant inlet temperature is 810°F. Average outlet temperature from each subassembly is 1050°F. (Exception: outlet temperature from 05 and 06 subassemblies is 1085°F.) Axial peaking factor = 1.2.

3. Maximum clad temperature include both a 1.33 factor for flow and power maldistribution effects on coolant temperature rise, and a 1.10 uncertainty factor. Maximum fuel temperatures include the 1.33 factor but no uncertainty factor.

*Approximate burnup intervals.

The assumptions used in the thermal calculations, basic to the core design and thermal analysis, are shown in Table 1-9.

Table 1-9. Assumptions for Thermal Calculations

(Based on a sodium film coefficient of 20,000 Btu/(hr)(ft^2)(°F))

Fuel Material	Clad Thermal Conductivity, Btu/(hr)(ft)(°F)	Fuel-Clad Interface Conductance, Btu/(hr)(ft^2)(°F)	Fuel Thermal Conductivity, Btu/(hr)(ft)(°F)
Oxide	13.5	1,500	1.7[a]
Carbide	13.5	1,500	10
Metal	14.5	40,000[b]	9[b]

[a]The fuel is assumed to have a central hole large enough to produce an "effective" fuel density of 85%, provided that the remainder of the jacket interior is filled with fuel of 100% density. This condition reduces the temperature rise through the fuel to 67% of that through a solid fuel pellet. The central hole is expected to form in oxide at centerline temperatures above 1600-1800°C.

[b]The fuel is considered to have expanded against the jacket, displacing the bond sodium, and to have an accompanying reduction in thermal conductivity.

The core configuration is shown in Fig. 1-15. Several conditions were considered in the positioning of the subassemblies. Symmetry was maintained, as closely as possible, to simplify analysis and to subject the several elements of each type to similar power conditions throughout the experiment. Also, to achieve the linear heat fluxes, the uranium enrichment and positions in the configuration were varied.

The positioning was also influenced by the sequence of removal and replacement. Instrumented subassemblies are located so that the loading and unloading of other subassemblies is not encumbered by instrumentation leads. It is planned to remove the instrumented subassemblies in the latter stages of burnup for each type element.

Two experimental loops at the core edge and one loop in the reflector are planned. Each subassembly type is to be tested up to about 15 heavy atom-percent burnup. The elements are to be destructively tested at predetermined sub-intervals of burnup.

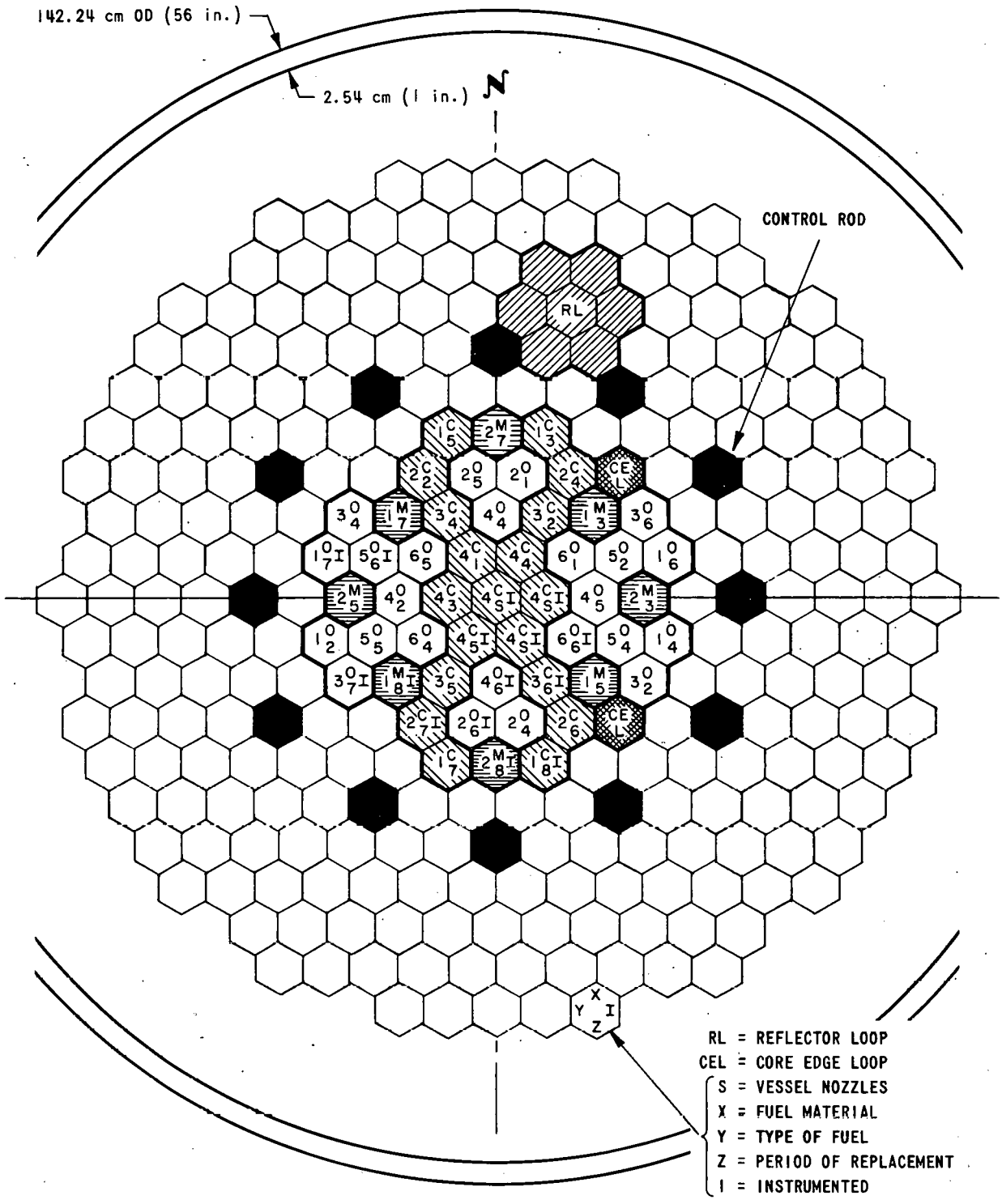

Fig. 1-15. Configuration for FARET Core I experiment

Control Rod Drive Mechanisms

Twelve identical control rod drive assemblies are mounted on a common lifting platform and support structure which, in turn, is supported by the top surface of the reactor vessel cover. The drive mechanisms control the axial movement of vertical drive shafts which extend downward through the vessel cover into the vessel interior. The bottom extremities of the shafts are fitted with grippers for connecting the shafts to the upper fittings of the control rods located in the reactor core.

Each control rod drive assembly is capable of raising or lowering its drive shaft and control rod over 24-in. at a velocity of 6 in./min. The drive shaft is electromagnetically latched to the drive mechanism. The electromagnet is attached to a travelling carriage which is driven by a pair of lead screws and a gear motor with a magnetic brake. To initiate a rapid shutdown (scram stroke), the electromagnet is de-energized.

Scram-stroke acceleration is attained by a pneumatic cylinder whose piston is connected to the upper end of the drive shaft. Deceleration of the drive shaft is accomplished by a hydraulic dashpot shock absorber.

The gripper jaws are actuated by the axial movement of a concentric shaft (within the drive shaft) that connects the gripper with a jackscrew actuating mechanism. The jackscrew mechanism can be driven only when the drive shaft is in the "down" or scrammed position. In this position, the motorized gripper drive mechanism's output shaft can be mechanically coupled to the jackscrew shaft by means of a solenoid. A concentric sensing shaft operates in conjunction with the gripper shaft to ensure positive engagement or disengagement of a control rod. Gastight metallic bellows are used with the concentric shafts to prevent the escape of gas and sodium vapor from the reactor vessel.

The function of the lifting platform is to vary the elevation of the grippers (in their "down" or scrammed position) over a range of several inches. For example, the lifting platform is driven downward by motorized jackscrew mechanisms to effect engagement between the grippers and the upper end fittings of the control rods. The platform is also used to lift the grippers clear of the control rods before the reactor vessel cover is raised for fuel handling.

Several control rod drive components are being prepared for test, or have been tested with the following results.

Electromagnet. An electromagnet was designed and fabricated to meet the requirements of a fast-acting shaft release device for scramming a control rod. The following performance characteristics were demonstrated in a separate test facility.

Gap dimension, in.	0.003
Coil current, amp	1.3
Coil potential, volt	6
Lifting capability, lb	1100
Load release time, sec	0.017
Temperature rise, °F	23

Shock Absorber. A dashpot hydraulic shock absorber and scram accelerator (modified standard pneumatic cylinder) were assembled together with the electromagnet and a dummy shaft. A pressure of 12 psig provided a 1.5-g acceleration. The shock absorber also exhibited acceptable performance characteristics, including a deceleration of about 4 g.

Bellows Shaft Seal. Specifications and drawings were prepared for the purchase of a welded-disc, nesting-type bellows capable of accommodating the movement of the control rod drive shaft. A facility was constructed to permit testing the bellows in a simulated reactor environment of argon gas mixed with sodium vapors produced by molten sodium at 1200°F. The bellows has exceeded 13,000 cycles with no leakage, and sodium or oxide deposition is apparently not sufficient to hamper the bellows' performance.

Electrical Components Test Facility. This facility is designed to test the reliability of electrical components in a dry argon atmosphere at 150°F. The assembly consists of a cylindrical, gastight container filled with argon gas which is electrically heated. For test purposes, a fractional-horsepower, geared, brake motor was installed and put under the proper load conditions. Other test units included three different types of switches and a self-synchronous generator driven by a smaller gear-motor. After about 180 hr of operation, both motors failed due to insulation breakdown. Operation of the test facility was suspended pending analyses of the motor failures.

Control Rod Gripper. A gripper similar to that used in the EBR-II reactor has been fabricated for test purposes. The principal difference lies in the main structural material: the FARET gripper is made of Haynes 25 alloy, whereas the EBR-II gripper is made of stainless steel Types 304 and 420.

This gripper will be tested on a dummy control rod while both are immersed in sodium at temperatures up to 1200°F. Briefly, the test facility includes:

(1) A gripper assembled on the lower end of a drive shaft.

(2) A scram accelerator and shock absorber assembly. The piston of the accelerator is attached to the upper end of the drive shaft.

(3) A welded-disc bellows to seal the drive shaft where it penetrates the nozzle of the electrically-heated sodium container.

(4) An electromagnet for lifting the drive shaft (and control rod). The magnet is coupled to a motorized lead-screw and ball-nut drive mechanism.

(5) Means for manual actuation of the gripper.

Reactor Vessel

Figure 1-16 shows the reactor vessel assembly within the cavity of the containment structure. As indicated by the legend, the vessel is of double-walled construction (20, 21), with a bolted and seal-welded extension (3), and a cover (1) which protrudes above the cell floor. At this point, the vessel is sealed to the cavity walls by a metallic expansion joint seal (5). The vessel is supported on a skirt (28) which, in turn, is anchored to the floor of the cavity.

The annulus between the double-walled portion of the vessel is filled with a NaK alloy. This alloy is used for detecting sodium outleakage and for heating the vessel.

Within the vessel are located a removable core support structure, and a neutron shield of canned, borated graphite (18). The core support structure is comprised of high- and low-pressure inlet plenums (26, 27) formed by the core grid plates, and an outlet coolant mixing chamber (14). This assembly is supported at the bottom of the vessel. Inlet and outlet coolant piping connections are made with special couplings.

The high- and low-pressure plenums service, respectively, core subassemblies which require high flow rates (fuel), and reflector subassemblies which require low flow rates. Each subassembly has an orifice which connects to the appropriate plenum. Flow from the high- to low-pressure plenum is fixed by orifices in the grid plates and in one or more reflector assemblies.

Safety and other aspects of two- and three-grid plate designs for the core support cylinder were compared, and hold-down forces on the subassemblies during full-power operation were calculated for both designs. The results indicated that a 150-lb subassembly will retain at least a 50-lb net holddown force with either design. In the three-plate design, the

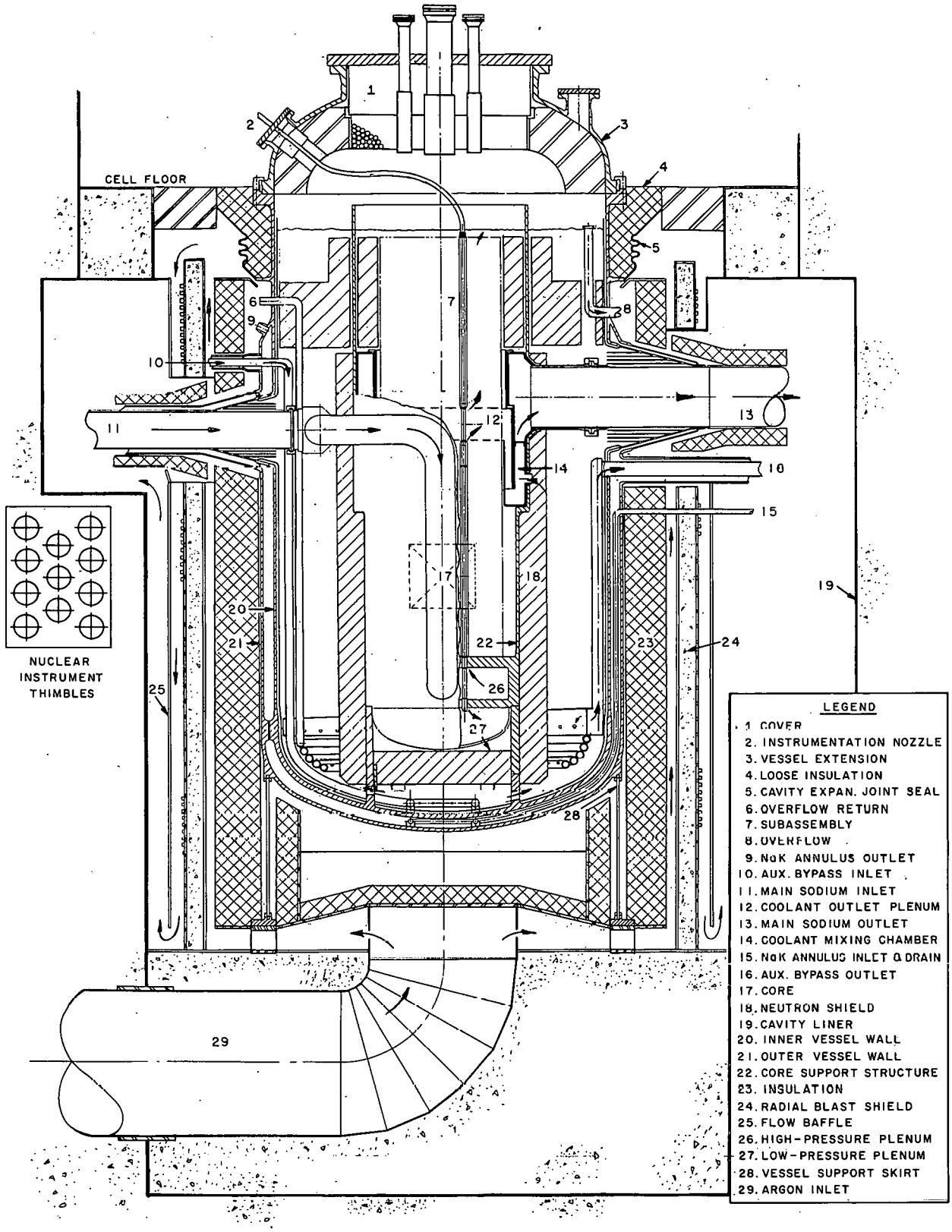

Fig. 1-16. Reactor vessel assembly within cavity

subassemblies seat on the top plate, above a low-pressure plenum, and penetrate the entire bottom plate. This design offered some advantages with regard to holddown. However, the two-plate design, with seating on the top plate above a high-pressure plenum, was selected because it was simpler and less costly to fabricate and permitted a shorter subassembly lower adapter.

A number of additional analyses were also performed for the reactor vessel. Leakage flow past the subassembly shielding extensions was calculated to be about 500 gpm. Pressure drop and shielding and heat barrier requirements between the hot (1280°F) leakage flow and cooler (1050°F) sodium in the vessel inside annulus were investigated. Pressure drop and/or heat exchange requirements for inlet plenum inlet lines, make-up line, and auxiliary bypass (drain) line were established.

A number of different core support grid configurations were analyzed in an effort to arrive at an efficient structure having acceptable stresses and deflections. Effects of transverse pressure and temperature gradients were taken into consideration. Application of thin-plate theory indicated the need for rows of reinforcing tubes between the two grid plates (6 ft dia.) to reduce deflection and to permit reasonable plate thicknesses. Further check analysis using beam theory as well as thin-plate theory showed that stresses were well below acceptable code values.

A vendor (Babcock & Wilcox Co.) has been selected for performing the engineering and manufacturing phase of the vessel design. This work is in two parts: (1) substantiation of the design sufficient to permit ordering the bulk of materials and (2) final engineering analysis and construction drawings and procedures. The first part has been completed and a report submitted to the Laboratory. This report contains the necessary initial details of design, stress analysis, cost estimate, and fabrication schedules and quality requirements.

Type 304 stainless steel has been specified. Because of the reactor vessel design operating temperature of 1150°F, the normal allowable composition range of the major constituents has been reduced to enhance the metallurgical stability of the alloy.

To maintain long-term dimensional stability and the low creep strain specified (0.0001 in./in. for a life of 15 years at 1200°F), the vendor extrapolated existing creep data from three different sources. As a result, a conservative stress level of 1300 psi was selected for the design. (Based on ASME Code, Sec. I, the allowable stress at 1150°F is 4500 psi.)

Reactor Vessel Cover Handling System

The FARET control rod drive cluster is isolated from the cell atmosphere by means of a large flexible bellows. (See Fig. 1-17.) The bellows makes a gastight connection between the reactor vessel cover and the cell annex. To permit fuel handling, the reactor vessel cover, with the attached control drive complex, is raised by a hoist into the cell annex.

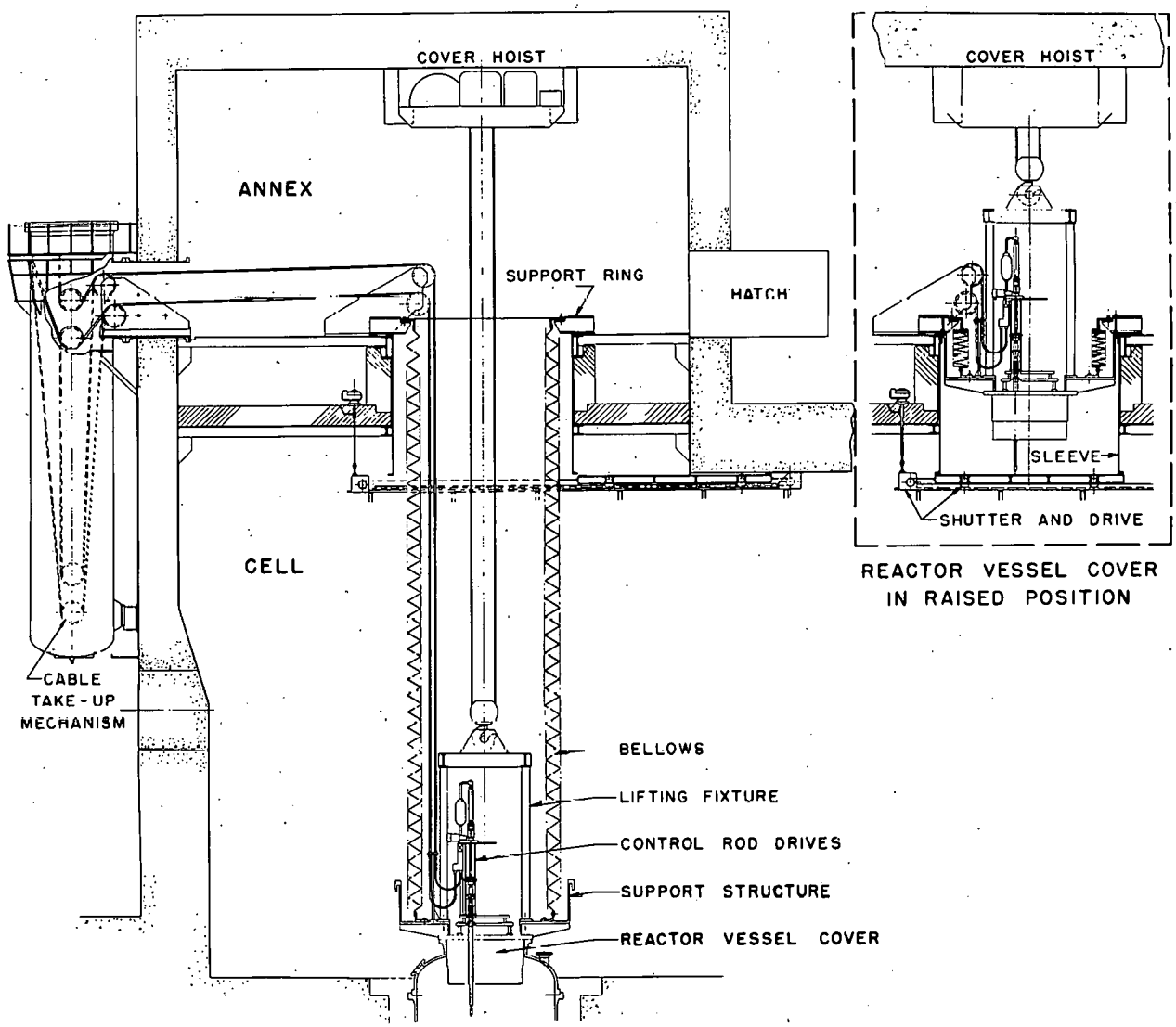

Fig. 1-17. Reactor Vessel Cover Handling System

The bellows is made of a double layer of elastomer-coated, nylon fabric with aluminum slats bonded between the two layers. The slats provide rigidity to the convolutions, yet permit the fabric to flex during movement of the bellows. The slats also lessen the overall diffusion through the bellows by reducing the effective leakage area. Nylon tapes are fastened to the convolutions to limit their travel and to support the weight of the bellows. Both ends of the bellows are provided with collars for attachment to metal flanges.

The reactor cover is lifted by means of a handling fixture and a hoist that is located below the ceiling of the cell annex. Multi-conductor control drive cables are attached to the reactor cover inside the bellows. These cables run over pulleys in the cell annex and are guided into a gas-tight tank located outside the annex wall. During the lifting operation, the extra cable length is taken up by a loop formed by the pulley counter-weight located inside the tank. When the cover is fully raised, it is secured to the annex sleeve (near the cell annex floor) by locking bolts. A shutter, mounted on a carriage and rails supported from the cell walls, is driven by a motorized chain drive to form an annex closure at the cell ceiling. Two inflatable seals are used to complete the gastight closure.

Conceptual design of the cover-handling system has been completed. Air and moisture permeability tests on candidate bellows materials are in process. Cable tank cover penetration leak rate and pressure tests have been completed. Average leakage rates of 0.04 $in.^3$/day per penetration at 30-psig differential pressure were determined.

Cell Annex Test Bellows. A shortened one-quarter scale test bellows has been fabricated to determine the effects of flexing at the stress points of the folds, leak tightness of the material and the metal flange connections, and the effects of differential pressures.

The bellows is constructed of a double layer of 0.018-in.-thick, hypolon-neoprene-coated nylon fabric, with aluminum slats (0.050 in. thick) bonded between the two layers. There are three complete convolutions, and a 2-in.-high collar at each end. Nylon tapes are fastened to the convolutions to limit their travel and to support the weight of the bellows. The test assembly measures 33 in. across flats on the outside and 27 in. across flats on the inside, with a fully extended length of 18 in.

The assembly has accummulated in excess of 1000 cycles with no detectable leakage.

1.2.3.2 Reactor-Related Tasks

Hydraulic Tests - Reactor Vessel

In the FARET vessel, up to 20% of the main inlet coolant flow is bypassed and subsequently mixed with the core outlet flow. Accordingly, a one-eighth scale, plastic model of the vessel was constructed to observe the bypass flow pattern and to ensure that adequate coolant flow through the core is maintained. Water was used to simulate the sodium coolant.

The model (Fig. 1-18) was designed such that the flow through the core (A), the flow past the upper reflector (B), and the bypass flow (C), could be adjusted in proportion to flowrates in the parent vessel. Three different

color dyes were injected simultaneously in the bypass flow at the entrance holes to the mixing chamber. High-speed photography was used to obtain a velocity profile over the full circumference within the mixing chamber. The film recording showed that adequate coolant flow through the core is maintained during simulated reactor scram conditions, first by flow reversal in the mixing chamber and then by coolant flow into the auxiliary outlet.

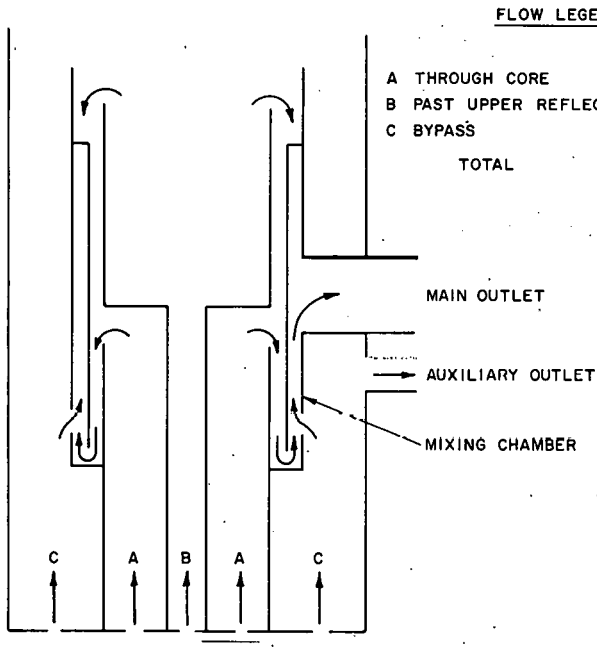

Fig. 1-18

Schematic of 1/8-scale reactor vessel model used for hydraulic studies

The effect of a 24-in.-diameter main outlet pipe rupture also was simulated. In this instance, it was necessary to vent the mixing chamber so that the water would not siphon below the core level.

Hydraulic Tests - Core Subassemblies

The water flow test loop shown in Fig. 1-19 was constructed for purposes of verifying the calculated flow characteristics of FARET core subassemblies. For these tests, the upper reflector of the subassembly was removed.

Concurrent tests were made to determine the holddown forces. In these tests, the reflector was simulated by balancing the hydraulic pressure on a piston connected to the subassembly. The results showed that a 100-psi pressure drop through the subassembly yielded a net holddown force of 80 lb. For the same pressure drop, the leakage past the lower grid annulus was measured to be 2.3 gpm.

The following pressure drop relationship was developed to correlate the water data to sodium at the appropriate temperature:

$$h = \frac{1}{170} w^{1.76}$$

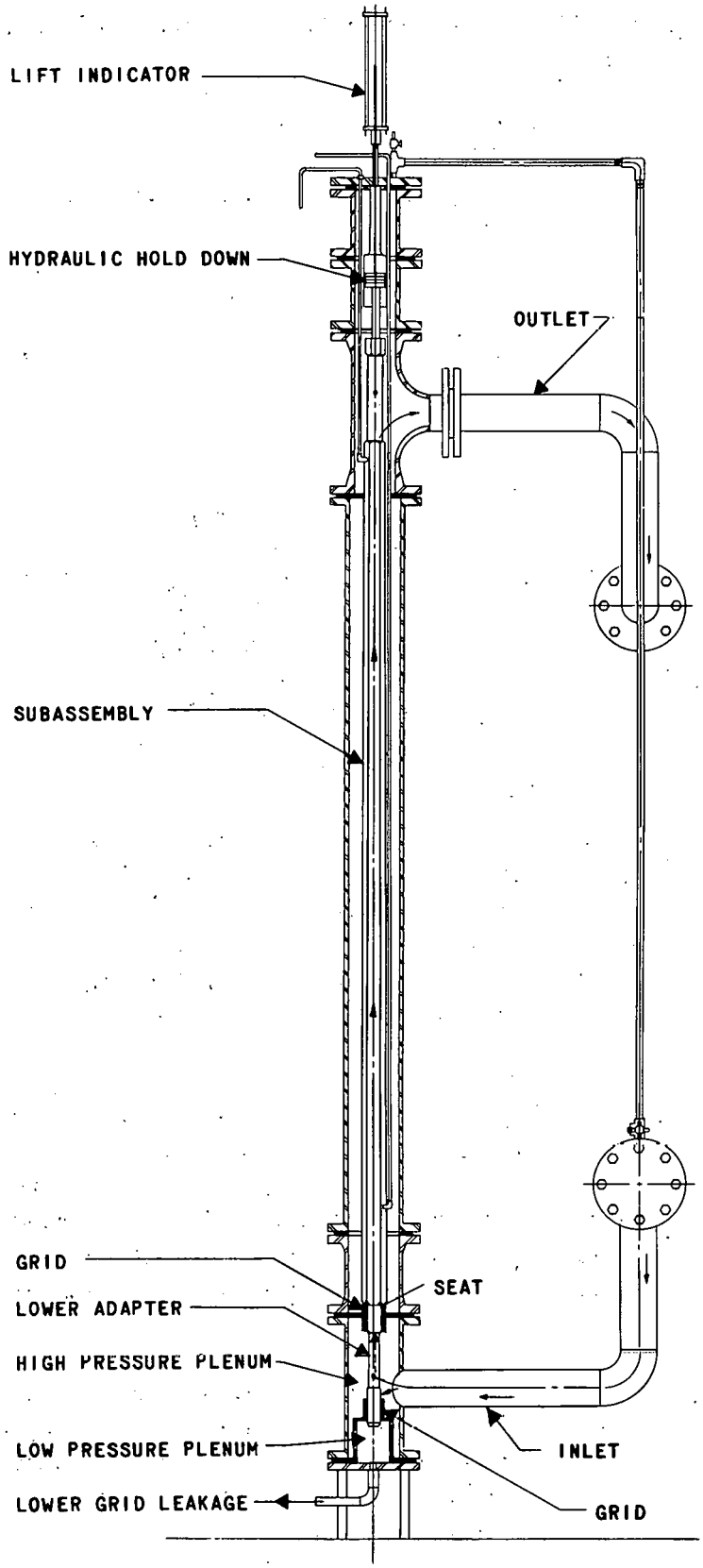

Fig. 1-19. Subassembly Flow Test Assembly

where h is the pressure drop (psi) in the test subassembly, and w is the flowrate (gpm) of sodium at 1000°F.

Fuel Subassembly Sodium Flow Test Loop

This loop, shown schematically in Fig. 1-20, is nearing completion. It will be used to determine or to verify the hydraulic characteristics and other design features of fuel subassemblies, control rods, and in-core instrumentation in a sodium environment up to 1200°F.

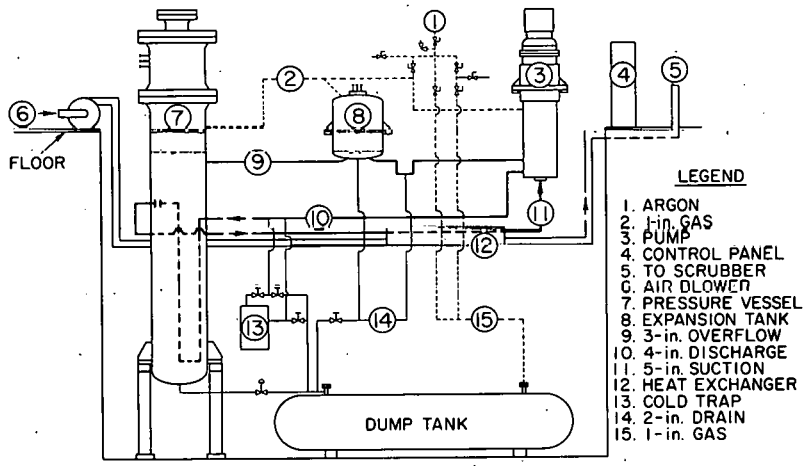

Fig. 1-20

FARET Fuel Subassembly Sodium Flow Test Loop

With reference to Fig. 1-20, the pressure vessel and pumping circuit are located in a pit (20 ft square, 25 ft deep) below floor level. The vessel will accommodate 19 FARET fuel subassemblies in a mock-up core support grid. The pump has a capacity of 800 gpm. Thus up to seven subassemblies can be tested simultaneously, using the highest flow rates expected in the reactor. Similar tests can be conducted on 19 subassemblies, but at lower flowrates.

Constructed of Type 304 stainless steel, the loop meets the requirements of Section VIII of the ASME code and the ASA-B31.1-1955 code for Pressure Piping, where applicable. Electrical rod-type heaters are used for heating and maintaining loop temperatures. Pipe stresses were calculated using the Kellogg Analytical Method. Strain gages have been installed to measure the potential high-stress points of the piping during the initial start-up.

Other loop features include (1) an argon gas system for maintaining an inert atmosphere above the sodium; and (2) a NaK-jacketed cold trap, a conventional plugging meter, and a Blake resistivity meter, for monitoring the quality of the 900-gal sodium inventory.

In-Core Instrumentation - Thermocouples

The scope of this effort includes design and evaluation of various material combinations for use as thermocouples and insulators in sodium-radiation environments ranging from 650°C to in excess of 1600°C.

High-Temperature Thermocouples. Thermocouples for measuring temperatures above 1600°C most likely will employ tungsten-rhenium alloy combinations.[4] Tests are underway to extend the known temperature-emf characteristics of these materials to temperatures above 2400°C. Bare wires are being used to eliminate "hot zone errors," i.e., possible shunting effects of any electrical insulation on the output signal.

Table 1-10. Temperature-emf Relationships for W-3% Re/W-25% Re Thermocouples

Temp., °C	Electromotive Force, mV		Temp., °C	Electromotive Force, mV	
	Argonne	Manufacturers		Argonne	Manufacturers
1000	18.290	18.242	2000	35.889	36.007
1200	22.265	22.192	2200	38.526	38.677
1400	26.053	25.956	2400	40.775	40.678
1600	29.613	29.551	2600	42.597	-
1800	32.905	32.922	2800	43.951	-

Table 1-10 lists the temperature-emf relationships for W-3% Re/W-25% Re thermocouples. The Argonne values were obtained by a least-squares fit to the test data. Over 97% of the test data agree to within ±1% of both the manufacturers' and the least-square values. These couples have been returned for long-term thermoelectric stability tests.

Other tests are in progress to establish temperature-emf relationships for W-5% Re/W-26% Re couples.

Resistivity of Refractory Oxide Insulators. Thoria shows particular promise for electrical insulation at high temperatures. It has a melting point of ~3300°C and is compatible with refractory metals and alloys being considered for sheathing and/or wire elements.

The resistivity of "crushable" and "vitrified" refractory oxide insulator beads is being determined. For control purposes, resistivity measurements have been made on alumina, using ASTM standard D257-61 procedures with minor variations.

Table 1-11. Resistivity of Vitrified Alumina at Various Temperatures

Temp., °C	Resistivity, ohm-cm	
	Measured	Literature
800	2×10^7	1×10^8
1000	3×10^6	1×10^6
1200	5.5×10^5	7×10^4
1400	1×10^5	1.5×10^4
1600	2×10^4	3×10^3
1800	3×10^3	5×10^2
1900	1×10^3	2.5×10^2

Table 1-11 lists the measured volume resistivity of "vitrified" alumina. Also listed are average values from the literature. In general, the measured values are higher.

The accuracy of the measured values is suspect in view of subsequent dimensional checks on the alumina beads. These checks

revealed a shrinkage of about 3%. Since shrinkage or further sintering could have adverse effects on thermocouple performance, a series of independent tests are underway to investigate this phenomenon.

Tests completed thus far have shown a 10% shrinkage in alumina beads after firing for 3 hr in a helium atmosphere at 1950°C; resistivity decreased to one-fourth the value at room temperature. Thoria beads, fired for 1 hr at 2600°C, evidenced a shrinkage of 5%.

In-Pile Tests. Table 1-12 lists four prototype thermocouples that were used successfully to measure the centerline temperature of UO_2 and $(PuU)O_2$ fuel pellets. In each instance, the wires inside and outside the fuel region were insulated with thoria and alumina, respectively. All couples were sheathed with tantalum (0.062 in. O.D.).

Table 1-12. Summary of In-Pile Thermocouple Tests

Test No.	Thermocouple	Fuel	Capsule Gas	Centerline Temp., °C	Duration, hr	Fast Flux, nvt x 10^{19}	No. of Cycles
1	W-5% Re, W-26% Re	UO_2	Argon	1050	810	2.9	30
2	W-5% Re, W-26% Re	UO_2	He	750	940	3.4	35
3	W-3% Re, W-25% Re	(UO_2PuO_2)	Argon	1150-1345	720	2.6	20
HI-1	W-3% Re, W-25% Re	UO_2	Argon	2300	~2	-	2*

*Sudden increase in temperature, corresponding to instrument limit, caused reactor shutdown. Test discontinued.

Moderate Temperature Thermocouples. Prototype thermocouples for measuring coolant temperatures are under test in a dry inert gas atmosphere at 650°C. These couples are made of chromel-alumel wires insulated with alumina, and are sheathed in stainless steel. Thus far, the couples have accumulated 1000 hr of operation and 10 thermal cycles from room temperature to 650°C without failure.

Additional thermocouple assemblies are being prepared for testing in a sodium environment.

In-Core Instrumentation - Flowmeters

Figure 1-21 shows sectional views of three types of flowmeters for measuring sodium coolant flow through a fuel subassembly.

The turbine flowmeter is designed for installation between the inlet nose piece and bottom reflector of a subassembly. It contains a turbine and an integrally-cast, 4-pole magnet (Alnico VB) which rotates within a miniature, high-temperature coil (0.5 in. I.D., 0.25 in. high). Other components and materials include a Type 304 stainless steel body, a Hastelloy C turbine shaft, and molybdenum bearings. In operation, the coolant rotates the turbine-magnet unit, inducing an a-c voltage in the coil. This voltage is converted to a direct current to indicate coolant velocity.

The electromagnetic flowmeter is designed for interchangeability with the turbine flowmeter. It consists of a Type 304 stainless steel body and electrodes, Alnico VB magnets, and soft-iron poles. Measurements made on a prototype assembly indicated an average magnetic flux of

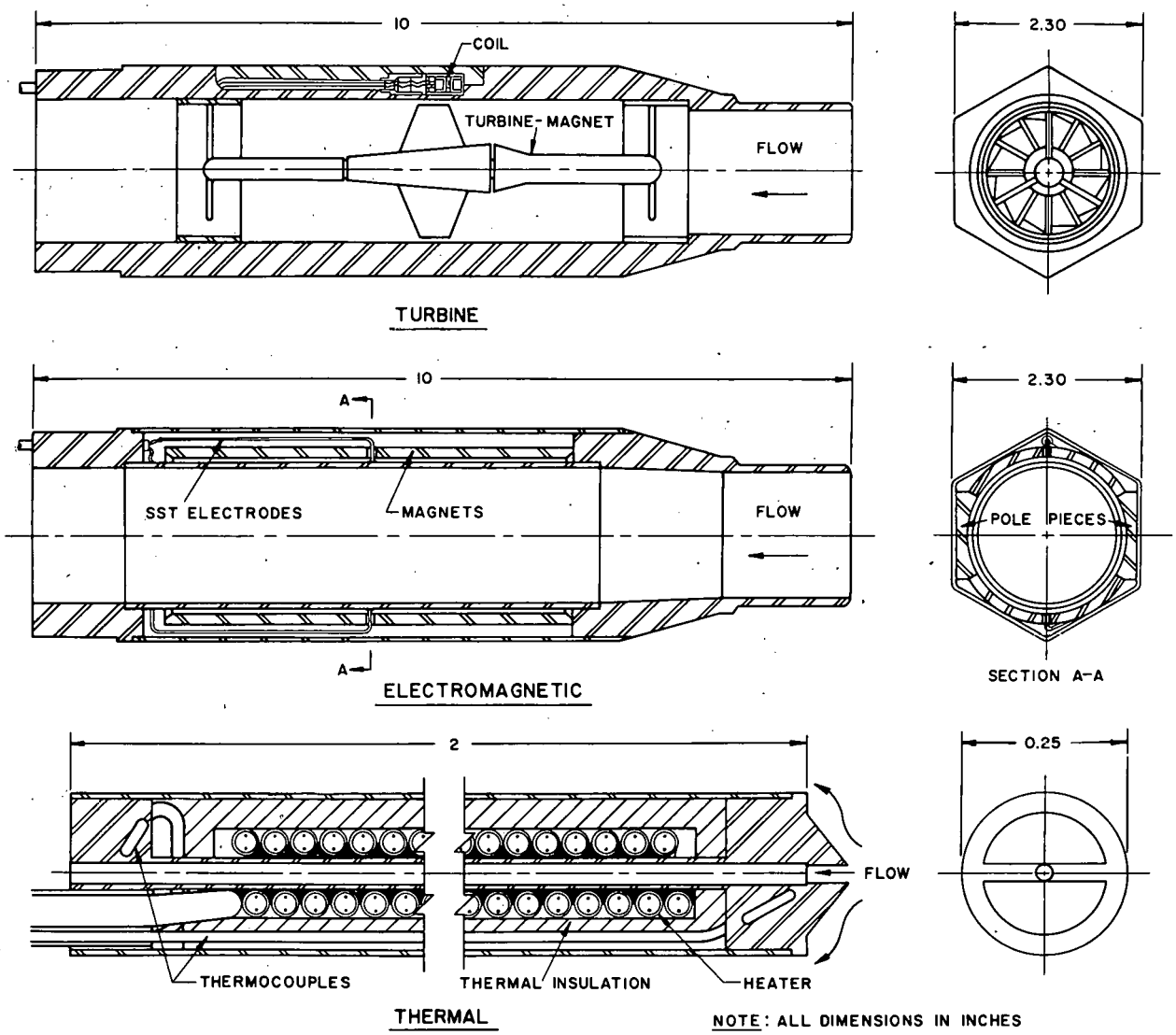

Fig. 1-21. Sectional views of turbine, electromagnetic, and thermal flowmeters for measuring sodium coolant flow through fuel subassemblies

410 Gauss and a corresponding output voltage of about 5.0 mV/(ft)(sec). Other configurations are being investigated to improve meter sensitivity.

The effect of temperature on magnetic flux also was studied. After 3 hr at 650°C, the flux was permanently reduced to 80% of the initial value. Further aging up to about 700°C is planned.

In the thermal flowmeter, a small amount of sodium flows through the cylindrical hole in the center of the meter. At this point, the sodium temperature is increased with the aid of a 150-W heater element. This section is thermally insulated to minimize heat loss to the surrounding sodium. Two chromel-alumel thermocouples are used to measure the temperature rise. At a constant heater power, the temperature rise is a function of the sodium flowrate. One unit is being fabricated for test purposes.

In-Core Instrumentation Lead Connectors

Two, commercially available, multi-pin connectors have been modified to effect a sodium-vapor-tight connection between lead wires and metering devices for use in experimental subassemblies. As shown in Fig. 1-22, the principal difference between the two connectors is the manner in which the seal is effected. One employs a gasket between the plug and socket. The other relies on pressurization to maintain a metal-to-metal seal.

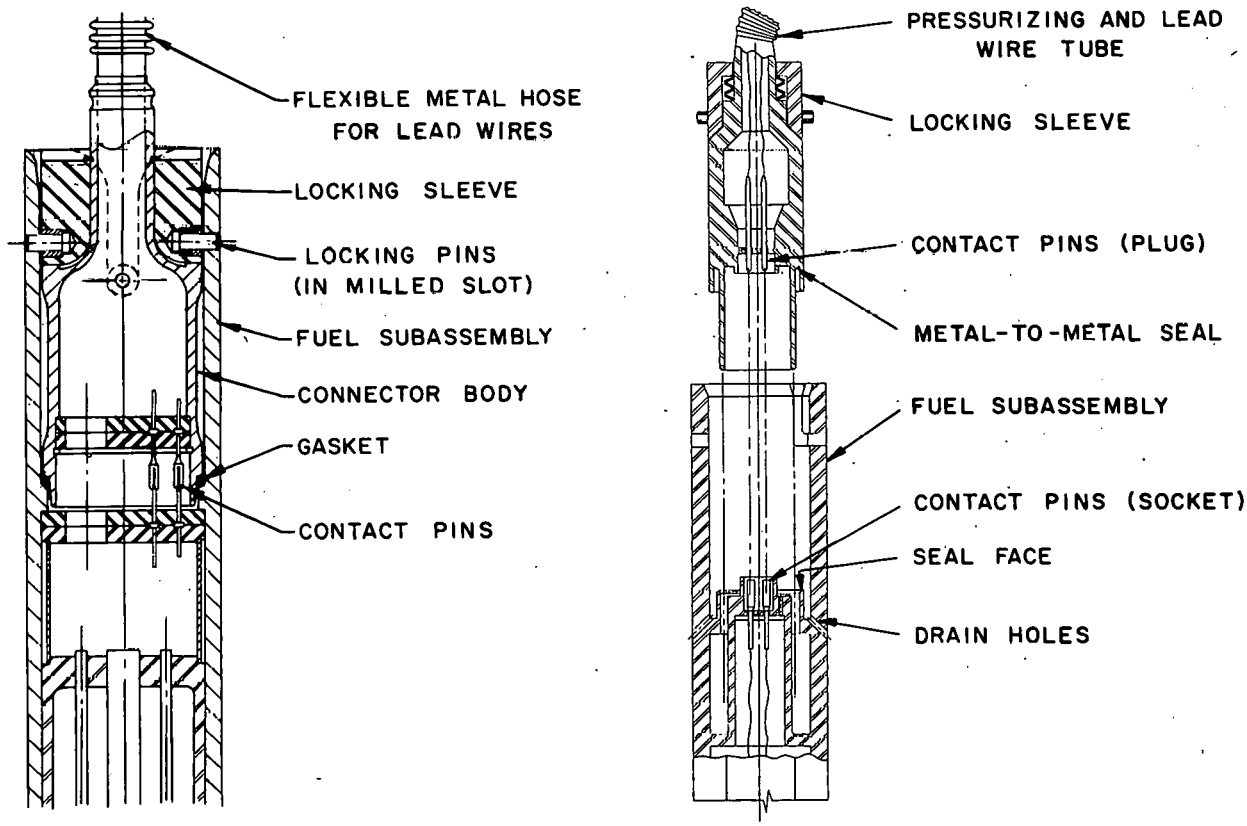

Fig. 1-22. Prototypes of gasket-sealed and metal-to-metal sealed lead wire connectors for instrumented fuel subassemblies

Both connectors are designed for remote-controlled assembly by a special grip and locking tool to be carried and operated by the fuel-handling machine. This tool latches onto and rotates the locking-sleeve pins into the milled slot, clamping the connector plug firmly to the fuel subassembly. Continued rotation of the tool-operating jaw disengages the latch from the installed connector.

Models of both sealing arrangements have been constructed for test purposes. Several types of commercial gaskets have been evaluated in a sodium environment at temperatures up to 1200°F. The most promising gasket seal consists of two half-rings of copper plated Inconel.

The pressurized metal-to-metal seal has been tested first in water and then in sodium at 700°F. In both tests, a gas outleakage less than 0.1 ft^3/day was maintained at 6 in. W.G. There was no evidence of water or sodium inleakage.

1.2.3.3 In-Cell Fuel and Equipment Handling Systems

These systems consist of the fuel-handling machine, wet fuel storage facility, subassembly cut-off machine, in-cell crane and hoist, scrap containers, special handling tools, and viewing devices. Their functions are best illustrated by a brief description of a typical fuel handling sequence:

(1) The fuel-handling machine is used to remove and transfer subassemblies from the reactor to the wet fuel storage facility.

(2) After the fission product decay heat has decreased to the prescribed level of 1 MW, the subassembly is removed into the fuel-handling machine and transported to the subassembly cut-off machine.

(3) Within the cut-off machine, the non-fueled sections are separated from the fueled section.

(4) The non-fueled sections are removed with special handling tools and deposited in the scrap containers.

(5) The fueled section is transported by the fuel-handling machine to the fuel transfer port, where it is lowered out of the cell into a shielded cask-carriage assembly.

(6) The scrap containers are also removed through the fuel transfer port with the aid of the in-cell crane.

All of these operations are performed by remote control and viewed through shielding windows.

Fuel-Handling Machine. The fuel-handling machine (Fig. 1-23) will be used for moving specific subassemblies into or out of the reactor vessel, the wet fuel storage facility, the subassembly cut-off machine, and for transporting fuel within the cell. During transport of irradiated fuel, it will provide for removal of the decay heat energy. The machine will also handle reflector subassemblies, neutron source rod and thimble, and control subassemblies. Finally, the machine will be capable of performing limited manipulations inside the reactor vessel, e.g., coupling of instrument lead connectors to certain subassemblies.

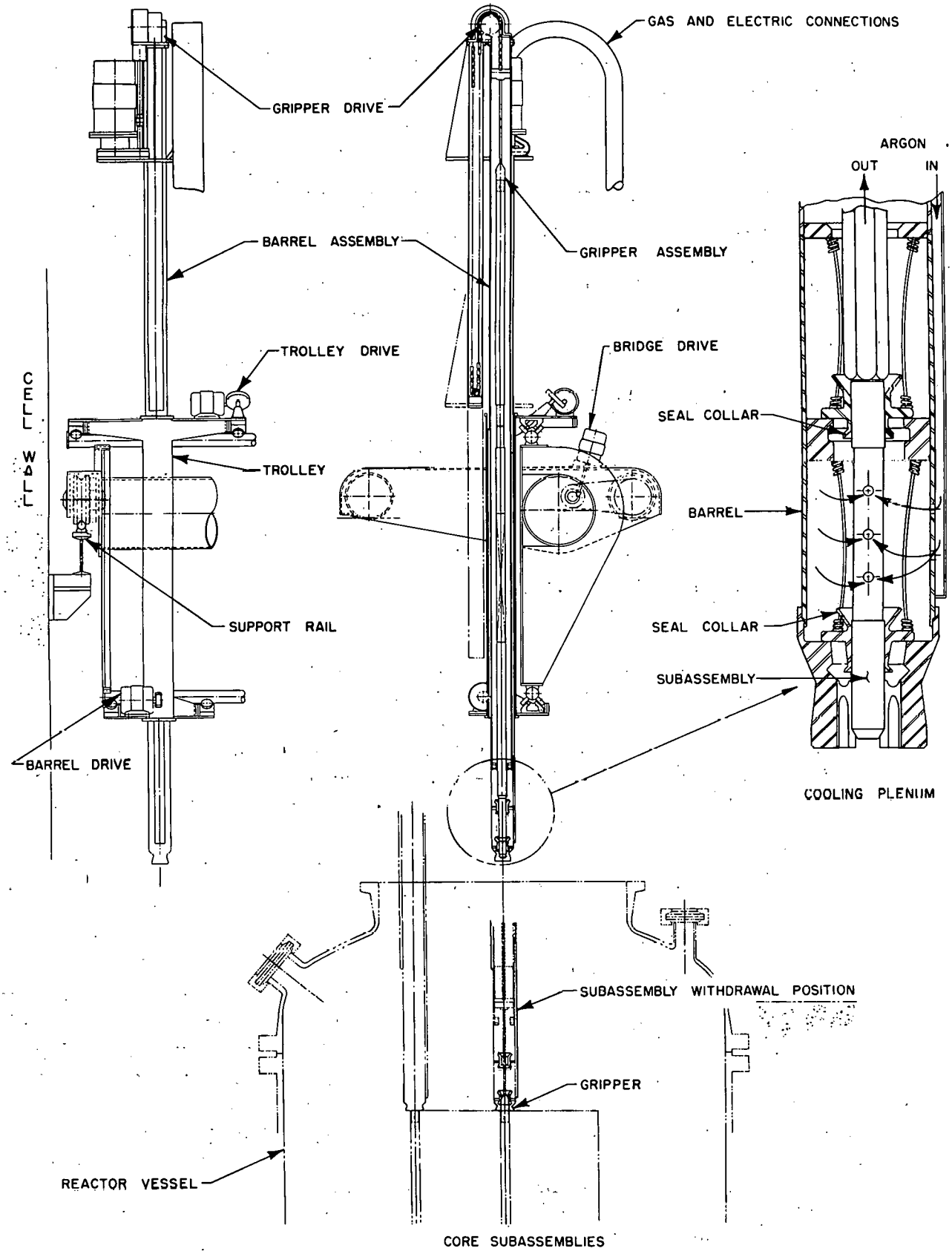

Fig. 1-23. Fuel-Handling Machine

The design of the machine has been largely completed. Several unique features have been incorporated to adapt the machine for its specific modes of operation in an argon atmosphere. These include:

(1) A remote-controlled, precision positioning and control system.

(2) A relatively high decay heat cooling capacity (3 MW).

(3) Arrangement of components in modular assemblies to facilitate their removal and replacement. With one exception, these modular assemblies can be removed through the fuel equipment port. The bridge drive is removed through a hatch in the cell ceiling.

(4) A force-limited gripper mechanism which limits the downward force on a subassembly to 200 lb, and the upward force to 1500 lb.

(5) An emergency power system to service the machine and its cooling system in the event of normal power failure during a transfer operation.

(6) Provisions for disengaging the barrel assembly. For example, should a subassembly become lodged, the barrel assembly can be detached and lowered, by means of the in-cell crane, into the disassembly pit.

Principal components, such as gripper and holddown assembly, trolley drive model, and bridge suspension system, have been fabricated. Independent tests of these components have been successfully completed. The Fuel Assembly Sodium Flow Test Loop has been enclosed to permit the entire machine to be tested in an argon and sodium vapor environment.

The unresolved design tasks are largely associated with the position-indicating and position-control system. Basic concepts have been established and specifications are being prepared.

The design of the cooling system for the fuel-handling machine is nearing completion. It provides for forced flow of argon through the machine during transfer of irradiated subassemblies. Although the cell atmosphere is also argon, the coolant circuit is a closed loop to minimize spreading of sodium vapor and radioactive contamination into the cell. The compressor, filters, vapor traps, heat exchanger, and argon supply tank are located outside the cell in an extension of the fuel and equipment transfer tunnel. Effluent gas from the fuel-handling machine is cooled by bubbling through a vessel containing refrigerated NaK (~45°F). This cooling arrangement also condenses any sodium vapor that may be entrained by the argon coolant.

Hydraulic and thermal analyses of the loop have been completed. A small-scale hydraulics experiment was conducted, using water and air to simulate the cooling media. Prototype components are being fabricated for more extensive testing of the system.

Wet Fuel Storage Facility. Irradiated fuel subassemblies will be stored in a sodium-filled tank until the fission product decay level corresponds to 1 kW of heat, which can be handled within the fuel transfer cask.

The storage tank is of double-walled construction and is cooled by circulating NaK through the annulus. The internal grid will accommodate 151 subassemblies in a non-critical array. Storage capacity was based upon reactor core size, time at rated power, cooling time in the reactor, and "down time" between shutdown of one core and startup of another. Subassemblies are lowered through loading ports in a shielded closure plug which is indexed to the storage grid.

Design of the storage tank, and conceptual design of the rotating cover has been completed. Areas requiring further development have been identified. These include the inflatable seals which isolate the tank cover gas from the cell, and the tank cover indexing mechanism.

A mock-up of the storage tank upper grid was constructed for purposes of evaluating a self-aligning upper guide bushing in the tank grid. After a series of tests with a dummy subassembly, it was determined that misalignment of ±17 degrees can be corrected to ±4 degrees with the aid of the guide bushing.

Subassembly Cut-Off Machine. As mentioned earlier, this machine will be used to separate the fueled and non-fueled sections of the all-welded, 178-in.-long subassemblies. Upon completion of the cutting operation, the 96-in.-long fueled section will be removed by the fuel-handling machine and lowered through the fuel transfer port into a shielded cask-carriage assembly. The cut-off machine includes an integrally-mounted manipulator for transporting the non-fueled sections to adjacent scrap containers.

Two types of cutters are under consideration: (1) collar-type tubing cutters for cutting through the Type 304 hexagonal tubing (0.040 in. thick); these have been used successfully in the EBR-II Fuel Cycle Facility; and (2) clipper-type cutters for severing instrument leads in certain subassemblies. The latter will operate through the gap produced by the tubing cutters.

During the cutting operations, the decay heat will be removed by suction flow of argon from the cell atmosphere through the subassembly. The effluent will be cycled through a blower-filter assembly outside the cell and then back into the cell.

Preliminary tests with a prototype lead cutter indicated that approximately 1,000 lb of force was required to shear 14 mineral insulated, stainless clad, instrument leads. Further tests will be made with various types and shapes of blades to determine blade durability and overall performance of the clipper-type cutters.

Operation of the subassembly cut-off machine and related equipment will be checked out in the mock-up installation shown in Fig. 1-24. Design of the machine base and other facilities for mounting the machine components has been completed. These facilities include an adjustable floor platform, cooling blower system, and manipulator. The floor platform permits mounting of the cut-off machine at the proper elevation relative to the viewing window and service penetrations. It also provides openings at the proper locations for scrap containers and cooling ducts. The cut-off machine base also supports the electrical and pneumatic service connections which operate the machine.

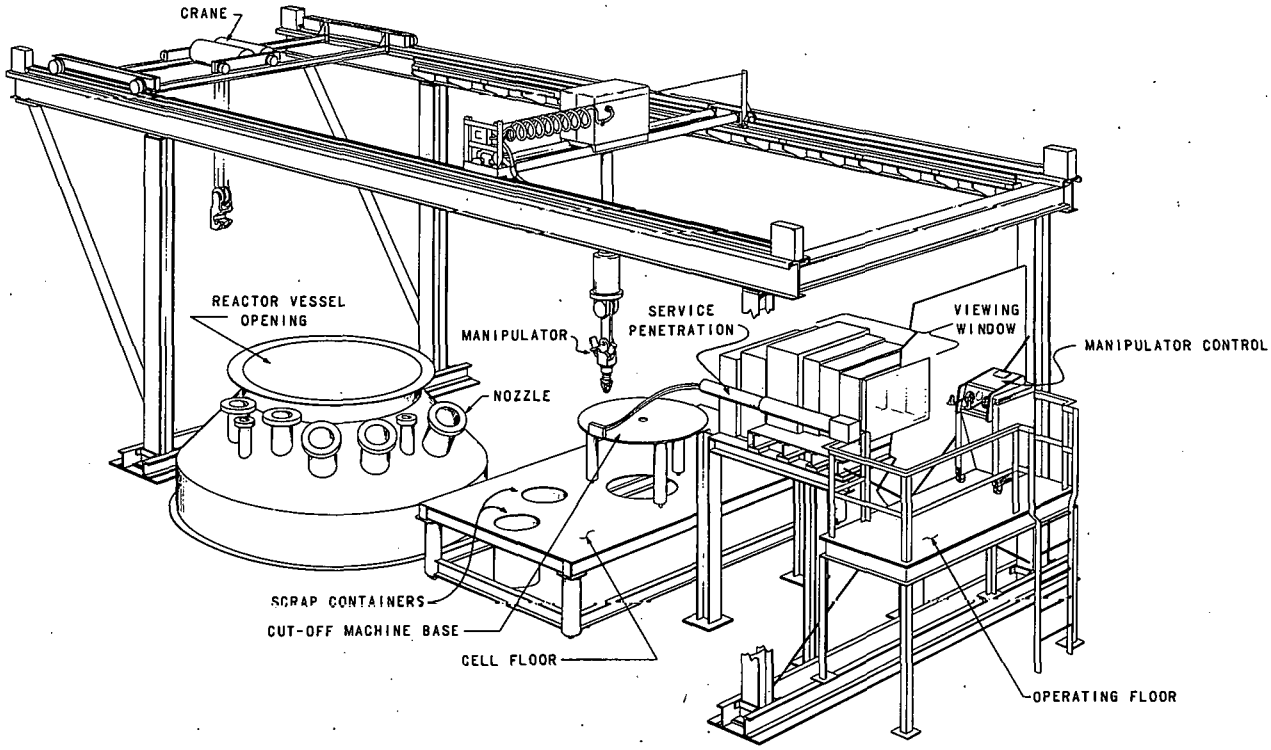

Fig. 1-24. Partially completed mock-up of subassembly cut-off machine supporting structure and related equipment

Fuel and Equipment Transfer Ports. Radioactive and nonradioactive core components and certain in-cell equipment are transferred into and out of the cell through the fuel and equipment transfer ports. Located in the south end of the cell, these concentric ports lead to a tunnel which extends beneath the rear cell area.

As shown in Fig. 1-25, empty or loaded casks are transported on a carriage in the tunnel and positioned beneath the transfer port. The carriage support frame is then raised to effect a seal between the cask and the transfer port. At this point, the closure plug of the transfer port is removed by the in-cell crane to facilitate subsequent transfer operations.

A test program has been implemented to evaluate the cask-to-fuel transfer port seal concept. The scope of this program includes:

(1) Applying a load of 40 tons (cask weight) to the seal at a speed of 2 ft/min, with various horizontal and vertical offset seal conditions.

(2) Simulating seismic conditions by imposing a lateral load of up to 7 ton.

(3) Stress determinations and seal leakage rates at pressures up to 60 psig.

Shielding Windows. A shielding window has been designed and specifications have been prepared. The specifications are in two parts. The first part deals with procurement of the glass slabs. The second part specifies the mode of fabrication and assembly.

With reference to Fig. 1-26, the window is composed of three 6-in.-thick slabs of 3.3-density glass (B-1, B-2, A-2), and an oil-filled tank unit. The tank interior is designed to accommodate two 4-in.-thick slabs of 6.2-density glass (T_2 and T_3), or two 8-in.-thick slabs of 3.3-density glass, with virtually no change in the viewing angles or in the shielding capability. The tank unit is removable from the exterior of the cell. Slabs A-2 and B-1 can be removed with in-cell manipulators and crane.

The shielding afforded by the window is equivalent to a 5-ft-thick wall of ordinary concrete. Calculations indicate that the light transmittance will vary from a minimum of 14.5% to a maximum of 22.5%, depending on the glass combination used. The minimum value is comparable to the light transmittance through windows installed in the EBR-II Fuel Cycle Facility.

Resistance of the multiple glass slab arrangement to high pressures and temperatures, and missiles has been demonstrated in a series of tests. In Test No. 1, a slab of 3.3-density lead shielding glass, measuring 29 in. long, 44 in. wide, $8\frac{1}{2}$ in. thick, was placed in a steel test fixture and pressurized with water to 160 psig. There was no leakage or failure. At this pressure, the maximum bending stress for the glass was calculated to be ~900 psi. This is three times the value calculated for slab B-2 (see Fig. 1-26) at a cell design pressure of 30 psig.

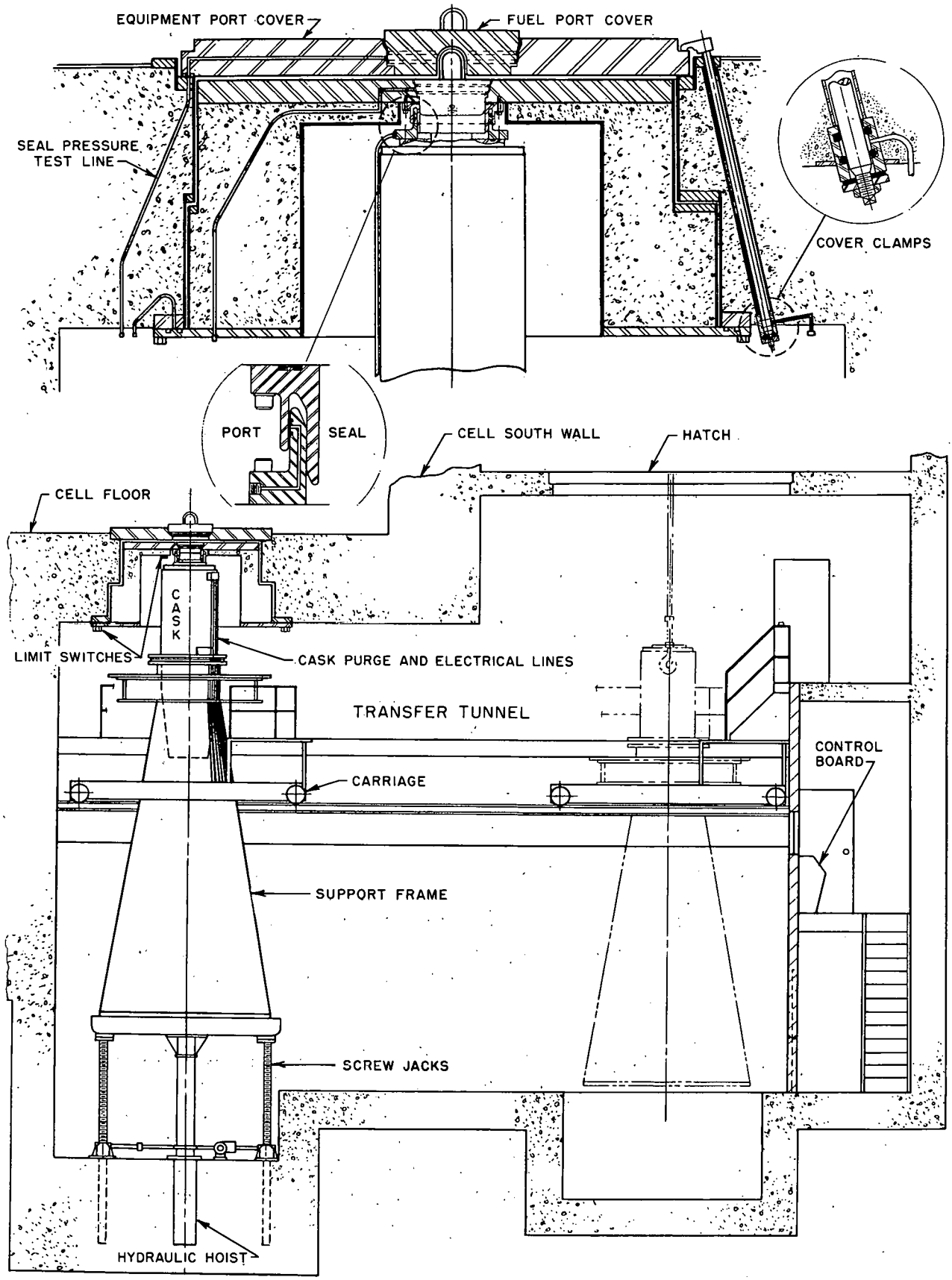

Fig. 1-25. Fuel and Equipment Transfer System

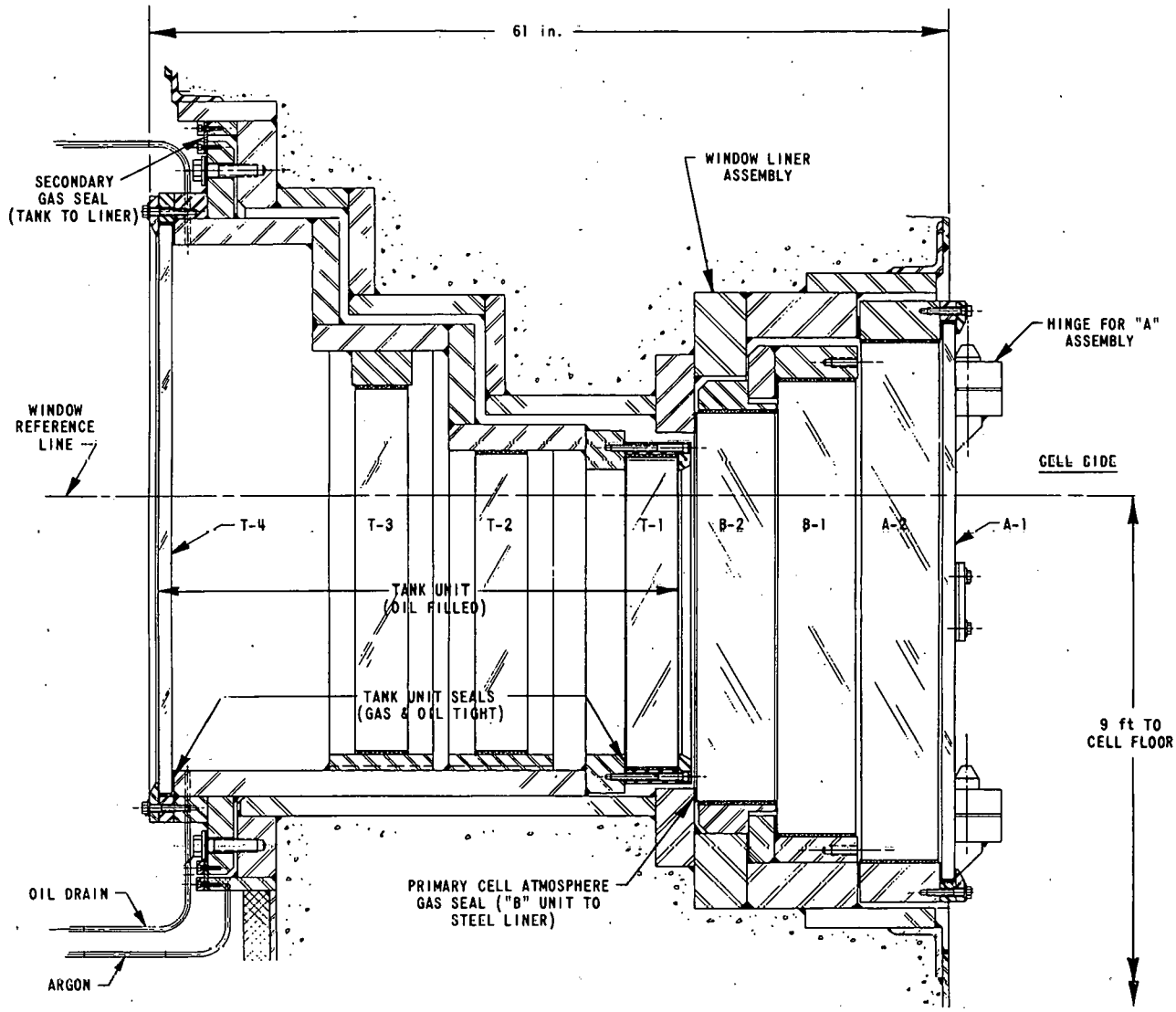

Fig. 1-26. Vertical section through FARET cell shielding window

In Test No. 2, the test slab was covered with another framed glass slab $8\frac{1}{2}$ in. thick and impacted with a 16-lb cast steel ball dropped from a height of 16 ft. The cover glass was damaged, but the underlying slab remained intact.

In Test No. 3, an assembly of two glass slabs was placed 10 in. distant from a bank of infrared heaters (nichrome elements in quartz tubes). Thermocouples were installed and the entire assembly was enclosed in a heat trap consisting of aluminum foil backed up with Transite panels. Several preliminary runs were made, during which 13.2 kW of power was supplied to the heaters for very short periods, followed by progressive reductions of power. Minor temperature rises were recorded by all thermocouples.

Next, a 1/2-in.-thick, tempered glass cover plate was installed 1 in. distant from the test slab. In order to resist higher temperatures, the gasket material used for the cover plate was 1/16-in.-thick lead sheet. During this test, power at 13.2 kW was applied for 20 min, then increased to 16.1 kW for 18 min. At this point, the corresponding surface temperatures were 490°F and 430°F for the cover plate, 260°F and 120°F for the first test slab, and 110°F and 90°F for the second test slab. There was no visible damage to either the test slabs or their gaskets (Koroseal 116).

In the final experiment, the glass cover plate was removed. A power of 13.2 kW was applied for 20 min, then increased to 16.1 kW for 11 min. At 340°F, the gasket of the first slab softened and flowed. At 342°F (front surface temperature), the glass cracked profusely, but remained in the frame. After the power was turned off, the back surface temperature remained essentially constant at 120°F for about 30 min. This observation suggests that, although cracked, the glass slab would serve as a good heat insulator. The second slab was not damaged.

Containment Penetrations. The containment structure will include numerous access penetrations for personnel and equipment, and for service interconnections. (See Fig. 1-27.) Each opening will be designed to maintain prescribed containment integrity and biological shielding tolerances. With one exception (MI-cable penetration), each opening can be tested periodically for leak tightness at a design pressure of 30 psig.

Considerable effort has been expended in developing a basic penetration design that will satisfy the requirements for the many different service interconnections. For example, Fig. 1-28 shows a test assembly of a "straight-thru" penetration to accommodate either electrical cables or small piping. In this instance, three prototype electrical connections were being evaluated with respect to leak integrity and radiation attenuation.

Leakage along the wire strands within the multi-strand conductors was of particular concern. Special cables, alleged to have low-leakage characteristics, were procured and tested without success.

Success was achieved by encapsulating the ends of commercially available cables in a potting compound and cable connector, as shown in Fig. 1-28. Each of the three cable connections indicated an argon leak rate of less than 0.03 ft^3/day at 30 psig. The total volume of gas outleakage from the test chamber was less than the prescribed leak rate of 0.5 ft^3/day at 30 psig.

A Co^{60} source (~1700 curie) was positioned on the "cell" side of the assembly in an effort to check the calculated gamma attenuation value of the penetration assembly. Two shielding plugs were installed and offset to eliminate any obvious streaming path. Nonetheless, a single streaming

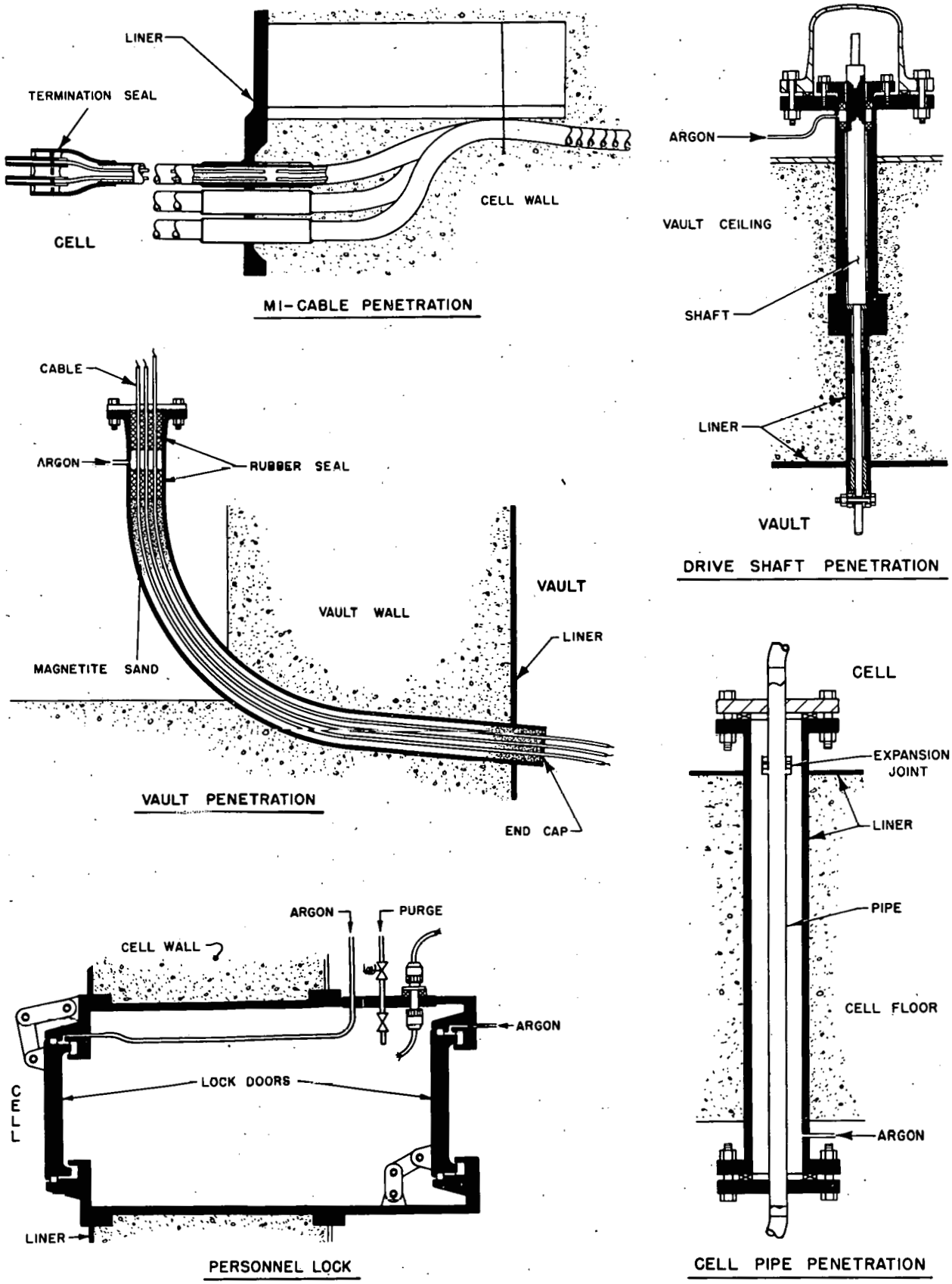

Fig. 1-27. Sectional views of personnel, equipment, and service penetrations through containment structure

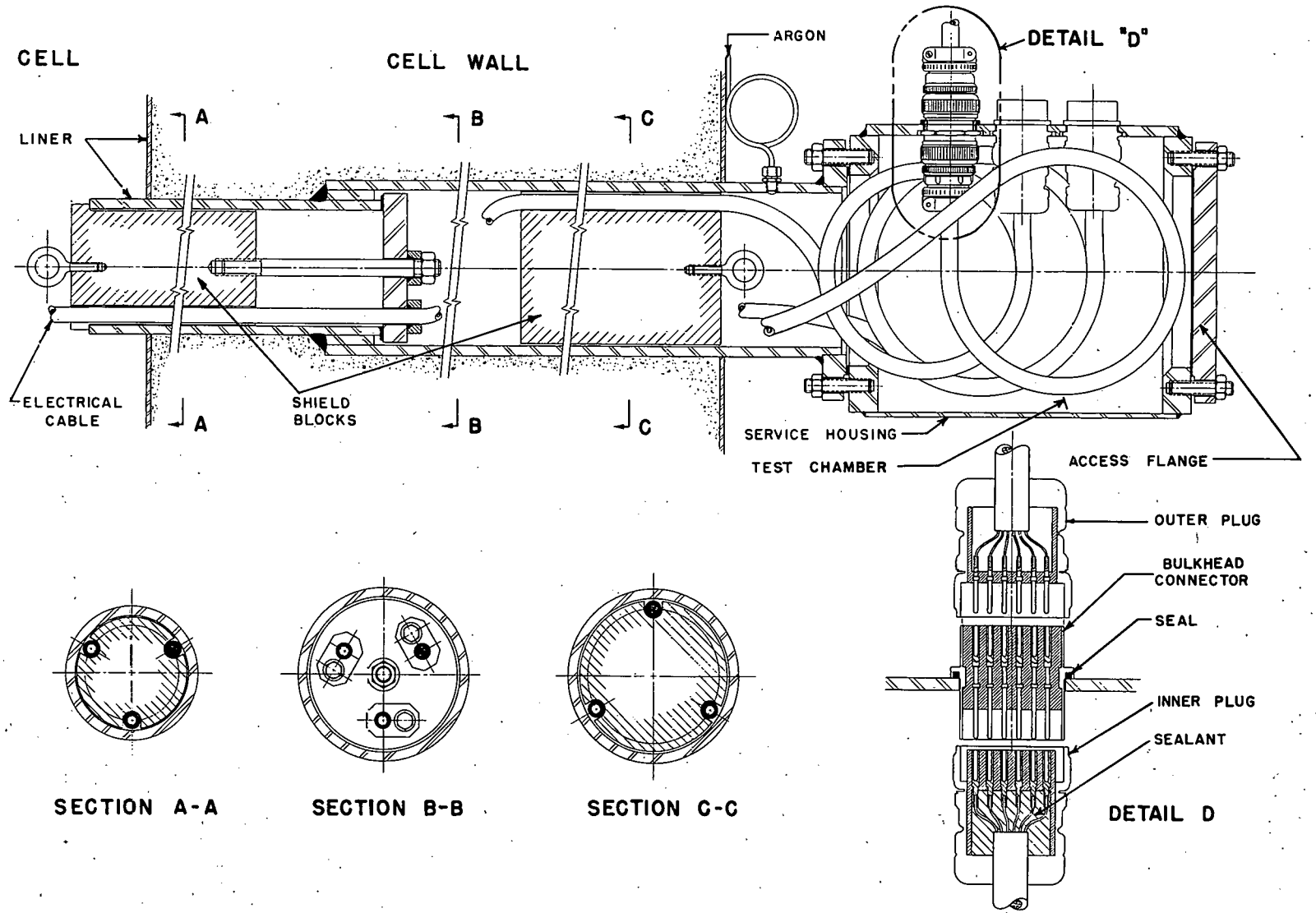

Fig. 1-28. Sectional views of test assembly used to evaluate leak integrity and radiation attenuation of electrical service penetration through containment cell

path of 7 R/hr intensity was detected over a 0.25-in.-square area on the opposite wall. Alternate shielding block configurations will be investigated in subsequent tests.

1.2.3.4 Preliminary Safety Analysis

The preliminary safety analysis of the FARET Facility was based upon the concept established by the Title-I design study. The findings of this analysis were compiled for limited distribution within the Laboratory and review by the Commission in August, 1964. The initial publication was supplemented by letter of February 8, 1965; with Supplement No. 1 in July, 1965, which extensively updated the detailed design description of the facility; and, finally, with Supplement No. 2 in October, 1965. General distribution of the integrated report is pending approval by the Advisory Committee for Reactor Safeguards.

As a result of this analysis it was concluded that:[3]

(1) Either the partial loss of coolant or coolant flowrate, or the dropping of a fuel subassembly into the core, which results in the collapse of a molten core, could lead to a nuclear accident with a mechanical energy release equivalent to detonating a 25- to 30-lb bare charge of TNT in the core. The consequences could include destruction of the reactor vessel, lifting of the reactor vessel cover, generation of other smaller missiles, ejection of sodium into the cell, and release of fission products from the molten fuel to the cell and cavity.

(2) The energy-absorption capabilities of the containment complex are significantly higher than the postulated release values. Structural analysis indicates that the proposed FARET containment system can absorb the dynamic effects of a 40-lb bare charge of TNT located at the core center. More specifically, the dynamic effects of the energy release are absorbed radially by a reinforced concrete shield which surrounds the reactor vessel, and vertically, by the cell roof structure. The maximum dynamic effect on the cell roof would involve ejection of the vessel cover and upper shielding extensions of the subassemblies (~50 ton). The vessel cover may impinge upon, but is not expected to penetrate the steel liner of the cell ceiling.

(3) Upward acceleration of the vessel cover withdraws the poison control rods. However, for reactor periods associated with the collapse of a molten core (<0.02 sec), the reactor would disassemble before any significant loads were imposed on the vessel cover. Hence, criticality could not be achieved by subsequent lifting of the cover and the control rods.

(4) For smaller accidents, which have longer reactor periods (>0.02 sec), the partition of energy during an exponential power excursion was shown (Fig. 1-29) to be a strong function of reactor period. As the reactor period shortens, most of the energy is retained in the fuel. Hence, the fuel is completely vaporized before a peak core pressure capable of disassembling the reactor is reached. (See Fig. 1-30.) Subsequent lifting of the vessel cover does not increase the severity of the accident.

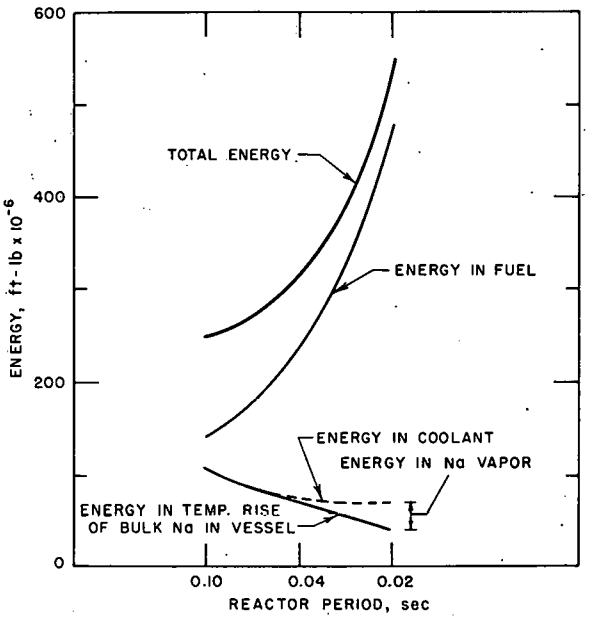

Fig. 1-29

Energy distribution at time of peak core pressure. (Initial power level = 50 MW(t); core filled with vapor at time of peak pressure.)

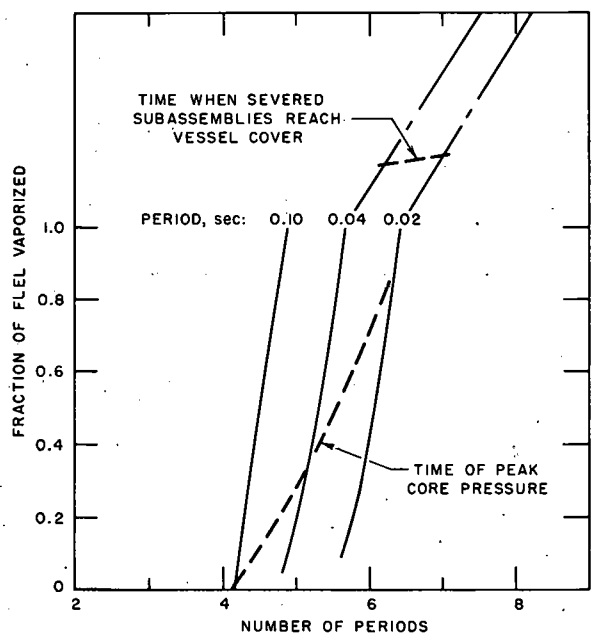

Fig. 1-30

Fraction of fuel vaporized as a function of number and duration of reactor periods. (Initial power level = 50 MW(t).)

(5) Substantial quantities of fission product-laden sodium coolant may be ejected into the argon atmosphere of the cell. Figure 1-31 shows the calculated resultant increase in cell pressure and temperature. The

calculations were based on a postulated leakage rate from the containment structure of 30 wt-%/day at 30 psig. Entrainment of the fission products released under these conditions would not pose undue hazards to surrounding populated regions.

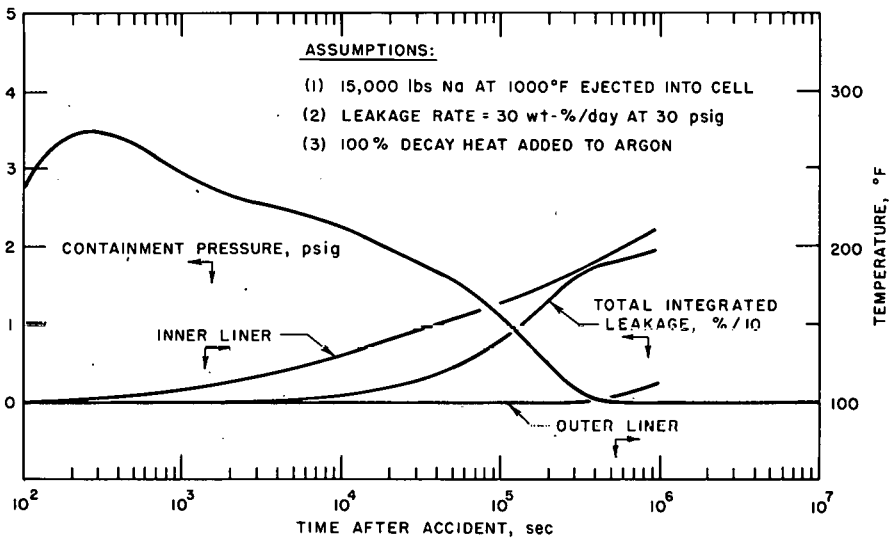

Fig. 1-31

Containment pressure, temperature, and leakage following maximum credible accident

In summary, to initiate a nuclear accident, several unusual and coincident conditions must prevail. For the situation to proceed to serious proportions would require simultaneous malfunction of many design safety features and, in most cases, coincident loss of administrative control.

That these events will occur in the proper coincidence or sequence is unlikely. Each experiment will be carefully planned, and its safety aspects meticulously analyzed. Zero power critical experiments, laboratory tests, and other verification techniques will be employed to ensure the safety of each proposed experiment. Subsequent reactor operations will be designed to limit available reactivity and accidental reactivity input rate. With any reasonable inherent shutdown mechanism, the reactor should not go above prompt critical and no explosive energy release should occur.

REFERENCES

1. W. R. Simmons, P. J. Persiani, and T. R. Bump, *Fast Reactor Test Facility (FARET) and Initial Experimental Program*, ANS-100 (April, 1965), p. 773.

2. P. J. Persiani, T. R. Bump, and W. J. Kann, *FARET Core I Fuel Irradiation Program and Reference Design*, ANL-7106 (October, 1965).

3. J. D. Geier (ed.), *Fast Reactor Test Facility*, Vol. I: Description and Program; Vol. II: Summary of the FARET Preliminary Safety Analysis; ANL-7168. (To be published.)

4. G. F. Popper and T. Z. Zeren, *Refractory Oxide Insulated Thermocouple Analysis and Design*, presented at High Temperature Thermometry Seminar, February 24-26, 1965, Washington, D. C. (To be published.)

1.3 ARGONNE ADVANCED RESEARCH REACTOR (AARR)

1.3.1 Project History and Status

Argonne National Laboratory has long recognized that continued progress in research involving nuclear radiation is contingent upon the availability of more specialized research reactor facilities with neutron fluxes of the order of 10^{15} or higher. Accordingly, the Reactor Engineering Division has, for the past several years, conducted a program to develop and evaluate design concepts of research reactors capable of producing neutron fluxes of these orders. The AARR is the latest concept which has evolved from this program.

The initial concept of AARR featured a pressurized, light-water cooled, beryllium reflected, flux-trap reactor with a maximum unperturbed thermal flux (in the flux trap) of 5×10^{15} n/(cm^2)(sec) at a power level of 100 MW.[1] Additional core physics investigations were carried out and tentative facility design layouts were prepared. The results of these efforts served as the basis of a preliminary feasibility and cost study performed by United Nuclear Corporation in 1962.

However, subsequent physics and heat transfer studies indicated the possibility of upgrading the reactor from 100 MW to 240 MW, and thereby producing unperturbed thermal neutron fluxes as high as 10^{16} n/(cm^2)(sec). It was recognized that such an increase would constitute an extension of existing technology subject to experimental confirmation. Nonetheless, the probability of success was deemed sufficiently high to warrent an initial facility design for ultimate operation at 240 MW. On this basis, a second cost study was undertaken and completed in 1963.

The engineering design and construction of AARR at Argonne was formally authorized by Congress late in fiscal 1964. On June 1, 1965, Burns and Roe, Inc. (New York) was selected as architect-engineer. Title-I design is expected to begin early in fiscal 1966.

During fiscal 1965, major efforts on the AARR Project were expended in the following areas:

(1) Revision and expansion of the prospectus to provide a definitive guide for the architect-engineer in preparing the Title-I design.

(2) Completion of core and system safety analyses as necessary to compile a Preliminary Safety Analysis Report.

(3) Core heat transfer analysis and experimentation.

(4) Initial studies on fuel thermal stresses and hydraulic stability.

(5) Fuel and control rod material fabrication process development, and irradiation testing.

(6) Reactor vessel stress analysis evaluations to determine feasible beam tube penetration layouts.

(7) Detailed conceptual design and development of in-reactor experimental facilities, with particular emphasis on facilities whose definitive design is contingent upon prototype testing and evaluation.

(8) Adaptation of the Department of Defense - National Aeronautics and Space Administration PERT/Cost System for use on the Laboratory's CDC 3600 computer, and initial application to the AARR project.

1.3.2 Conceptual Design

This section describes the fundamental concept of AARR which served as the basis for the Preliminary Safety Analysis Report and for negotiating the services of the architect-engineer.

Figure 1-32 is an artist's concept of the buildings and supporting facilities. Overhead power lines terminate at an electrical substation located behind the Reactor Containment Building. Also not shown is an underground pedestrian tunnel which leads from the Laboratory and Office Building to the nearby CP-5 Facility.

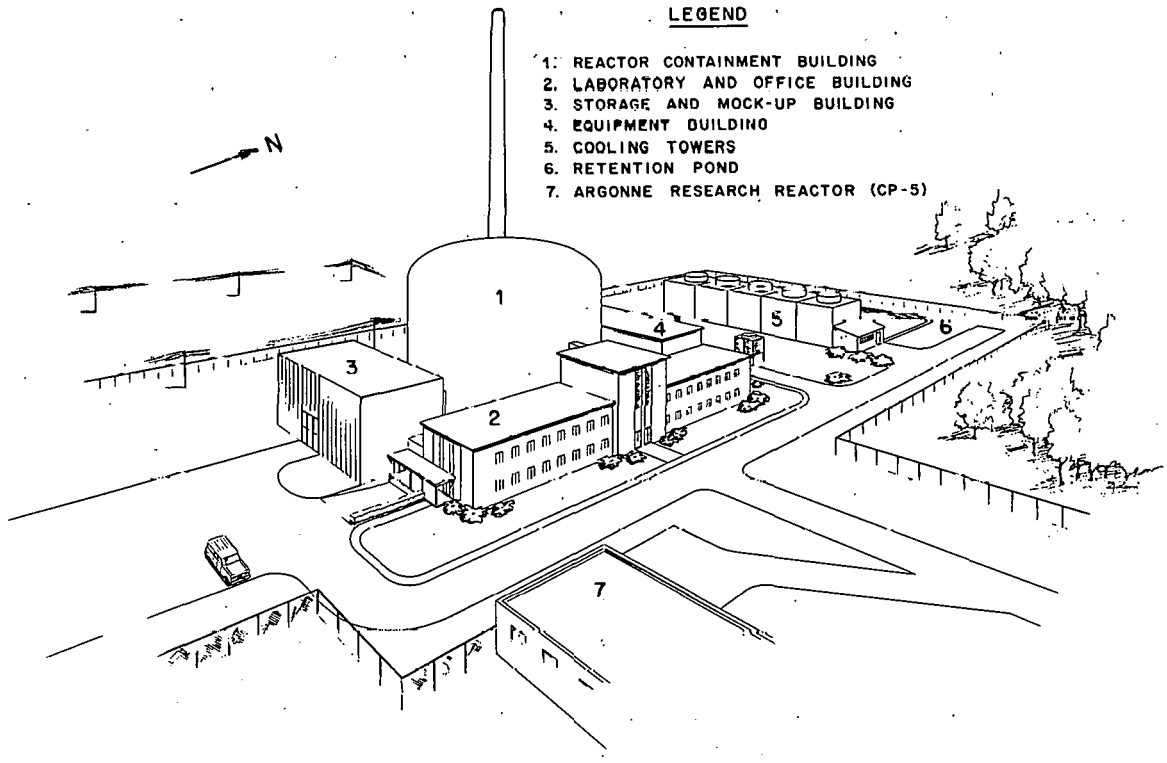

Fig. 1-32. Artist's concept of Argonne Advanced Research Reactor

1.3.2.1 Reactor Containment Building

Structural Components and Services

This building measures 122 ft in diameter and 106 ft in overall height, with 14 ft below grade and 92 ft above grade. Designed for reactor containment, the structure consists of a steel dome (0.5 in. thick) above grade, and reinforced concrete walls and foundation below grade.

The building houses the reactor and experimental facilities, the fuel handling canal, and certain primary system equipment which requires heavy shielding. The remainder of the primary system is installed on the lower level of the Equipment Building. Components are located in an area which communicates directly with the lower level of the Reactor Building and forms an integral part of the reactor containment volume.

The reactor vessel is located in a concrete-shielded pit filled with water, with the core centerline a few feet above the main floor level. Except for small areas near the building access air locks, the entire main floor area around the reactor is available for experimental equipment. In order to provide maximum floor space for specific beam tube experiments, the reactor vessel pit is located off-center with respect to the building centerline. The resultant distance from shield face to building wall will permit a range of neutron beam lengths varying from 33.5 ft to 55 ft.

A wide balcony, extending around the periphery of the building, is also available for controls and instrumentation for the various experiments. Located 12 ft above the main floor level, this balcony communicates directly through a personnel air lock with the second floor of the Laboratory and Office Building. A narrow observation balcony is located 34 ft above the main floor, at a level corresponding to the top of the reactor shield pool.

The fuel-handling canal with its specialized areas, a small high-level cave, and the control rod drive room (immediately below the reactor) are located on the service floor. Certain heavily-shielded equipment is installed in pits below the service floor level.

Other facilities within the building include a 40-ton rotary crane, which services the main floor level; miscellaneous cranes and hoists for handling samples, fuel, and transfer casks in the canal; and a personnel elevator.

Normal access to the building is through two personnel air locks from the main and second floors of the Laboratory and Office Building, or through an equipment air lock from the Storage and Mock-Up Building. Other openings in the building include emergency air locks, and penetrations for system piping, utilities, and ventilating and exhaust ducts.

Reactor Components and Auxiliaries

Core. The reference core is fueled with 0.040-in.-thick plates containing 37 wt-% UO_2-stainless steel cermet (0.030 in.), clad with stainless steel (0.005 in.). These plates are welded or brazed to form 0.040-in. coolant channels in subassemblies which are essentially rhomboidal in cross section.

These subassemblies, in turn, are disposed in a hexagonal geometry (18 in. across flats, 18 in. high) around a central hexagonal flux trap (internal thermal column) which is approximately 5 in. across flats. Insofar as possible, the subassemblies are oriented such that the fuel plates are perpendicular to a core radius. Fuel plates in subassemblies immediately surrounding the thermal column and, also, those near the outer periphery of the core, are graded in loading. This is done to reduce the peaking of neutron flux (and consequently, heat flux) which would occur in these zones if a uniform loading were utilized throughout the core.

Use of a UO_2-stainless steel cermet, rather than a uranium-aluminum dispersion-type fuel represents a departure from established research reactor technology. However, a number of advantages are afforded by this approach:

(1) Longer core life - 90 days at 100 MW as compared with 12 days for the aluminum core, or 37 days at 240 MW. This is achieved by virtue of the greater critical mass permissible in the highly-absorbing stainless steel core, and the correspondingly higher allowable uranium burnup per unit of available excess reactivity.

(2) Greater structural strength and stability in the presence of high-velocity coolant flow.

(3) Elimination of corrosion as a consideration in designing fuel plates for operation at elevated temperatures required for high-power-density cores.

(4) The epithermal spectrum (median fission energy = 8 eV) minimizes post-shutdown buildup of xenon and samarium as an impediment to subsequent startup during the first 75 days of core life at 100 MW, or 27 days at 240 MW.

Control Rods. The reactor is controlled by twelve, blade-shaped rods. Six of these rods are oriented radially within the core; the others are located around the outer periphery of the core. Each rod is approximately 0.200 in. thick and is composed of europium oxide-stainless steel cermet clad in stainless steel.

Reflector. The core is surrounded radially by a beryllium reflector, approximately 12 in. thick. The reflector is penetrated by coolant passages and other openings designed to accommodate various experimental facilities.

Experimental Facilities. These facilities include:

(1) A hexagonal flux trap (internal thermal column) in the center of the fuel region. The flux trap can be used either for long-term irradiations in the production of milligram quantities of transuranium isotopes, or for accelerated irradiations of materials of interest. In addition, the flux trap is traversed by a 1/2-in.-I.D. hydraulic rabbit tube to facilitate short-term exposures.

(2) Four $1\frac{3}{8}$-in.-I.D. and six 2-in.-I.D. vertical thimbles which terminate in the beryllium reflector.

(3) Eight 3-in.-I.D. vertical thimbles. These thimbles are oriented radially in the water reflector-shield region between the beryllium reflector and the reactor pressure vessel.

(4) Two 5/8-in.-I.D. hydraulic rabbit tubes which terminate in the beryllium reflector.

(5) Twelve horizontal blind beam tubes, with respective inside diameters ranging from $2\frac{3}{4}$ in. to $6\frac{1}{4}$ in. These tubes extend into the beryllium reflector; ten are roughly tangent to the core periphery, while two are radial to the core vertical center line. Two of these beam tubes can be used for 400-meter, time-of-flight experiments.

(6) Two $4\frac{1}{4}$-in.-I.D. horizontal through-tubes which penetrate the beryllium reflector.

Three supporting facilities are contemplated:

(1) A reactivity measurement facility, which is essentially a duplicate of the AARR core configuration. It will be used by reactor operators and by experimenters to measure reactivity effects of new cores and experiment loadings without interfering with reactor operation.

(2) A core disassembly area, which is located in an isolated wing of the fuel storage and handling canal. This area will be used to disassemble and inspect cores containing spent or ruptured fuel elements without danger of contaminating the entire canal.

(3) A high-level cave, which is located near one end of the storage canal. It will facilitate examination and evaluation of freshly irradiated specimens.

Coolant Systems. The reactor is moderated and cooled by recirculating approximately 30,000 gpm of light water through the core and the reflector. Reactor-generated heat is transferred through primary heat exchangers to a secondary water system which rejects the heat in cooling towers.

The primary coolant system is designed for a normal operating pressure of 750 psig and a maximum water temperature of 250°F. Cooling water at 135°F (or lower) enters the vessel through a 30-in. nozzle at the top, flows downward through the core and reflector and exits at a temperature of 158°F (for 100 MW) or 190°F (for 240 MW) through a 30-in. outlet at the bottom of the vessel. From this point, the effluent flows through a bank of six parallel heat exchangers into a common header. This header is connected to three primary circulation pumps. Two of these pumps are normally in operation and return the primary coolant to the reactor through a full-flow strainer close to the reactor inlet.

The primary system includes two emergency and shutdown cooling circuits. Both circuits are completely independent of each other as well as of any other part of the main circulation loop. The two primary emergency-shutdown pumps are connected to a constant power supply line (Class A power).

Primary water is degassed and purified in a bypass system which also serves to pressurize the primary system.

Secondary system cooling water is circulated through the shell sides of the primary heat exchangers and the contained heat is rejected to the atmosphere through five cooling towers. The secondary system is equipped with five circulating pumps which operate in a fashion similar to the primary system pumps, i.e., four are for normal operation, and one is a spare. Two secondary emergency-shutdown pumps are connected to the constant power supply.

The cooling towers also serve as a heat sink for auxiliaries such as the cooling system for experiments, the primary purification system coolers, and the reactor pool and canal cooling system. Water from the latter system also may be cycled through chilling equipment installed adjacent to the canal.

Make-up water for the cooling towers is obtained from the nearby Chicago Sanitary and Ship Canal via an existing water treatment plant on the Argonne site. Since this water contains high concentrations of chloride ions and is oxygen saturated, the tubes in the primary heat exchangers are made of Inconel rather than stainless steel. This is done to avoid the stress corrosion problems associated with the use of stainless steel in water having a high chloride content. Auxiliary system heat exchangers also will use

this water, but at much lower temperatures. The cooling surfaces in these units will be Alclad aluminum.

Fuel Handling. After reactor shutdown, the spent core is cooled by forced circulation until the afterheat has decayed to a level where adequate cooling can be effected by natural convection.

With the aid of the building crane, the reactor vessel refueling cover is removed to expose the core. The core cartridge is lifted from the vessel through the surrounding pool, moved laterally, and lowered through a water-filled chute to a transfer tank. This tank is located on the bottom of the fuel handling and storage canal. The core is deposited on a hydraulically-operated transfer cart inside the tank and transported to a position directly below the water-filled storage area. The storage area crane is used to lift the core out of the transfer tank, and deposit it in the storage area. Within this area, the core is cooled by natural convection until it can be removed, dismantled, and shipped to an off-site processing plant.

The core is disassembled by remote-controlled equipment in an isolated cell adjacent to the storage area. This cell is serviced by a separate cooling system. Spent cores with known, or suspected of having, cladding failures are transported directly to this cell. This is done to prevent contamination of the entire storage canal by released fission products. A small, high-level cave is located adjacent to the disassembly cell, and provision is made for direct transfer of fuel subassemblies from the canal into the hot cave for close examination.

The core disassembly area is also used to load undamaged fuel subassemblies in casks for off-site shipment. These casks are brought, through the vehicle air lock, into the Reactor Containment Building. They are lowered (by the building crane), through a hatch in the experiment floor level, directly into the storage canal. The hatch is just inside the air lock opening and located so as not to interfere with any beam tube experiment or equipment.

Samples which have been irradiated in vertical thimbles in the reactor are also removed through the fuel transfer chute to the canal. They are then transferred into the hot cell for examination, or placed in casks for shipment from the building.

Instrumentation and Control. Nuclear instrumentation is provided to monitor the complete range of reactor operation, from startup to power. Twelve instrument channels are used in conjunction with four modes of control, or three channels per mode. Thus two-out-of-three logic will prevail, in the event of equipment malfunction, to minimize the frequency of

unnecessary reactor shutdown. Automatic control is used in the power range to reduce operator manpower, to provide steadier operation, and to switch control modes in a consistently safe manner.

In general, the logic of the control system operates sequentially to reduce power, or to effect complete shutdown, depending on the nature and the degree of urgency associated with the system malfunction, if known. Fast shutdown (scram) is initiated under all other conditions of urgency.

Analog instrumentation is employed for rapid and accurate recording of data on reactor operations. Provisions for the future use of digital computer control are being incorporated into the design.

Containment building atmosphere is monitored continuously to provide advance warning and to initiate automatic precautionary confinement actions upon detection of abnormal radiation levels. The environmental monitoring system also provides background data for low-level experimentation.

1.3.2.2 Laboratory and Office Building

This building contains the reactor control room, and laboratories, offices, and service facilities for use by personnel engaged in the operation, maintenance, and conduct of experiments in the reactor facility.

These facilities are disposed on three floor levels. The main floor contains a reception area, the control room, eight offices, a technicians' laboratory, drafting room, conference room and an assembly room for Operations personnel. Two offices and one laboratory are provided for Radiation-Safety personnel. Also located on the main floor are instrument and electrical shops, water closets, and locker rooms for all personnel.

On the second floor are located eight offices, fifteen laboratories, and other personnel facilities; these are available for use by scientists and engineers engaged in reactor experiments.

Below the main floor are four counting rooms and three laboratories. They are located to facilitate direct pneumatic or hydraulic transfer of test specimens between them and the fuel-handling canal and/or hot cave.

The three floors are serviced by a personnel and freight elevator (10-ton capacity).

1.3.2.3 Storage and Mock-Up Building

As the name implies, this building provides space for mock-up assembly of experiments prior to installation into the reactor. It also contains a storage vault for new fuel, a stock room, a machine shop, and storage space for miscellaneous reactor equipment when not in use, e.g., beam hole plugs, transfer casks, etc.

The mock-up area is connected directly with the Laboratory and Office Building, and communicates through the equipment air lock with the Reactor Building. Motor trucks carrying reactor equipment may be driven into the Storage and Mock-Up Building and, if necessary, may be backed through the equipment air lock into the Reactor Building.

Equipment mock-up assembly and repair operations are serviced by a 10-ton bridge crane.

1.3.2.4 Equipment Building

The major portion of the service floor level of this building constitutes a containment cell which houses most of the primary system equipment. This includes the primary pumps, heat exchangers, and the purification and degassing systems. This cell also contains auxiliary cooling systems for the fuel-handling canal, reactor shield, and certain irradiation test facilities and supporting equipment. Normal access to the cell is from the service floor of the Reactor Building, and only during reactor shutdown. The building is also penetrated by large, removable, sealed plugs to facilitate installation and removal of equipment directly from outside the structure.

Two other cells are located on the service floor. One contains two shielded 40,000-gal waste dump tanks, demineralizers, and other liquid waste treatment equipment. Two additional waste storage tanks, each of 56,000-gal capacity, are located underground outside the building. The other cell houses a walk-in filter plenum. This plenum contains 60 AEC high-efficiency filters which may be used to process all air exhausted from the Reactor Building and the primary system equipment cell. Both cells communicate with the main floor of the Equipment Building.

The main floor and second floor contain refrigeration equipment for the fuel-handling-canal-cooling system, air conditioning equipment for the Reactor Building, make-up water demineralizers and storage tank (30,000-gal capacity). Other equipment includes the station battery and emergency diesel-generator sets, all electrical switchgear for the facility, two booster blowers for the prefiltered air exhaust system, and two, half-capacity exhaust fans which discharge to the 250-ft stack.

1.3.3 Supporting Research, Design, and Development

1.3.3.1 Preliminary Safety Analysis

A major portion of the analytical work necessary for the Preliminary Safety Analysis Report was completed during fiscal 1965. An initial draft of the findings, based upon the conceptual design described above, was compiled for informal review by the Laboratory Reactor Safety Review Committee.

However, because of unique problems associated with preparing a PSAR in advance of any design work by an architect-engineer, it was decided to revise the report format drastically and base the findings upon Title-I design criteria and requirements. This revision was in progress at the end of the year.

The results of the analytical effort are incorporated in the following sections.

1.3.3.2 Mark-I Core Development

Analytical and Experimental Heat Transfer

The scope of the heat engineering effort included a steady-state parameter study, supporting experimentation, and transient analyses. This section describes the nature and the preliminary results of the steady-state analysis and experiments.

The criterion used in the thermal design of AARR is to operate the core at the maximum power density consistent with safety and the production of maximum neutron flux for research purposes. The design conditions for the initiation of local boiling at the hot spot on the fuel surface are conventionally used in reactors similar to the AARR to yield a steady-state design that is conservative. However, the degree of conservatism must be related to the transient behavior of the reactor during inadvertent power excursions or operational mishaps. Accordingly, the thermal design has concentrated on estimating system conditions that could promote fuel melting. In this regard, the occurrence of a critical heat flux or flow instability could cause fuel melting. Critical heat flux is defined as the heat flux that causes an insulating barrier of vapor at the interface of the fluid and heat transfer surface. Flow instability is defined as a nonrepetitive flow excursion initiated by hydrodynamic conditions in a flow channel that cannot be sustained during steady-state operation.

Table 1-13 lists the thermal characteristics of the core that were used in conjunction with the preliminary safety analysis of AARR.

Limitations on the thermal performance are based on the coolant channel that experiences the maximum thermal load. The factors listed are applied simultaneously with the channel space decreases noted.

Table 1-13. Design Data Used in Thermal Analysis

Radial max./avg. plate power density ratio	2
Axial max./avg. plate power density distribution	See Fig. 1-33
Factors	
Fluid temperature rise	
Average plate power density	1.11
Flow rate	1.08
Film temperature rise	
Local plate power density	1.27
Flow rate	1.06
Accuracy of film coefficient, %	25
High power density channel spacing, in.	
Nominal	0.050
Minimum	0.040
Average power density channel spacing, in.	
Nominal	0.040
Average	0.030
Inlet temperature variation, °F	3
Pressure variation, equivalent in temperature, °F	2
Heat transfer area, ft^2	672
Scaling allowance	None

Steady-State Parameter Study. The purpose of this study was to determine the effect of inlet coolant velocity and temperature, and uniform channel spacing deviations on the inlet pressure required to suppress local boiling. In addition, estimates were made of the critical heat flux and flow instability limits, using the Zenkevich-Subbotin correlation,[2] and the trend of flow instability calculations, using the STDY-3 code.[3]

The solid curves in Fig. 1-34 are typical results of these calculations for the design data listed in Table 1-13. The dashed lines provide an estimate of the power increase factor that can be used to predict the power level at which fuel melting can be expected. For example, at 100 MW, with an inlet coolant velocity of 45 ft/sec and an inlet temperature of 135°F, local boiling is suppressed with an inlet pressure of 275 psia. Under these conditions, the power level at which fuel melting will occur is 1.87 x 100 MW = 187 MW. The parenthesized value of 1.5 is the estimated power increase factor based on the Zenkevich-Subbotin correlation.

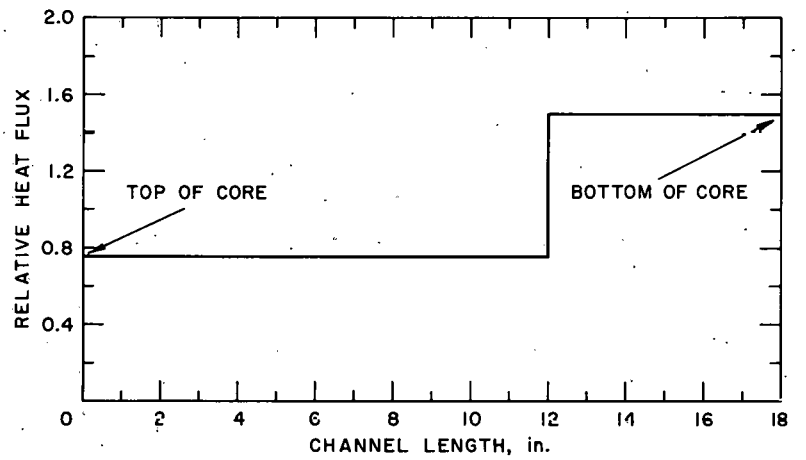

Fig. 1-33. Axially-skewed heat flux distribution used for thermal analysis of AARR core

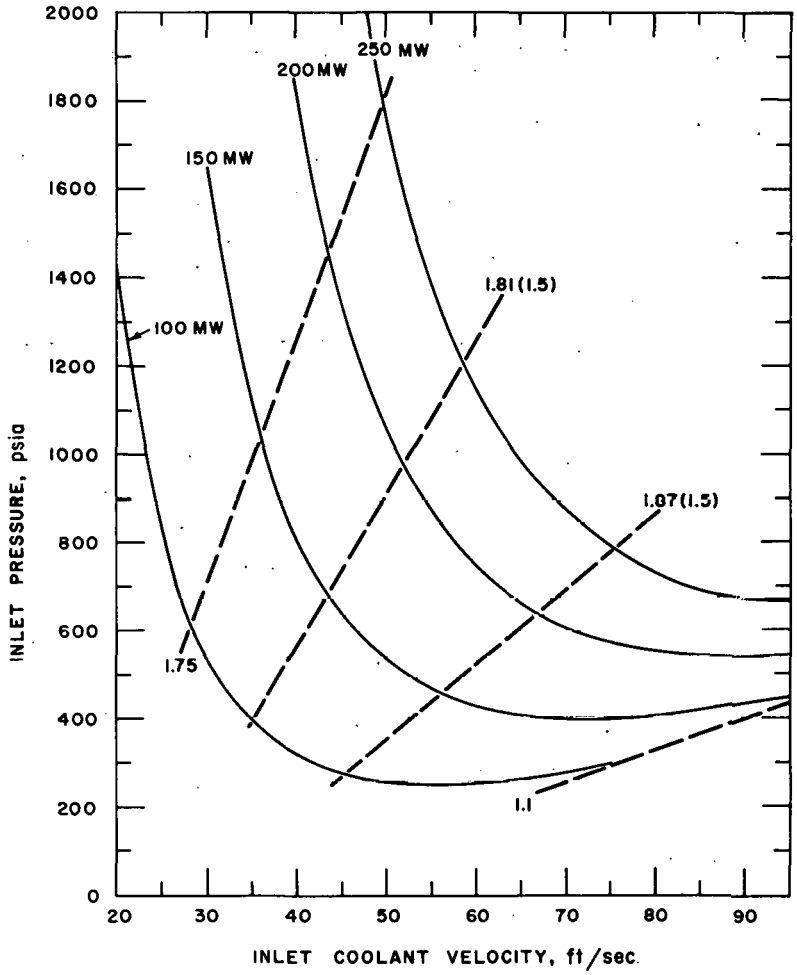

Fig. 1-34. Calculated steady-state thermal performance. Solid curves show threshold conditions for local boiling. Dashed lines indicate power increase factor for predicting power level at which fuel melting will occur.

The steady-state operating conditions chosen for the reactor are: inlet pressure of 750 psia, inlet coolant velocity of 45 ft/sec, and inlet temperature of 135°F. The selection of pressure is based on beam tube design considerations that favor limiting the inlet pressure to 750 psia. It was also necessary to estimate the conditions that would permit attaining the goal of 240 MW operation with a power increase factor of 1.25.

At these conditions, local boiling is suppressed at the hot spot for power levels below 160 MW; the ratio of critical heat flux to the maximum operating heat flux at 100 MW power level is 3.6; and the power level for fuel melting is estimated to be 250 MW and 288 MW, based on critical heat flux and flow instability estimates, respectively.

As stated earlier, these safety margins must be related to the transient behavior of the core in order to properly assess the degree of conservatism involved in the design. This aspect of the design is discussed in Section 1.3.3.3.

Experimental Program. The experimental program is intended to provide verification and/or guidance for the heat transfer analyses. The scope of this program will include steady-state, transient, and shutdown-emergency cooling tests. Only the steady-state tests have progressed to the preliminary data stage. Two separate loops, using a 1500-kW, d-c power supply, were made operational to satisfy the requirements for testing single and parallel channels. The single-channel tests have the potential for obtaining the type of data needed to determine the conditions at which flow instability and critical heat flux will occur. The parallel-channel loop provides a facility for checking the results of the single channel tests for application to the reactor core.

A series of tests were made on three test sections in the single-channel loop. Table 1-14 summarizes the maximum operating conditions for each significant test. Also listed for comparison are the heat fluxes determined from the Zenkevich-Subbotin critical heat flux correlation, and estimated power levels at which flow instability can be expected.

Table 1-14. Summary of Steady-State Tests

Test Section[a]	Inlet Conditions		Exit Conditions		Total Power, kW	Average Heat Flux, 10^6 Btu/(hr)(ft^2)	Max. Heat Flux, 10^6 Btu/(hr)(ft^2)		Estimated Power for Flow Instability, kW	Remarks
	Velocity, ft/sec	Temp., °F	Press., psia	Temp., °F			Experimental	Correlation		
I	51	147[a]	615	453[b]	372	3.94	-	-	362	Actual burnout occurred.
II	43	138	620	431	304	3.28	4.69	4.57	316	Actual burnout occurred.
III	43.3	122	620	402	285	3.01	4.3	5.22	335	Terminated before burnout.
III	48	126	620	431	347	3.67	5.1	4.8	363	Terminated before burnout.
III	55.3	134	620	433	387	4.15	5.84	5.12	413	Actual burnout occurred.

[a]Test sections I and II had sharp corners; test section III had rounded corners.

[b]Possible error of 20°F. Test section had local channel deflection of <0.020 in. at 2 in. from end of heated length.

These preliminary results indicate that for AARR conditions, single-channel data can be applied to parallel-channel systems so long as the proper core pressure drop is maintained. Also, the Zenkevich-Subbotin correlation looks promising for determining design and operation limits. Additional tests will be made in both the single- and the parallel-channel systems in order to verify the above findings.

Mechanical Design, Stress Analysis, and Hydraulics

During the last part of fiscal 1965, Division personnel collaborated with Nuclear Utility Services on the initial scoping of thermal and hydraulic stress problems in the AARR fuel subassembly and core support grid.[4] This effort was intended primarily to ascertain the nature and magnitude of stresses to be anticipated, and to serve as a basis for planning a more detailed analytical and experimental program in fiscal 1966.

As a result of this effort, three major areas were identified as amenable to quick estimates: thermal stress, channel closure, and fuel plate stability. The latter also was singled out for extended analytical and

experimental treatment. Additionally, a detailed study will be made of the transient thermal stresses caused by sudden changes in coolant conditions and in power levels. Two distinguishing features of this study are the inclusion of internal energy generation and simultaneous cooling through a boundary conductance. Although both have been neglected in past studies, they are now considered essential since it is clear that a predetermined design conservatism cannot be established solely from a knowledge of possible thermal stress cracking during cooldown.

Static thermal stress problems were included in the study by Nuclear Utility Services, with particular reference to the cladding where the maximum stress occurs. Generalized stresses were computed for the condition of central supports (fuel plate spacers); these data are being evaluated.

The Plastic-Sass model used in the NUS study provided interim conclusions regarding plate bowing, expressed in the form of a channel closure ratio:

$$R_{uc} = 1 - \frac{\text{minimum channel spacing}}{\text{nominal channel spacing}}.$$

Computed values ranged around 0.3. They were based on the use of a central spacer and certain assumptions with respect to radiation-induced growth of the plates. However, independent irradiation experiments performed by Argonne at Idaho indicated the computed values were overly conservative. Further studies will be made, with emphasis on sensitivity to material properties.

Among the problems of stability encountered, that of the elastic response of the fuel plates and subassemblies to the reactor core flow and thermal environment is being considered at greater length. Theoretical results obtained thus far indicate it may be possible to investigate more complex models without proceeding immediately to assumptions that decouple the thermal and hydraulic aspects of the plate stability problem.

A model core support plate and special dummy fuel boxes are being fabricated for the purpose of performing stress-deflection tests on the plate under various hydraulic loads.

Fuel Material Fabrication

Consistent with the original intent of using existing technology wherever possible, the AARR fuel material fabrication development program has continued to draw heavily from the BORAX-V, SM-2, and PM-1 core technology and the Enrico Fermi Core B development work. In general,

extension of the technology to produce an improved fuel capable of meeting the high performance requirements of AARR has been successful. The major problem has been one of achieving the desired degree of consistent quality control.

The development program was initiated with a survey of existing stainless steel cermet technology. This study concentrated on evaluation of the basic processes used to fabricate the above-mentioned reactor fuels, and the improvements generated from the Fermi Core B development activities. Since the completion of the survey, work has continued in two principal areas: improvement of cermet homogeneity, and assessment of mechanical properties of the fuel materials (37 wt-% UO_2-SST) in both the unirradiated and irradiated conditions. The high-performance AARR design requires the use of nominal 85% T.D. UO_2 in a matrix of Type 347 stainless steel. Cermet ratios vary from a nominal 6 wt-% UO_2 in SST, up to 37 wt-% UO_2 in SST. Use of low-density UO_2 spherical particles with the accompanying reduction in crushing strength has required certain original investigations.

Four basic processes were investigated to determine the effect of each process on oxide dispersion. Three of these processes have been selected for further evaluation to determine their relative capabilities for producing flat fuel plates to close dimensional tolerances:

Process No. 1 - a loose powder metallurgy process - involves blending and compaction of loose UO_2 and stainless steel powder by conventional techniques. The compact is enclosed in a stainless steel envelope, and hot rolled into a long, thin, flat plate.

Process No. 2 - a process using UO_2 particles encapsulated in stainless steel - involves cold die-extrusion of the steel-covered UO_2, with an organic binder, into a flat plate. This flat plate cermet is then densified, enveloped in a stainless steel jacket, and hot rolled to final dimensions.

Process No. 3 - an all-sintering densification process - involves a modified procedure for blending and initial compaction of loose UO_2 and stainless steel powders into a "green" compact cermet. This cermet is enclosed in an all-stainless steel powder compact of the same consistency. The complete "green" compact is then fixed at the sintering temperature of stainless steel to form a fully densified, full-size fuel plate which requires less than 10% cold reduction to final dimensions.

At present, Process No. 1 appears to be the most practical for the AARR. Blending and compaction studies have established several basic requirements for achieving the desired quality of dispersion fuel plates. Correlations between oxide particle crushing strength and dispersion homogeneity have been made. Figure 1-35 shows the type of oxide break-up incurred with UO_2 spheres of various crushing strengths when fabricated

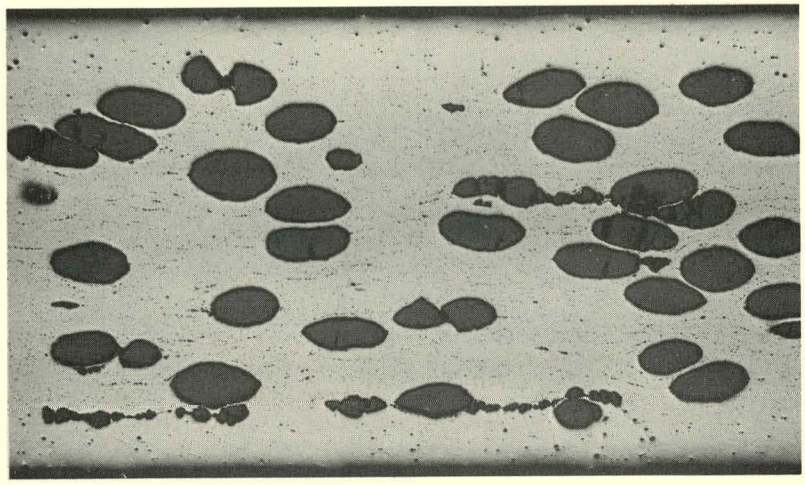

High fired, 95% T.D. UO_2

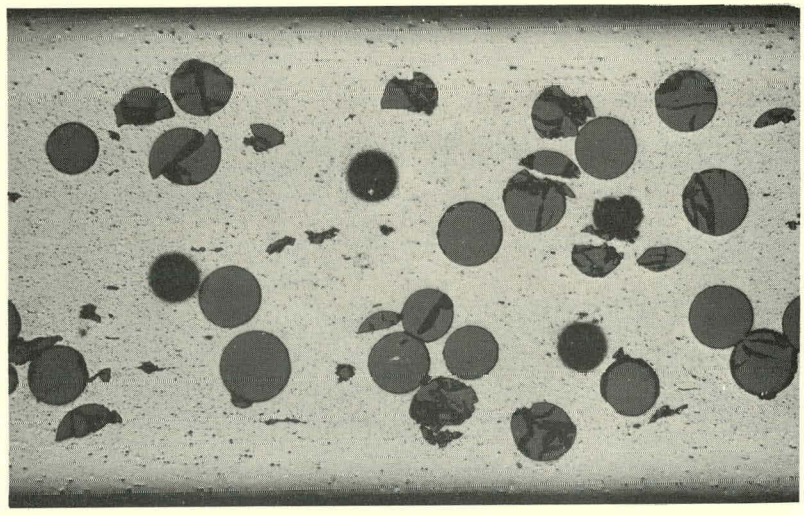

Sol-Gel, 98 % T.D. UO_2

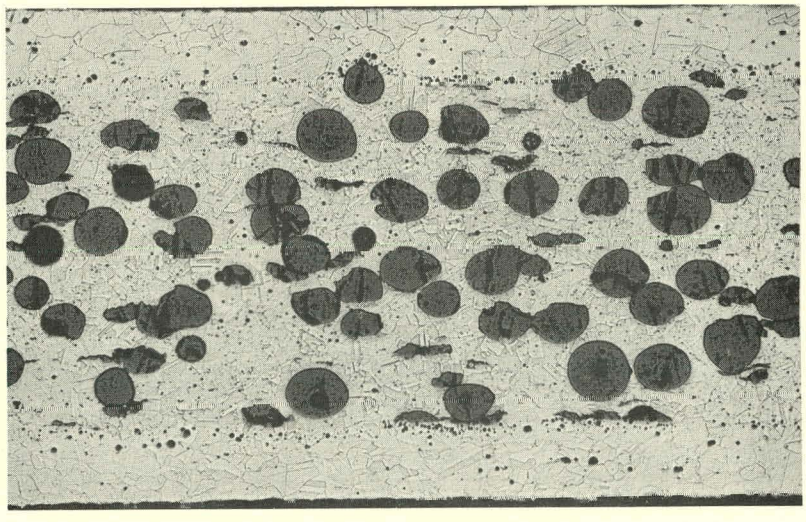

Flame fired, 85% T.D. UO_2

Fig. 1-35. Microstructures of 0.040-in.-thick fuel plates rolled with different types of UO_2

into plates by optimized hot-rolling procedures. Of all the oxides studied, the very-high-crushing-strength Sol-Gel UO_2 evidenced the least fragmentation. Additional quantities of UO_2 made by the Sol-Gel process are being procured to determine if a material of 85% T.D. can be produced consistently. The effect of reduced density on crushing strength of this material also will be evaluated.

Optimization studies at Battelle Memorial Institute and demonstration studies at Westinghouse and Sylcor have indicated that random orientation of UO_2 spheres in a stainless steel matrix can be made to produce a quality of homogeneity adequate to provide the desired soundness of matrix structure in 37 wt-% UO_2-SST cermets. Close quality control was required to achieve the desired structure. A reference process has been established for making this material, with special emphasis being given to the size and properties of the materials and ultimate fabrication into flat plates.

Initial irradiation performance tests were conducted by the Phillips Petroleum Company in the ETR-G-12 and the MTR-L-51 loop facilities. The low temperature and power density MTR irradiations were made to determine if an open porosity condition existed in the 97+% dense matrix of the all-sintered process fuel plate. After three cycles, it was determined that no serious fission product leakage should be expected.

The ETR irradiations were performed on 37 wt-% UO_2-Type 347 stainless steel cermets made by BMI (Process No. 1) and by Martin Co. (Process No. 2). The test conditions are listed in Table 1-15. In the table, B-6 denotes the plates made by Process No. 1, and M-1 the plates made by Process No. 2.

Table 1-15. Calculated ETR Irradiation Test Conditions for AARR Fuel Plate Specimens Containing 37 wt-% UO_2 in a Type 347 Stainless Steel Matrix

(Nominal oxide density = 80-85% T.D.)

	Cycle 70				Cycle 71			
Plate No.	Avg. Fiss. Rate, f/(gmU)(sec)	Avg. Ht. Flux,[a] Btu/(hr)(ft^2)	Avg. Burnup, % U^{235}	Avg./Max Surface Temp., °F	Avg. Fiss. Rate, f/(gmU)(sec)	Avg. Ht. Flux, Btu/(hr)(ft^2)	Avg. Burnup, % U^{235}	Avg./Max. Surface Temp., °F
M-1-926	1.49×10^{14}	1.37×10^6	8.6	240/282	1.57×10^{14}	1.33×10^6	21[b]	226/295
M-1-923	1.49×10^{14}	1.37×10^6	8.6	240/282	-	-	-	-
M-1-933	-	-	-	-	1.57×10^{14}	1.45×10^6	~13	233/306
M-1-925	1.49×10^{14}	1.37×10^6	8.6	240/282	1.57×10^{14}	1.33×10^6	21[b]	226/295
B-6-947	2.11×10^{14}	1.69×10^6	12.8	314/368	2.17×10^{14}	1.56×10^6	27[b]	295/327
B-6-952	-	-	-	-	2.17×10^{14}	1.67×10^6	~15	304/343
B-6-943	2.11×10^{14}	1.69×10^6	12.8	314/368	-	-	-	-
B-6-945	2.11×10^{14}	1.69×10^6	12.8	314/368	2.17×10^{14}	1.56×10^6	27[b]	295/327

[a]Maximum heat flux = 2×10^6 Btu/(hr)(ft^2).

[b]Total burnup for both cycles.

The net measured swelling in the fuel plate having the highest burnup was less than 3%. The highest burnup in these tests corresponds roughly to twice the average burnup in the 37 wt-% fuel at the end of core life in the AARR.

Extensive post-irradiation examination of the specimens is planned. The effect of burnable poison additions on the 37 wt-% UO_2-SST cermets also will be evaluated.

Fuel Assembly Development

A reference process for fabricating flat plates into close-tolerance rhomboidal assemblies has been established. During the course of developing techniques for jigging and bonding the 27-plate composites, six full-size subassemblies were made. Variations in the coolant channels were ultimately held to less than 0.0015 in. A seventh subassembly was incorporated in a full-size dummy fuel assembly. (See Fig. 1-36.) Overall tolerances on width, depth, and irregularities due to angular displacement and straightness were held to approximately ±0.015 in.

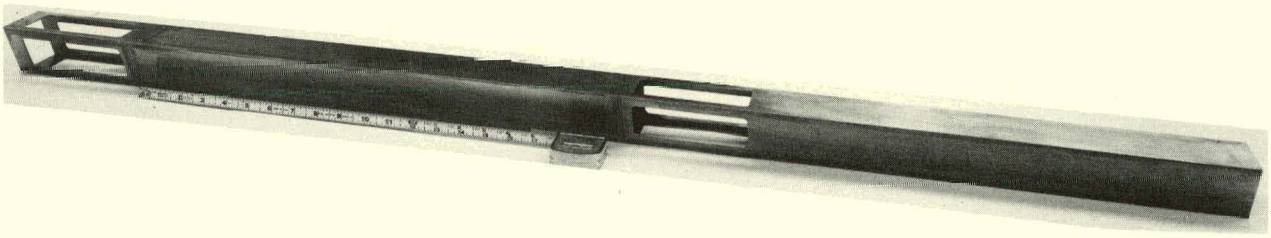

Fig. 1-36. AARR Full-Scale Dummy Fuel Assembly

Major emphasis has been on the attainment of complete bonding between the spacer wires and the fuel plates. This is important for strength and for heat transfer considerations. Special procedures for application of the braze material and preparation of the wires and plates for brazing are being evaluated in an effort to achieve a sound bond between all surfaces.

Consistent quality control is vital to the economic assembly of fuel plates in their respective subassemblies. Since the coolant channels are 0.040 in. deep, approximately 1.25 in. wide, and 20 in. long, post-fabrication examination of all joints in the 27-plate and the 47-plate assemblies will be extremely difficult as well as costly. Figure 1-37 shows a model 27-plate fuel assembly fabricated of Type 347 stainless steel by the Pyromet Corporation under subcontract to Argonne. Also shown is the microstructure of a typical sound braze between the spacer and fuel plate.

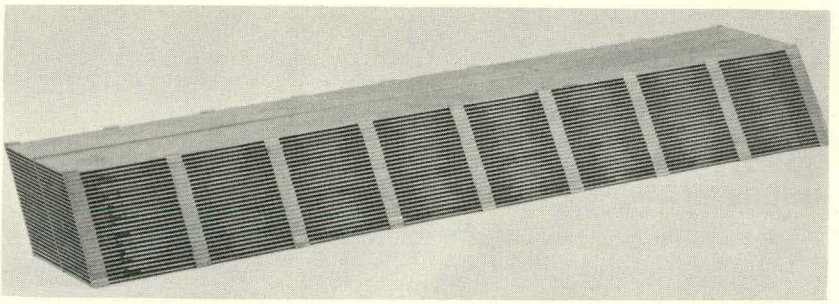

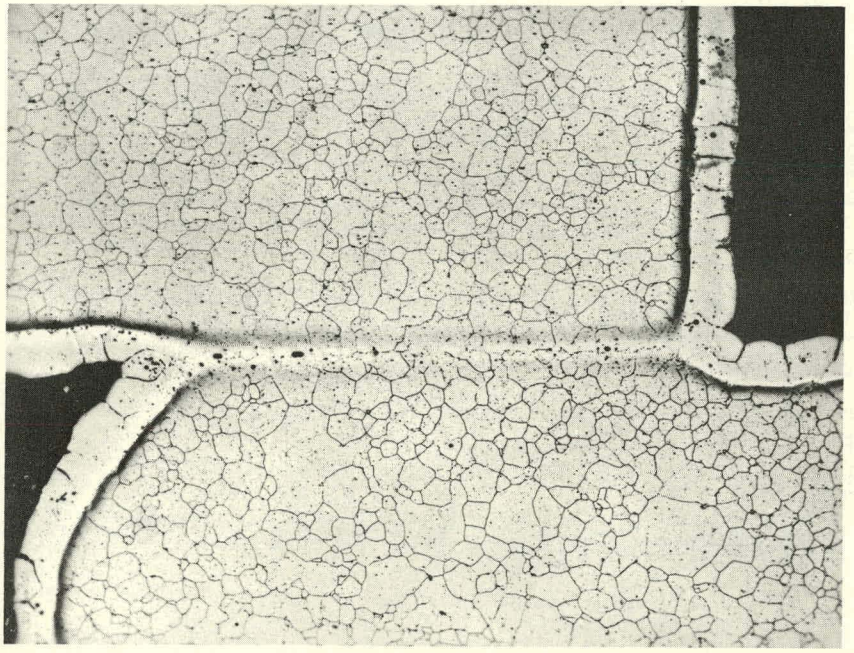

Fig. 1-37. (Top) Type 347 stainless steel model of 27-plate rhomboidal fuel assembly. (Bottom) Typical spacer-to-plate joint brazed with GE J8100 at 2135-2145°F for 2 hr. (Etched with 50% HNO_3 at 1.8 V for 40 sec.) 100X

Control Blade Material

Because of the heat limitations of high-density control materials in the very high gamma flux environment anticipated in AARR, attention has focussed on the lower-density, rare earth control materials. Blades of europium oxide-stainless steel cermets, in particular, were procured for physics evaluations in the AARR critical facility, for hydraulics tests, and for corrosion tests. These blades measure 0.200 in. thick, 5.500 in. wide, 22 in. long, and contain cermet cores 0.180 in. thick, 5.250 in. wide, and 18.00 in. long.

Control blade cermets containing 44, 45, and 53 wt-% $Eu_2O_3 \cdot 2TiO_2$ in Type 347 stainless steel, and 38 wt-% $Eu_2O_3 \cdot 2HfO_2$ in Type 347 stainless steel, were obtained from the Martin Company and Sylcor. Only the 53 wt-% europia-titanate and 38 wt-% europia-hafnate cermets approximate the net

neutron absorption characteristics of the 37 vol-% Eu_2O_3-SST cermet tentatively selected as a reference material. The other cermets will be evaluated to determine their effective "blackness," starting with proportions of oxide to stainless steel used in the Army reactors.

Some problems were encountered in stabilizing the Eu_2O_3 with 2 molar additions of HfO_2, and with fabrication of the full-size blade. Also, blistering was experienced during fabrication of the 53 wt-% $Eu_2O_3 \cdot 2TiO_2$-SST cermet blade. Special post-rolling treatment was required to resolve the blistering problem and to yield sound, full-density blades.

1.3.3.3 System Dynamics and Transient Analysis

Process Control Analysis

To assist in the design synthesis of appropriate AARR process control schemes, a mathematical model has been constructed which describes the instantaneous relationships between the control variables (flow, pressure, temperature) and reactor power. The point reactor neutron kinetics approximation is employed, with sectionalized thermal modeling of the reactor core, reflector, and primary heat exchangers. Coupled to these relationships for the primary system are those necessary to describe the dynamic behavior of the components which comprise each control loop. The latter relationships contain adjustable parameters whose values influence control performance.

The model is premised on the following preliminary control concepts:

(1) Coolant temperature is controlled at the outlet of the primary heat exchangers. This control is effected through automatic variation of the heat exchanger secondary flow, with anticipation provided through measurement of instantaneous power in the core and heat exchangers.

(2) Changes in primary system pressure are incurred by changes in coolant volume, which will be controlled through automatic variation of the degasification bleed. Constant feed from the pressurization pumps is assumed. The effect of surge tank air volume on pressure variations is considered.

(3) Coolant mass flow rate is monitored through a venturi and temperature measurement, and is controlled by an automatic drive for the primary pumps bypass flow valve.

(4) Reactor power is controlled automatically by a servo rod drive system using power range neutron detectors as input, periodically calibrated through measurement of reactor thermal power. Reactor power control is considered effective during performance studies of the process control loops.

The final overall plant model was programmed for an analog computer which was used to determine system performance. In these computer studies, constant mass flow of coolant to the reactor was assumed, based upon the assumption that the coolant temperature control system would hold temperature changes to within ±2°F, thereby limiting density changes to approximately 0.1%. Computer results on temperature control justified the assumption of constant mass flow.

The purpose of the analog studies was to determine feasibility of control concepts and examine plant performance in terms of control stability. The control goals formulated for steady-state operation were:

(1) Coolant temperature: ±1°F

(2) Coolant mass flow: ±1%

(3) Pressure: ±1%.

The results indicate that stable plant performance can be achieved with commercially available control components. Plant performance was studied under conditions of rapid power demand (0.5%/sec to 5%/sec). Close control was obtained on all parameters, indicating the feasibility of realizing the steady-state control goals. It is expected that closer system control can be demonstrated through additional computer studies directed toward optimization of control system parameters.

Transient Analysis and Safety Studies

Preliminary estimates of AARR dynamic behavior were made utilizing a modified version of a core model employed to predict the transient responses of HFBR.[5] The model describes core thermal properties and associated reactivity effects as they respond to various induced changes in steady-state conditions. Point reactor neutron kinetics equations are used in conjunction with a sectionalized thermal model which yields instantaneous material temperatures and steam generation in core regions where fuel plate surface temperatures exceed the local boiling point.

In addition, the model treats thermal conditions in a core coolant channel considered most susceptible to thermal failure. It includes the core hot spot and the effects of engineering design safety factors. Prediction of fuel plate burnout is made by comparing transient hot spot conditions therein with the Zenkevich-Subbotin steady-state burnout correlation.[2]

The model was programmed for an analog computer and a series of problems were completed which describe the transient response of the AARR core to a variety of reactivity disturbances introduced at equilibrium reactor power levels of 100 MW and 1 MW. The reactivity insertions consisted of step and ramp functions, with magnitudes ranging to well above

prompt critical. Input reactivity ramps were chosen such that the total insertion occurred in 33 ms, which is the coolant transit time through the core. Briefly, results indicated:

(1) The power response is stable, i.e., there is no evidence of significant power oscillations following the initial power burst.

(2) The effect of decreased initial power is to decrease the magnitude of peak power obtained during the short-term response.

(3) For the same total input reactivity, the effect of ramp rather than step insertion is to reduce peak power by factors ranging from 0.8 for \$0.75 reactivity to 0.5 for \$1.50 reactivity when initial power is 100 MW. No appreciable difference between the power response to steps or ramps is observed when initial power is 1 MW.

(4) For step reactivity insertions, the short-term power peak is reached within 13 ms after application of the step when initial power is 100 MW. When initial power is 1 MW, and the reactivity exceeds prompt critical, the time required to achieve short-term power peak is increased to a maximum of 60 ms for a \$1.00 step insertion.

(5) For the ramp reactivity insertions, the short-term power peak is reached within 6 ms after termination of the ramp (33 ms duration) when initial power is 100 MW. When initial power is 1 MW, and the reactivity exceeds prompt critical, this delay time is increased to a maximum of 52 ms after termination of a \$1.00 ramp.

(6) Reactivity compensation by steam voids is not significant for subprompt critical reactivity insertions.

(7) The threshold value of input reactivity which causes hot spot failure is approximately \$0.90 step insertion at initial reactor power of 100 MW. Burnout heat flux at the hot spot occurs in approximately 40 ms after application of the step. For ramp insertions, the corresponding threshold value is extended somewhat, ranging from \$0.90 to \$1.00. For the \$1.00 ramp, burnout heat flux at the hot spot occurs in approximately 14 ms after termination of the ramp.

For both step and ramp insertions at 1 MW reactor power, the threshold value of input reactivity for hot spot failure lies in the range \$1.10 to \$1.25. Burnout is reached in approximately 48 ms after application of a \$1.25 step, and 40 ms after termination of a \$1.25 ramp.

Three simulated operational abnormalities were also studied. These included: (1) continuous withdrawal of a control rod; (2) injection of cold water into the reactor; and (3) partial voiding of internal thermal column (ITC).

Case 1: A startup accident was simulated with the reactor critical at essentially zero power (2.4×10^{-4} watts) followed by the continuous addition of reactivity at a rate of $\$6.4 \times 10^{-2}$ per second. Since negligible reactivity compensation is developed (due to inherent feedback mechanisms) until reactor power reaches 1 MW, the initial portion of this problem was solved using a digital code (RE-101) without feedback. Values of reactivity, neutron density, and delayed neutron precursor concentrations were obtained for 1 MW power. These values were used as input conditions for the analog studies of the problem with feedback.

After initiation of the transient, the time to reach 1 MW power is 15.75 sec. At this time, total reactivity is \$1.01 and the reactor period is approximately 50 ms. Power continues to rise exponentially for an additional 140 ms to a level of approximately 12.5 MW. At this level, sufficient feedback reactivity is developed to reverse the exponential power rise. The ensuing power rise is accompanied by sufficient feedback reactivity such that the power rises nearly linearly with time. At 100 MW, which is reached 17.66 sec after initiation of the transient, the power rise rate is approximately 40 MW/sec. Termination of this excursion before hazardous conditions develop is considered well within the capabilities of the AARR safety systems.

Case 2: The consequences of injecting cold water into the reactor was examined by simulating the effects of instantaneous reduction in inlet water temperature from 135°F to 35°F. Although the physical realization of this condition is not feasible, it is considered to represent the theoretical upper limit insofar as the resulting power excursion is concerned. The transient was initiated from a simulated equilibrium reactor power level of 100 MW, with full coolant flow.

The reactivity produced due to cold water injection is that resulting from the combined effects of the negative temperature coefficients in the core and the positive coefficients in the ITC and Be reflector. However, in the simulation, no credit was taken for the beneficial effects of either the ITC or the Be reflector.

The net reactivity rises rapidly following reduction of inlet water temperature, and reaches a maximum value of approximately \$0.60 at 40 ms. The resulting power rise reaches a peak value of 240 MW at approximately 45 ms after initiation of the transient. Conditions at the hot spot remain well below the critical values required for burnout.

Case 3: In this study, it was assumed that uniformly distributed voids are swept into the ITC with the bulk water stream at a velocity of 4 ft/sec. This produces a linear reactivity addition at a maximum rate of \$12/sec, with a possible total reactivity addition of \$4.5. Control rod scram was assumed, with a high-flux signal occurring at a power level 30% above

nominal, a 25-ms rod declutching delay followed by 4-g acceleration of five of the six in-core control rods.

If the reactor is operating at 100 MW, the power level rises rapidly to a maximum value of 250 MW in approximately 90 ms after the beginning of the transient. The control rod high-flux trip point (130 MW) is reached in approximately 20 ms, and the action of the safety system is effective in limiting the net reactivity to a maximum of $0.60 and then shutting the reactor down. Local boiling conditions are reached at the hot spot, but heat fluxes remain well below critical values.

Similar calculations based on an initial reactor power level of 1 MW, indicate that the reactor will be shut down without damage, provided the control rod high-flux trip point is set for the low-power range.

1.3.3.4 Component Design and Evaluation

Reactor Vessel

A conceptual design of the pressure vessel and internals has been completed. (See Fig. 1-38.) Designed for 800 psig and 350°F, the vessel measures 8 ft in diameter and approximately 24 ft long. Selection of vessel material and final arrangement of the vertical and horizontal irradiation facilities is contingent upon completion of a comprehensive stress analysis.

Preliminary stress calculations were made on an all-stainless steel vessel. These calculations were based on an elastic deformation analysis in accordance with ASME Boiler and Pressure Vessel Code, Section III: Nuclear Vessels (1963 Edition). This analysis revealed that a large proportion of the wall stress is caused by differential thermal expansion. This is to be expected because of the high heat generation in the wall, and the low thermal conductivity - high expansion coefficient of stainless steel. Also, the yield strength for stainless steel decreases very rapidly with temperature. In this instance, the code-recommended stress limits exceeded the yield strength. Consequently, stainless steel-clad, carbon steel (SA 212 B) is being considered as an alternate vessel material.

Accurate theoretical stress analysis at the vessel midplane is difficult because of the large number and proximity of penetrations for beam tubes. Moreover, the penetrations are not normal to the vessel; rather they are tangent to an 18-in.-diameter inner circle. To date, approximate stresses at the beam tube penetrations have been computed by ignoring the existence of other nozzles. Total stresses were mapped by the method of superposition.

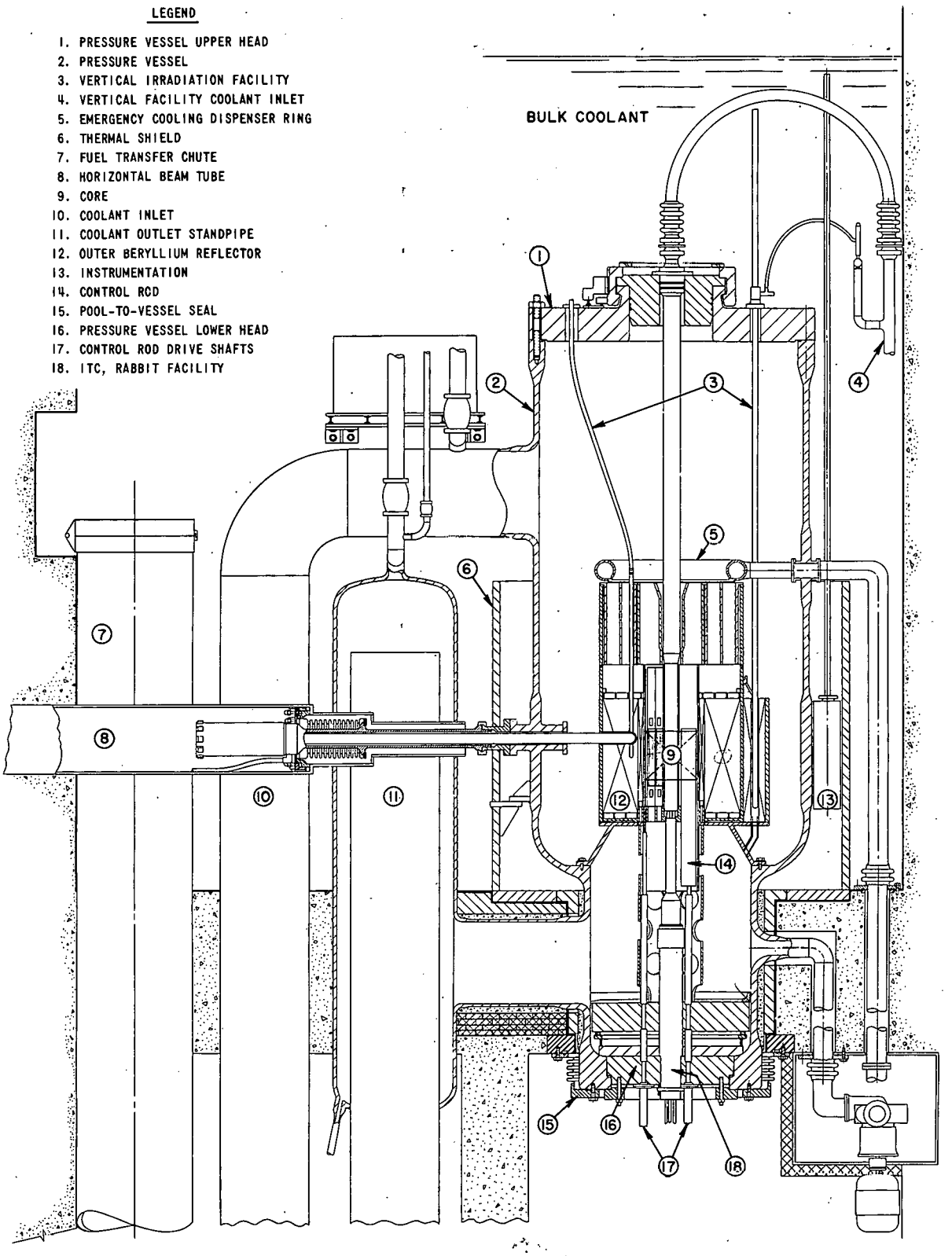

Fig. 1-38. Conceptual design of AARR pressure vessel

However, stress approximations in the vicinity of the nozzles are essential in determining the maximum feasible number of beam tubes. Therefore, a computer program has been written to calculate the stresses in the vicinity of a reinforced circular hole. The machine output is then used to evaluate the stress concentration factors for different combinations of plate thickness, outlet wall thickness, and outlet diameter. An outlet-wall thickness of 2 in. has been tentatively selected, based on a stress concentration factor of ~2.2 at the critical point. This will be re-examined when more reliable information on gamma heating is available and the beam tube layout is completed.

Experimental Facilities

Horizontal Beam Tubes. The function of the horizontal beam tubes is to furnish a collimated beam of high-intensity thermal neutrons leading from the core to the experimental face of the biological shield. Environmental conditions within the vessel require that the tubes be designed to withstand (1) a collapsing pressure of 800 psig; (2) thermal stresses created by gamma heating; and (3) irradiation damage from sustained exposure.

Figure 1-39 shows a conceptual design of the blind beam tubes proposed for use in the AARR. (A similar design is contemplated for the through-tubes.) Basically, the design is characterized by a bolt-breech mechanism for connecting the tubes to their respective nozzle openings in the reactor vessel, and for making the transition to the penetration in the shield tank and biological shield. The bolt-breech connection is also employed to facilitate remote-controlled assembly or disassembly of the beam tube for repair or replacement.

With reference to Fig. 1-39, the blind beam tube assembly comprises six major components: (1) aluminum beam tube; (2) stainless steel shield penetration; (3) stainless steel beam tube adapter; (4) collimator (not shown); (5) bolt-breech connectors; and (6) shield tank transition bellows. The integrated assembly performs four major functions:

(1) Seals the beam tube to the vessel nozzle against 800-psig pressure.

(2) Seals the tube adapter to the stainless steel shield penetration in the biological shield.

(3) Compensates for thermal expansion, misalignment, and movement of the tube between the reactor vessel and stainless steel shield penetration.

(4) Provides initial collimation of the neutron beam.

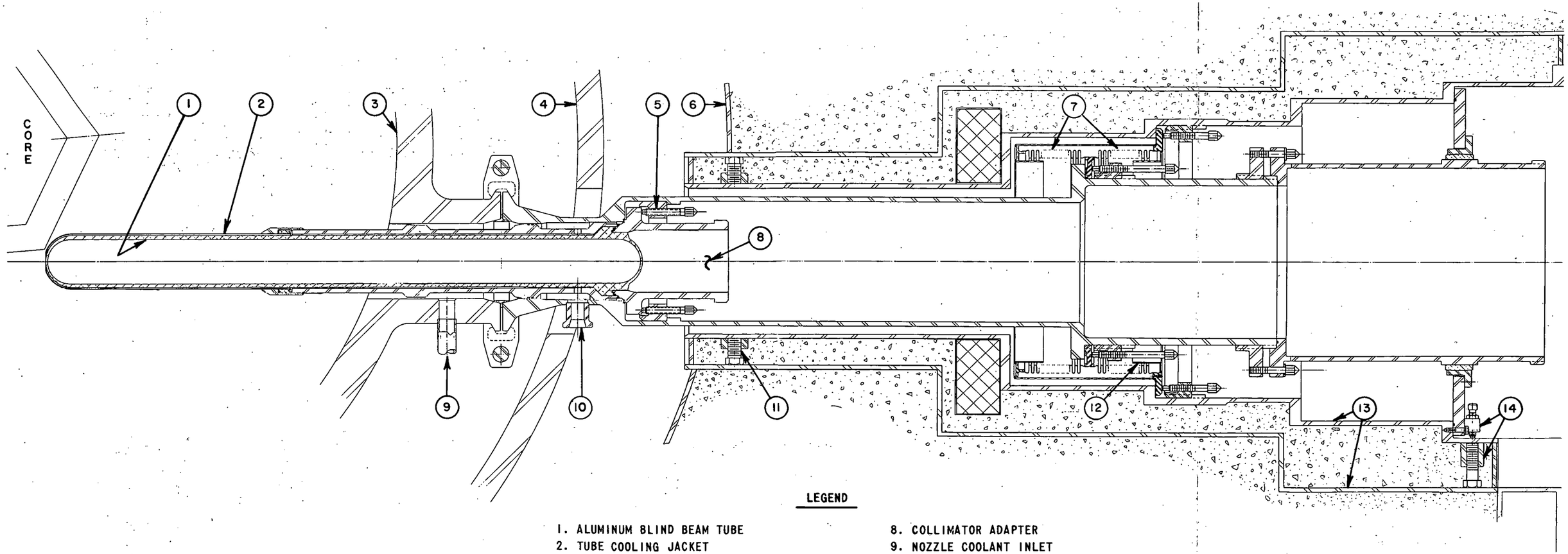

LEGEND

1. ALUMINUM BLIND BEAM TUBE
2. TUBE COOLING JACKET
3. REACTOR VESSEL
4. THERMAL SHIELD
5. BOLT-BREECH CONNECTORS
6. SHIELD TANK
7. SHIELD TANK TRANSITION BELLOWS
8. COLLIMATOR ADAPTER
9. NOZZLE COOLANT INLET
10. BEAM TUBE COOLANT INLET
11. ALIGNMENT BOLTS
12. ADAPTER BREECH LOCK
13. BIOLOGICAL SHIELD LINERS
14. ALIGNMENT BOLTS

Fig. 1-39. Plan view of conceptual blind beam tube installation in AARR

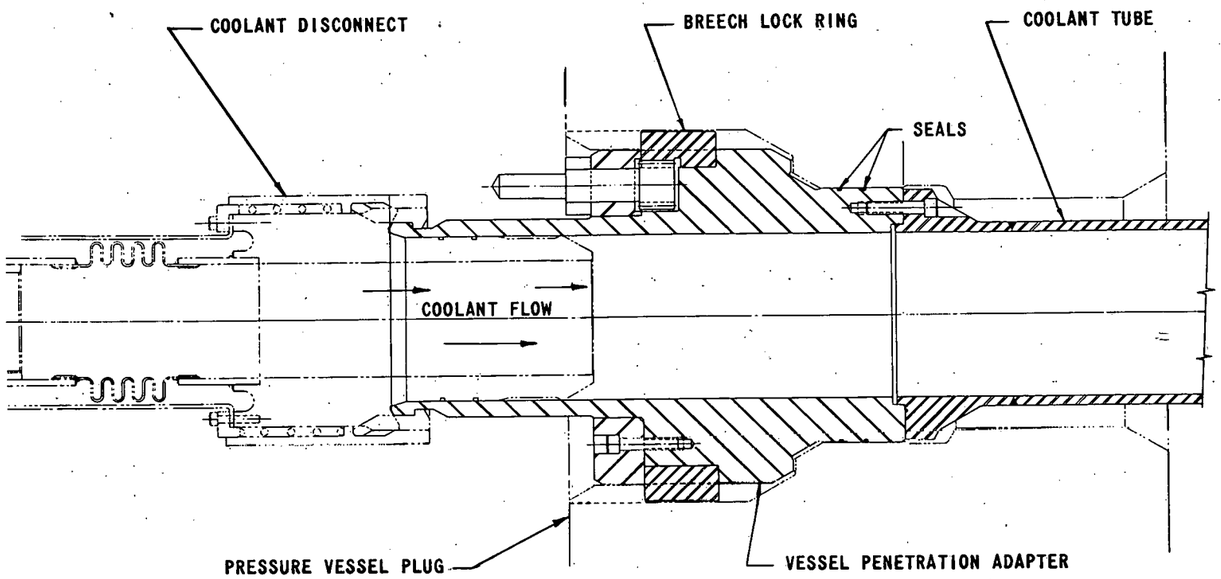

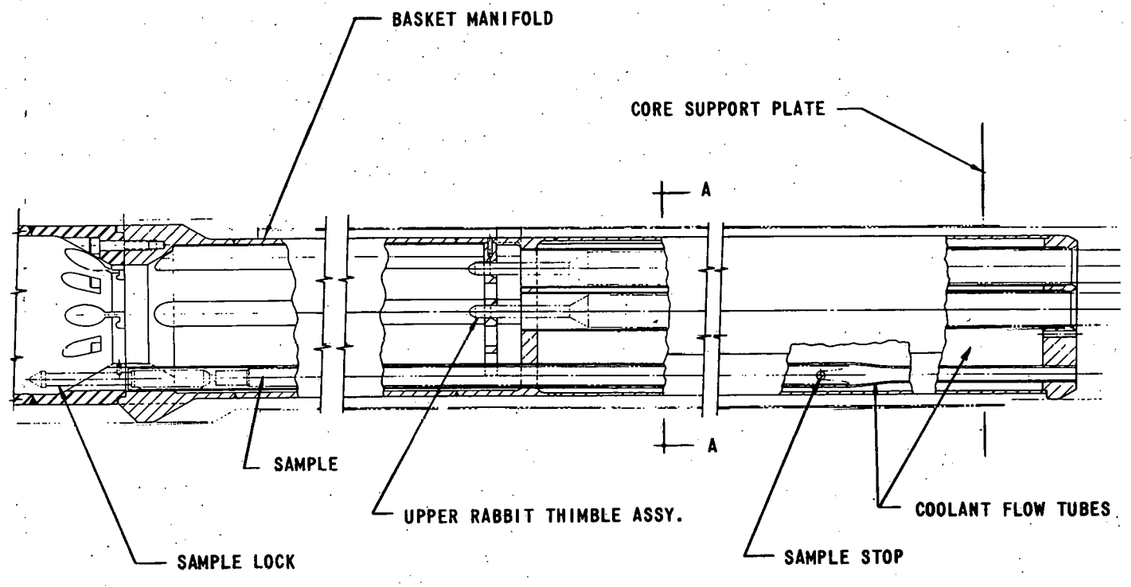

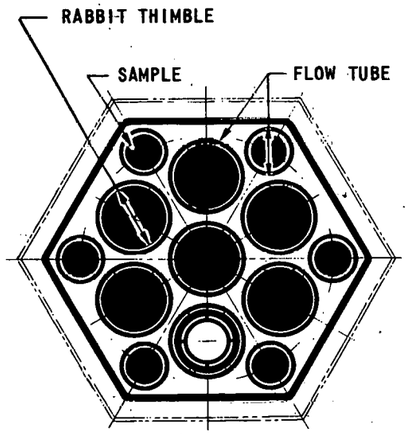

SECTION A-A

COMPOSITE SECTION SHOWING RABBIT THIMBLE IN PLACE

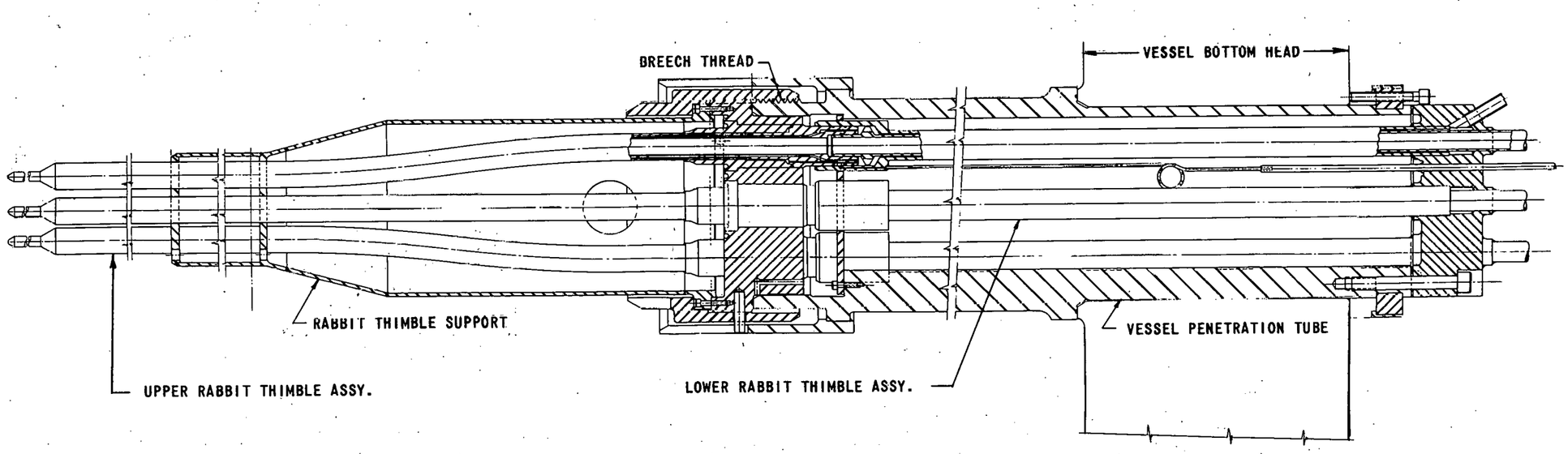

Fig. 1-40. Sectional views of upper and lower Internal Thermal Column Assembly

Briefly, the beam tube consists of an aluminum pressure tube encased in a thin-walled aluminum jacket. Both jacket and tube are inserted into an aluminum sleeve which lines the opening in the reflector. The sleeve is sealed to the reflector shroud. Cooling water enters through the beam tube adapter and flows through the annulus formed by the tube and jacket toward the tip of the beam tube. At this point, the flow reverses, enters the annulus formed by the sleeve and jacket, and ultimately discharges into the reactor vessel.

A preliminary stress analysis of the beam tube was completed, by Franklin Institute, early in March, 1964. In general, thermal gradients and stresses were determined in order to set the bounds for the allowable wall thicknesses of the aluminum tube. A two-dimensional, electrical analog was used to determine the temperature distribution and cooling requirements. The results showed that the temperature can be kept below 300°F with flow rates of 11 to 12 ft/sec, and inlet coolant temperatures up to 175°F.

A prototype blind beam tube will be fabricated to facilitate further development and refinement of the conceptual design.

Vertical Facilities. A review of the vertical facilities by various experimenters has reflected an increase in the number and type to be installed in the Internal Thermal Column. More specifically, design layouts are being prepared to accommodate six basket-type (long-term exposure) and seven hydraulic-operated (short-term exposure) rabbit facilities.

The most promising arrangement is the interlocking assembly shown in Fig. 1-40. The upper half contains the six baskets. It is sealed to and supported by the central shield plug which penetrates the vessel top closure. The integral assembly is removed prior to fueling operations. The lower half contains seven, re-entrant rabbit facilities which penetrate the vessel bottom head and supporting structure. This assembly remains stationary during refueling operations.

The core zone apparatus within the hexagonal I.T.C. tube is cooled by primary coolant from either of two sources, the discharge being made into the main stream below the core support plate. The shown method (Fig. 1-40) uses independently monitored primary coolant from a branch loop which enters through the top head of the vessel closure into the coolant tube. (See Item 4, Fig. 1-38.) The coolant flows downward into the basket manifold where it cools both the baskets and the outer tube of the rabbit facilities. A second method would extract primary coolant from the upper portion of the reactor vessel through holes in the coolant tube and, utilizing the reactor core pressure drop, would effectively cool the apparatus in the same manner.

The seven hydraulic rabbit facilities are operated and cooled independently by auxiliary water systems. Connections to these systems are made through the bottom vessel head.

The rabbit tubes terminate in one of several common or paired unloading stations in the canal adjacent to the hot cell in the Laboratory and Office Building. At this point, the encapsuled specimen is either (1) temporarily stored in the canal; (2) loaded into a shielded cask for off-site shipment; or (3) inserted in a secondary, pneumatic rabbit system for rapid delivery to the experimenter's laboratory.

A prototype of the I.T.C. apparatus will be built to verify the hydraulic parameters, structural adequacy, and ease of handling, maintenance, and repair.

REFERENCES

1. D. H. Lennox et al, *Status Report on the Argonne Advanced Research Reactor*, ANL-6451 (November, 1961).
2. B. A. Zenkevich and B. I. Subbotin, *Critical Heat Fluxes in Subcooled Water with Forced Circulation*, Atomnaya Energiya 3, 149 (1957).
3. R. S. Pyle, *STDY-3: A Program for the Thermal Analysis of a Pressurized Water Nuclear Reactor During Steady State Operation*, WAPD-TM-213 (June, 1960).
4. *Preliminary Stress Analysis of the AARR Fuel Assembly*, NUS-242 (June 15, 1965).
5. J. M. Hendrie and H. J. C. Kouts, *Preliminary Hazards Summary Report on the Brookhaven High Flux Beam Research Reactor*, TID-14771 (May, 1961).

1.4 EXPERIMENTAL BOILING WATER REACTOR (EBWR)

Plutonium Recycle Experiment

1.4.1 Summary

Early in 1962, the Division of Reactor Development requested Argonne National Laboratory to participate in the Plutonium Recycle Program, with particular emphasis on the research that could be explored experimentally in the EBWR Facility. The purpose of the joint Argonne-Hanford program which evolved as a result of this request is to obtain information on the use of plutonium fuel in light-water, thermal reactor systems. Such utilization could be made in either an all-thermal plutonium recycle system, or in the thermal part of a mixed fast-thermal reactor complex.

Development of either concept requires essentially the same physics information, in particular, basic data on the isotopic behavior of plutonium as it is irradiated in a thermal reactor. Therefore, it is desirable that the experiment be made as simple as possible; so that it will yield the necessary information in a form which is readily amenable to analysis. Accordingly, the following considerations were regarded as significant: (1) that modifications to EBWR be kept to a minimum; (2) that EBWR should remain a boiling-water system; and (3) that it be used primarily as an irradiation facility, rather than in support of an active reactor development program.

During the fiscal reporting period, the principal efforts of the Reactor Engineering Division were focussed on activities related to conversion of the EBWR to meet the needs of the program. These activities ranged from preventive maintenance of auxiliary systems and piping, to rigorous inspection, repair, modification, and/or replacement of major components and systems. Concurrent efforts in direct support of the program included: (1) development of a reference core design and an improved control rod assembly; (2) establishment of a pressure vessel material surveillance program; and (3) participation in the preparation of the safety analysis report[1] on the proposed Plutonium Recycle Experiment.

1.4.2 Plant Inspection, Modifications, and Maintenance

Argonne's participation in the Plutonium Recycle Program was prefaced by a rigorous radiographic, ultrasonic, magnaflux, and dye-check inspection of all critical primary systems and components comprising the EBWR plant complex. The observations made during the course of this inspection resulted in numerous repairs, modifications and a materials surveillance program, all designed to ensure safe and reliable operation of the plant.[2]

1.4.2.1 Reactor Pressure Vessel

The upper half of the vessel interior was subjected to a series of non-destructive and destructive tests. These tests were triggered by visual and dye-penetrant inspections which revealed numerous surface defects in the Type 304 stainless steel cladding. This cladding consists of eight butt-welded panels (0.109 in. thick, 32 in. wide, 110 in. long) that are spot-welded to the wall of the SA 212B steel vessel.

Many of the defects were disclosed as through-cracks by introducing nitrogen at 800 psig between the cladding and the vessel wall, and covering the clad surfaces with a foaming detergent. (See Fig. 1-41.) The through-cracks were clearly defined in five of the eight panels. No through cracks were found in the other panels.

Approximately 40 linear feet of cracks were alternately ground and inspected with a dye penetrant. In general, the cracks appeared to increase in size and number, suggesting origination at the clad-wall interface. (See Fig. 1-42.) These operations were extended through the clad-wall interface and slightly into the vessel wall. Boat samples (1/2 in. wide, $2\frac{1}{2}$ in. long) of the cladding, which included some SA 212B material, and strips of the vessel clad (1/2 in. wide, 8 in. long) were subjected to rigorous chemical and metallurgical tests, including bend tests. In all cases, there was no evidence of crack propagation into the vessel wall. Corrosion of the interfaces was limited to a thin film of mill scale (Fe_3O_4). There was no evidence of local pitting or gross generation of iron oxide (Fe_2O_3).

The lower half and lower head of the vessel were not examined because of high radiation levels and inaccessibility posed by the core support structure and thermal shield. However, it was observed that cracking of the clad was most severe in the steam dome area, with progressively less cracking below the water line.

Tests were also made on (1) remnants of Type 304 clad, SA 212B material which were salvaged during initial fabrication of the vessel in 1955; (2) a clad test plate fabricated by the vendor in 1959; and (3) a section removed from the vessel in 1960. In all cases, similar cracks were observed, but again there was no evidence of crack propagation into the vessel wall. Photomicrographs of sections through the clad, spot weld, and vessel wall indicated that the cracking originated at the clad surface rather than at the clad-wall interface.

The foregoing inspections and supporting tests have not clearly defined the actual mode of fracture in the cladding. However, the observations made during these tests support the belief that it is highly improbable that subsequent cracks will propagate into and impair the integrity of the vessel wall. The cladding was never calculated as a strength factor of the vessel; it was installed to inhibit corrosion of the SA 212B vessel material. Partial removal of this protection (see Fig. 1-43) has resulted in total

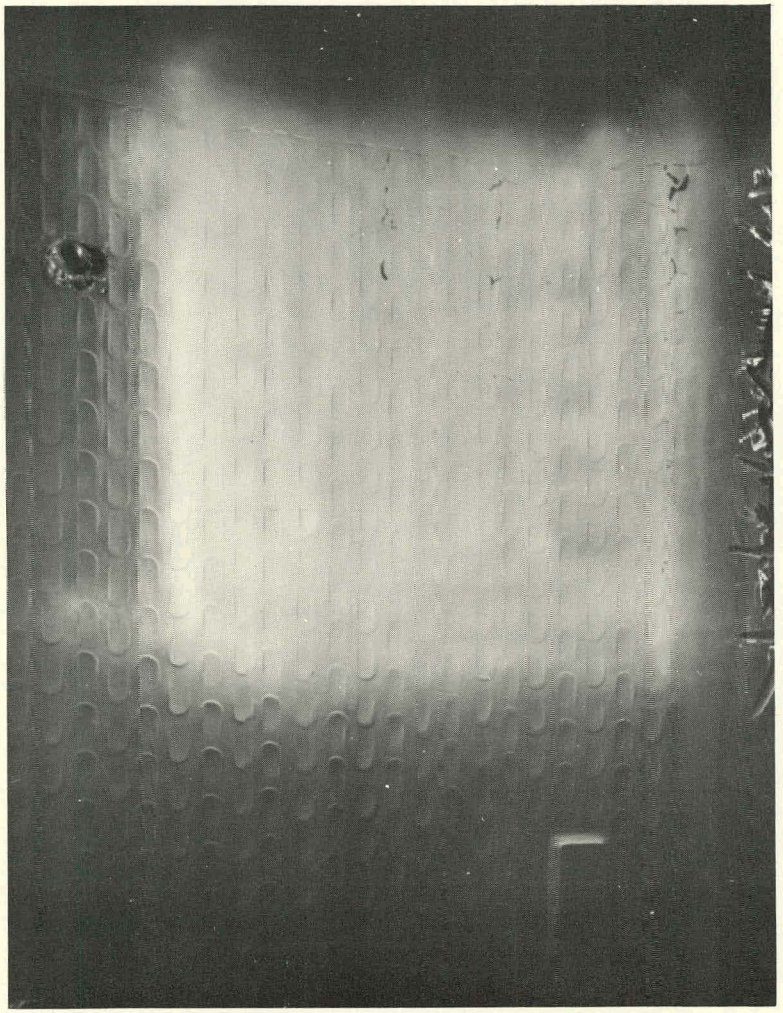

Fig. 1-41. Typical dye-penetrant indications of cracking in Type 304 stainless steel cladding

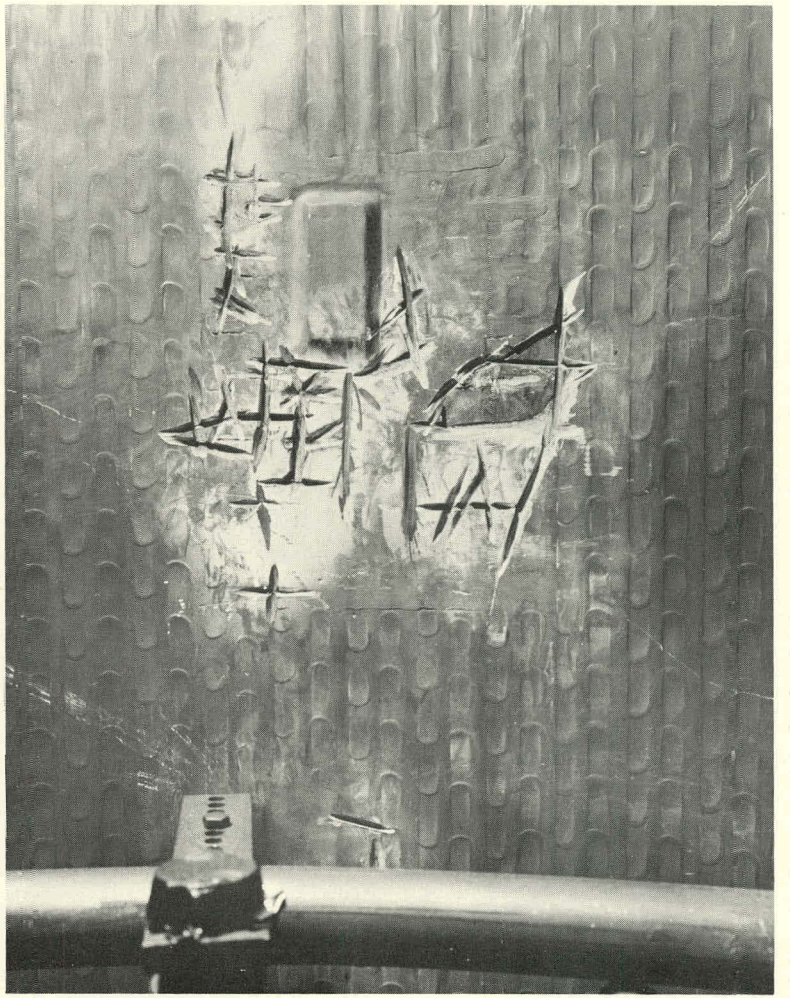

Fig. 1-42. Post-grinding appearance of panel having greatest number of initial "surface defects." Also see panel No. 8 on Fig. 1-43.

exposure of about one square foot of SA 212B material to the reactor coolant. Inasmuch as it is not proposed to reclad these areas, a vessel materials surveillance program has been established to monitor for possible adverse changes in the cladding and carbon steel wall during subsequent operations.

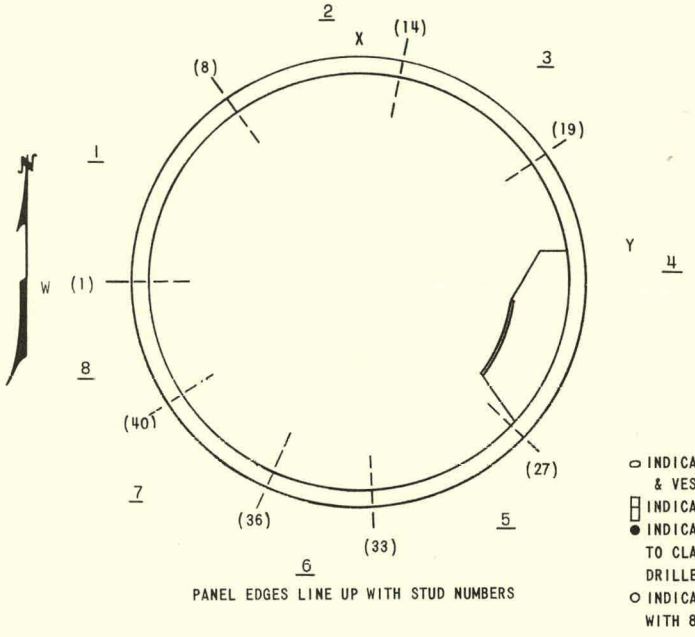

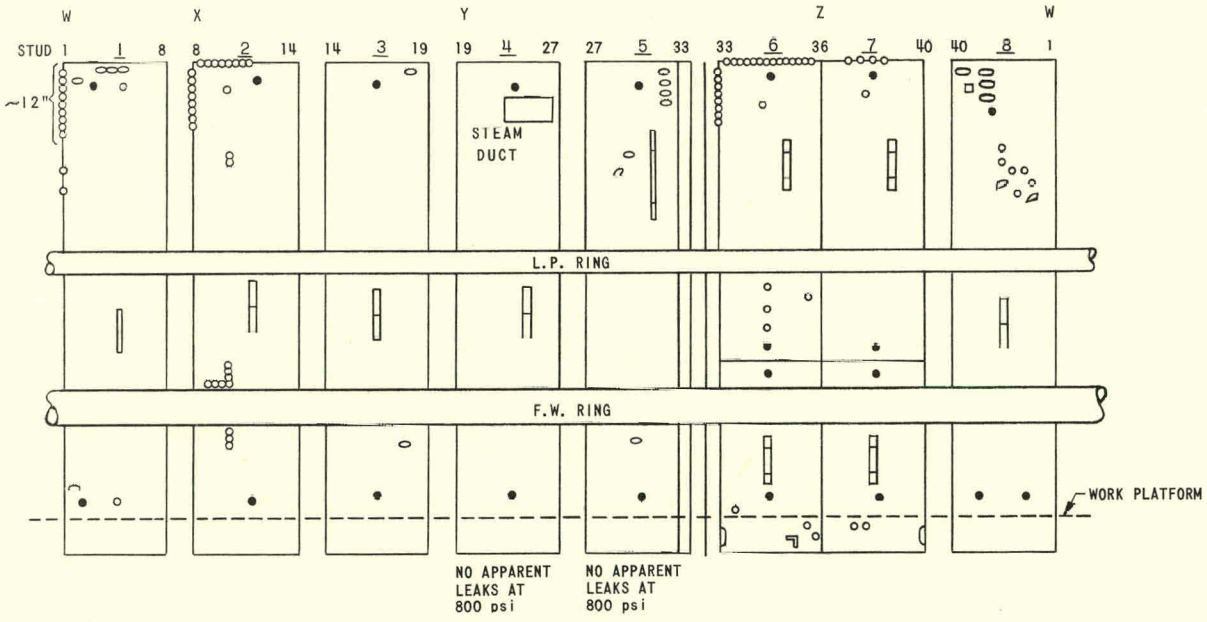

Fig. 1-43. Pictorial summary of EBWR vessel inspection, showing areas of vessel material exposed by removal of boat and strip specimens

This surveillance program has involved a comprehensive literary and photographic documentation of the current state of the cladding and base metal. An optical depth micrometer has been used to establish corrosion reference points for the SA 212B steel. During scheduled shutdown periods, similar measurements will be made to determine the extent and significance of any evidence of additional corrosive attack.

Dye-penetrant tests of the cladding will be made and the results compared with reference photographs to identify the onset of new cracks. These tests will be conducted on four areas of the upper course of cladding. Specifically, they include two panels (one in the water zone, one in the steam zone) that were clear of surface defects, and two panels (in the same zones) that showed evidence of surface cracks. To facilitate these tests, the upper shock shield (which covers the clad region in the water zone) has been modified. This modification consisted of installing two removable panels over the cladding areas to be monitored in this zone. No changes have been made in the steam zone since sufficient area is available for inspection and testing.

Dye-penetrant tests also will be made on the exposed surfaces of the SA 212B base metal to determine whether cracking has been initiated. Detection of any incipient cracks will be cause for re-evaluation of the experimental program.

Surveillance of the vessel base metal will include radiation effects. Five capsules, each containing 15 specimens, have been prepared for this purpose. Two capsules will be installed in each of two "bare" and two "shielded" irradiation test thimbles located adjacent to the core. Accelerated irradiation of the specimens in these thimbles will provide advance warning of any potential structural changes that may be induced in the vessel itself. The fifth capsule will be located in the steam dome.

Subject to experimental verification, the steam dome region will be modified to include an improved steam-water separating baffle. Designed for installation on the existing core riser, this baffle consists of an inverted, perforated, truncated cone fabricated from 1/8-in.-thick stainless steel Type 304. Its effectiveness will be determined by comparison with reactor operating conditions without the baffle installed. If successful, improved steam-water separation should allow operation at higher power levels ($\geq$40 MW) and thus accelerate the Plutonium Recycle Experiment.

1.4.2.2 Removal of Forced Circulation Tees

The original EBWR design included provisions for future conversion from a light-water, natural circulation system to a system which would permit experimentation with both forced circulation and heavy-water operation.

One provision consisted of four 6-in. pipe extensions of nozzles located at the bottom of the vessel. These extensions terminated in pipe tees in the subreactor room and in close proximity to the control rod drive mechanisms.

Although one branch of each of three tees was connected to a blowdown system, radioactive corrosion products collected in their side branches and could not be removed. (It is believed that introduction of air during past experiments resulted in entrainment of the products to the far recesses of these branches.) Consequent high radiation levels precluded personnel access for maintenance of the control rod drives. The fourth tee, which is connected to the water purification system, has never accumulated any significant amount of radioactive products.

To prevent any future buildup of highly activated products, the other three tees were replaced with vertical, tapered pipe sections. Those sections are also connected to a blowdown system and are valved at the bottom to facilitate periodic cleanout.

1.4.2.3 Primary System Piping Welds

Radiographs of the Kanigen-plated steam piping and the balance of stainless steel piping revealed a very high percentage of defective welds. These defects ranged from unfused weld roots and voids, to longitudinal, transverse, and crater-type cracks. Repair of the steam piping was effected, in part, by welding two half-shells over the defective welds. The stainless steel piping was repaired by the conventional technique of grinding out and rewelding. All repair welds were inspected radiographically.

Similar inspection of the high-pressure boric acid system resulted in replacement of all piping and fittings. A completely new piping arrangement was installed, with improved routing of the absorber material, and with one-third the number of welds.

Sonic wall thickness measurements indicated that the condensate piping was sound and relatively unaffected by water corrosion. However, radiographs revealed several cracked welds. These cracks were ground out and rewelded. Since the maximum pressure in these lines is about 12 psig, the welding requirements are based primarily on mechanical loading and vibration.

1.4.2.4 Primary Purification System

A review of the operating history of this system revealed numerous failures of the canned-rotor pumps, and instances where the subcooler heat exchangers did not meet design performance specifications. These pumps and subcoolers were replaced with larger-capacity counterparts. The corresponding piping and valving was revised and instrumented consistent with improved efficiency, reliability, and flexibility of operation.

1.4.2.5 Feedwater Full-Flow Filters

The feedwater system is equipped with four full-flow filter units. Units No. 1 and No. 2 are constructed of carbon steel with roll-bonded stainless steel cladding; they represent the initial installation. Units No. 3 and No. 4 are constructed throughout from Type 304 stainless steel; they were installed during modification of EBWR for 100-MW operation.

Units No. 1, No. 3, and No. 4 were adjudged amenable to repairs or reinforcing in order to meet code requirements. However, the entire longitudinal seam of Unit No. 2 was cracked beyond economical repair. Since sufficient filtering capacity is provided by three filters, Unit No. 2 was removed from service.

1.4.2.6 Retubing of Main and Recovery System Vent Condensers

Both condensers were completely retubed with 18 BWG Admiralty brass tubes. Inspection of the 6063-T831 aluminum Alclad tubes in the main condenser showed severe pitting on surfaces exposed to the circulating cooling water. Moreover, eddy-current measurements on 26% of the 1158-tube complex revealed that 234 tubes has less than 75% of the original wall thickness remaining.

The original aluminum tubing in the vent condenser also showed evidence of corrosion similar (but to a lesser degree) to that which necessitated retubing of the main condenser.

Inhibited Admiralty brass tubing was specified as the alternate tubing material. Available data on water chemistry and corrosion product distribution indicates that the brass constituents will not introduce any significant corrosion problems. Treatment of the circulating coolant has been adjusted consistent with the change in tube material.

In addition to retubing the main condenser, the desuperheater-deaerator piping arrangement was modified to eliminate back-pressure buildup of radioactive gases in the deaerator vent line. These gases ultimately leaked through the packing of the deaerator safety valve into the containment building. The modification consisted of cutting the common piping between the two components, sealing off the desuperheater side, and adding a diffuser plate on the deaerator side to prevent impingement of the steam on the condenser tubes.

1.4.2.7 Containment Shell Main Air Lock Doors

Structural analysis of these doors indicated that the fillet welds between the stiffeners and the door plates were prone to overstressing, depending upon the stress-intensification factors employed. Subsequent

magnaflux testing of these fillets revealed three partially cracked welds on the inner door. These cracks were ground out and re-welded.

As a precautionary measure against further fillet weld cracking, reinforcing members were welded on both inner and outer doors. Extreme care was exercised to minimize heating and consequent warpage of the doors. The success of these operations was evidenced by subsequent leak tests on the doors and door seal faces. There was no measurable leakage.

1.4.3 Supporting Research, Design, and Development

1.4.3.1 Reference Core Design

The reference core (Fig. 1-44) measures 5 ft in diameter and is designed to accommodate a total of 147 fuel subassemblies (effective fuel length = 4 ft) loaded in three zones as follows: 36 plutonium test fuel subassemblies in a central, square zone (Pu); 60 enriched uranium subassemblies in an intermediate zone (E); and 51 natural uranium subassemblies in the outer zone (U).

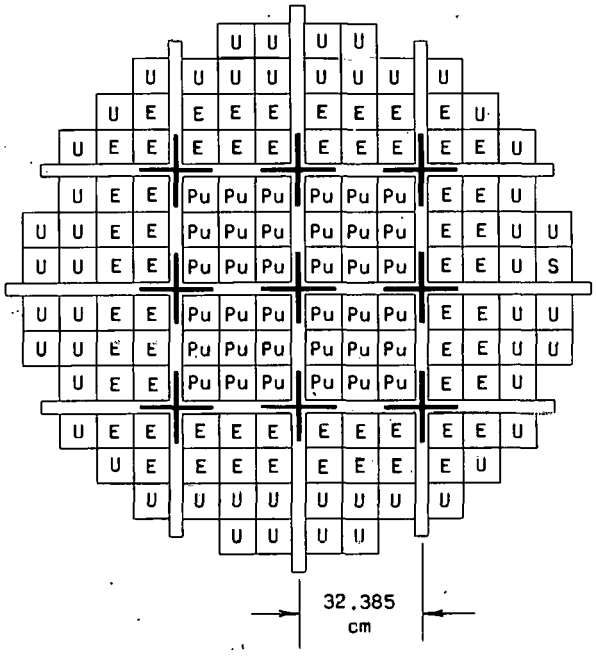

Fig. 1-44. Plan view of reference core loading for Plutonium Recycle Experiment

Fuel Subassemblies. Each fuel subassembly contains 36 Zircaloy-2 tubes arranged in a square lattice. Each tube measures 0.372 in. O.D., with a wall thickness of 0.025 in.

The fuel in the central test subassemblies is composed of 1.5 wt-% PuO_2 - 98.5 wt-% depleted UO_2 mixed oxide, which is loaded into the tubes by vibratory compaction. Unlike their counterparts in the intermediate and outer zones, the subassemblies in the central zone are of a "take-apart" design, to facilitate withdrawal and replacement of individual fuel tubes. This feature is essential to the conduct of periodic analyses for isotopic content as a function of fuel burnup. Figure 1-45 shows these and other details of the plutonium test fuel subassemblies for the central zone.

Subassemblies in the intermediate zone are fueled with UO_2 pellets enriched to 6 wt-% U-235. The composition includes a burnable poison: 0.158 wt-% Eu_2O_3 and 0.0288 wt-% Sm_2O_3. These pellets are mechanically

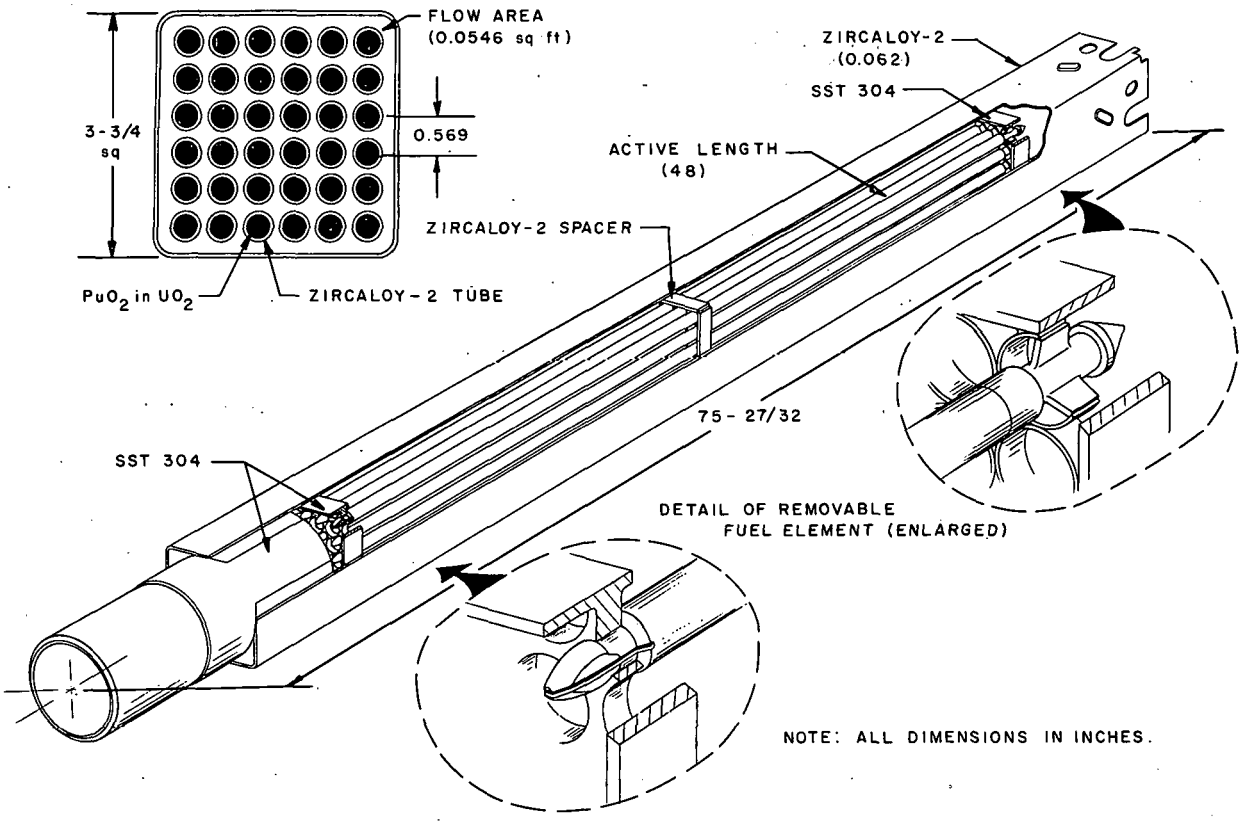

Fig. 1-45. Sectional views of Plutonium Test Fuel Subassembly

loaded into the Zircaloy-2 tubes. Subassemblies in the outer zone are loaded similarly, but with natural UO_2 pellets.

After being loaded, each tube is evacuated, backfilled with dry helium or mixed argon-helium gas at atmospheric pressure, and sealed with Zircaloy-2 plugs welded at each end. Prior to welding the top end plug, a stainless steel spring is compressed above the fuel rod. The primary purpose of the spring is to maintain a gap for collection of fission gas released during irradiation of the fuel to a design burnup of ~25,000 MWd/tonne. A gap of 5.5 in. is maintained above the fuel in the central, plutonium-bearing elements, while a gap of 3.5 in. is maintained above the enriched uranium and the natural uranium fuel rods. The spring also serves to prevent shifting of the fuel rod during shipment or loading into the reactor.

The fuel tubes in each subassembly are supported and positioned at each end by a stainless steel grid, and at the center by a Zircaloy-2 spacer grid. Each support and spacer grid, in turn, is contained within, and fastened to, a 3.75-in.-square can (0.062-in. wall). The can is fabricated from rolled, formed, and welded Zircaloy-2 strip stock. All subassemblies are positioned in the core support grid by respective locating-tip, bottom-end fittings.

Control Rods. After completion of the 100-MW experimental program, but prior to unloading the fuel, the reactor vessel was filled with water to facilitate examination of the nine control rods. These included eight rods made of 2% boron-stainless steel, and a center rod made of hafnium. One rod at a time was disconnected from its drive mechanism and lifted out of its guide shroud sufficiently to expose the poison section and the Zircaloy-2 follower. The surfaces of these components were then scanned with a strong light and a mirror. Questionable areas were scrutinized with the aid of a boroscope.

The surfaces of all rods were covered with the usual reddish-brown iron oxide. Although the hafnium rod had accumulated 100,000 cycles during the course of the transfer function measurements, it appeared to be in good condition. Upon completion of the examination of all control rods, the hafnium rod was transferred to the fuel storage pit pending use in future oscillation tests.

The only defect noted during this examination was a missing rivet head in the transition zone of a boron-stainless steel rod. When this rod was subjected to a "rap and wedge" test, two more rivet heads broke loose. Microscopic examination of the rivet shanks indicated that failure was promoted by intergranular cracking combined with severe mechanical distortion. It is believed that owing to the differential thermal expansion between Zircaloy-2 and stainless steel, sufficient strain (0.010 cm at 250°C) developed in the outermost rivets to cause a shear-type failure of the rivet shank.

Because of the questionable condition of approximately 400 of the rivets used in the eight rods, and the fact that rods of greater reactivity worth were desirable for the plutonium recycle core, eight highly-enriched, 2 wt-% boron-stainless steel rods and one hafnium rod were ordered. The new hafnium rod will be used as a spare.

Several changes were made in the design of the boron-stainless steel rods. As shown in Fig. 1-46, the riveted transition sections were replaced with tongue-and-groove joints. These joints eliminate the stress due to differential thermal expansion of the poison and follower materials by allowing relative motion to occur between the dissimilar sections. When assembled, the control rod components are held in alignment by a central, 1/2-in.-square stainless steel bar. This bar is integral with the cross guide follower and extends throughout the length of the control rod. It is secured by a threaded end which is tack-welded in place. By removing the handling tip from the upper end of the control rod, the rod may be disassembled for ease of handling or independent replacement of either the poison or follower section.

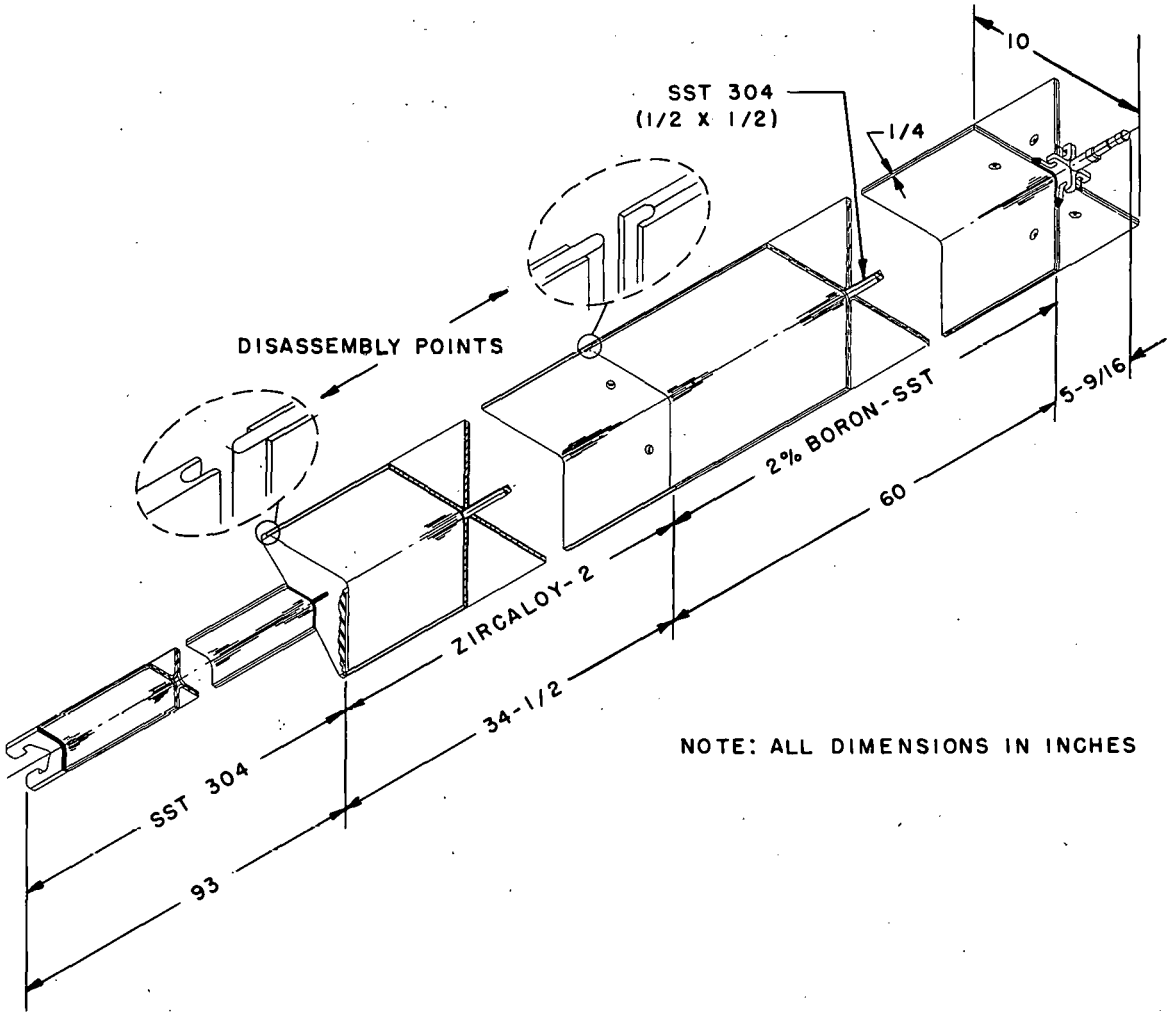

Fig. 1-46. Sectional views of control rod for Plutonium Recycle Core

1.4.3.2 Plutonium Fuel Storage Rack

Prior to being transported to an off-site processing plant, irradiated fuel subassemblies will be stored, for a predetermined decay period, in the water-filled storage pit which is adjacent to the reactor vessel.

While this method of storage provided a simple solution to the shielding problem, it did pose a criticality problem. Calculations based on loading plutonium-fueled subassemblies into the original storage rack within the pit indicated that the amount of absorber material was insufficient to reduce multiplication much below 30. Therefore, the rack has been replaced with an assembly designed to limit k_{eff} to less than 0.811.

The new rack is similar in size and shape to the old one. The differences are limited to the number of storage openings and the amount of absorber material incorporated in the egg-crate-type structure. There

are 143 openings (as compared to 148 in the old rack). Each opening measures $4\frac{1}{16}$-in. square, with intervening walls of 1/4-in. thick stainless steel plates which contain 1.4% natural boron. The walls of the old rack were fabricated from 1/8-in. thick stainless steel and 1 wt-% natural boron-stainless steel plates.

1.4.3.3 Heat Transfer Characteristics and Hydrodynamics of Pu Recycle Core

Past experience with EBWR has shown that the hydrodynamic characteristics are adequate to permit sustained operation at power levels well above 40 MW. The plutonium recycle core is composed entirely of rod-type fuel subassemblies which are geometrically very similar to those used in the "spike" region of the Core IA loading during operation to 100 MW. Since the average power density in the new core will be lower than that in Core IA, it is expected that the operation with the new elements will be free of hydrodynamic difficulties.

Although the power distribution and the average hydraulic equivalent diameter in the plutonium core are somewhat different from the values found in Core IA, it is expected that the recirculation flow rate will be similar to that measured in Core IA at 42 MW. Because of this and the aforementioned observations, some experimental values from Core IA operation have been incorporated into the following calculations in order to predict more accurately the actual operation of the plutonium recycle core.

A number of power-void iterations were carried out using two codes programmed for the IBM-704 computer: the PDQ neutron diffusion theory code, and the CHOPPED hydrodynamic program. The CHOPPED code is a revision of RECHOP which has been used extensively for EBWR calculations. The new code features a faster iteration procedure; thus it was possible to generate relationships between local average void fraction and power level at a given burnup.

Figure 1-47 is a composite plot of the hydrodynamic characteristics calculated for an initial power level of 42 MW. Plots (1) and (2) show the radial and axial power density distributions, respectively. The highest average (and the peak) power density occurs in the first shim zone. Plot (3) indicates a fairly uniform inlet velocity distribution even though the natural uranium zone has a much lower power density than the other core zones. This occurs because the outer zone receives a large share of the driving head in the upper riser, while the friction loss is low because of the low void fraction in the zone. Finally, plots (4) and (5) show, respectively, the variation in radial exit void fraction and the axial behavior of the void fraction at the average power density in each zone.

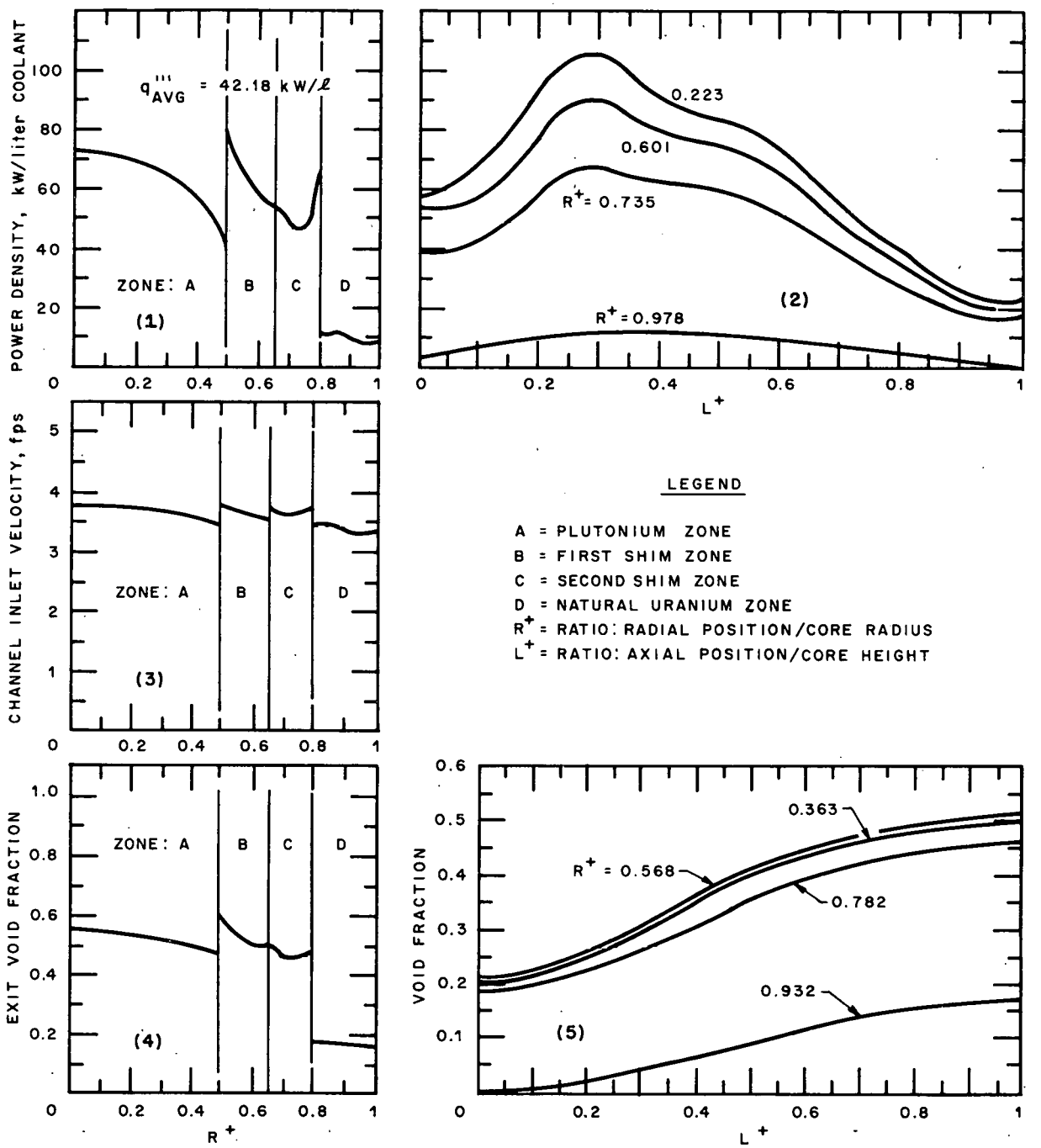

Fig. 1-47. Calculated hydrodynamic characteristics of Plutonium Recycle Core for an initial power level of 42 MW

Table 1-16 lists the most significant heat transfer characteristics of the core that were derived from the same computer program. The maximum heat flux [191,000 Btu/(hr)(ft^2)] occurs at the innermost edge of the first shim zone at a height of about 1.1 ft, and is well below the predicted burnout flux [~800,000 Btu/(hr)(ft^2)]. All power densities are expressed per liter of coolant contained within the fuel element boxes.

Table 1-16. Heat Transfer Characteristics of Plutonium Recycle Core at 42 MW and Zero Burnup

Reactor Power, MW	42	Plutonium Zone	
Operating Pressure, psig	600	Average Power Density, kW/liter	61.75
Operating Temperature, °F	489	Total Power, MW	15.06
Average Steam Void Fraction[a]	0.262	First Shim Zone	
Average Steam Void Fraction[b]	0.210	Average Power Density, kW/liter	64.98
Equivalent Diameter of Coolant Channel, ft	0.0461	Total Power, MW	12.32
Total Core Heat Transfer Area, ft^2	2327	Second Shim Zone	
Core Power Density, kW/liter		Average Power Density, kW/liter	50.58
Average	42.17	Total Power, MW	10.96
Maximum	130.5	Natural Uranium Zone	
Core Heat Flux, Btu/(hr)(ft^2)		Average Power Density, kW/liter	10.59
Average	61,600	Total Power, MW	3.66
Maximum	191,000	Fuel Centerline Temperature, °F	
Total Recirculation Flow Rate, lb/hr	7.51 x 10^6	Core Average	881
Average Steam Quality at Core Exit	0.0235	Core Maximum	1672
Estimated Carryunder	0.264	Integrated Fuel Conductivity, watt/cm	
Subcooling at Core Inlet, Btu/lb	2.0	Core Average	5.2
		Core Maximum	16.1

[a]Based upon coolant volume in fuel box.

[b]Based upon coolant in typical core lattice.

A study was also made to determine the sensitivity of the time-dependent isotopic changes to the local average void fraction. While some effect is apparent, the differences are not great enough to justify the extensive instrumentation required to obtain accurate measurements of local void fraction. Corrections will be made on the basis of previous calculations and measurements of reactor power level.

1.4.3.4 Reactor Kinetics

Transfer function measurements will be made prior to each successive increase in power to predict the highest level of stable operation. Digital sampling equipment will be used in conjunction with a binary noise reactivity input to obtain the middle- and low-frequency portion of the transfer function curves. This method of measurement provides the maximum amount of information in a minimum of time. The high frequencies will be obtained by sinusoidal control rod movement.

A change-over from the IBM-704 to the CDC-3600 computer has necessitated revision of the codes which reduce the digital data to transfer function information. These codes include the operations of auto-correlation, cross-correlation, and noise rejection. Revision of the codes is scheduled for completion in early fiscal 1966.

REFERENCES

1. B. J. Toppel, P. J. Vogelberger, Jr., and E. A. Wimunc, *Safety Analysis Associated with the Plutonium Recycle Program*, ANL-6841. (To be published.)

2. N. Balai, C. R. Sutton, E. A. Wimunc, and R. F. Jones, *Inspection, Evaluation, and Operation of the EBWR Reactor Vessel*, ANL-7117 (November, 1965).

1.5 ARGONNE RESEARCH REACTOR (CP-5)

1.5.1 Stress Analysis of Vessel Coolant Distribution Plenum

During the evaluation of CP-5 for proposed operation at powers up to 10 MW, it was recognized that enhancement of the core heat transfer characteristics at these powers would necessitate a marked increase in coolant flow rate through the fuel assemblies. It was also recognized that increasing the flow rate would reflect an increase in pressure drop through the assemblies. The limiting factor would be the stresses imposed on the reactor vessel coolant distribution plenum.

A theoretical stress analysis of the plenum had been performed during the early design stages of the CP-5 reactor. In the absence of any reference data for such a complex structure and loadings, the calculations were based upon conservative assumptions which yielded a plenum design rating of 20 psi. However, a review of the reactor operating history revealed that the maximum coolant pressure drop across the plenum has never exceeded 14.5 psi. In-reactor measurement was impractical; therefore, in order to verify the calculated design value, an essentially identical mock-up of the plenum was constructed for a comprehensive stress analysis up to the rated value of 20 psi, and then to destruction.

The shape and complexity of the installed plenum is evidenced by the mock-up unit shown in Figs. 1-48 and 1-49. Both constructional and environmental factors were considered during its fabrication and subsequent testing. These included fabrication according to the original drawings, using the same material (Type 1100-0 aluminum) and techniques. Radiation and corrosion damage over an 11-year period in the reactor was considered insignificant. With respect to radiation, the total integrated neutron flux (nvt) for neutron energies greater than 0.13 keV is less than 10^{18} n/(cm^2)(sec). Limited studies show no significant changes in aluminum up to 10^{20} nvt.

In-reactor forces affecting the plenum were also considered. As mentioned previously, the plenum pressure increases consequent to

increased coolant flow rate and pressure drop through the fuel assembly. Conversely, since the subassembly is seated in the plenum by gravity, the external force on the plenum at this point decreases as the internal pressure increases. Therefore, the following variables were used to simulate reactor dynamics over the entire operating range:

Metal temperature	10°C to 60°C
External loading (dead weight at each fuel assembly location)	0-200 lb
Internal pressure	Zero to metal yield threshold and, finally, to destruction

Strain gauges were installed on the basis of a Stresscoat analysis. This analysis gave the directions of the principal normal surface stresses and, also, some indication of the interior bending moments. (See Fig. 1-48.) In this manner, the effect of a particular load on the plenum could be measured.

Analysis of the test data indicated a maximum differential pressure of 19.5 psi without permanent deformation of the plenum. Failure of the mock-up occurred at 61 psi. When extrapolated to actual operating conditions, with the plenum submerged in 72 in. of heavy water, the corresponding values are 22.3 psig and 63.8 psig, respectively.

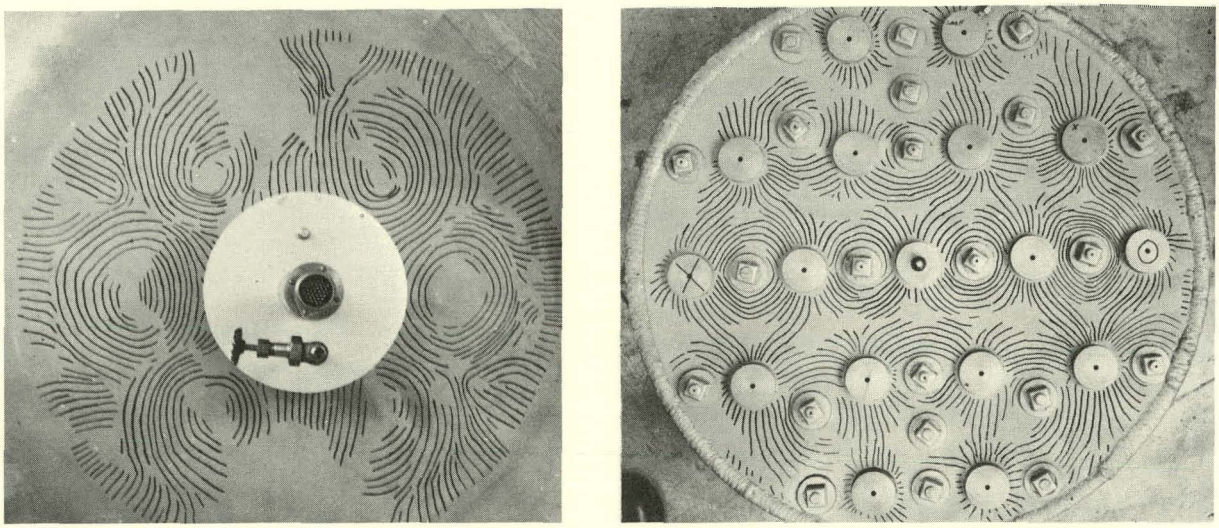

Fig. 1-48. Stress patterns on (left) bottom and (right) cover plates of CP-5 plenum mock-up. (Patterns are outlined in ink for legibility. Stresscoat No. 1207; 18 psig; 73°F.)

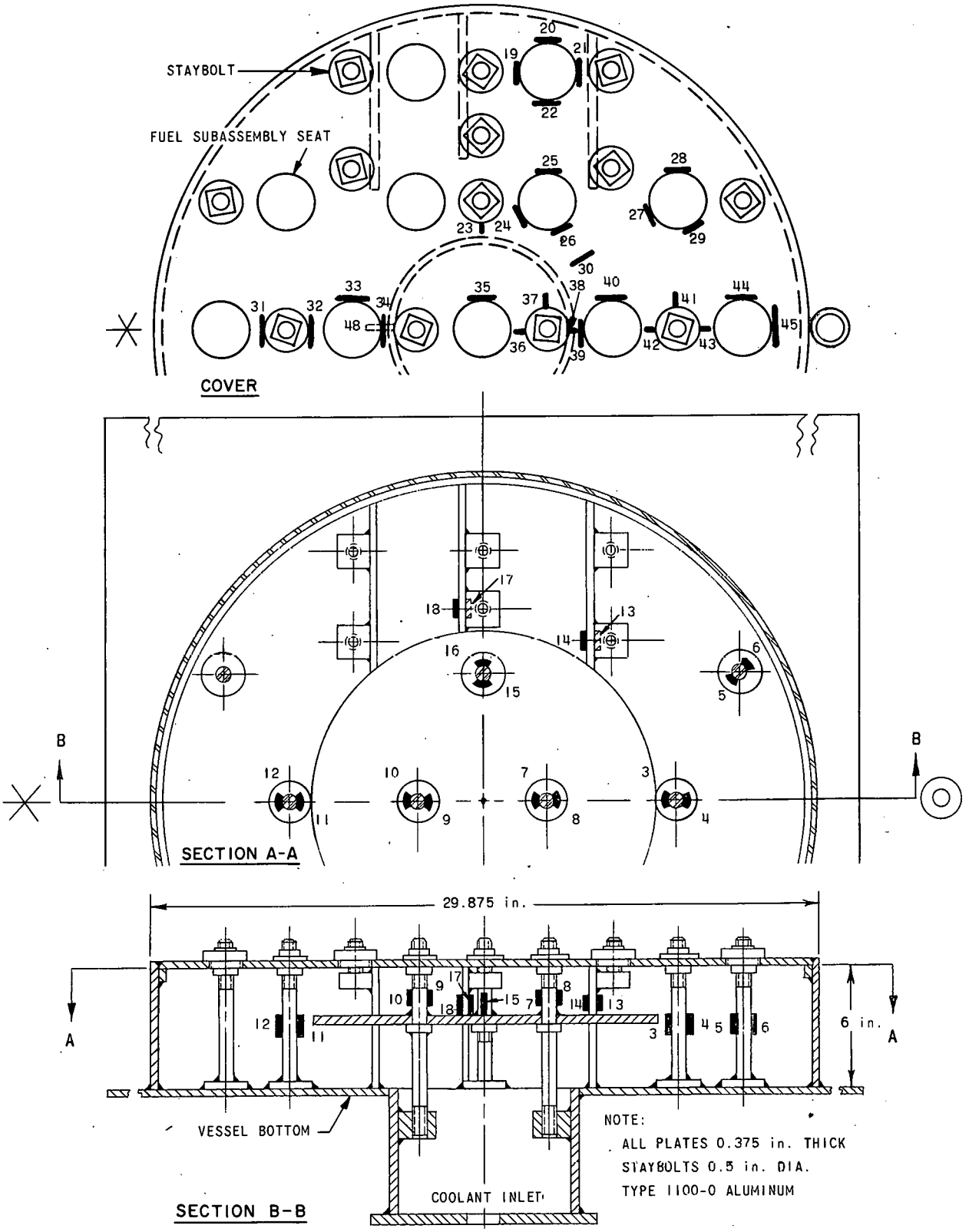

Fig. 1-49. Sectional views of CP-5 plenum mock-up, showing location of strain gauges

1.6 ARGONNE NUCLEAR ROCKET PROGRAM

1.6.1 Objective and Scope

The objective of the Argonne Nuclear Rocket Program is to determine the technical feasibility and potential of a refractory metal-fueled, fast reactor system for spacecraft propulsion. This includes establishment of the estimated performance of the rocket system and an investigation of its advantages and limitations short of a full-scale reactor test.

Three major avenues of effort have been identified as essential to the successful achievement of the program goal. These are: (1) development and testing of fuel elements; (2) development of a core structure and testing of its structural integrity; (3) establishment of adequate and reliable reactor control capability.

1.6.2 Reference Systems

Two reference systems have been selected to facilitate investigation of these problem areas: a 100,000-lb-thrust topping cycle, and a 10,000-lb-thrust bleed cycle. The comparative sizes and design parameters of both systems are shown in Fig. 1-50.

In each system, the reactor consists essentially of a cylindrical core of W-UO_2 cermet fuel elements contained within an Inconel X-750 pressure vessel. This vessel is surrounded by a preheater section and a radial beryllium reflector. The latter also contains twelve, pneumatically-driven, cylindrical control drums spaced at 30-degree intervals around the core periphery. In the fuel shutdown position, the 120-degree poison sector of each drum is adjacent to the core. Startup is accomplished by rotating the drums 180 degrees, thereby replacing the poison sector with a 240-degree beryllium sector.

In the topping cycle (Fig. 1-51), hydrogen propellant is pumped into the entrance manifold of the regeneratively-cooled nozzle and then up through the respective nozzle tubes. The flow continues into an extension of the nozzle which surrounds the core, and emerges into a forward plenum between the pressure vessel and the preheater-radial reflector-control drum section. At this point, a fraction of the flow is cycled through the fueled preheater; the remainder passes through and cools the reflector-control drum section.

The total flow merges in an after plenum where it is ducted to the topping turbine. Here, a small stream is bled off to power the control drum drives. From the turbine, the propellant is discharged into the forward plenum upstream of the reactor, where it cools the core support plate and

axial reflector before entering the active core region. From the core, hydrogen at 4500°F passes through a short plenum, and exhausts through the convergent-divergent rocket nozzle.

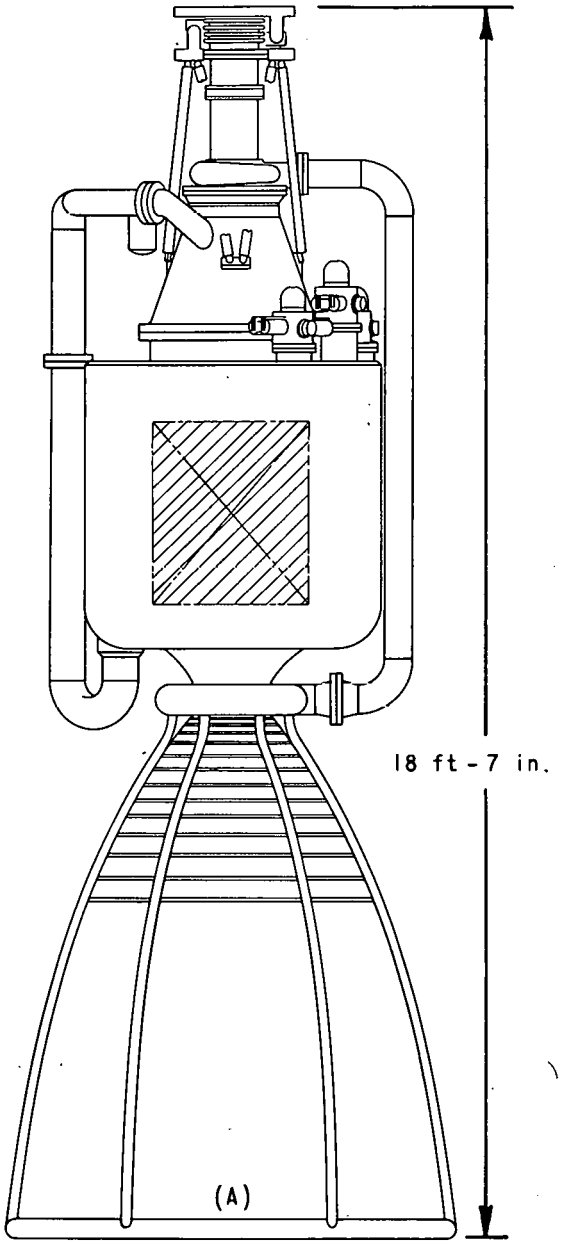

DESIGN PARAMETERS

SYSTEM	(A)	(B)
REACTOR CORE POWER, MW	2,000	213
SPECIFIC IMPULSE, sec	836	813
THRUST, lb	100,104	10,000
OPERATING TIME, hr	>1-10	>1-10
RESTART CAPABILITY, cycles	3-40	3-40
HYDROGEN FLOW RATE, lb/sec	119.7	12.27
ENGINE WEIGHT, lb	20,813	2,860

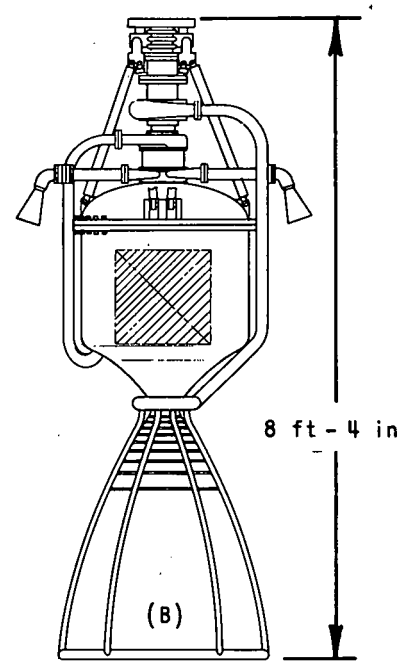

Fig. 1-50. Comparative sizes and design parameters of (A) 100,000-lb-thrust topping cycle and (B) 10,000-lb-thrust bleed cycle selected for feasibility studies of refractory metal-fueled, fast reactor rocket systems

In the bleed cycle, hydrogen is bled from the nozzle to operate the turbopump, mixed with the cover gas, then passed through the turbine and exhausted overboard. Elimination of the preheater results in a weight saving, which is important in small engine applications.

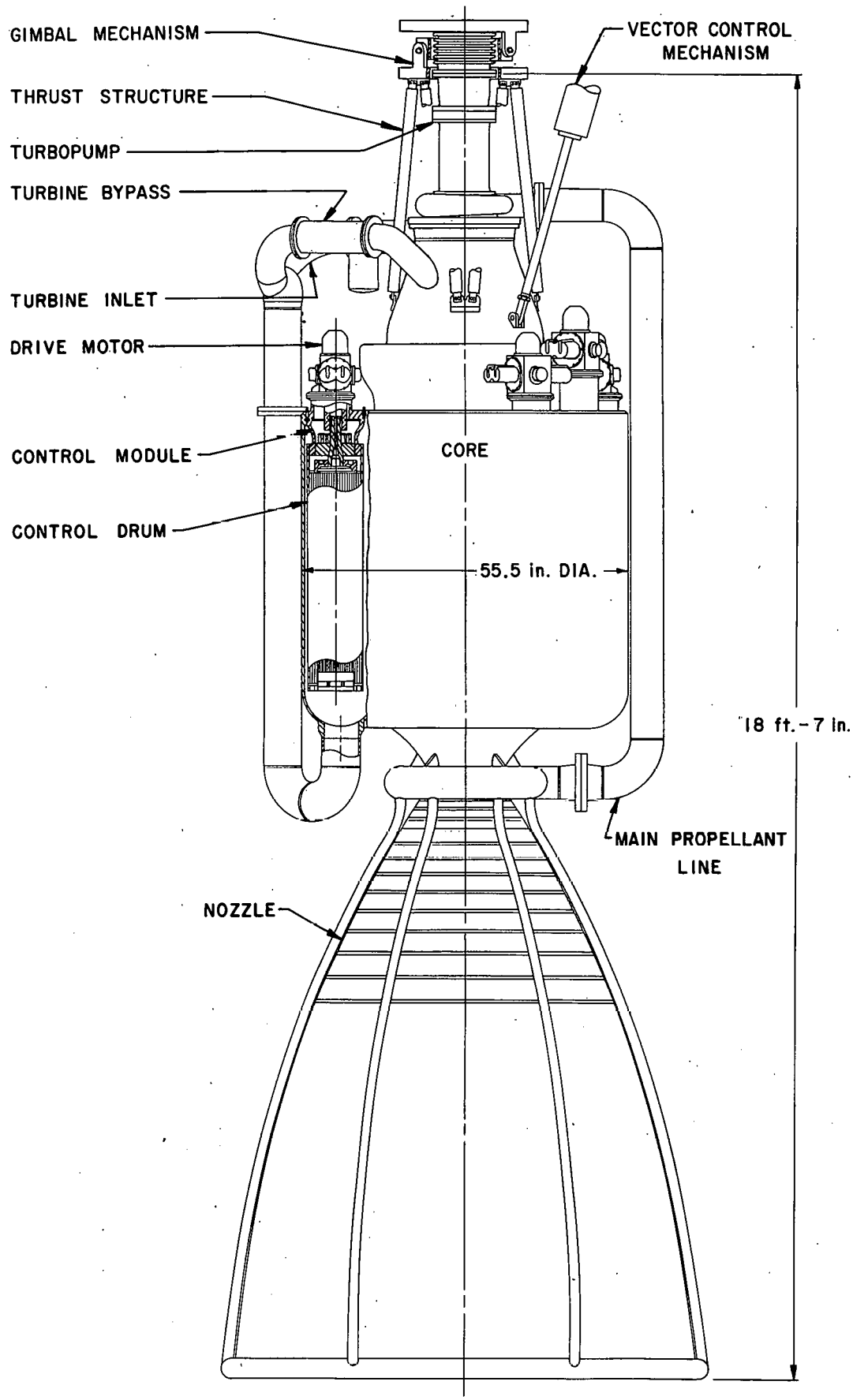

Fig. 1-51. 100,000-lb-thrust refractory metal-fueled fast reactor rocket engine

Current programmatic efforts are directed toward defining the design and development problems associated with the 10,000-lb-thrust bleed cycle.

1.6.3 System Analysis

System analysis comprises four parallel efforts: (1) steady-state analysis, (2) uncertainty analysis, (3) system dynamics analysis, and (4) analysis of advanced concepts. The objective is to predict the operating characteristics of the rocket engine and thus to provide numerical guidance for design decisions.

A portion of the analytical effort has been allocated to writing, procuring, and/or reprogramming of computer codes to perform the complicated analyses required for this reactor. Some of the codes that are available as a result of this effort are:

(1) FRANTIC - an adaptation of an AGN code (HECTIC II) that calculates steady-state flow and temperature distributions in a variety of parallel multi-channel configurations.

(2) OPTIONAL GEOMETRY - a versatile code for computing compressible flow, heat transfer and pressure drop in single channels.

(3) DESIGN - developed at Lewis Research Center, this code provides a nozzle design consistent with various input parameters.

(4) NOZZLE - calculates the axial variation in coolant pressure, temperature distributions, nozzle wall temperature, and heat flux in a given nozzle design.

(5) BIRDIE - a steady-state cycle analysis program that is readily adapted to any pumping cycle and system configuration.

(6) SHUTDOWN - calculates the fission product heat release rates and the integrated power as a function of time, for various shutdown schedules.

(7) PSA-II - a parametric analysis to determine optimum reactor core configurations and engine operating characteristics for various limiting conditions.

(8) TABHP; TABTP - subroutines developed at Los Alamos to calculate accurately the properties of para-hydrogen.

1.6.3.1 Steady-State Analysis

Steady-state analysis can be subdivided into (a) calculation of design point conditions, and (b) calculation of conditions at part load, once the reference design is relatively firm. Problems of particular concern are (1) adequate cooling of the support and containment structure; (2) temperature distributions and gradients in the reactor fuel; and (3) proper coolant flow distribution throughout the system.

The primary mode of operation of the nuclear rocket is to bring it rapidly (<30 sec) from very low power to full power, operate at full power over the entire thrusting period, and then shut down quickly. However, there are situations where it is desirable to operate at less than full power. For example, analysis of the aftercooling problem indicated that considerable hydrogen could be saved if fission product decay heat produced during the full-power run could be dissipated while operating at partial power prior to thrust termination. Figure 1-52 shows an example of the aftercooling heat load for two operating schedules, both producing 7.2×10^6 MW-sec of thermal energy. Tabulated below is the percentage of total propellant required to remove this heat as a function of coolant temperature for the case of constant power generation.

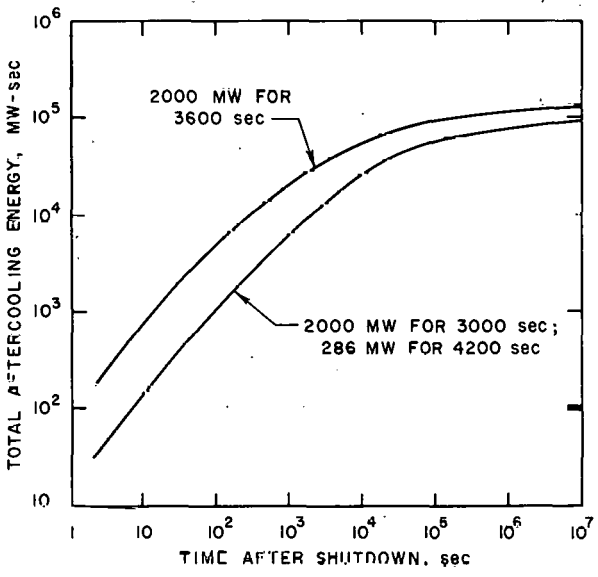

Fig. 1-52. Integrated aftercooling power vs. time after shutdown from 7.2×10^6 MW-sec operation at various power-time schedules

Temp., °R	Aftercooling Propellant, percent of total used in powered flight
1,500	5.03
2,000	3.66
2,500	2.88
3,000	2.37
3,500	2.01
4,000	1.68
4,500	1.38

During low-power operation, the allowable coolant temperature is primarily a function of nozzle cooling limitations. Some of the problems associated with operating at partial power are: (1) the thermal radiation heat load on the structure does not decrease with power while the cooling capability does, (2) flow redistribution, caused by changes in friction factors and orifice coefficients, (3) flow choking, resulting from sonic flow in various reactor regions, and (4) operation in transition and laminar flow regimes in the core.

1.6.3.2 System Dynamics Analysis

The primary objective of this analysis is to demonstrate feasibility of stable control consistent with maximum system performance. To this end, various turbopump operating characteristics, control schemes, operational procedures, and nuclear transients are evaluated in terms of their effect on overall system stability plus regional temperatures and pressures as a function of time. The ultimate goal is to provide controllability such that the effect of reactivity feedback on system dynamics need not be considered a limiting factor in the core design.

It is believed that with available servo control technology, accurate, stable control can be accomplished regardless of the reactivity feedback which may be encountered. For example, by providing closed inner loop control of power, with band-width beyond the frequency corresponding to the core thermal time constant, random fuel temperature variations can be virtually eliminated. Also, random flow fluctuations up to about 10 cps can be eliminated. Control of flow noise reduces the low-frequency component of dynamic load on the core structure due to thrust variations at power. Depending on the flexibility of the engine support structures and propellant tank, a 5% variation in thrust could produce up to 0.2 g axial load on the core, in addition to that due to flow friction.

The degree to which these objectives can be attained is contingent upon the influence of the so-called period effect in the neutron kinetics, the influence of stall and cavitation problems in the pump, and the inherent noise in the system. To these, of course, must be added the speed with which the control drums and flow control valves can be actuated.

A dynamic analog computer model of the rocket engine system was constructed and a practical closed loop control system was synthesized. The latter system was used to control transients between 10% and 100% of thermal power. Power buildup times ranged between 7 and 10 sec. An important result of this study was that control and startup from a moderately low-power range was analytically demonstrated for the fast reactor engine system. Typical results are shown in Fig. 1-53.

1.6.3.3 Advanced Concepts Analysis

The scope of this analysis includes (1) the effect of various turbopump pumping cycles (hot bleed, heated bleed, topping, split-flow topping) on engine operating parameters and weight, (2) the effect of tapered coolant channels on allowable core power density, and (3) parametric studies to optimize engine weights.

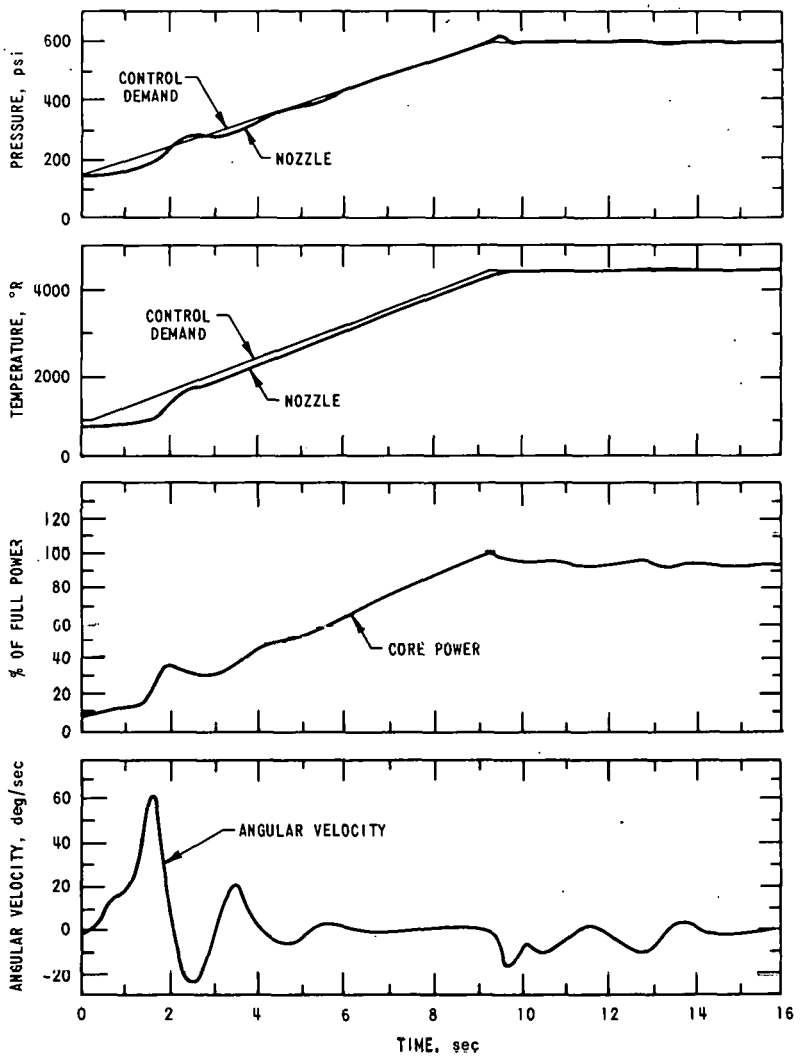

Fig. 1-53. Chamber pressure, temperature, core power, and control drum velocity during 9-sec startup from 10% power

The optimum engine will be operated at as high a temperature as possible, the upper limit being determined by the particular mission, and the engine weight as a function of propellant temperature. Other factors such as nozzle cooling capability, number of engine restarts required, fuel element creep rates, etc. can also limit the maximum propellant temperature. The choice of an optimum set of engine parameters is impossible without a well-defined mission. The parametric analysis, therefore, provides "trade-off" data to rocket designers on how particular design changes affect engine performance.

For example, Fig. 1-54 shows the engine weight-thrust characteristics of a hot bleed turbopump engine system powered by fast reactors fueled with either U-235 or U-233 in a tungsten matrix. Initial neutronic calculations of critical core volumes indicated that Al_2O_3 reflectors imposed an unacceptable weight penalty on the system. Therefore, the parametric study was limited to Be-reflected cores.

The Parametric Systems Analysis Code (PSA-II) was used to evaluate heat transfer-limited core geometries. Promising geometries were then iterated with the critical-volume data to yield a reactor that is simultaneously critical and heat transfer limited. In general, the study revealed that engine weights are relatively insensitive to core L/D ratios ranging from 0.75 to 1.2. Thus other considerations such as minimum shielding weight or control capability will be the prime variables in selecting the ultimate core geometry.

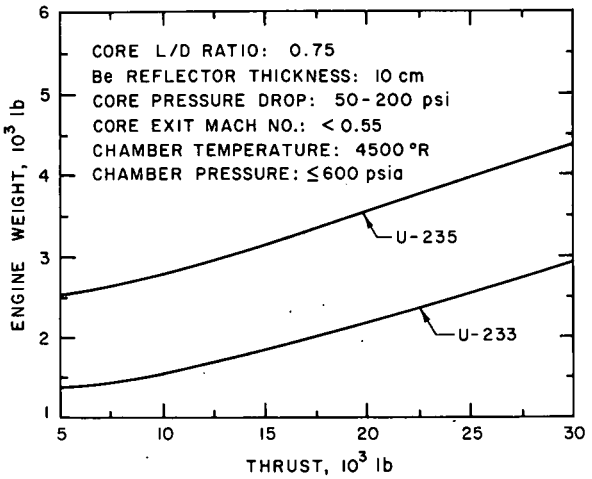

Fig. 1-54. Weight-thrust characteristics of U-235- and U-238-fueled, hot bleed turbopump engine systems

1.6.4 Fuel Element Development and Testing

1.6.4.1 Steady-State Tests

The objectives of these tests are:

(1) To determine the extent of UO_2 migration and/or loss as a function of hydrogen temperature, pressure, and velocity.

(2) To determine the extent of gross erosion of fuel element surfaces by high temperature, high-velocity hydrogen.

(3) To identify any cracking or distortion due to thermal expansion differential between fuel and structural materials, creep, the presence of high vapor pressure solids or included gases, or chemical changes in the fuel matrix.

The extent of UO_2 loss is of primary importance to the overall program relating to reactor control. The control span must be shown to be wide enough to compensate the excess reactivity required to offset UO_2 loss during operation. Accordingly, fuel subsections will be exposed (~2 hr) to hydrogen at a pressure of about 50 atm, with temperatures ranging up to 2450°C, and mass velocities up to 54.8 gm/(cm^2)(sec).

Post-test evaluations will include gross dimensional and weight changes, chemical analysis, metallography, and electron probe microanalysis. An absolute filter in the hot gas exhaust of the test loop also will be checked for traces of natural uranium.

1.6.4.2 Thermal-Cycling Tests

Knowledge of the effects of cyclic temperature variations on the fuel elements is essential to establishing whether the reactor is capable of multiple restart and pulsed cooling. Such cyclic effects can be caused by the difference in thermal expansion between the tungsten matrix and the UO_2 fuel; by loss of oxygen from the UO_2 at elevated temperatures; or by recrystallization of the tungsten. Other related causes and effects may be revealed during the course of the tests. For example, the thermal expansion differential may have a hysteretic effect on the expansion characteristics of the cermet; this could influence markedly the overall design and control of the reactor.

The nature of the initial thermal cycling tests will involve exposure of fuel element subsections to hydrogen at a constant pressure of ~50 atm, a hydrogen mass velocity of 3.15 $gm/(cm^2)(sec)$ and the following heating-cooling cycles:

(1) Heat linearly from 25°C to 2450°C in 5 min; cool down same way; 5 cycles.

(2) Heat linearly from 25°C to 2450°C in 3 min; cool down same way; 2 cycles.

(3) Same as (2), but increase to 5 and 10 cycles.

(4) Heat linearly from 25°C to 2450°C in 1 min; cool down same way; 5 cycles.

1.6.4.3 Rapid-Cooling Tests

Minimization of reactor startup time is vital to hydrogen economy. Assuming control feasibility, the elasped time depends upon the effects of transient thermal stresses that may be generated in reactor components during startup. Such stresses could also affect the multiple restart and pulsed cooling capability of the system.

The defined purpose of rapid-cooling tests is to obtain insight into the ability of the fuel elements to withstand extreme thermal shock. More specifically, fuel subsections (with all 331 flow passages open) will be heated relatively slowly to 2450°C and then cooled suddenly with a pulse of hydrogen at room temperature, or lower.

1.6.5 Argonne Hydrogen Flow Facility

The foregoing tests will be conducted in two test loops which comprise the Argonne Hydrogen Flow Facility (Bldg. D-311).

1.6.5.1 Building D-311

The basic structure consists of two test cells (North and South), with an intervening wall of concrete block, and an adjacent control room which services both test cells. Each cell measures 20 ft long and 18 ft wide, with a minimum headroom of 12 ft-4 in. The outer walls of the cells are reinforced concrete, 2 ft thick. The reinforced concrete wall between the cells and the control room is 3 ft thick. This wall is penetrated by windows (3 ft square) for visual access to both cells. Metal doors are provided for personnel access to each cell; these doors will be open whenever hydrogen is flowing into the test cells. The gas manifolds and piping leading to one nitrogen and four hydrogen tank trailers are installed on the north side. The 1200-kW-d-c power supply is mounted on a concrete pad on the south side of the building. Finally, the roof of the cells is made of structural plastic and clipped in place, so that it can be blown off easily in the event of an explosion.

1.6.5.2 Hot Hydrogen Test Loops

Figure 1-55 is a schematic of the larger of the two loops. It is designed to operate with power inputs up to 1000 kW. The smaller loop is scaled down to operate at inputs up to 50 kW. In both loops, hydrogen is cycled from the high-pressure storage trailers, through a system of pressure-regulating valves, to an electrical-resistance heater mounted in the lower end of a water-jacketed pressure vessel. Here, the gas is heated to temperatures up to 2450°C, and then passed over the fuel specimens mounted in the upper end of the pressure vessel. From the vessel, the gas flows through a water-cooled heat exchanger, a conventional flow control valve, and discharges to the atmosphere.

With reference to Fig. 1-55, the heater-pressure vessel assembly is located in a pit (8 ft square x 8 ft deep) in the South Cell. A separate hydrogen coolant line is installed downstream of the heater. The hydrogen in this line is used to effect rapid cooling of the fuel specimens.

Two heater designs are in various stages of development and evaluation. One unit features a single gas flow passage, and the other 19 smaller, parallel passages. Both are discussed in a later section.

Pressure Vessel. The pressure vessel is basically an 8-in., Schedule 80, mild steel pipe, 66 in. long. It is surrounded by a water-cooling jacket designed to remove 60 kW of heat. The bottom end of the vessel is connected to, but insulated from, the top of the heater support flange. The top end is connected to the transition section of the heat exchanger. The pressure vessel is designed to accommodate either the single- or the multi-passage heater.

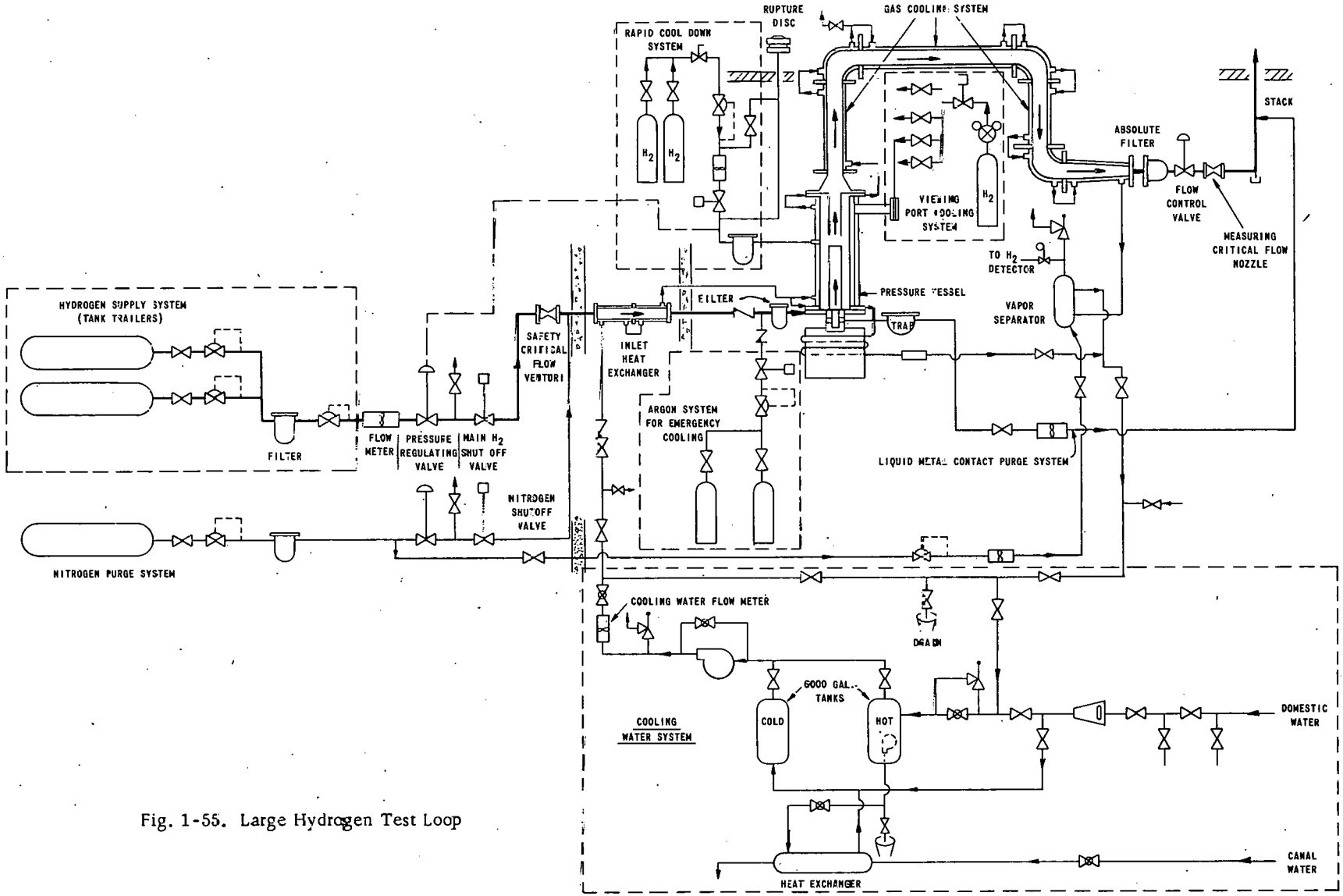

Fig. 1-55. Large Hydrogen Test Loop

Four viewing ports are installed at various elevations to permit pyrometers to sight on:

(1) The outer surface of the heater assembly near the bottom.

(2) The exit end of the heater.

(3) The inlet end of the test fuel subsection.

(4) The surface of the holder at a point corresponding to the back end of the test fuel subsection.

The windows in the ports are cooled by the flowing hydrogen, which also serves to sweep vapors that might condense on the inner surfaces. A 3/4-in. pipe line penetrates the vessel wall at a point between the top of the heater and the inlet to the test specimen holder. This line is used to introduce hydrogen for the transient cooling tests.

Other attachments include six thermocouple stations for monitoring the vessel wall temperature, and a small insulated vessel. The latter contains the liquid metal bath into which the bottom ends of the heater tubes are immersed. This bath is blanketed with hydrogen which is cycled down from the heater and bled to the atmosphere.

Gas-Cooling System. The purpose of this system is to cool the hydrogen effluent from the pressure vessel to a degree where it can be passed readily through an absolute filter, a flow-regulating valve, and a metering critical flow nozzle.

As shown in Fig. 1-55, this system consists of two vertical and two horizontal sections. Each section is simply a water-jacketed, Schedule 40, carbon steel pipe of specific length and diameter. These values, and corresponding gas temperature differentials prevailing in each section are listed below:

Section	Diameter, in.	Length, ft	Gas Temp., °C	
			In	Out
First vertical	4.0	9	2450	1800
First horizontal	2.5	14	1800	900
Second vertical	1.0	9	900	400
Second horizontal	1.0	11	400	200

The transition section between the pressure vessel and the first vertical section features a tungsten liner. The purpose of this liner is to maintain a layer of stagnant hydrogen between the bulk of the hot gas and the carbon steel wall. Similar liners made of molybdenum are used to protect the two hotter elbows, and a stainless steel liner is installed in the elbow leading to the filter.

Power Supply. The power supply consists of four rectifiers, each capable of delivering 10,000 amperes at 30 volts. Thus full-power operation can be realized at 30, 60, and 120 volts, and 3/4-power operation at 90 volts. The specific output rating for each rectifier unit is as follows:

Volts, d-c	1.5-30
Amperes	500-10,000
One-minute output, amp (max.)	25,000
Maintained automatic voltage regulation at 30 V, %	±0.5
Time to restore output voltage to preset value, sec	0.5

In addition to manual control, work is underway on a power supply that will respond to a control voltage input. Briefly, the design criteria are as follows:

(1) Input voltage should be in the range of zero to 30 volt, d-c, and the input power should not exceed 1 watt.

(2) For slow shutdown and control at the set point, the power supply should respond to a ramp input of ±15 volt/sec, and, also, to a 1-cps sine wave of 2.4-volt amplitude.

(3) Rapid shutdown should be achieved within 0.2 sec, and must be effected by opening a contact in the normal power supply safety circuit.

Water-Cooling System. The functions of the water-cooling system are:

(1) To preheat and maintain at a constant temperature the hydrogen entering the heater-test specimen assembly.

(2) To cool the pressure vessel.

(3) To cool the effluent hydrogen flowing through the main heat exchanger.

During the course of a steady-state test, the pressure in the hydrogen storage tanks will decrease from 2200 psia to about 800 psia. If the gas is initially at 300°K and is assumed to expand adiabatically, its temperature will decrease to about 225°K. Thus provision must be made for preheating and maintaining the hydrogen at a constant heater inlet temperature. This is accomplished in the inlet heat exchanger, which is a water-jacketed, 1-in. Schedule 40 carbon steel pipe, 20 ft long. The exchanger traverses the North Cell.

The cooling water system consists basically of a primary closed loop and a secondary open loop. In the closed loop, chemically treated water is pumped from a 6,000-gal cold storage tank through the inlet heat exchanger, the pressure vessel jacket, the main heat exchanger, and into a hot storage tank. A water flow rate of 80 gpm corresponds to an overall increase in water temperature of 45°C (neglecting cooling by incoming cold hydrogen) and permits a steady-state run of $1\frac{1}{4}$ hr. This time can be increased by as much as a factor of two by having both storage tanks filled with cold water and then dumping the effluent hot water.

The hot water in the storage tank is cooled by passing it through a small heat exchanger into the cold storage tank. This exchanger is cooled by an open loop of canal water.

Hydrogen-Nitrogen Supply. Four trailers, each containing 40,000 SCF of hydrogen will sustain three hours of operation at a flow rate of 23.7 gm/sec (equivalent to 36,000 SCFH).

The nitrogen supply is interconnected to the hydrogen system. It is used only to purge the cold system prior to the introduction of hydrogen.

During normal shutdown, the heater is cooled with hydrogen. Upon loss of hydrogen, the heat removal would be accomplished by a regulated supply of argon.

1.6.5.3 Prototype Heaters

Design calculations performed by the RE-329X code indicated that a heater with a nominal rating of 1000 kW would be required to heat the hydrogen over the proposed temperature range. The choice of heater materials was limited to tungsten or rhenium. Although more expensive, rhenium was selected because: (1) it is much easier to fabricate; (2) it has better stress-rupture properties up to at least 2600°C; and (3) at high temperatures, its electrical resistivity is almost twice that of tungsten.

As mentioned earlier, two prototype heater designs were developed for performance-evaluation tests in the large loop. One unit features a single gas flow passage, and the other 19 smaller, parallel passages. The overall heat transfer and flow characteristics are similar, i.e., both have a pressure drop of about 34 psi at rated operating conditions.

The single-flow-passage heater is an assembly of two concentric tubes having the following dimensions and tolerances:

	Active Length, in.	Diameter, in.		Wall Thickness, in.			H_2 Annulus, in.
		I.D.	O.D.	Top	Center	Bottom	
Outer tube	32.50	2.401	-	0.167	0.086	0.167	0.036
Inner tube		-	2.330	0.210	0.100	0.210	

The wall thickness of both tubes is stepped to produce a given heat generation rate as a function of axial length. The positions of the steps were determined by parametric heat transfer calculations. The annulus is maintained by small-diameter thoria balls. These balls are positioned in sockets machined in the inner tube.

Both tubes are welded together at their upper ends; exit slots are provided for the hydrogen. At the bottom ends, the outer tube is fastened to a massive electrode, and the inner tube is fastened to a thick copper rod that dips into a molten metal bath. The purpose of the bath is to permit free differential thermal expansion of the tube without interrupting the electrical circuit. The single-flow-passage heater is designed to operate at about 52.8 volts and 17,650 amperes.

In the 19-flow-passage heater, each passage is formed by two concentric tubes having the following dimensions and tolerances:

	Active Length, in.	Diameter, in.		Wall Thickness, in.			H_2 Annulus, in.
		I.D.	O.D.	Top	Center	Bottom	
Outer tube	18	0.250	-	0.040	0.021	0.040	0.020
Inner tube		-	0.210	0.069	-	0.026	

All tube assemblies are "headered" into a rhenium plug at the top end of the heater. This plug, in turn, is mounted in a massive tungsten sleeve that supports the heater and completes the electrical circuit at the top. As in the case of the single-flow-passage heater, the bottoms of the tubes extend into a liquid metal bath. The 19-flow-passage heater is designed to operate at about 26.8 volts and 34,900 amperes.

1.6.5.4 Loop-Heater Performance

50-kW Loop. Successful shakedown tests were made with a nickel mock-up of the single-passage heater, using first nitrogen and then hydrogen. However, subsequent hydrogen tests with the rhenium counterpart indicated a heater ΔP considerably greater than predicted. Since hydrogen flow rate is not critical in this loop, the flow was derated one-third, i.e., to 19.6 SCFM. This resulted in a ΔP of about 45 psi at two-thirds flow and power. Under these conditions, and a power of 26 kW, the sample temperature was about 57% of the computed adiabatic gas temperature, indicating considerable heat loss.

Several modifications in the heater-sample holder system resulted in some reduction of heat loss. In addition a three-dimensional heat transfer code (HECTIC) was used to obtain a measure of detailed temperature distributions in the heater tube and tungsten muffle. The results of this

study indicated (1) significant heat losses were occurring from the heater tube to the muffle; and (2) that these losses could be offset by operating the heater at higher power without increasing its temperature excessively.

This was done in two stages of subsequent loop operation: first, to produce a sample temperature of 2360°C at a power of 38.8 kW, and then 2420°C at a power of 40.3 kW. As of December 1, the heater has accumulated 3.48 hr of operation, producing sample temperatures in excess of 2400°C, with no evidence of heater deterioration.

1000-kW Loop. Both prototype heaters have been modified as a result of failures experienced during initial operation of this loop. Failure of the single-passage heater was traced to inability of the thoria balls to maintain alignment of the gas flow annulus. In this instance, the rhenium tubes were repaired for use in the modified heater (Mark-II). In addition, the thoria balls have been replaced with rhenium wire spacers, and a massive tungsten muffle has been installed to complete the current path. Fabrication is underway, and the unit is scheduled for testing in April, 1966.

Failure of the 19-flow-passage heater was related to the tube support structure, i.e., the top-end rhenium plug and the tungsten muffle. A stress-analysis model was evolved that predicted, quantitatively, the actual mode of failure. The information obtained from this model has also been incorporated in the top-end design of the Mark-II single-flow-passage heater.

1.6.6 Structural Mechanics

The objectives of the structural mechanics program are to develop analytical models and experimental facilities for assessing the structural integrity of the reference design. A set of typical structural loads based on the NERVA-RIFT system is being used as a guide.

1.6.6.1 Deformation Analysis of a Grid Plate Support Structure

This analysis was performed for a circular support structure consisting of two flat parallel plates, interconnected by a grid work of equally-spaced structural members. Closed form solutions of the deflection equation and its derivatives were found which are sufficiently accurate to provide realistic estimates for an engineering deformation and stress analysis. The analytical method also can be applied to determine the deformation of grid structure beams.

Acrylic plastic models of beam and circular plate grid structures are being fabricated in order to experimentally verify the analytical results.

1.6.6.2 Possible Influences of Anisotropy on Plane Strain Thermal Stress Solutions

In certain core and fuel element thermal stress calculations, the internal complexity of the component to be studied precludes exact treatment of the problem. It has been proposed that such elements be modeled by homogeneous elastic solids possessing various types of anisotropy; also, that the anisotropic constants be selected to reflect the gross behavior of the detailed internal structure. For this reason, various studies have begun on the possible effects of anisotropy on thermal stresses. The simplest form of anisotropy considered was that of transverse isotropy, i.e., where the elastic properties in one preferred direction differ from those on any plane transverse to this direction, while in the transverse plane there exists no preferred direction.

For plane strain and torsionless rotational symmetry, it has been shown that a given problem for a transversely isotropic solid may be replaced with an equivalent isotropic problem having material constants bearing a known relation to the anisotropic material constants. Such an anisotropic model was used to determine the relative effects of various anisotropic constants on stresses due to radial temperature variations in a long circular cylinder possessing transverse isotropy.

The general trends of this model indicated that an in-plane Young's modulus greater than that in the axial direction, coupled with an axial thermal expansion greater than the in-plane expansion, always causes an increase in thermal stress above that computed on an isotropic basis using in-plane values. Similarly, reductions in stresses are the result of an exact reversal of these conditions.

1.6.6.3 Reduced-Scale Model Tests

The primary objective of these tests is to determine the size of the model that will reveal the response of a cluster of fuel elements to a known load input.

Initial tests were made to determine the response of densely-packed, aluminum cantilever beams to lateral, sinusoidal-forcing functions. Similar tests were made on single beams for purposes of comparison. Briefly, the results were as follows:

(1) Beam clusters varied significantly in amplitude of vibration from that of a single beam.

(2) The damping ratio for a single beam was <0.02.

(3) Modes shifted only with additional restraint such as banding together the previously free ends.

(4) Significant damping (with tight mounting joints) can be achieved only by intentionally introducing lateral forces between the beams.

1.6.6.4 Vibration Exciter Facility

This facility will be used in developing models for dynamic stress and deformation analysis of reactor components. These will include fuel elements and assemblies, reflector components, support structures, and control systems. The pertinent specifications of the facility are:

Force output:	10,000 lb, sinusoidal; 9,000 lb, rms random
Frequency range:	5-3000 cps
Amplitude accuracy:	±1 db
Power amplifier:	60-kW output
Stroboscopic system:	Simultaneous visual, photographic, and data recording of vibrating test specimens.

The operating characteristics of the facility have been checked out, and training of operator personnel is underway.

1.6.6.5 Shell Stability Analysis

In attempting to minimize the thickness of certain cylindrical shell structures to reduce gamma heating and reactor weight, it was found that the existing pressure differences could cause collapse. In lieu of increasing shell thickness, alternate stabilizing methods were considered. A proposal to provide stability by placing the shell in tension proved unworkable due to the excessively large values of tension required to significantly raise the critical collapse pressure. A second possibility was to stiffen the shell with regularly-spaced axial ribs. Analysis of this shell structure entails replacing the original isotropic model with an anisotropic model.

Accordingly, two independent analyses were carried out. The first was based on a modification of known formulas derived from Taylor's equation for the stability of orthotropic cylinders. The critical pressure expression which resulted was based on the assumption that Poisson's ratio is zero. The second analysis was similar to that used for deriving the classical critical pressure expression for an isotropic cylindrical shell. It included

a non-zero Poisson's ratio and, while yielding much more elaborate formulas, produced only minor changes in the computed critical pressure.

The stabilized model shell represented a highly redundant structure. Even the assumption of construction to perfect dimensions and symmetry was likely to obviate a complete theoretical stress and deformation analysis. Thus in order to gain some insight into the stress and deformation behavior and to provide at least a rough comparison with the experimental data, a cursory theoretical analysis was made of the shell deformation in the normal cross-sectional plane midway between the end plates. The basic assumptions included elastic behavior, perfect symmetry with respect to the axis, no instabilities, and the absence of bending stresses in the axial direction, i.e., a shell of infinite length. Further considerations of stability were undertaken on an initial experimental basis.

1.6.6.6 Experimental Study of Shell Deformation and Stability

The instrumentation of a shell that may fail as a result of instability requires careful consideration. Even though an area of incipient failure may be localized, the region in which it can occur is rather large. To survey such a large region with strain-gage instrumentation would have constituted a formidable undertaking. One method under study consists of gluing a continuous band of birefringent plastic to the shell interior, and monitoring this coating with a rotating mirror. The underlying principle of the proposed method is based on the utilization of correction factors ordinarily required to convert the strains determined by photoelastic measurements into strains that would be developed in an uncoated part subjected to the same plane or bending loads. Further development of this method is being carried out. Thus far, results reveal good agreement between methods at positions away from reinforcing ribs.

Section 2

FAST REACTOR RESEARCH AND DEVELOPMENT

2.1 Advanced Systems and Concepts

2.1.1 1000-MW(e) Metal-Fueled Fast Breeder Reactor Concept

Four divisions of the Laboratory, including Reactor Engineering, participated in a preliminary design study of a metallic uranium-plutonium-fueled, sodium-cooled, 1000 MW(e) fast breeder reactor for central station power plant application. The purpose of the study was to present metallic fuels in a fashion somewhat comparable to four industrial studies of a ceramic-fueled counterpart.[1] A formal report will be issued late in fiscal 1966.[2]

Design Considerations. As in the case of the referenced studies, emphasis was placed on topics related to the fuel in order to permit electrical energy cost estimates for the fuel cycle. Conceptual design of the fuel element and subassembly was carried out to a depth sufficient to ensure that remote fabrication of the fuel units could be performed routinely. Layouts of the overall reactor concept were prepared, as necessary, to indicate core and blanket arrangements, to show a primary coolant flow path, and to suggest a refueling scheme. Finally, design compatibilities were investigated to ascertain that a design synthesis had been achieved.

In all nuclear-powered central station plants, the degree of fuel burnup is a major economic consideration, since portions of the fuel cycle cost are inversely proportional to this factor. The reactor design is also influenced by the burnup level; for example, in the reactivity allowance for burnup, and the provisions for fuel change in a reasonable time. In the metal-fueled concept selected, the interplay of burnup and thermal-neutronic performance is particularly strong because a significant portion of the core volume is reserved for accumulation of fission product gas.

This accommodation for fission-product gas results from using a particular burnup model. In this model, the fuel is regarded as arbitrarily weak, and the cladding is assumed to act as a tube pressurized according to the degree of burnup desired. Restrained by the metal, the gas expands the fuel from its as-cast density to a final density determined to be a reasonable minimum for decrease in fuel thermal conductivity and for neutronic performance.

A cladding of 20 wt-% titanium-vanadium alloy was selected because of its strength characteristics, low neutron absorption, and good compatibility with the fuel and sodium coolant. A low coefficient of expansion and good thermal conductivity combine to result in lower thermal stress than

for stainless steel at a given heat flux. Ductility, high strength up to 650°C, and favorable creep rate make this alloy a promising material for the fast neutron environment at temperature and exposure time of interest. Also, it can be fabricated into small-diameter, thin-walled tubes.

Table 2-1. Fuel Element Design and Performance Characteristics

Average Burnup in Discharged Fuel, %		6
Fuel Element Composition, vol-%		
Vanadium-20 wt-% Titanium Cladding		31
Expanded U-Pu-9 at-% Ti Fuel		69
Fuel Pin:	As Cast	Expanded
Density, gm	17	12
Diameter, in.	0.150	0.174
Length, in.	34	36
Fuel Tube		
Outside Diameter, in.		0.210
Wall Thickness, in.		0.018
Fuel Enrichment as Charged ($Pu_f/Pu + U$), wt-%		
Inner Zone		13.5
Outer Zone		17.5
Thermal Data		
Average Linear Power, kW/ft		6.6
Hot Spot Cladding Temperature, °F		1126
Hot Spot Fuel Centerline Temperature, °F		1439
Heat Flux, Btu/(hr)(ft^2)		
Maximum		6.9×10^5
Average		4.1×10^5

Fuel Elements. Table 2-1 lists the pertinent fuel element design and performance characteristics. The wall thickness of the titanium-vanadium cladding tube was selected to give the highest amount of fuel per element for a given burnup. The outside diameter is near the optimum, based on comparing the two opposing factors of fabrication cost and plutonium inventory cost.

The fuel elements are assembled into subassemblies as shown in Fig. 2-1. Tubular spacers are employed to achieve an acceptable pressure drop across the subassembly. The tops of the 20.5-ft-long subassemblies extend above the sodium coolant level so that refueling can be performed with visual aid.

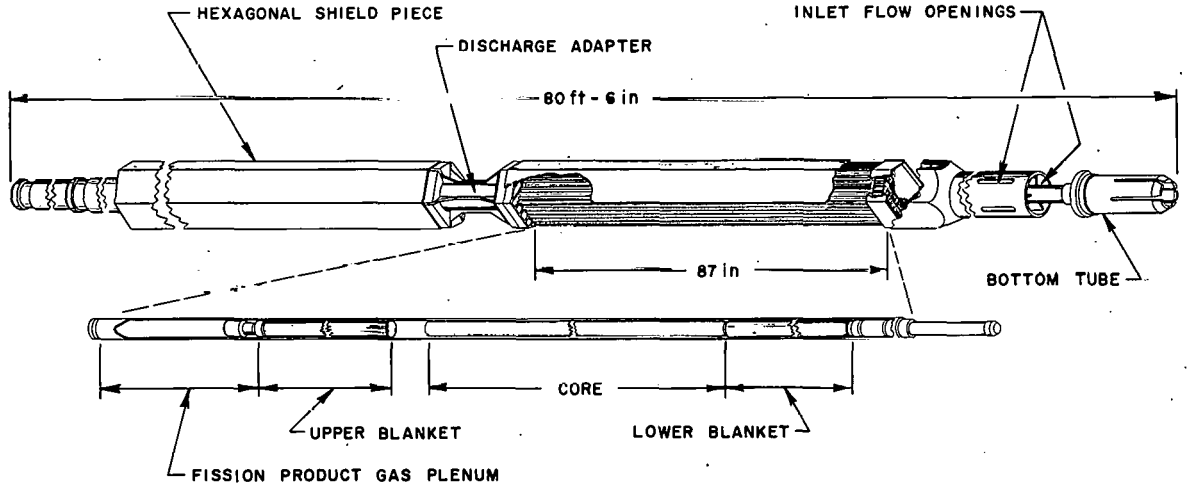

Fig. 2-1. Components of fuel subassembly for 1000 MW(e) metal-fueled fast breeder reactor study

Modular Core. A ring of six core modules was selected to provide the heat for generating 1000 MW of electricity. (See Fig. 2-2.) The size of the module was based on the sodium density change effect on reactivity. A significant Doppler reactivity effect was incorporated by specifying a ring of beryllium at the radial boundary of each core. The thickness of

uranium blanket between cores was chosen so that each module is essentially an independent chain-reacting unit.

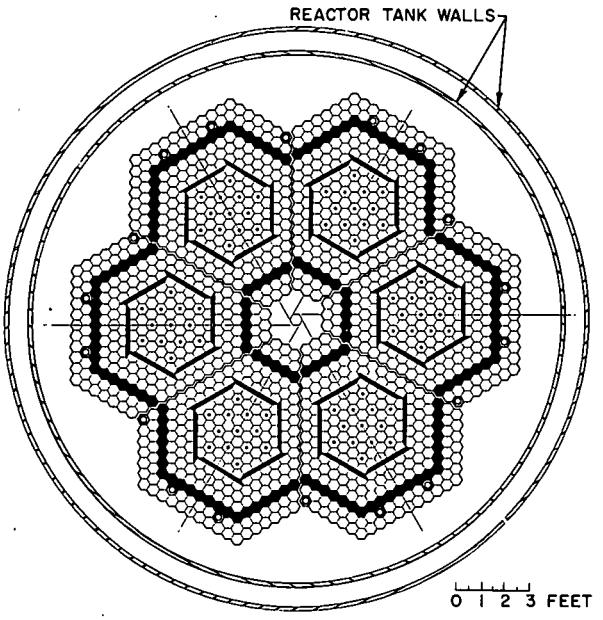

Fig. 2-2. Horizontal section of reactor at midplane

Each module (Fig. 2-3) contains a core of 61 fuel subassemblies. The outer 24 subassemblies are of higher enrichment to improve power flattening. These units in combination with the inner radial blanket subassemblies have appropriately located beryllium to form the inner beryllium zone. Although the radial uranium blanket is thin, it has good breeding characteristics because the outer beryllium zone is backed up by a stainless steel reflector.

In each module, the fuel subassemblies and two rows of blanket subassemblies are locked radially by the differential expansion between a titanium pivot plate and a stainless steel drive plate. These plates act at two levels on the lower adapter of each subassembly. Radial clearances which exist between subassemblies at the refueling temperature are removed before the approach to criticality. This is accomplished by raising the system temperature part way to the operating coolant inlet temperature.

Control Rods. Twelve enriched boron carbide control rods are housed in respective subassemblies in each core module. (See Fig. 2-3.) In addition, there is a regulating rod at each core axis. All rods are cooled by upward flowing sodium suitably orificed to preclude rod flotation. A grid just below the rotating plug holds down each control rod guide tube to prevent unseating of the control rod-containing subassembly should binding occur during upward rod movement.

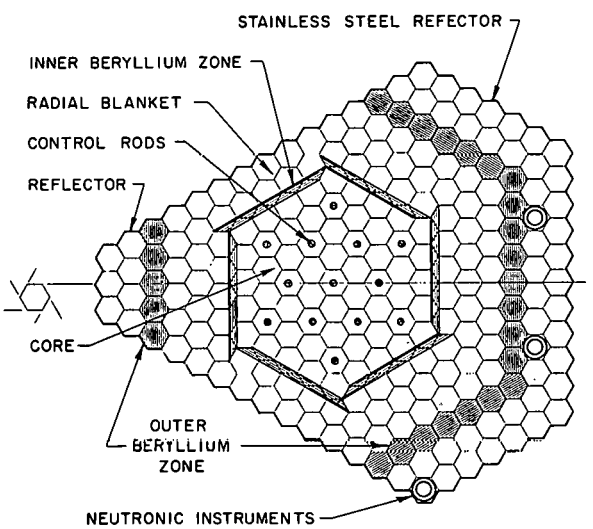

Fig. 2-3. Section of one module

Primary Sodium Circuit. This circuit consists of a reactor inlet-flow plenum common to the six core modules, a common discharge into the reactor tank region above the fuel subassemblies, and six loops joined to these plena. As shown in

Fig. 2-4, each loop features a vertical, sodium-to-sodium heat exchanger which receives sodium at 1000°F directly from the reactor; a vertical, free-surface, variable-speed, centrifugal pump; and a check valve. The number of loops was based on extrapolating a developed pump design to large sizes. Location of the pump in the cold leg permits minimum pressure in the secondary sodium for preventing radioactive primary sodium from entering the secondary system, should a leak develop in the heat exchanger.

Turbine-Generator. The turbine-generator complex that matches the reactor outlet temperature of 1000°F will consist of two 500-MW(e) units. These units will operate at a primary steam pressure of 1800 psig, and primary and reheat steam temperatures of 900°F.

Fuel Cycle. The refueling cycle is 206 days, with an annual plant load factor of 80% and 6% average burnup in the core. Reactor characteristics are based on replacing one-third of the core, one-sixth of the inner blanket zone, and one-ninth of the outer blanket zone at each refueling cycle. Replacement of one-third of the core minimizes the total conceivable accumulation of reactivity (due to fresh fuel slumping) to less than the shutdown control margin. The reactivity loss over such a cycle is about 3% $\Delta k/k$.

A fuel-handling procedure is postulated beginning with disengagement of all control rods from their respective drives to permit rotation of the top shield. (See Fig. 2-4.) A removable plug exposes the entire area of a module for replacement or relocation of a subassembly. It is proposed that a spent subassembly be lifted into a sodium-filled cask for transport to storage within a fuel-cycle facility.

The fuel-cycle facility consists of the on-site components to process discharged fuel, refabricate processed fuel into fuel elements, and dispose of wastes. Remote-controlled pyrochemical processes and fabrication techniques were selected because of the short-term, fuel cooling requirements (15 days) and, also, because certain of the major steps have been successfully demonstrated on a plant scale with irradiated fuel in the EBR-II Fuel Cycle Facility.

Fuel Cycle Costs. Fuel cycle costs were based on a reactor design having the characteristics listed in Table 2-2, a plant load factor of 80%, a 9% per annum charge on working capital, and a value of $10 per gram of fissionable plutonium. The unit-energy costs for metallic fuels, at both 6 and 7 at-% burnup, are listed in Table 2-3.

Conclusion. Based on the results of the referenced studies[1] and the present study, it is not possible at this time to make a firm selection of a specific fuel material for future fast reactors. Unresolved fuel performance

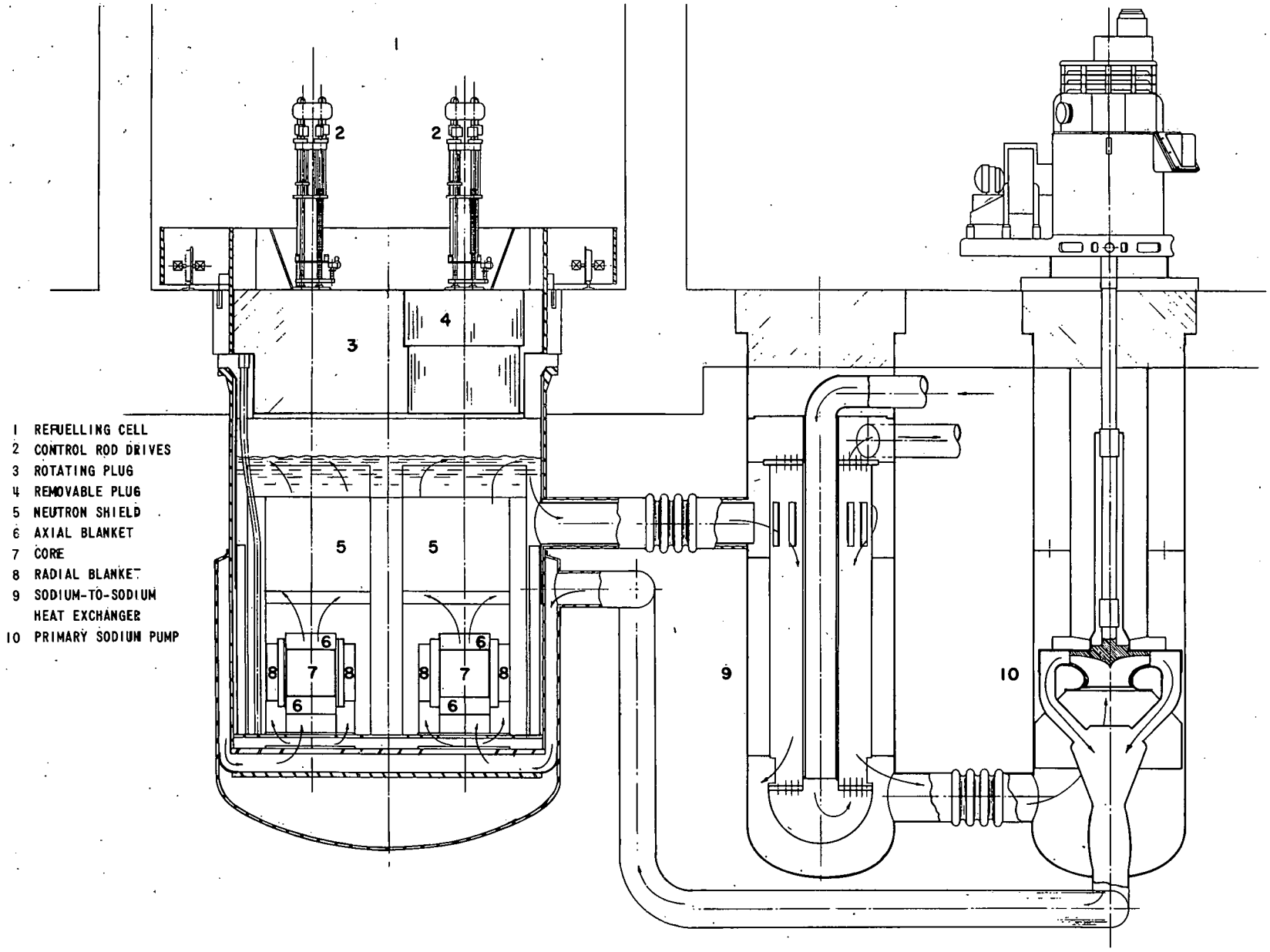

Fig. 2-4. Vertical section of reactor and one of six primary sodium loops

capabilities, lack of knowledge of complete system optimization, uncertain costs of fuel processing and fabrication, relative influence of fuel type and design on plant safety, and the uncertainties in the change with time of the cost and availability of fertile and fissile materials support the present course of deferred selection. Concentrated research and development on any fuel type, plus eventual commercial application by industrial firms, would make changes to an alternative fuel very difficult.

Table 2-2. General Reactor Features and Performance Data

Breeding Ratio	1.48
Core Breeding Ratio	0.64
Doubling Time for Reactor Fuel, yr	7.6
Gross Reactor Power, MW(t)	2513
New Plant Output, MW(e)	1000
Primary Sodium Outlet Temperature, °F	1000
Primary Sodium Flow Rate, lb/hr	10^8
Maximum Sodium Velocity in Core, ft/sec	24
Core Volume per Module, liter	785
Equivalent Core Diameter per Module, ft	3.46
Core Height, ft	3.0
Core Power Density, kW/liter	
Average	450
Maximum	650
Fraction of Power Generated in Core	0.85

Core Composition, vol-%

	Inner Zone	Outer Zone
Sodium	39	42
Stainless steel structure	9	8
Control region	6	-
Fuel Element	46	50
	100	100

Table 2-3. Fuel-Cycle Costs for Metallic-Fueled System

Core Burnup, at-%	6.0	7.0
Processing, $/kg		
Fabrication		
Core and axial blanket	155	155
Radial blankets	100/65	100/65
Chemical Processing	60	60
Spent Fuel Shipment	-	-
Unit Energy, mill/kW-hr		
Fabrication	0.61	0.52
Chemical Processing	.28	.25
Shipping	-	-
Pu Credit	-0.47	-0.45
Working Capital	.61	.60
Total	1.03	.92

2.1.2 Engineering Design and Cost Study of Large Steam-Electric Generating Units

A study of the influence of steam conditions on thermal efficiency and capital cost of turbine-generator plants for 500 MW(e) and 1000 MW(e) stations was completed by United Engineers and Constructors, Inc., in collaboration with Division personnel.

Briefly, the study was carried out to a depth sufficient to assist in the evaluation of sodium-cooled, fast reactor concepts for central station power application. It included the general design, arrangement, thermal performance, and installed cost of eight, steam-electric generating units. The operating characteristics were determined by Division personnel to be within the scope of the evaluation program.

Cost estimates were prepared in accordance with the Federal Power Commission Uniform Code of Accounts. More specifically, the estimates included all materials, labor, and equipment from the inlet steam line to the turbine-generator building, through the high-voltage transformer.

The merits of this study are best illustrated by the pertinent results summarized in Table 2-4. They indicate that:

Table 2-4. Influence of Steam Conditions on Thermal Efficiency and Capital Costs of Turbine-Generator Plants for 500 MW(e) and 1000 MW(e) Nuclear-Powered Central Stations

Steam Condition, psig - °F/°F	Net Thermal Efficiency, %	Capital Cost, $/Net kW
500-MW(e) Station		
3500-1000/1000	42.6	52.06
2400-1000/1000	41.8	50.99
1800-900/900	39.7	52.17
1000-Dry and Saturated	33.2	66.26
1000-MW(e) Station		
3500-1000/1000	42.9	46.26
2400-1000/1000	42.1	44.98
1800-900/900	39.8	48.37
1000-Dry and Saturated	33.5	60.62

(1) The 2400-1000/1000 steam cycle reflects the lowest capital cost investment for either station, and is only 2% less efficient than the 3500-psig case.

(2) The 1800-, 2400-, and 3500-psig steam cycles exhibit significant improvement in cost and thermal performance over a steam cycle representative of current, water-cooled, nuclear reactors.

(3) Selection of an 1800-900/900 steam cycle for fast reactors would not significantly penalize the electric-generating part of the plant. Moreover, the reduced temperature requirements may alleviate critical material problems in certain reactor designs. Or the 1800-psig cycle may allow greater temperature differentials to be used in heat exchange equipment for a given reactor top temperature over the 2400-1000/1000 or 3500-1000/1000 steam cycles.

The foregoing study represents the first phase of an overall effort on fast power reactors. The next phase will include a similar appraisal of the sodium-heated, steam-generator portion of the power plant.

2.2 Materials and Components

The development of advanced fast breeder reactors for safe and economical power generation is contingent upon the availability of suitable materials and components. Their availability, in turn, is contingent upon the results of comprehensive screening and evaluation tests in facilities designed to simulate the anticipated operating environments. These environments will include intense fast neutron irradiation and/or sodium coolant at temperatures as high as 1200°F. In addition, the coolant may contain varying amounts of impurities, i.e., carbon, oxygen, fission products, etc. Unless controlled or removed, the buildup of these impurities could affect adversely the physical and mechanical properties of materials and components. Thus the screening facilities should provide for the simultaneous evaluation of auxiliary or in-line systems and components for monitoring, controlling, or removing these impurities.

All of these factors are being considered in the design and conduct of the fast reactor materials and component development program at Argonne. The nature of this program, the related test facilities, and the progress during fiscal 1965 are described briefly in the following subsections.

2.2.1 1200°F Materials and Component Evaluation Loop

When completed, this loop will provide for maximum flexibility in operation and comprehensive evaluation of materials and components in sodium at temperatures up to 1200°F and at flow rates up to 184 gpm.

Constructed of 4-in. Type 304 stainless steel piping, the basic loop consists of a d-c electromagnetic pump, a surge tank, cold trap, plugging meter, blanket gas system, valves, and dump tank. Other provisions include:

(1) A gas-quality-monitoring system. This system consists of a pair of electronic devices which continuously monitor the oxygen and water content of the blanket gas. These devices produce an electrical output proportional to the concentration of the measured impurity.

(2) A portable sodium distillation unit. This unit consists of a sodium sampling chamber, vacuum system, support framework, and associated instrumentation. It will be used to monitor samplings of sodium for impurities. These data will be correlated with the results of plugging meter tests to determine their effect on meter performance.

(3) A modified Falex Wear Tester. Used to evaluate wear properties of bearing and shaft materials at various speeds and loadings, this commercially available tester has been modified for similar tests in sodium up to 1200°F. Briefly, the tester consists of a sodium vapor isolation housing, drive motor, shaft block and support, force transmission device, and related instrumentation.

(4) A bellows-sealed valve. Installed between companion flanges, this valve, along with others, will be evaluated as an "in-line" component of the loop.

(5) Finally, the loop piping will be surveilled. For this purpose, a section of the piping has been fitted with Conoseal flanges. In this manner, the Type 304 section can be removed and replaced with counterpart sections of other materials. Performance of the flanges also will be evaluated.

Electrical signals from various loop and test instrumentation will be continuously recorded and stored on punched tape in a digital-data-logging system. This system includes a circuit which can produce a graphic display of the stored data in a large number of modes, as selected by the operator. Thus rapid analyses of the data can be made as the test progresses.

The status of the loop is as follows. Components such as the bellows-sealed valve, dump tank, and electromagnetic pump are in various

stages of procurement and installation. Modification of the Falex Wear Tester was completed, and preliminary check-out tests are underway. The gas-quality-measuring equipment has been received and is undergoing similar check-out tests.

2.2.2 High-Temperature (1200°F) Sodium, Long-Term Environmental Test Loop

This loop was built in 1957, primarily to evaluate the integrity of a d-c electromagnetic pump tube and current conductor in dynamic sodium (25 gpm) at 1550°F. Since that time, it has been used for material compatibility tests in sodium at 1200°F.

Constructed of 2-in., Type 304 stainless steel piping and fittings, the vertical loop (10-gal capacity) is equipped with a d-c pump at the bottom, and an expansion tank at the top. The expansion tank (6-in. pipe, 14 in. high) contains flowing sodium into which the test materials are immersed. A 4-in. pipe section and gate valve are mounted on top of the tank, so that the test specimens may be removed without contaminating the sodium with oxygen. A plugging meter is used to measure the oxide content.

To date, the loop has accumulated 12,000 hr of testing, including 8,000 hr at 1200°F. The time element is important, since there is no provision in the loop for cold trapping or hot trapping operations. Thus a careful check of the mass balance of this system with metallic impurities in the "as-received" sodium should indicate a "solubility rate" of the Type 304 pipe material in 1200°F sodium.

Chemical analysis of sodium samples indicated an increase in Fe content from 2 ppm (as received) to 40 ppm, while the Ni content increased from 2 ppm to 8 ppm. There was no measurable evidence of chromium. Vanadium content increased from 4 ppm to 1500-2000 ppm. This increase is attributed to vanadium cladding specimens that were exposed in the expansion tank.

The modest increase in Fe and Ni is encouraging, with respect to compatibility of Type 304 stainless steel for sustained operation with sodium at 1200°F.

2.2.3 Material Compatibility Test Facility

This facility is being used to determine the self-welding characteristics of various material combinations when immersed in static sodium at temperatures up to 1200°F. Other test parameters include material geometry, surface finish, loading, and sodium quality.

In operation, couples of like or unlike specimens are positioned in an electrically-heated autoclave filled with sodium of a predetermined quality. The autoclave is essentially a 12-in.-long pipe (12 in. O.D.) welded at the bottom and flanged at the top. Loadings are transmitted to the samples through a bellows-sealed, push-rod assembly which is an integral part of the flanged closure.

Couples of Type 304 stainless steel are in test. Their configurations represent the curved seating surface of subassemblies and the flat core support grid in the EBR-II. The objective is to determine the compatibility of Type 304 beyond the operating temperature of EBR-II (700°F), up to and including 1200°F.

2.2.4 1200°F Furnace - Tensile Testing Machine

A 1200°F sodium atmosphere furnace has been constructed for use in conjunction with a universal tensile test machine. The purpose of this unique combination is to isolate and assess the relative effects of operating variables on the mechanical properties of thin-walled tubes simulating, for example, fuel element clad. These variables will include high-temperature sodium, fast neutron irradiation, tension, compression, and biaxial stresses up to and including bursting pressure.

The furnace is designed to test in tension or compression an 8-in.-long, 0.50-in.-O.D. tubular specimen immersed in sodium at temperatures up to 1200°F. It consists of an electrically-heated stainless steel tank (8-in. pipe, 14 in. long). The tank bottom includes a chuck which engages the lower end of the test tube. This chuck and the tank are an integral part of a rod extension which, in turn, is engaged by the lower gripper of the tensile test machine. The upper end of the specimen extends through the bellows-sealed tank closure and is engaged by the upper gripper of the tensile machine. This arrangement permits elongation or compression of the tubular specimen while maintaining a leak tight argon atmosphere above the hot sodium. Biaxial stresses can be applied simultaneously by pressurizing the specimen (with inert gas) through an upper end fitting. The tensile machine may then be programmed to cycle the stressed tube through any predetermined stress range.

Plans are to develop stress ranges and ultimate bursting pressures for unirradiated tube materials in air and in sodium at temperatures up to 1200°F. Similar tests will be performed on the same lot of tubing after exposure in a combined irradiation, high-temperature sodium environment. It is believed that this program will lead to differences in cyclic stress ranges and ultimate rupture strengths which may be due primarily to fast neutron irradiation.

The first series of tests will be made on unirradiated EBR-II blanket element tubing. Preparatory tests have been made: (1) to determine the minimum L/D ratio for tube specimens; (2) to determine the effect on burst pressure of using an internal rod (fuel) to displace a known volume inside a pressurized tube; and (3) to develop simple stress-strain curves for "as received" and "sodium soaked" tubes. In addition, steps have been taken to obtain EBR-II blanket tubes with various nvt histories.

2.2.5 Sodium Vapor Trap Development

A compact vapor trap has been developed which is capable of removing sodium vapor from argon gas vented at flows up to 40 ft^3/hr from a 1200°F sodium system.[3]

Briefly the trap consists of an 8-in. length of 2 in., Schedule 40 stainless steel pipe. Contained within the pipe is a series of concentric rings and discs of stainless steel. These baffles are sloped downward in the vertically-mounted pipe. The outlet of the trap is maintained at a temperature slightly above the melting point of sodium. In operation, the sodium-inert gas flow impinges on the baffles. The gas flows through the baffles, whereas the sodium droplets deposit on the baffles and return by gravity to the bulk sodium in the system.

The efficiency of a vapor trap is defined as the ratio of liquid sodium returned, to the total sodium vapor available for trapping. Accordingly, at flow rates of 5 ft^3/hr and 20 ft^3/hr, the measured efficiencies were 97% and 99%, respectively.

2.2.6 Self-Seeking Sodium Level Probe

Designed for either automatic or manual operation, this probe provides continuous indication of the sodium level in a vessel without physically contacting the sodium. More specifically, it consists of a solenoid (2 in. O.D., 2 in. long) which operates in a stainless steel thimble installed in the vessel to be monitored. The probe is suspended by flexible, electric-conducting tapes which are connected to a motorized take-up drum mounted on top of the vessel.

In operation, the solenoid forms one branch of an a-c excited bridge. Bridge balance is dependent on the solenoid inductance. Inductance, in turn, is dependent upon the resistance of the environment surrounding the thimble. For example, the inductance increases as the resistance decreases when the probe traverses the gas space and enters the sodium region. The electronic circuitry employed enables the operator (1) to manually drive the probe up or down, or (2) to select a circuit which automatically raises or lowers the probe as the sodium level changes. This circuitry is described elsewhere.[4]

The probe was tested in a small vessel (4 in. O.D., 3 ft high) which was partially filled with sodium. The vessel was electrically heated from room temperature up to 1200°F. Accuracy was based upon statistically repeating a level determination for a constant, known level. In each instance, the indicated level was within ±0.5 in. over the entire temperature range.

This device is being used to monitor sodium level in a 1000-gal, sodium supply tank which services a reactor engineering test facility.

2.3 Sodium Quality Control

The corrosive action of molten sodium is due largely to its impurity content, and several methods have been developed to control this content. While these methods are adequate for current sodium systems which operate at relatively low temperatures, they are inadequate for sodium temperatures that will prevail in the next generation of fast reactors. Therefore, studies and experiments are underway to either improve the old methods or to devise new measures for monitoring impurities in sodium up to 1200°F.

2.3.1 Sodium Quality Measurement Loop

Constructed of 2-in., Type 304 stainless steel piping, this closed loop is designed to accommodate three different methods for simultaneously analyzing the impurity content in sodium at various flow rates and temperatures. Sodium at 239°F is drawn from the center of a 5000-gal, model EBR-II primary tank. In order to check the accuracy of the analytical methods, the equilibrium oxide content at 239°F is increased by adding sodium peroxide.

The methods under study include a distillation apparatus, a plugging meter, and a resistivity meter. In operation, the distillation technique consists of withdrawing a sodium sample from the loop into an equally hot cup inside an evacuated container. The cup overflows, presumably giving a measured volume of sample. This sample is distilled, under vacuum, leaving the solid impurities in the cup. The apparatus is then dismantled, the impurities are dissolved, and their concentrations are determined by standard analyses.

The plugging and resistivity meters are "in-line" measuring devices. Neither has been placed in operation pending resolution of difficulties with the distillation apparatus. These difficulties range from loss of sodium sample due to sputtering, to nonuniform samples due to meniscus variation and wetting of the cup.

2.3.2 Drybox Sodium Sampling Test Loop

This small, all-welded, Type 304 stainless steel loop is being operated to determine the feasibility of using a portable drybox to provide a protective inert gas atmosphere during sodium sampling for impurity analyses. Designed for operation at sodium temperatures up to 1200°F, the loop components include electric heaters, an electromagnetic pump and flowmeter, and a small test section. The drybox is intended to provide controlled access to the test section. If successful, the portable feature of the drybox will allow similar servicing of more than one facility.

Amalgamation analyses of sodium samples removed thus far have been inconclusive and evidence the need for marked improvements in the technique. Chromatographic analysis of the cover gas indicates a high oxygen and moisture content. Diffusion of oxygen through the semipermeable glove fabric is suspected. Partial improvement has been effected by using gas purification trains of magnesium perchlorate to remove moisture, and NaK bubblers to remove oxygen. A more efficient purification train is required for the cover gas.

REFERENCES

1. *An Evaluation of Four Design Studies of a 1000 MW(e) Ceramic Fueled Fast Breeder Reactor*, Prepared by Reactor Engineering Division, Chicago Operations Office, U. S. Atomic Energy Commission, COO-279 (December, 1964).

2. L. E. Link, et al, *1000 MW(e) Metal-Fueled Fast Breeder Reactor Concept*, ANL-7001. (To be published.)

3. E. L. Kimont, *Engineering Development of a Practical 1200°F Sodium Vapor Loop*, Trans. Am. Nucl. Soc., 8, No. 1, 147 (June, 1965).

4. A. G. Hosler and F. A. Smith, *Impurity and Liquid Level Measurements for the FARET Loop*, Proc. Conference on Application of High-Temperature Instrumentation to Liquid-Metal Experiments, ANL-7100. (In press.)

Section 3

LIQUID METAL HEAT TRANSFER RESEARCH PROGRAM

3.1 Objectives

The objectives of this program are: (1) to acquire theoretical and experimental data on the thermodynamic properties and characteristics of liquid metals during single phase, boiling, and two-phase flow in forced convection systems; (2) to develop instrumentation and other metering devices essential to the accurate measurement and correlation of these high-temperature parameters; and (3) to use these data to derive new methods or to improve engineering computations traditionally employed in designing liquid metal heat transfer equipment or in predicting temperature gradients in reactor coolant channels.

3.2 Two-Phase Adiabatic Flow of Sodium

This experiment was designed to provide fundamental information on forced convection two-phase flow of sodium over the following range of operating variables:

Pressure, psia	2-17
Temperature, °F	1300-1650
Boiler Inlet Velocity, fps	1-5
Boiler Power Density, kW/liter	0-200
Liquid Superheat, °F	10-100
Quality	0.0005-0.01
Vapor Volume Fraction	0-0.87
Slip Ratio	5-100
Frictional Pressure Loss, in. H_2O	0-40
Boiling Operation, hr	1000

Primary emphasis was placed on the measurement and correlation of vapor volume fraction, quality, and two-phase frictional losses in an adiabatic test section. The secondary objective was to evaluate the performance of certain instrumentation, particularly the use of electromagnetic flowmeters for void fraction measurement.

The experimental apparatus used in these tests is shown schematically in Fig. 3-1. The loop is constructed of Type 316 stainless steel tubing (0.500 in. O.D., 0.035 in. wall) through which sodium is circulated at a maximum of 4 gpm. Both electromagnetic flowmeters featured kerosene-cooled permanent magnets and were calibrated by differential pressure measurements across the venturi section. Liquid levels in the venturi legs and the condenser well were continuously monitored by analog-type, 10-kc eddy-current gauges constructed of alumel and chromel wire for use at high

temperatures. Void fractions in the 24-in.-long rectangular test section were recorded by a traversing gamma-attenuation assembly, using a Tm-170 source. These outputs were compared with oscillograph records of flowmeter performance. The boiler is of the homogeneous type, with a maximum heat input of 10 kW. Boiling occurred at the boiler exit, or further downstream, and was limited to a low vapor quality range. All free sodium surfaces were blanketed with argon gas. These surfaces served as pressure control and measurement stations.

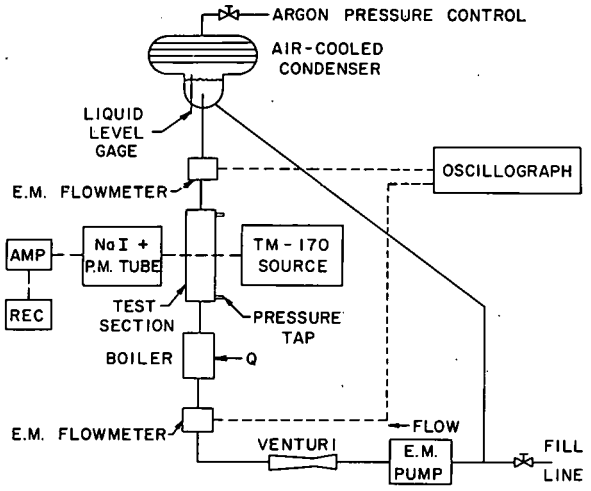

Fig. 3-1. Schematic of boiling sodium loop used for two-phase heat transfer studies up to atmospheric pressure

The following qualitative results and conclusions are based upon observations made during operations totalling 4200 hr at temperatures between 1300°F and 1650°F. To begin with, the range of liquid superheats obtained prior to the initiation of boiling was rather low when compared with values reported by other experimenters. Further, there is evidently a decrease in average superheat requirements with time, as shown in Fig. 3-2. Note that in the early stages of the experiment, the amount of superheat was unpredictable, whereas later measurements showed a much narrower scatter range. This phenomenon of liquid superheat is related to the more general problem of flow and boiling stability in a closed loop. At low pressure, the violent temperature and specific volume changes which accompany the onset of boiling lead to oscillatory conditions. These conditions cannot be called stable or "steady state" by any combination of reasonable assumptions and/or "averaging" techniques. Therefore, for purposes of correlating void fraction and pressure loss data, a stable condition was assumed to be achieved whenever (1) the pressure fluctuations were small compared to the absolute value; (2) the boiler inlet flow was steady; and (3) the time-averaged void fraction at a point was constant for a time sufficient to collect data. In general, stability was achieved at pressures greater than 7 psia, so that the correlated data presented here cover the range from 7 to 17 psia.

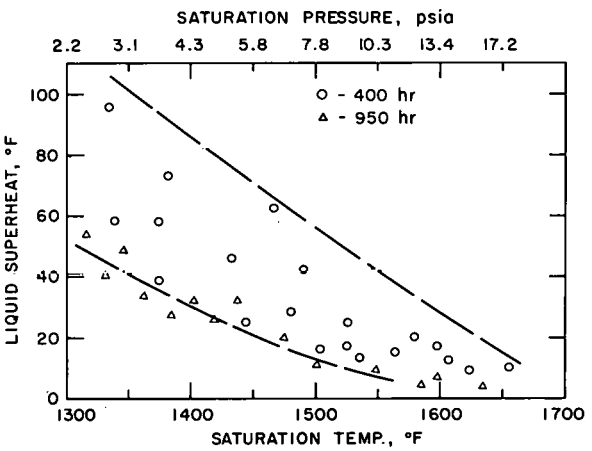

Fig. 3-2. Effect of system pressure and total boiling time on liquid superheat requirements at inception of boiling

Analysis of the void fraction data indicates that the electromagnetic flowmeter method is adequate for measurements in vertical upflow of two-phase liquid metals - at least up to some value of void fraction limited by the continuity of the liquid film on the duct walls. Operation of the flowmeter is based upon the assumption that, at constant magnetic flux, the output is a function of liquid velocity only, i.e.,

$$\alpha_i = 1 - K_1E_0/K_0E_1 \tag{1}$$

where α_i is the "ideal" void fraction; E_0 and E_1 are flowmeter outputs in the all-liquid and two-phase regions, respectively; and K_0 and K_1 are calibration constants.

Figure 3-3 shows a typical set of flowmeter data compared with uncorrected readings obtained from the gamma-attenuation apparatus. The flowmeter results are generally lower. This discrepancy was attributed to the change in two-phase electrical conductivity with increasing void fraction. Therefore, the following equation, implicit in the actual void fraction, α, was theoretically derived to account for this change in conductivity:

$$\alpha_i = A\alpha \frac{1 + f(\alpha)(\rho_f t/\rho_w h) + 1/S_c}{1 + \rho_f t/\rho_w h + 1/S_c} \tag{2}$$

where A, t, h, and S_c are geometric constants for a rectangular duct; ρ_f and ρ_w are electrical resistivities of the liquid and duct wall, respectively; and $f(\alpha)$ is the correction factor for the change in conductivity. This factor can be expressed as:

$$f(\alpha) = (2+\alpha)/2(1-\alpha) \tag{3}$$

or

$$f(\alpha) = \exp(3.8\alpha) \tag{4}$$

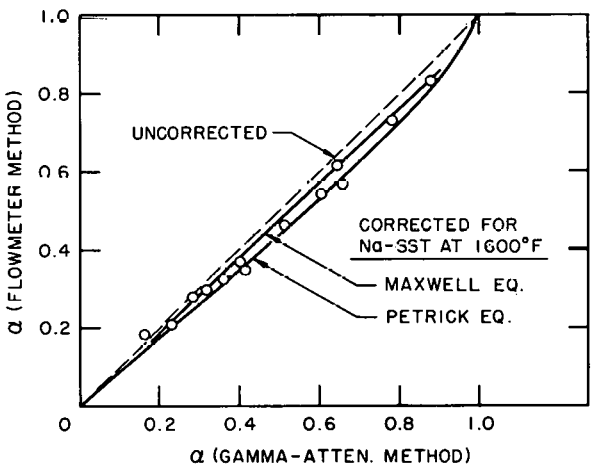

Fig. 3-3. Comparison of void fractions determined by flowmeter and gamma-attenuation methods

Equation (3) is a theoretical expression due to Maxwell, while Eq. (4) is an empirical expression derived from magnetohydrodynamic generator studies by Petrick at Argonne.

Both of these corrections are plotted in Fig. 3-3. The important quantity here is the electrical resistivity ratio, ρ_f/ρ_w. If the liquid resistivity is much smaller than that of the wall, then the choice of $f(\alpha)$ is not very

critical; however, as this ratio approaches unity, the correction and choice are important. In the present system, i.e., sodium-stainless steel, the ratio is low, so the importance of the correction is minimized. Some low-temperature experiments with various materials will be carried out to determine the correct factor. The relative simplicity of the flowmeter measurement implies an attractive application to higher temperature systems such as the Nb-1%Zr-Na system described in the following section. Such a system has a resistivity ratio close to unity in the 1800-2100°F range, so the correct $f(\alpha)$ must be known.

For higher-quality flows, a quality factor must be introduced into Eq. (1). The flowmeter-oscillograph system used to record voids was fast enough to follow liquid velocity variations in the vicinity of the flowmeter; both slug and annular flow regimes were encountered there, according to the instantaneous output of the flowmeter. Thus the system should also prove useful for transient boiling studies.

Detailed comparisons of the pressure drop and slip ratio data with existing correlations for sodium were not made. The qualities were very low, so that a definite dependence of two-phase friction factor on quality was not clear. However, the slip ratios were definitely higher than counterpart values determined from correlations of steam-water data. There may be either a systematic measurement error in quality measurement, or non-equilibrium effects. For example, if the qualities are not as high as calculated from the equilibrium case, then the actual slip ratios are lower than the calculated range listed at the beginning of this section.

A more comprehensive description of the foregoing tests is being prepared for publication as an ANL topical report.

3.3 Boiling Sodium Studies

3.3.1 2100°F Boiling Sodium Test Facility

When completed, the facility shown in Fig. 3-4 will be used to extend the foregoing studies up to a temperature of 2100°F, and a pressure of about 8 atm. Variables to be investigated will include boiling heat flux and temperature difference up to the critical heat flux, boiling and adiabatic two-phase pressure drop, vapor volume fraction, slip ratio, and boiling stability parameters. Loop operation is scheduled for January, 1966.

Constructed primarily from Nb-1%Zr tubing (0.500 in. O.D., 0.035 in. wall), the loop is contained within a chamber which will be evacuated to 10^{-7}-10^{-8} torr. Major components of the loop include a thermal radiation-heated boiler, an adiabatic riser section, a radiating coil condenser, and an electromagnetic helical induction pump.

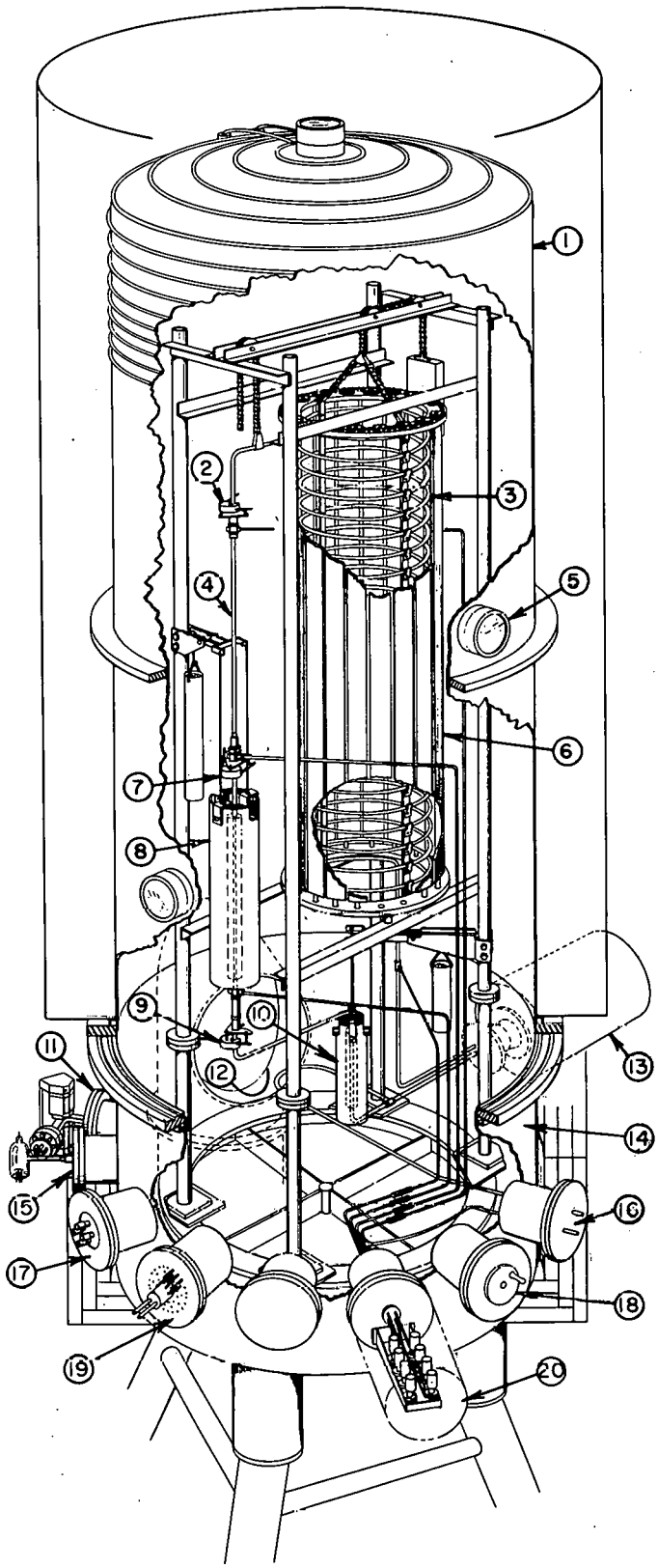

1. VACUUM CHAMBER COVER
2. ELECTROMAGNETIC FLOWMETER (VOID FRACTION)
3. THERMAL RADIATING COIL CONDENSER
4. ADIABATIC RISER SECTION
5. VIEWING PORT
6. SHUTTERS
7. ELECTROMAGNETIC FLOWMETER (VOID FRACTION)
8. BOILER SECTION
9. ELECTROMAGNETIC FLOWMETER (FLOW RATE)
10. PRE-HEAT SECTION
11. PARTIAL-PRESSURE ANALYZER
12. VACUUM PUMP PORT
13. ELECTROMAGNETIC PUMP
14. VACUUM CHAMBER BASE
15. IONIZATION GAUGE
16. SODIUM LINES FROM DUMP TANK
17. POWER FEEDTHROUGHS
18. ROTARY FEEDTHROUGH FOR SHUTTER MECHANISM
19. THERMOCOUPLE AND COOLANT FEEDTHROUGHS
20. PRESSURE TRANSDUCERS

Fig. 3-4. Schematic of 2100°F boiling sodium test facility

The boiler section consists of a thick-walled Nb-1%Zr tube (2 in. O.D., 0.312 in. I.D., 24 in. long) surrounded by twelve, closely-spaced tungsten heating elements. These elements are surrounded by thermal radiation shields constructed of tantalum. This radiant heat is conducted through the tube wall to the liquid metal flowing inside the tube. Thermocouples are placed at various radial and axial locations in the tube wall so that both the heat flux and the inside wall temperature may be determined. Heat fluxes ranging up to 10^6 Btu/(hr)(ft^2) are anticipated.

Electromagnetic flowmeters are located at the boiler inlet, between the boiler and riser section, and at the riser outlet to obtain the flow rates and void fractions of the two-phase mixture. Pressure taps and thermocouples are also located at these points for the determination of absolute pressure, pressure drop, and energy balances.

Heat is removed from the loop by a thermal radiation coil condenser. This condenser contains 26 coils arranged on an 18-in. coil diameter, with a 2.5-in. space between coils. Heat loss from the condenser is controlled by operating a shutter mechanism.

Temperature measurements are to be made with twenty-five W-25% Re/W-3% Re and forty chromel/alumel ungrounded junction thermocouples enclosed in hermetically-sealed, niobium-1% zirconium sheaths (0.0625 in. O.D.). Choice of the refractory metal conductors allows high temperature measurements to be made, limited only by the alumina insulation to a maximum working temperature of approximately 2600°F.

Eight primary pressure measurements are to be made, using Type 304 stainless steel diaphragm transducers: four transducers for absolute measurements and four for differential readings. Maximum operational differential or absolute pressure for any one diaphragm is 200 psia. Diaphragm motion will be sensed with a linearly variable differential transformer. Signals will be fed to a Model CAS-2500 Carrier System. This system, consisting of a power supply, oscillator, amplifier, demodulation, and a phase-sensitive rectifier will be used to obtain a d-c output proportional to the diaphragm displacement. Overall system error is expected to be within ±2%.

Analog data from thermocouples, pressure transducers, flowmeters, the boiler and pre-heater, and the liquid metal pump will be read on a Hewlett Packard-Dymec Model 2010D data-acquisition system. This system consists of a crossbar scanner, an integrating digital voltmeter, a preamplifier, a tape punch coupler, a punch power supply, and a Teletype BRPE-11 paper tape punch. Provisions have been made so that the punched paper tape output can be fed directly into a Model 160A computer programmed for data reduction.

3.3.2 Prototype Heater Development

The feasibility of using thermal radiation to generate fairly high and uniform heat fluxes in liquid metals has been demonstrated. Three heaters have accumulated a total of 750 hr operation in a small-scale, forced convection test loop. This loop was operated to obtain single-phase (500 hr) and boiling (250 hr) heat transfer data on upward flow of NaK in a vertical tube under constant heat flux conditions. The test parameters included heat fluxes ranging up to 62,000 Btu/(hr)(ft^2), flow rates up to 416 lb/hr, and liquid metal temperatures up to 1400°F.

The single-phase data were in good agreement with correlations developed by Lyon[1] and Dwyer.[2] During two-phase operation, boiling was generally accompanied by a "bumping" noise and flow instabilities.

An electron-bombardment heated boiler section also is being developed for future use with the Nb-Zr loop. The heater section will consist of a Nb-1%Zr tube (anode) encircled by either tungsten or thoriated-tungsten emitters (cathode). This heating arrangement will be surrounded by shielding, the inner shield being at the same electrical potential as the cathode. Emitted electrons will be directed to the anode by an accelerating voltage. Heat fluxes well above 10^6 Btu/(hr)(ft^2) are anticipated.

Two small-scale electron-bombardment heating experiments were conducted to investigate geometric and mechanical factors involved in the construction of a high-flux heater. During both tests, the sodium was sufficiently subcooled so that no boiling occurred. In the first test, thermocouples at various positions on the anode outer surface gave identical readings at given heat fluxes, indicating uniformity of flux. Heat fluxes up to 8000 Btu/(hr)(ft^2) were obtained. Limitations of the available power supply necessitated termination of the test at this value. With increased power input (voltages up 20,000 V and currents up to 1 A), heat fluxes ranged to 20,000 Btu/(hr)(ft^2). Thermocouples in the anode wall recorded temperature increases up to 8°F/sec.

Subsequent tests are pending heater modification, improvement of operating vacuum level, and better matching of the 200-kW power supply to the heater circuit.

3.4 Evaluation of Traditional Liquid-Metal Heat Transfer Design Computations

At the outset, these "traditional" engineering computations are limited to those which rely upon direct use of heat transfer coefficients in designing heat exchangers for, and predicting temperature gradients in coolant channels of, liquid metal-cooled reactors. The inference is that usage of these coefficients is all-inclusive. This is not true. For example,

when expressed as Nusselt or Stanton numbers for turbulent flow of non-metallic fluids, heat transfer coefficients are, for most practical purposes, functions only of Reynolds and Prandtl numbers. With liquid metals, however, these coefficients also depend significantly on other characteristics of the system to which they are applied.

The procedure used to evaluate these traditional methods is as follows: Detailed profiles of local fluid temperature distributions are plotted from mathematical analyses based on first principles. These distributions are then used to compute heat transfer coefficients, duct surface temperatures, and heat transfer rates. Related experiments are performed in support of these computations. Comparisons are then made with counterpart values predicted by the traditional engineering methods. The ultimate objectives are: (1) to identify and resolve the discrepancies in these methods; and (2) to effect improvements such that repetitive basic mathematical analyses need not be performed for each prediction.

A detailed description of these analyses and their reflections on traditional engineering prediction methods has been published.[3] The important aspects of these studies are summarized here, along with some more recent results.

3.4.1 Heat Transfer in Double-Pipe Heat Exchangers

Investigations related to liquid metal heat exchangers have concentrated on relatively simple, double-pipe units of various configurations. Extensions to cross-flow and shell-and-tube exchangers as well as to boilers and condensers are planned for the future.

The results of these analyses, when interpreted in terms of heat transfer coefficients and predictions of heat transfer rates, indicate the following. With co-current flow, fully developed local channel heat transfer coefficients are never larger than values corresponding to the boundary condition of uniform wall flux, but can be significantly less than values corresponding to the boundary condition of uniform wall temperature. With counter-current flow, the coefficients are never less than values corresponding to the boundary condition of uniform wall temperature, but can be significantly larger than values corresponding to the boundary condition of uniform wall flux. In addition to their dependence on Reynolds and Prandtl numbers, the actual values of these coefficients are a complicated function of the exchanger operating conditions, and the effect is an important one for liquid metals. It was also found that the extremely high local heat transfer rates in the thermal entrance regions contribute significantly to the overall heat transfer rate of these heat exchangers. Since traditional design relations do not account for either of these observations, their predicted heat transfer rates, heat exchanger lengths, and their interpretations of experimental data can be seriously inaccurate.

Improved design relations have been formulated to include the quantities η and ϕ. The quantity η is defined as the ratio of the actual fully developed overall heat transfer coefficient to the overall heat transfer coefficient generally used in the traditional relations. The quantity ϕ, called the "Effectiveness Coefficient," is used to multiply the exponential terms in the customary relationships[4] used to compute heat exchanger effectiveness or efficiency. The basic form of the traditional relationships is modified, only when necessary, to include these quantities. For example, when η and ϕ are both unity, these relationships apply in their simplest forms.

Both quantities are themselves complicated functions of the exchanger operating conditions. Detailed tabulations of the respective values for concentric tube co-current flow exchangers are being compiled for publication. Significant improvements in accuracy of predictions resulting from the use of these parameters have been verified experimentally.[5]

For the counter-current flow exchangers, relatively simple procedures for assessing the parameter η have been developed; representative values over wide ranges of operating conditions have been obtained. Procedures for the determination of ϕ, however, are still in the exploratory stage.

The detailed analyses of the double-pipe heat exchanger required extensions of the classical Sturm-Liouville system related to the mathematics of boundary value problems.[6] In the case of the counter-current flow exchanger, these extensions revealed certain important aspects that appear to be new in the field of applied mathematics.[3] These "new aspects" are intimately related to the computational procedures that are being explored. Experimental procedures for determining both η and ϕ have been developed in support of the analytical program.[7]

3.4.2 Temperatures in Reactor Coolant Channels

As mentioned earlier, first principles are also used to derive improved relations for predicting temperatures in liquid metal coolant channels. Equation (5) is typical of these relationships. In this instance, the formulation is used to predict surface temperatures for a channel with a non-uniform, lengthwise heat flux distribution:

$$(\xi_S - \xi_B) = \sum_{k=0}^{\infty} R_k F^{(k)} \qquad (5)$$

where

$$F^{(k)} \equiv d^k F / dz^k$$

$$F^{(0)} \equiv F$$

Detailed definitions of the terms are given in Reference 3. Briefly, the left-hand side of Eq. (5) represents a dimensionless temperature difference between the channel surface (ξ_S) and the bulk coolant (ξ_B). On the right-hand side, F represents a dimensionless heat flux which is a function of a dimensionless axial position variable z. The quantities R_k can be likened to generalized thermal resistance coefficients which depend on the duct geometry, Reynolds number, and Prandtl number; they are independent of the actual flux distribution. The coefficient R_0 is equal to $2/Nu(\infty)$, where $Nu(\infty)$ is the appropriate Nusselt number for a uniform flux distribution. Also, $R_k \to 0$ as $k \to \infty$. When the heat flux is uniform, $F^{(k)} = 0$ for $k > 0$, and Eq. (5) reduces to the customary definition of the heat transfer coefficient.

For non-uniform flux distributions, $F^{(k)} \neq 0$; however, for most cases of practical interest, only the first few terms of the infinite series need be retained. Thus with the coefficients R_k known, Eq. (5) becomes a relatively simple expression to use for predicting channel surface temperatures under these conditions. On the other hand, Eq. (5) can be divided by F to achieve the equivalent inverse of the usual heat transfer coefficient (on the left-hand side). However, the coefficients obtained in this manner will depend upon the heat flux distribution and channel length. Subsequent use of these coefficients for specific flux distributions could result in unnecessarily cumbersome computations.

Values of resistance coefficients R_k were determined for liquid sodium flowing through a parallel plane channel, and applied to a cosine heat flux distribution. With operating conditions typical of current fast reactor designs, the single R_0F term of Eq. (5) gave sufficiently accurate predictions of the duct surface temperature. On the other hand, more terms were required for similar predictions based upon operating conditions that might prevail in future fast reactor systems. Further, in extreme cases, the approximations upon which Eq. (5) is based become invalid, and a more general relationship had to be used.[3]

REFERENCES

1. R. N. Lyon, *Liquid-Metal Heat Transfer Coefficients*, AIChE Trans., 47, 75-79 (1951).

2. O. E. Dwyer, *Eddy Transport in Liquid-Metal Heat Transfer*, AIChE Journal, 9, No. 2 (March, 1963).

3. R. P. Stein, *Liquid Metal Heat Transfer*, Advances in Heat Transfer, Vol. III, (eds.) T. F. Irvine and J. P. Hartnett (New York: Academic Press, Inc.).

4. M. Jakob, *Heat Transfer*, (New York: John Wiley and Sons, 1957), Vol. II, pp. 208, 211. Also see E. R. G. Eckert and R. M. Drake, Jr., *Heat and Mass Transfer*, (New York: McGraw-Hill Book Co., Inc., 1959), p. 482.

5. R. L. Merriam, *An Investigation of Liquid-Metal Heat Transfer in a Co-Current Flow, Double-Pipe, Heat Exchanger*, ANL-7056 (June, 1965).

6. R. P. Stein, *The Graetz Problem in Co-Current Flow, Double-Pipe, Heat Exchangers*, ANL-6889 (November, 1964).

7. R. P. Stein, *A Method for the Determination of Local Heat Fluxes in Liquid Metal Heat Exchangers*, Proc. Conference on Application of High-Temperature Instrumentation to Liquid-Metal Experiments, ANL-7100. (In press.)

Section 4

MAGNETOHYDRODYNAMICS

4.1 Potential of Liquid-Metal MHD Cycles for Central Station Power Systems

On the basis of advances in liquid-metal magnetohydrodynamics and similar advances in reactor and materials technology, a power system is evolving which has a strong potential for successful development. This system features a liquid-metal MHD generator coupled to a nuclear reactor heat source. The concept can be developed either as a compact power source or as a topping unit for a conventional steam plant which functions as the sink or bottoming cycle. It should be noted that a fossil-fuel-fired boiler using a liquid-metal coolant also can be employed as the heat source. The heat transfer characteristics of liquid metal are superior to those of water, and the boiler would operate at the highest cycle temperature with a low vapor pressure.

The details of the various analytical and experimental efforts in support of this concept are described in ANL-6954.[1] They are summarized briefly in the following subsections.

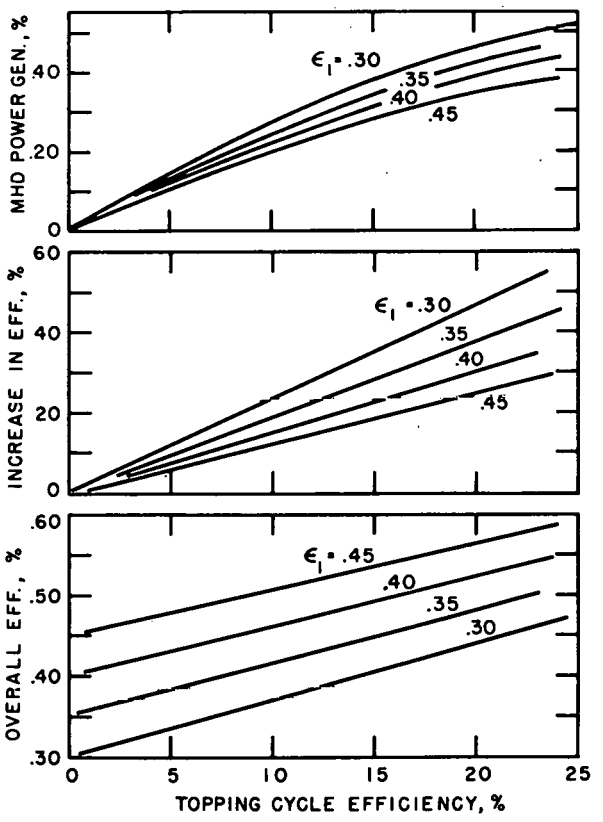

Fig. 4-1. Overall cycle efficiency, percentage increase of cycle efficiency, and percent of total power generated by MHD topping cycle vs. topping cycle efficiency and steam plant efficiency

4.1.1 Efficiencies of Binary Cycles

The overall efficiencies of a binary power cycle using a MHD topping cycle were computed by combining the efficiencies of the topping cycle with steam-plant efficiencies in the following manner:

$$\epsilon_c = \epsilon_{mhd} + (1 - \epsilon_{mhd})\,\epsilon_{sc}, \qquad (1)$$

where ϵ_{mhd} is the efficiency of the topping cycle and ϵ_{sc} the efficiency of the steam bottoming cycle.

The overall cycle efficiency, percentage increase of the cycle efficiency, and the percent of the total power generated by the MHD topping cycle are shown in Fig. 4-1 as a function of the topping cycle efficiency and the base steam-plant efficiency. From Eq. (1) it is apparent that the overall efficiency of the binary cycle increases with increasing efficiency of the topping cycle. Moreover

efficiencies greater than 50% are readily obtained when the base steam-plant efficiency (ϵ_{sc}) is equal to or greater than 40% and the topping cycle efficiency is 15% or greater. Maximum overall cycle efficiency is generally reached when the secondary steam cycle is operated at maximum allowable temperature conditions. As the sink temperature is increased, the decrease in the efficiency of the topping cycle is more than offset by the increase in the steam cycle efficiency. The end result is a maximization of the overall cycle. By combining Eq. (1) with the topping-cycle data, the following results can be deduced:

(1) If an alkali metal is specified as the working fluid, the maximum potential efficiency of the overall cycle ranges between 55% and 60%, and results from either a potassium- or cesium-steam binary cycle. The liquid-metal topping cycle operates between a temperature range of 2240°F and 1100°F, and produces 35% of the total power. The bottoming steam plant is assumed to be the equivalent of a modern supercritical plant, such as the Eddystone unit, operating at 4000 psi and 1050°F. The efficiency of such a plant was assumed to be ~0.45 after upgrading the published Eddystone efficiency of 0.407. The upgrading results from the elimination of boiler inefficiency and stack losses.

(2) The maximum potential efficiency of the mercury-steam binary cycle is ~56%, or slightly lower than that for the cesium- or potassium-steam binary cycle. This is based on a source temperature of 1540°F and a condenser temperature of 1100°F. If the sink temperature is decreased to 440°F, the overall cycle efficiency decreases correspondingly to ~47%, even though the efficiency of the topping cycle increases substantially. From a thermodynamic viewpoint, mercury is the superior working fluid. It has several major drawbacks, however. The principal drawback is its rapidly rising vapor pressure at high temperature. Other drawbacks are (a) poor wettability and heat transfer characteristics which require the use of additives; this tends to increase operational problems considerably; (b) limited availability; and (c) relatively high cost. The feasibility of the high-pressure mercury system is questionable.

(3) For the medium temperature range (1100-1600°F), mercury-potassium alloy and potassium appear to be the most promising working fluids for the liquid-metal cycle. Overall cycle efficiencies up to 50% appear possible. The MHD topping cycle can have an efficiency as high as 15% and its maximum working pressure would be below 75 psi.

(4) The working fluid most suitable for a pure MHD power cycle appears to be mercury.

The attractiveness of the calculated cycle efficiencies is apparent. The incentive for development of the cycle, therefore, must be dictated by strictly economic considerations. Although no detailed economic studies have been made, the results of a preliminary study tend to indicate a favorable economic argument.[1]

4.1.2 MHD Generator Tests

The efficiency of a MHD generator operating with two-phase mixtures depends upon (1) the nature of the flow; (2) the conductivity of the two-phase fluid; and (3) the degree to which the total liquid flow interacts with the magnetic field. . Because the flow pattern of a two-phase mixture changes from a dispersion of gas in liquid to a dispersion of liquid in gas as the mixture quality is increased, the conductivity of the fluid changes sharply.

Accordingly, two different types of generators have been fabricated for testing in a NaK-N_2 loop. The first is a variable-area generator which operates with a two-phase mixture wherein gas is dispersed in the liquid. For this type of flow, the mixture quality is generally quite low ($<5\%$) and the corresponding void fractions are less than 90%. As the mixture quality is increased beyond 10%, the degree of dispersion increases and the interaction between flow and magnetic field decreases sharply.

Hence, for the very high void, highly-dispersed liquid flow regime, a second, film-type generator will be investigated. In this generator, the liquid is separated from the vapor by impingement on the lower channel where the high-velocity film interacts with the magnetic field. Thus separation and power generation occur simultaneously in the generator. The efficiency of this type of generator will be a function of the degree of separation, the skin friction, and momentum losses.

4.1.3 End Losses in MHD Generators

In an MHD generator channel of finite aspect ratio (finite ratio of length to width), the actual power density is less than the value calculated for a channel of infinite aspect ratio. This difference is due to current loops at both ends of the channel. The net effect is one of providing a conduction path between the electrodes. This path acts as a shunt resistance in parallel with the load. Thus for a given load and generated emf, both the net load-current and the voltage load-coefficient are reduced.

The problem of end losses in an MHD channel of variable cross section does not appear to have received any attention in the published reports. However, this type of channel has been proposed and used in the cycle analyses summarized earlier. Therefore, studies were undertaken to determine the feasibility of inserting insulating vanes to reduce or eliminate these end losses. These studies were made on an electrical analog, using Teledeltos conducting paper.

The effectiveness of a vane configuration was judged by the gain in the maximum possible efficiency of the generator, as compared with the unvaned case. For example, a channel with an aspect ratio of 2 would be capable of offering a maximum efficiency of 40.4%. When inserted on the

center-line, a single, long vane increased the efficiency to 52.1%. Of all the vane configurations studied, the most promising one increased the efficiency capability to 66%. This configuration involved multiple vanes of varying length. Further gains may be secured by employing channels with larger aspect ratios. For example, with the same vanes, a channel with an aspect ratio of 4 would be capable of a maximum efficiency of 74%.

The analog predictions were checked with the aid of a plexiglass model generator. This model was used to circulate a solution of lithium sulphate in demineralized water. Velocities ranged up to 7 ft/sec. Attempts to use d-c current had to be abandoned because of excessive polarization, even at the higher velocities. With the use of a-c current, satisfactory confirmation was obtained for the case of a single, long vane. Plans are to extend these tests to include the multiple vane configurations.

4.1.4 Two-Phase Nozzle Studies

Two, rectangular, converging-diverging nozzles with high aspect ratios have been tested, using air-water mixtures as the working fluid. The purpose of the tests was to obtain data on the critical flow rates, critical pressure ratios, pressure profiles, and exit void fractions in the diverging portion of the nozzles.

The first nozzle had an exit-to-throat area ratio of 2 (throat area = 1 x 0.125 in.; exit area = 2 x 0.125 in.). With this nozzle, qualities ranged from 0.0001 to 0.1 at initial pressures from 30 to 80 psia. Velocity ratios measured at the exit plane varied from 0.5 to 40.0. Ratios less than 1.0 were obtained when the flow stream overexpanded in the diverging portion of the nozzle. Overexpansions, indicated by the measured pressure profiles, occurred only for qualities less than 0.01. Validity of the velocity ratios for qualities greater than 0.01 is suspect because of the inability to accurately measure the extremely high (>90%) void fractions that occur in this quality regime.

The second nozzle, with a throat area three times larger than above, exhibited substantially different performance characteristics. Slip ratios, calculated from void fraction measurements over the same quality range, were consistently below 1.0. The averaged value was 0.75.

The differences between the two nozzles are subject to further analyses and testing. However, the present data indicate that two-phase nozzle efficiencies as high as 90% are not unreasonable to anticipate with a properly designed nozzle.

4.2 Condensing Injector Studies

The feasibility and potential of the two-phase liquid-metal MHD power cycle depends, to a large extent, on the condensing injector. In this unit, which is upstream of the MHD generator, the vapor phase is condensed and a high-stagnation-head liquid is generated. This liquid then passes through the generator wherein electrical energy is produced by interaction with the magnetic field.

Developed primarily for use as a boiler feedwater pump, the condensing injector has been generally regarded as a low-efficiency device. However, recent experimental and analytical studies have indicated that the performance of the injector can be very high. More importantly, that it can generate very large stagnation pressures - a mandatory requirement for the liquid metal MHD cycle.[2-5]

Completed cycle analyses at Argonne[1] have shown there are large geometry, fluid, and parameter ranges of interest which have not been covered by the referenced investigations. These analyses have clearly pinpointed three major parameters which essentially control the injector performance. They are: (a) the area contraction (ratio of the combined area of liquid and vapor at the injection point to the area at the minimum diameter of the mixing region); (b) the Mach number of the inlet vapor stream; and (c) the inlet liquid to vapor pressure ratio. Therefore, a program is underway to evaluate the effect of these parameters on injector performance.

The first phase of this program has been completed.[6] It entailed preliminary experiments with steam-water mixtures in a closed loop. (See Fig. 4-2.) The cross section of the injector was designed to simulate a unit that would be used in conjunction with the magnet to supply the transverse field. In addition, movable baffles were installed in the combiner and diffuser sections. These baffles could be positioned at various angles to effect changes in the contraction ratios. The portion of the nozzle relative to the narrowest section of the combiner also could be varied. Finally, instrumentation was installed to measure temperature, pressure, and flow rates during loop operation, and to enable determination of energy partition.

Operation over a limited range of steam-water mixtures, temperatures, pressures, and fluid velocities indicated a condensing injector efficiency of 2% in converting enthalpy to kinetic energy. (The Carnot cycle efficiency for an overall power cycle would be much higher.)

Similar experiments will be conducted with various working fluids to further explore the potential of the injector for improved performance. For example, the next series of tests will be made with Freon-11. This refrigerant was selected because of its low latent heat, greatly reduced power requirements, and similarity to the ultimate working fluid: liquid metal.

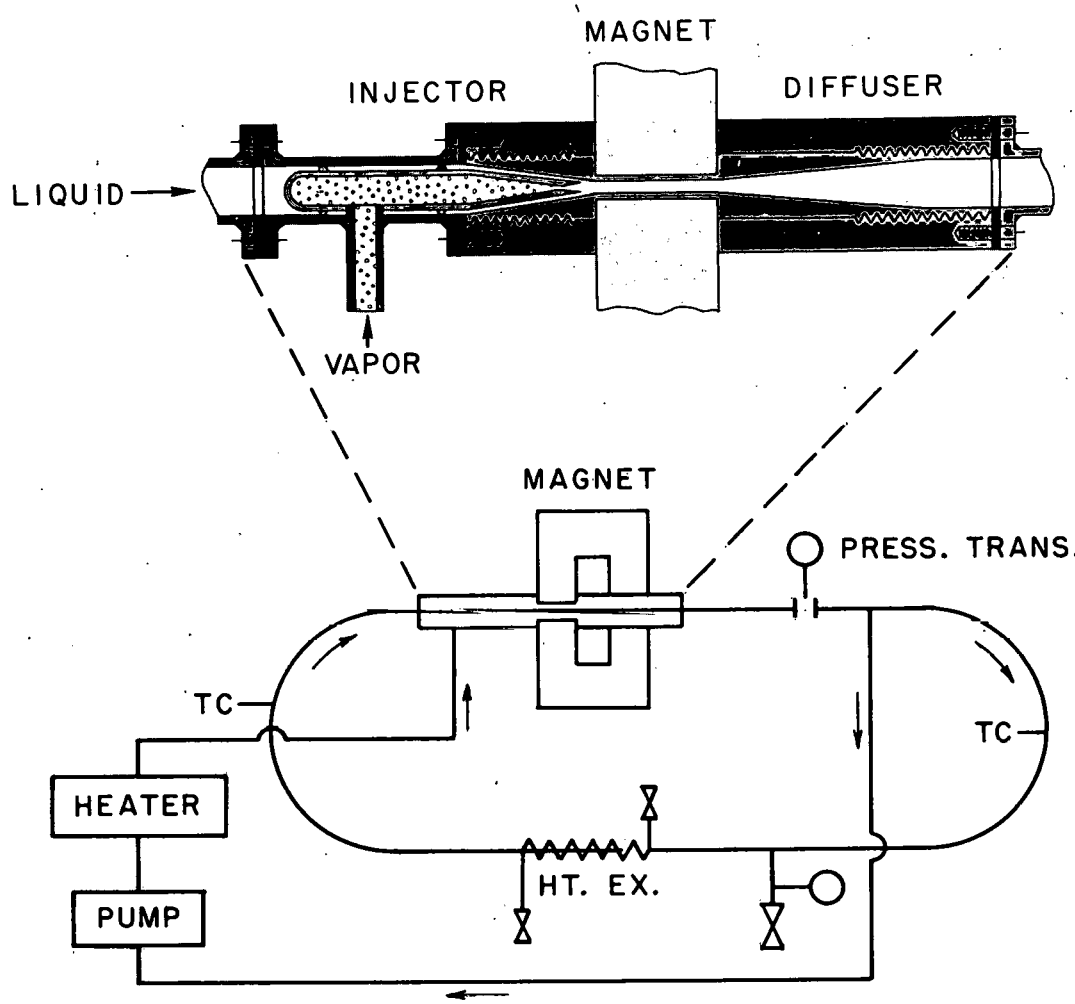

Fig. 4-2. Schematic of condensing injector test loop assembly. Inset shows enlarged cross section of injector

4.3 Production of a-c Current from MHD Generators

The purpose of this investigation was to determine the feasibility of producing alternating current from a liquid-metal MHD generator. As shown in Fig. 4-3, the concept is based upon the formation and acceleration of liquid metal slugs through separate ducts in a magnetic field. Electrical power pulses produced in this manner are of high current and low voltage. By means of a transformer, they are converted to pulses of high voltage and low current. Finally, a positive pulse from one generator duct is combined with a negative pulse from the other duct to produce an alternating current waveform.

For test purposes, NaK slugs were driven by nitrogen gas pulses. (Note: In a prototype cycle, liquid metal of low vapor pressure would be driven by a liquid metal of high vapor pressure. The driving fluid would be vaporized in a reactor. Upon leaving the generator, the vapor would be condensed and returned to the reactor to complete the cycle.) Instrumentation was installed to furnish voltage, current, and pressure as a function of time.

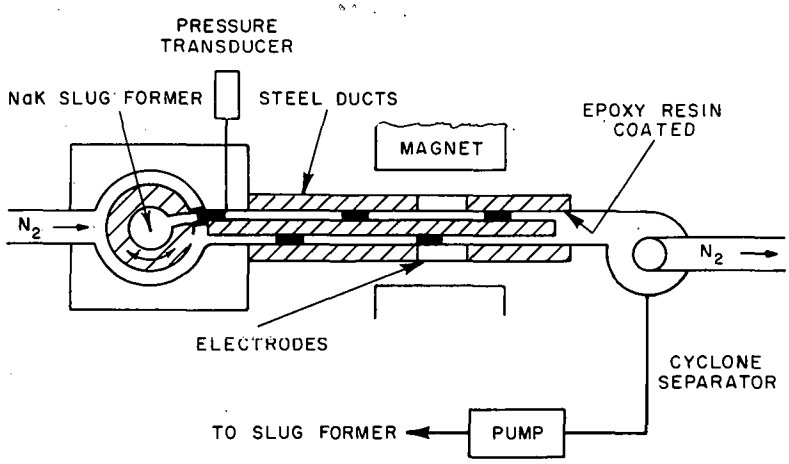

Fig. 4-3. Schematic of experimental liquid-metal MHD assembly used to study feasibility of generating alternating current. Valve in slug former alternately forces slugs of NaK and nitrogen into two ducts which penetrate the magnetic field. Electric pulses generated in this field are transformed and combined to produce an a-c waveform.

Analyses of data taken at 30 cps indicated that the slugs were reproducible and of constant resistivity. However, optimum driving energy was not achieved because of improper timing of the gas pulses. With improved timing it is believed that frequencies up to 60 cps are possible.

4.4 Use of Electromagnetic Field to Control Liquid Metal Condensation Rates

One major component of all vapor power generation cycles is the heat rejector, usually a condenser. Its performance characteristics in water cycles are well known; however, in liquid-metal systems, especially those designed for operation in low- or zero-gravity environments, abnormally low condensation rates will result if no innovations are introduced.

One innovation designed to control and to increase condensation rates is the use of an electromagnetic field. This concept employs the principle of electromagnetic pumping to accelerate the electric-conducting liquid (condensate) by its interaction with an electromagnetic field. The acceleration is independent of gravitational forces and results in a controllable heat transfer rate by thinning the condensate film.

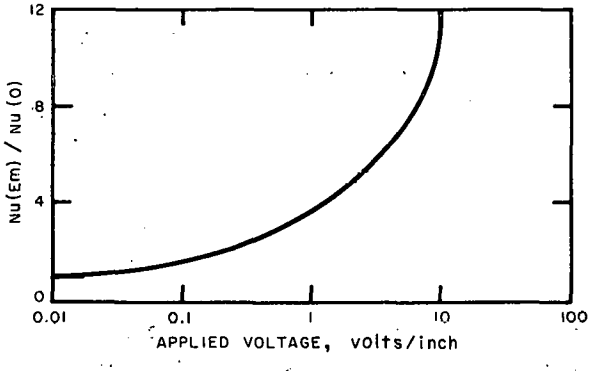

Fig. 4-4. Relative increase of condensation Nusselt number with an electromagnetic field

An extensive theoretical study has revealed that condensation rates can be increased substantially in this manner. For example, Fig. 4-4 shows the results of a calculation based on

condensing sodium at 1 atm and 1630°F on a 1-ft-square plate, with the parameter $c\Delta T/h_{fg} = 0.001$ and a constant magnetic field of 20 kilogauss. The ratio of the Nusselt number with, to that without, an electromagnetic field, increases markedly as the applied voltage is increased.

The merits of this innovation are subject to experimental confirmation.

4.5 Significance of Heat Transfer in MHD Generators

A theoretical study of combined natural and forced convection in liquid metal flow through an electromagnetic field has been completed. The primary objective was to determine the effect of temperature gradients in the liquid on the operating characteristics of an MHD generator.

Briefly, it was found that during transient startup:

(1) Significant flow (hence, power) and temperature oscillations can occur if the Rayleigh (Ra) and/or Hartmann (M) numbers are large. These numbers are a measure of the magnetic field strength and the free convective forces, respectively.

(2) That these oscillations can be prevented by allowing the magnetic field to become fully established in the liquid before pumping is initiated. (See Fig. 4-5.)

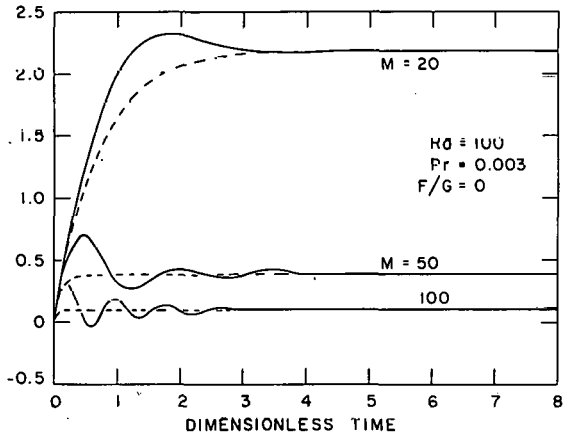

Fig. 4-5. Effectiveness of fully-established magnetic field (dashed curve) in preventing flow oscillations during transient startup of MHD device

(3) That knowledge of the Hartmann and Rayleigh numbers is sufficient to determine when the contribution of free convection to the overall heat transfer rate between the channel walls and liquid should be considered. In particular, if $M > 5 + (Ra/40)$ the contribution is less than 10% and can be neglected.

It was also found that a magnetic field sufficiently flattens the velocity profile so that, in many cases, the flow can be considered one-dimensional. A relationship between the Hartmann number and the aspect ratio (γ) was also established. This relationship shows when a one-dimensional approximation (max. error = 5%) can be made in calculating the ratio of the flow rate to the pressure gradient. Also, when free convection is not important and $M \gtrsim 38.5$, all rectangular channels may be considered as parallel-plate channels.

REFERENCES

1. Michael Petrick and Kung-You Lee, *Liquid MHD Power Cycle Studies*, ANL-6954 (June, 1965).

2. G. A. Brown, *An Analysis of Performance Data from the NUOS Condensuctor Test Facility with a New Theory for the Variable-Area Condensuctor*, Joseph Kay and Co. Inc., Cambridge, Mass., Report 44 (1961).

3. J. Miguel and G. A. Brown, *An Analytical and Experimental Investigation of a Condensing Ejector with a Condensable Vapor*, Paper No. 64-469, First AIAA Annual Meeting, June-July, 1964.

4. Lance Hays, *Investigation of Condensers Applicable to Space Power Systems, Part II: Jet Condensers*, Electrical Optical Systems Report 1588 - Final II (November, 1962).

5. R. P. Rose, *Steam Jet Pump Analysis and Experiments*, WAPD-TM-227 (June, 1960).

6. E. S. Sowa, *The Liquid-Metal Linear Generator*, Proc. AMU-ANL Conference on Direct Energy Conversion, Argonne, Ill., ANL-6802 (November, 1963), p. 181.

Section 5

FAST REACTOR SAFETY RESEARCH AND DEVELOPMENT

5.1 Sodium Expulsion Studies

During accidental power excursions and/or loss of sodium flow in fast reactors, the primary coolant may be expelled by at least two physical mechanisms: (1) a pressure pulse generated by rapid thermal expansion of fuel components and adjacent thin layers of coolant; and (2) an explosive rate of vapor generation that follows superheating of the coolant. Which, if either, of these mechanisms occurs depends primarily on the rate of energy input and the thermophysical and transport properties of the fluid. At present, both mechanisms are only partially understood; hence, it is impossible to accurately predict the circumstances under which coolant will be expelled. These circumstances and the consequent phenomena (pressure transients and channel voiding) must be understood and predictable if safe operating limits of a reactor are to be established.

Accordingly, a combined experimental and analytical program is underway to determine (1) the conditions which promote expulsion of coolant from a simulated reactor channel; (2) the magnitude of the resulting pressure transients; (3) the velocity of the expelled coolant; and (4) to develop a theoretical model of the expulsion mechanism. Preliminary to the liquid-metal expulsion program, exploratory tests will be made with light water in order to refine experimental techniques and to observe the physical response of the coolant. Parameters of interest in the water tests are (1) the time required to complete acceleration of the water; (2) measurement techniques to determine this time; (3) pressures developed during the accelerations; and (4) general knowledge related to the dynamics of the expelled column of liquid, such as voids as a function of time.

The physical design of the water experiment consists of a quartz pipe (1 in. I.D., 24 in. long) which contains an electrically-heated, Type 304 stainless steel tube (0.750 in. O.D., 0.005 in. wall, 10 in. long). The annulus between the pipe and tube is filled with water. Power transients are simulated by pulse heating the stainless steel tube, using the energy stored in a bank of twenty, 12-volt diesel truck batteries. The pulses are controlled by a heavy-duty circuit breaker. Water pressure is measured by a strain-gauge pressure transducer. Rate of void formation and velocity of the initially stagnant water are determined from a high-speed camera recording of the entire test.

This experimental technique yields excellent square-wave power inputs (linear energy release rates), of variable magnitudes and durations. During system check-out tests, the maximum power obtained was about 5000 A at 100 V (~0.5 MW), with a rise time of 1 ms, and a duration of about 35 ms.

Perhaps the most critical and difficult measurement is that of the pressure transients. Frequencies of the order of 5000 cps were anticipated. Therefore, several strain-gauge pressure transducers were purchased and tested in a shock tube and in a vessel subjected to sudden, predetermined pressure transients. All units exhibited excellent response and fidelity. Moreover, it was established that frequencies up to 8000 cps could be obtained. Coincidentally, this frequency is also the upper limit for the recording oscilloscope to be installed.

The tests with light-water are scheduled for early fiscal 1966. Variables to be explored will include: (1) power inputs up to 0.5 MW, applied for 10 ms and up to 100 ms; (2) annular gaps from 0.050 in. to 0.625 in.; water columns up to 2 ft above the heated surface; and (3) initial water temperatures ranging from 60°F to 210°F.

Concurrent with these tests, an analytical model has been derived and a computer program is being written to solve the differential equations. Given the initial state of the system, i.e., temperature, pressure, liquid level, channel geometry, physical properties of the coolant and cladding, and energy generation rate, the program will be able to compute pressure pulses in the coolant, and the velocity of the expelled fluid. Although the model will accommodate any functional forms of energy generation rates, three specific types will be studied initially: impulse, step, and step-exponential.

5.2 Reactor Control and Stability

The safe operation of a nuclear reactor is dependent on system stability under all operating conditions. For example, the BORAX reactors were unstable at high power levels. On the other hand, instability of EBR-I occurred at low coolant flow rates. Thus it is vital that the region of stable operation be accurately predicted during the early stages of reactor design.

Current methods of predicting system stability consist of working with a linearized model or of directly applying Liapunov's stability theory to the non-linear model. Application of the non-linear model with respect to global stability requires a system to be stable despite disturbances of any magnitude. This requirement is unrealistic because a reactor which is globally unstable may be stable in a smaller region. Accordingly, Liapunov functions are being sought which are suitable for finite-size disturbances and which define the region of stable reactor operation in terms of its operating parameters.

Large reactor cores also pose the problem of controlling variables which are a function of space and time, i.e., neutron flux, fuel temperature, and coolant flow. Time-consuming measurements of these

variables at a finite number of points reflect the desirability of a control program which will automatically manipulate a prescribed number of control rods to fulfill a specified performance criterion (e.g., optimal burnup).

Work to date has consisted of examining the general requirements of an input reactivity distribution as a function of space and time. Both modal and nodal approaches are being employed to develop suitable approximations. Ultimately, the study will be extended to include power feedback.

5.3 Digital Control of EBR-II

At present, the EBR-II reactor plant is controlled manually, with one exception: neutron flux is controlled automatically during operation at constant power. Desired changes in primary coolant temperature are effected by manual adjustment of sodium flow rates in both the primary and secondary systems. In addition to these adjustments, manual manipulation of control rods is required to fulfill demand power requirements.

In order to eliminate these time-consuming operations, a program has been instituted with the ultimate objective of achieving automatic demand control response ranging from 10% to 100% of full power. The first phase of this program will be confined to automating control of the secondary sodium flow with the aid of a digital controller. If successful, the control functions of this unit will be expanded progressively to include primary sodium flow and, ultimately, neutron flux control. Accordingly, an analysis has been made of the overall plant control requirements, and specifications have been prepared for the digital controller.

5.4 Fuel Meltdown Studies: TREAT Loops

Fast reactors typically contain more fuel than is required to achieve a minimum critical mass. This characteristic, coupled with the short prompt neutron lifetime in these reactors, conceivably can produce a severe nuclear accident if a fuel meltdown is followed by rapid reassembly into a more compact configuration.

Accordingly, the Transient Reactor Test Facility (TREAT) is being used for the experimental investigation of (1) the complex factors which promote fuel failure; (2) the nature and degree of fragmentation; and (3) the movement and ultimate reassembly of the fissionable material. In these experiments, fast reactor fuel elements are subjected to transient nuclear heating designed to simulate core environmental conditions that might prevail during an accidental power excursion. The scope and sequence of the meltdown experiments includes:

(1) Single elements in the absence of coolant under adiabatic conditions.

(2) Single elements in a pool of stagnant sodium.

(3) Single, pre-irradiated elements with and without the presence of sodium coolant.

(4) Single elements in dynamic sodium.

(5) Clusters of fuel elements and, ultimately, a full-sized subassembly in dynamic sodium.

5.4.1 Experimental Facilities

Successful execution of the foregoing experimental program has necessitated the engineering development of special capsules, test loops, and auxiliary equipment (1) to facilitate the particular phases of the program; and (2) to isolate the consequences from the parent TREAT facility.

Small Package Loop. The integral sodium loop (Fig. 5-1) is one of three units being used for meltdown studies of single fuel elements. Designed for installation in a dummy TREAT fuel subassembly, the portable unit consists of the sodium flow circuit, electromagnetic pump, transformer, heaters, and associated instrumentation. Electrical and blanket gas connections are made through the upper end fitting. The only expendable component is a removable insert tube which houses the test fuel element.

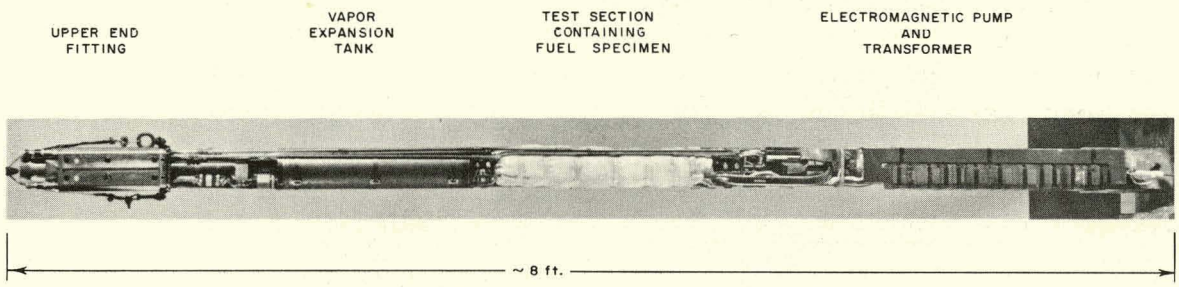

Fig. 5-1. Small TREAT loop preparatory to installation in dummy TREAT fuel subassembly

Supporting equipment includes a transparent plastic housing, appropriate manipulating equipment for remote-controlled handling of radioactive elements, and a shielded cask for transport of the elements to Argonne for subsequent examination and analysis. Figure 5-2 shows the housing installed preparatory to removal of the loop from the TREAT reactor. The housing is pressurized with inert gas to prevent inleakage of reactive air during loop removal and insertion into the shielded cask.

Several tests were performed successfully on EBR-II-type fuel elements in stagnant and in dynamic sodium. In each instance, the element was exposed to reactor transients of progressively increasing severity until its failure threshold was exceeded. Failures were produced with test fuel temperatures registering as high as 1285°C. A typical failure is shown in Fig. 5-3. Integrated power releases have ranged up to 143 MW, with pressure pulses up to 45 psi.

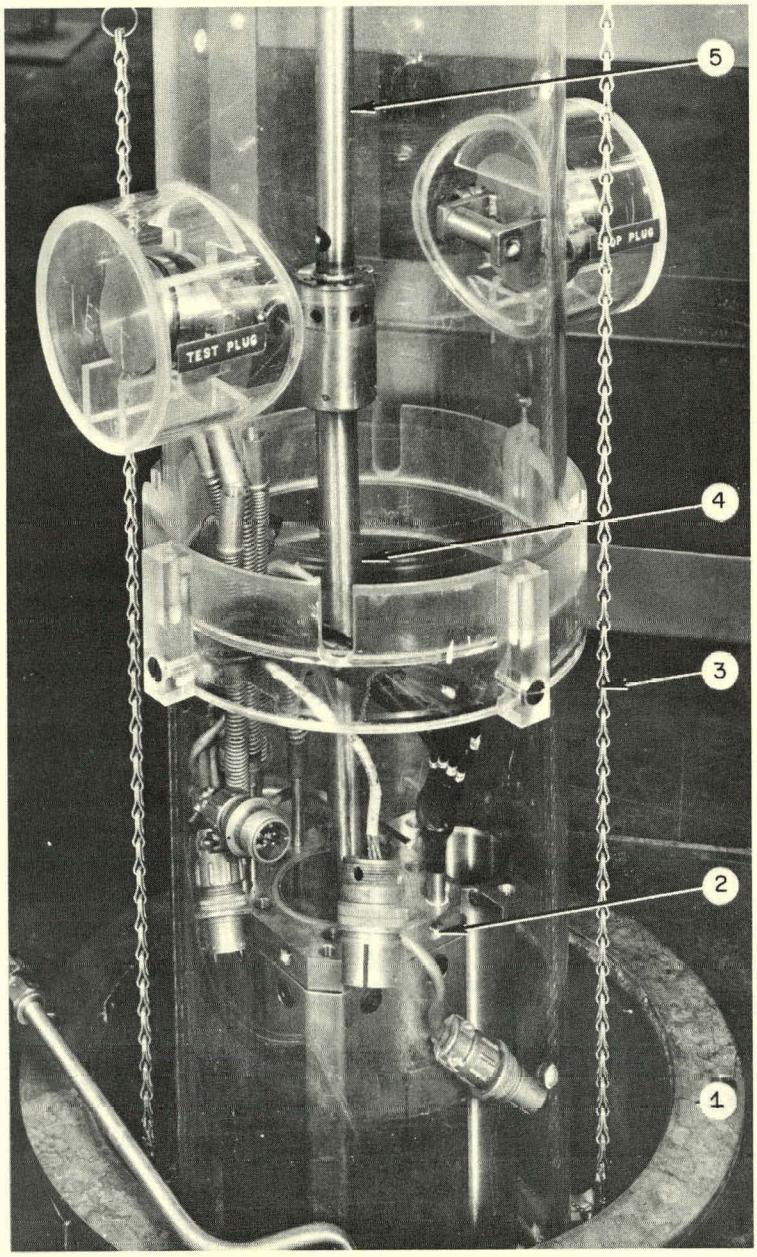

Fig. 5-2. Inert atmosphere containment used during loading and unloading of small TREAT loop: (1) reactor pit; (2) loop housing; (3) lift chain; (4) test section; (5) manipulator.

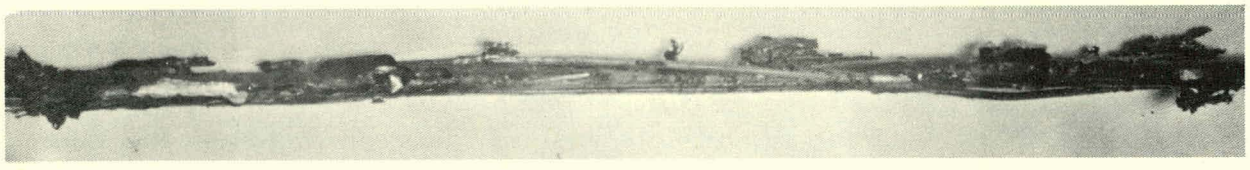

Fig. 5-3. EBR-II-type fuel element tested to failure in stagnant sodium. Rupture of cladding was attributed to internal pressure buildup. At time of failure, the test loop experienced a peak pressure of 45 psia. Had the element remained intact, the fuel would have achieved a centerline temperature of 2000°C. Total energy released equalled 935 watt-second per gram of fuel.

The entire complex of equipment has been transferred to the Reactor Physics Division for continued execution of the experimental program.

Large TREAT Loop. The physical construction and location of the small package loops limits the meltdown studies to simultaneous exposure of seven EBR-II-type fuel elements (0.75 in. I.D., 17.5 in. long). Thus in order to extend the studies to a full-sized subassembly (3.8 in. I.D., 92 in. long), a large sodium loop has been designed and is now under construction.

Unlike its packaged counterparts, this loop is a semi-permanent part of the TREAT reactor. As shown in the artist's concept (Fig. 5-4), only the in-pile test section is removable. This section is interconnected through special Conoseal flanges to 3-in. inlet and outlet sodium lines. These lines extend through the shielding into the sub-reactor room which contains the balance of the loop components.

The in-pile test section is located vertically in the center of the core. Sodium enters at the top and flows down through an outer concentric channel. At the base of the test section, the flow is baffled upward through the central region, which contains the test specimen, and into the outlet piping to complete the cycle.

The effluent piping leads to a settling tank hydroclone in the sub-reactor room. This tank serves to trap any particles of melted fuel that may be entrained by the sodium. Other loop components in the sub-reactor room include:

(1) A 500-gal sodium storage tank located at floor level. This tank serves as a reservoir for the sodium during recirculation of the coolant through the loop or during once-through flow through the test section. The tank is fitted with flanges to accommodate immersion heaters and liquid-level indicators.

(2) A dump tank located below floor level. This tank receives the bulk of sodium flow during once-through mode of operation.

(3) Five 4-in. bellows-sealed P-K ball valves. These valves are used to control the desired mode of sodium flow, and to isolate the loop from the test section during removal of the latter.

(4) An electromagnetic pump - rectifier assembly to circulate the sodium.

(5) A bypass cold trap, downstream of the pump, to reduce the oxide content of the sodium.

(6) A plugging indicator, to monitor the impurity level in the sodium.

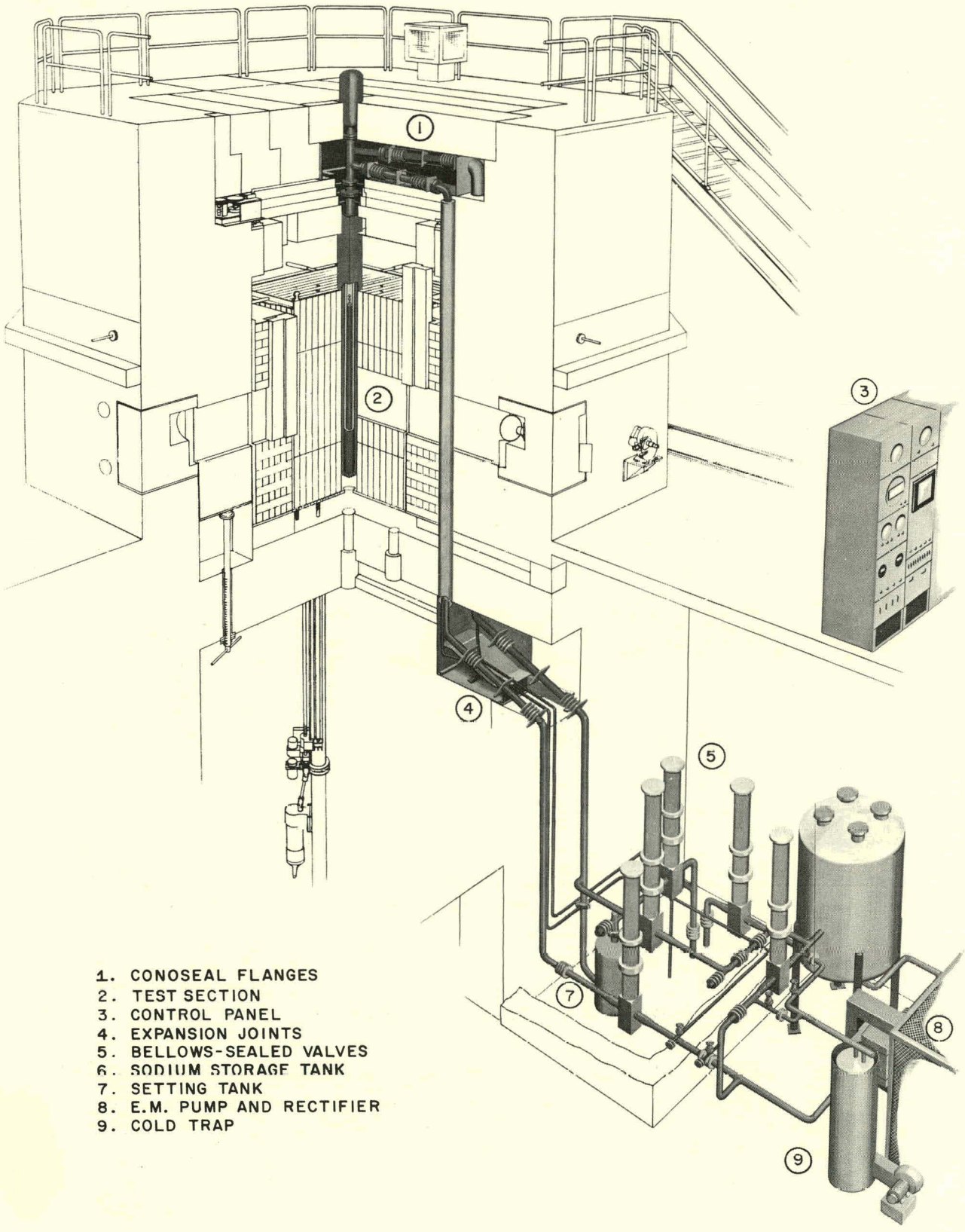

Fig. 5-4. Artist's concept of Large TREAT Loop installation for fuel meltdown studies

In addition, the loop is equipped with resistance heaters, instrumentation and circuitry, and a scrubbing gas transfer system. The latter is used to remove sodium and radioactive contaminants during displacement passage of gas from the dump tank to the storage tank.

Prior to each meltdown run, sodium will be recirculated through the loop and test section to establish equilibrium conditions. At this point, the flow mode will be switched to once-through; this will be done by remote control from the reactor console. Immediately thereafter, the reactor power transient will be initiated to effect fuel meltdown. Once-through flow can be maintained for 90 sec. Upon completion of the test, the electromagnetic pump will be shut down, and the sodium in the test section and piping allowed to solidify. Thereafter, the test section will be removed into a shielded cask and transported to a high-level cave for examination and analysis of the melted specimen.

The status of the large TREAT loop is as follows. The transport cask and carriage have been completed. Fabrication of the test section and installation of the loop components is underway. Figure 5-5 shows the components that were installed during the reporting period. In addition,

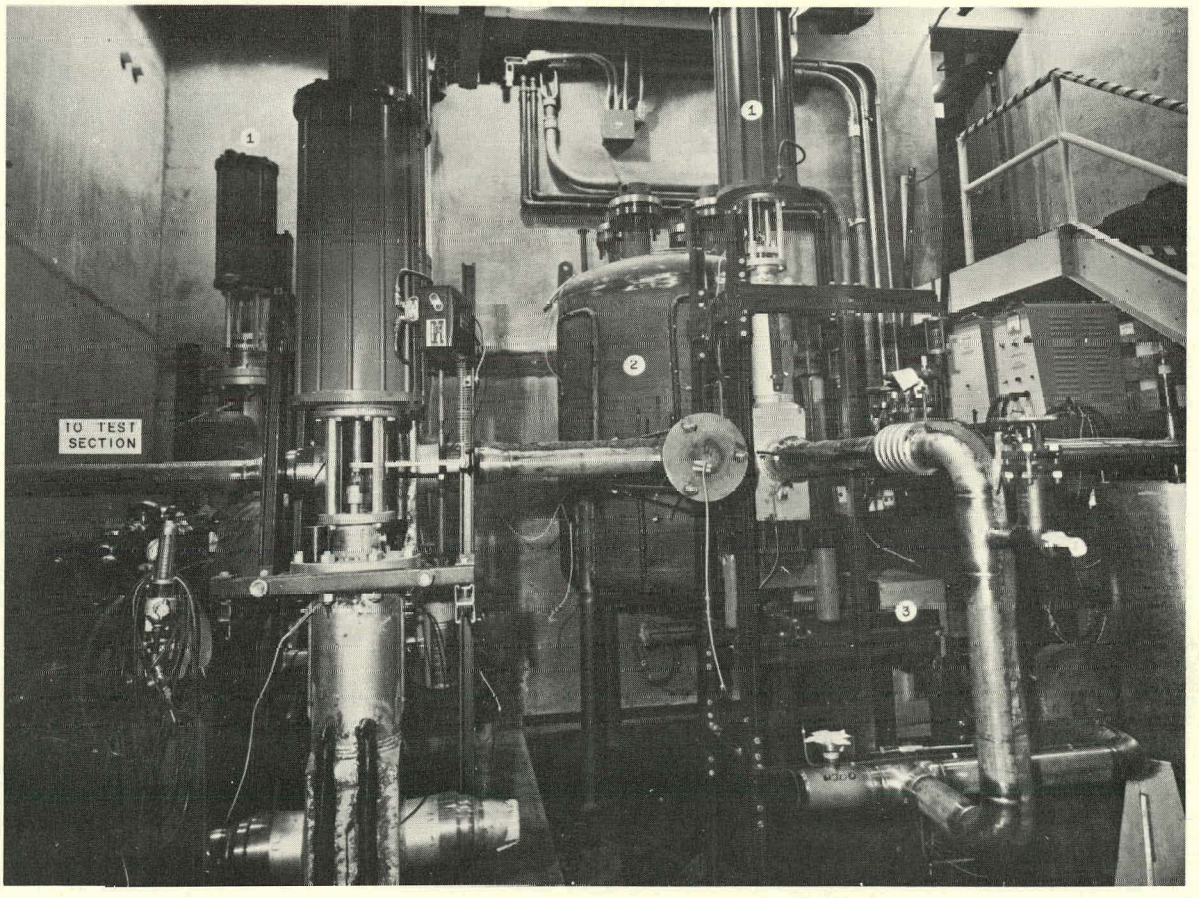

Fig. 5-5. Partial installation of loop components in sub-reactor room: (1) three of five bellows-sealed flow control valves; (2) 500-gal sodium storage tank; (3) electromagnetic pump and rectifier assembly

all of the electrical circuitry and control instrumentation is in position at the reactor building.

Finally, a safety analysis of the loop installation has been completed; publication of the findings is pending local and AEC review.

5.5 A Critique on Current Assessment of Radiation Damage in Reactor Pressure Vessel Steels

Limited ANL statistics on three heats of SA 212B, and U. S. Steel data on SA 212B and SA 302B pressure vessel steel, indicate that current methods of assessing radiation damage to these materials are inadequate for at least two reasons:

(1) The effects of steel-making practices on radiation sensitivity of the steels are unknown.

(2) The only test procedure that yields data on notch sensitivity is unreliable.

Table 5-1. Summary of Steel-Making Practices for SA 212B Heats Studied at Argonne

Source	Plate Thickness, in.	Ingot Treatment and Plate Final Heat Treatment
EBWR	4 2-3/8	Al treated, five grain, ASTM A-300; normalized and tempered
SL-1	1 (roll bonded)	Lukens composite plate*
ASTM E10 1959 Ref. heat	4	Al treated, five grain, ASTM A-300; quenched and tempered

*Not cast to ASTM A-300 specification.

The ANL data were obtained from EBWR surveillance programs and examinations of EBWR and SL-1 shell material. Table 5-1 lists the significant steel-making practices associated with the three heats of steel investigated. Figure 5-6(A) shows the disparity in the impact resistance of specimens prepared from each heat. Significant NDT (nil-ductility temperature) gradients across the wall thickness were also observed. These are plotted in Fig. 5-6(B).

Similar disparities in impact resistance are evidenced by comparison plots of U. S. Steel, NRL, and WAPD data on 1959 reference heats of SA 212B and SA 302B pressure vessel material.[1] (See Fig. 5-6(C)). The NDT values published by these laboratories are listed in Table 5-2. These values were determined from drop-weight tests.

Interpretations of radiation damage to vessel materials are further obscured by the test procedure used to determine loss in resistance to crack propagation. This test measures the energy required to fracture a notched test specimen. Conventionally, a minimum of three specimens are impacted to determine an average value. However, because of space limitations in available irradiation facilities, the test is usually confined to a single specimen.

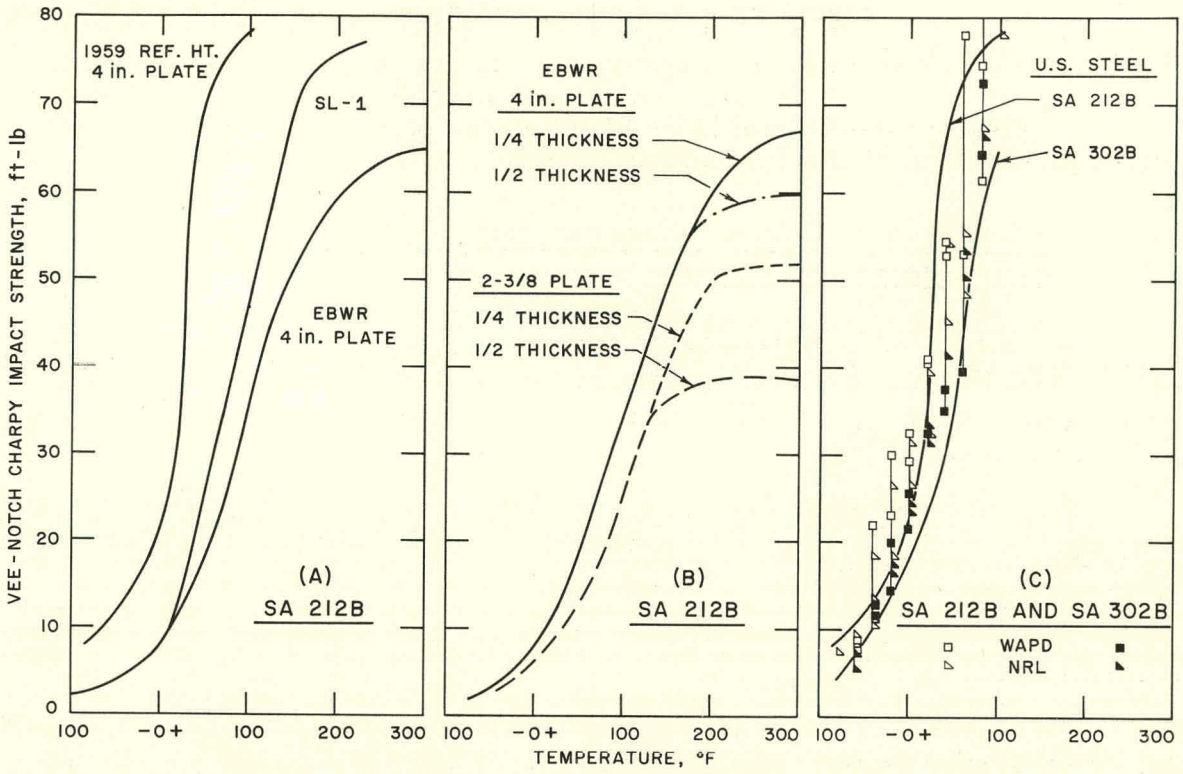

Fig. 5-6. Comparison plots of impact resistance data on SA 212B and SA 302B pressure vessel steels

Table 5-2. NDT Data for 1959 Reference Heats of SA 212B and SA 302B

Laboratory	SA 212B	SA 302B
U. S. Steel	-57F	-13F
NRL	-30	+10
WAPD	-45	-10

There is evidence that the test machine is also prone to yielding erroneous data. Unpublished minutes of the ASTM Committee on Design and Testing Methods reveal substantial variations in impact data on standardized Watertown Arsenal specimens.[2] This committee studied the calibration of impact test machines at five different sites, including Argonne. The Argonne machine yielded data within permissable deviations (±2 ft-lb) at the lower impact levels (~20 ft-lb). However, at intermediate and high impacts (~50 and 100 ft-lb), increasingly higher impact strengths were indicated. The source of error was traced to the design of the anvil supports. Similar test machines at the other four (unidentified) sites were also found to yield erroneous data.

Courses of action are fairly obvious and require prompt expansions of existing structural materials irradiation test programs. Specifically, data are needed for statistical evaluations of steel-making practices for the SA 212B and SA 302B steels. The need is particularly acute for the interpretation of irradiation damage to the first generation of power

reactor pressure vessels. These vessels are being monitored, almost exclusively, with specimens of heats other than those from which they were fabricated. Parallel programs also are needed to either refine or to replace the current impact test procedure. In the latter case, a nondestructive technique is preferable.

5.6 Experiment vs. Analysis of Core Support Grid

A series of tests was conducted to verify the analytical method of Marchertas for computing stresses and deflections in reactor core support grid structures.[3] In general, the test data were in relatively good agreement with predictions.

Figure 5-7 shows the physical design of the core grid mock-up and supporting structure. The grid assembly consisted of two circular plates interconnected by nineteen rods distributed on a hexagonal lattice with respect to the center of the plates. This assembly, in turn, was supported at the periphery by milled slots in a 6-in.-thick steel plate.

The test structure was instrumented in two diametral directions with SR-4 strain gages. Rosettes were used to measure the radial and tangential strains at the surfaces of the plates. Three temperature-compensating gages were installed: two between the plates, and one on the bottom of the structure. Strain gages were wired, respectively, to one d-c and two a-c galvanometers. Mechanical dial gages were arranged so that detailed deflection measurements could be made near the plate edge supports. Four additional gages were installed to indicate relative deflection of the support plate under load. In this event, the turnbuckles were adjusted to correct the induced deflection.

Nineteen separate loads were applied to the top plate (above each rod position) by adjusting the screwjacks attached to the bottom of the rings pictured in Fig. 5-7. A dial gage was fastened to measure the diametral change in each ring under load. For convenience, the dials were calibrated to show a specific load, i.e., 500 lb, 1000 lb, etc. The top of each ring was pinned to a flat plate which, in turn, was supported by four posts from the base support.

Figure 5-8 shows a typical comparison between analytical and experimental radial and tangential stresses. The small deviations may be attributed, in part, to departures from the "ideal" structure considered in the analysis, e.g., the very small number of rods per given area. A detailed description and evaluation of the analytical-experimental effort is given in ANL-6781.[4]

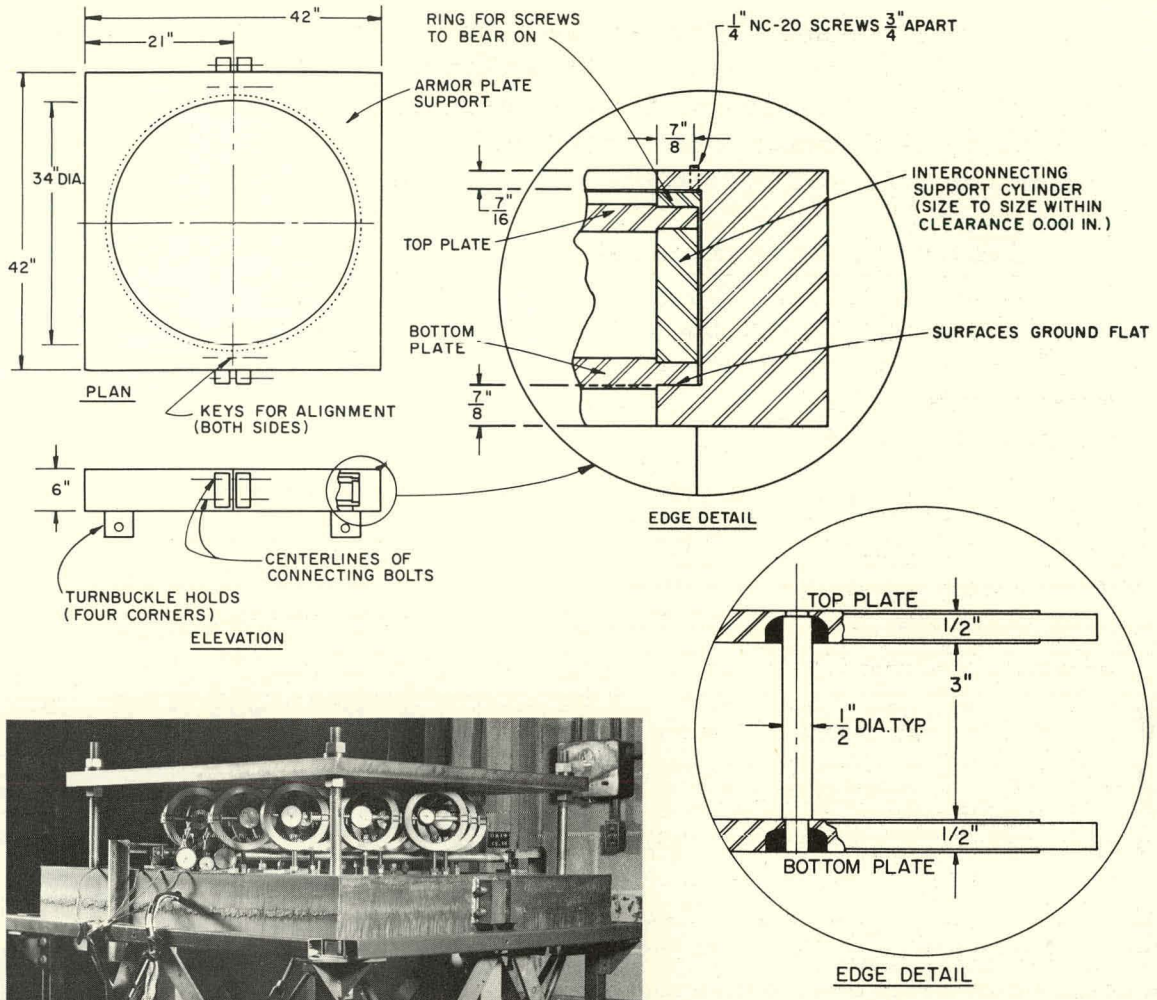

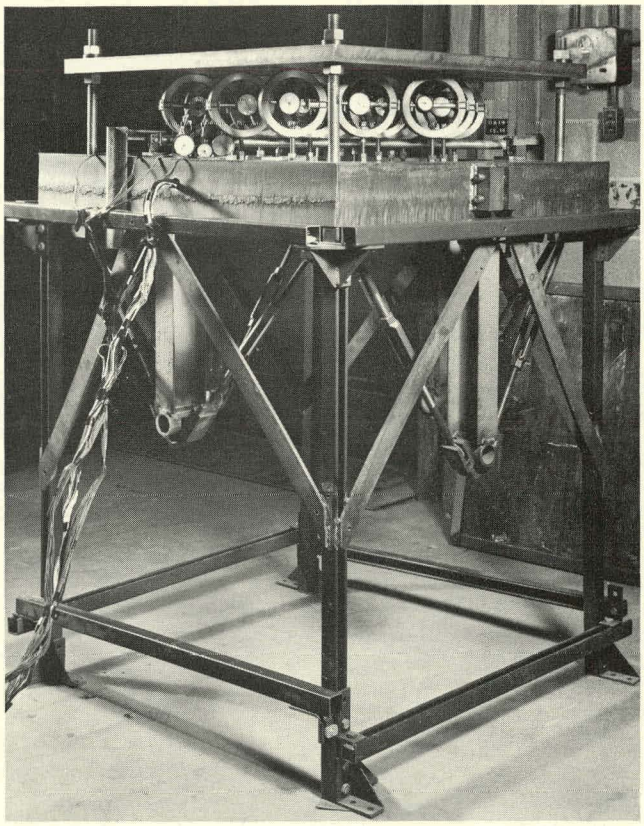

Fig. 5-7. Mock-up of core support grid assembly and test loading arrangement

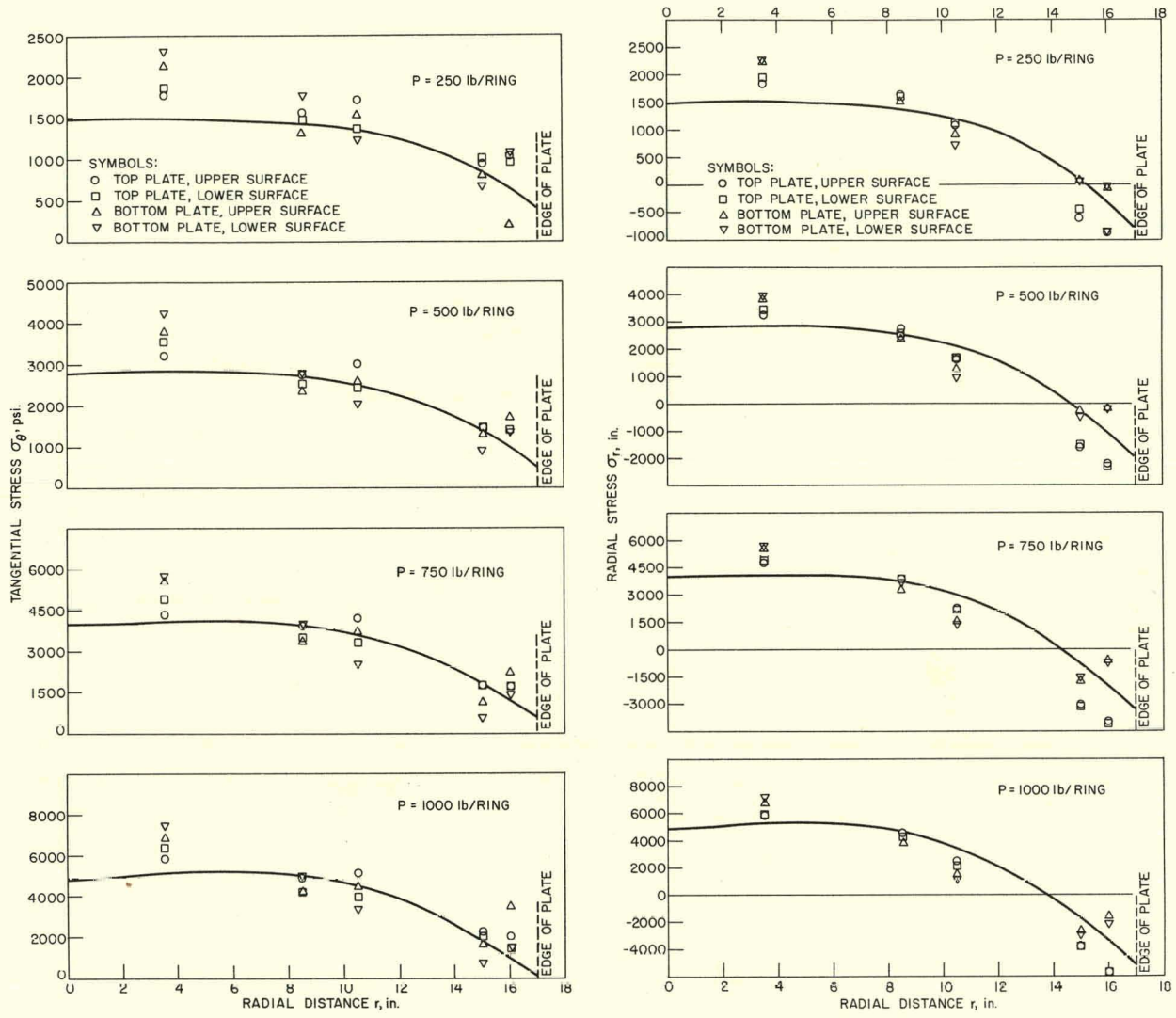

Fig. 5-8. Comparison between analytical and experimental distributions of tangential and radial stress in mock-up core support grid

REFERENCES

1. A. V. Alger and L. F. Porter, *Evaluation of Reference Pressure Vessel Steels for Neutron-Irradiation Studies*, U. S. Steel Report, Project No. 40.002-066(4) (1964).

2. A. L. Bement, Minutes of ASTM Committee E10-Sub II Meetings held on October 22, 1963 and September 22, 1964.

3. A. H. Marchertas, *Analysis for Determination of Nuclear Reactor Grid Structure*, PhD Thesis, University of Nebraska, March 10, 1963.

4. A. H. Marchertas, S. H. Fistedis, and R. O. Brittan, *Analytical and Experimental Investigation of a Nuclear Reactor Support Structure*, ANL-6781 (March, 1965).

Section 6

STUDIES AND EVALUATIONS

6.1 Use of High-Temperature Process Heat as Part of a Total Nuclear-Energy Source

Although a large fraction of our energy consumption in the future will be non-electrical, almost no progress has been made to satisfy these demands with nuclear reactors. Projections of coal, petroleum, and gas reserves and consumption are always hazardous, but current estimates indicate that some basic realignment of energy usage probably can be expected before the end of the century. At such time, it will become necessary for nuclear reactors to supply heat, particularly for high-temperature chemical or metallurgical processes. The temperature requirements of this energy market range from 1500 to 4000°F.

Recent advances in nuclear reactor technology for rocket propulsion, for the General Electric 710 reactor, and for the UHTREX experimental facility indicate that high-temperature gas streams (2000-2700°F) can be produced with reasonable core lifetimes. Accordingly, a preliminary study was made of the potential use of such streams as heat sources for iron ore reduction and pelletizing; production of alumina and aluminum; production of cement; production of fertilizer; and petrochemical processing.

The results of this study[1] indicate that, in addition to conventional electric power generation, nuclear energy has potential applications in:

(1) Alumina and aluminum production, when used as a total energy source at an ore site. Use of high-temperature process heat specifically for calcining alumina will be small, compared to electric power output.

(2) Cement production, using air as the heat transfer medium, either as part of a large, dual-purpose complex such as an electric generating-desalinization plant, or as a mobile plant operating in newly developing areas.

(3) Calcining and/or sintering ores (e.g., taconite) at mine sites, again using air as the heat transfer medium, in very large operations (>5 million tons/year).

In many cases where nuclear energy appears to be useful because of competitive energy costs, an additional economic incentive comes from freedom of site location, i.e., by eliminating the need to transport large quantities of raw materials to sources of fossil fuel or hydroelectric power, or to ship fossil fuels to processing sites. This siting advantage is

particularly valuable in the aluminum industry, where the ores average about 25% metal, as contrasted with the iron industry, where some ores range from 50 to 70% metal.

Nuclear energy does not appear useful in the fertilizer and petrochemical industries, since both utilize large cheap sources of hydrocarbons as fuel and also as basic raw materials. Similarly, iron ore reduction requires either carbon or hydrogen as a reductant, which must also be obtained from cheap raw materials. For these industries, it is difficult to conceive of a situation, at least in the near future, where a raw material will be cheap enough for use in the process and not also cheap enough to be used as fuel. Nuclear electricity would have to be very inexpensive to produce electrolytic hydrogen for ammonia production or iron ore reduction so long as supplies of coal and natural gas last.

On the other hand, ore pelletizing could provide a use for nuclear heat, since the process does not require a reductant. Present-day mine-site pelletizing plants range upward in size from 5 million tons/year, with heat requirements ranging from 1 to 2 million Btu/ton. Assuming a large plant of 10 million tons/year, with a heat requirement of 1 million Btu/ton, the thermal power requirement is found to be 385 MW. A nuclear power plant to provide this amount of heating to an air stream at 2200°F might be interesting. It might also be interesting to combine this plant with an electricity-generating plant to power electric reducing furnaces. A nuclear-powered pelletizing plant, in possible conjunction with electric power generation, is sufficiently promising to warrant a detailed economic analysis.

If and when high-temperature, nuclear process heat is used, undoubtedly it will also be economical to produce electricity and low-temperature steam at the same location. The relative balance between high-, moderate-, and low-temperature heat will, of course, be dictated by local economics. Whatever the balance, the need exists for a large, nuclear reactor capable of delivering part of its energy at temperatures in the range 1500 to 3000°F; and the technology for developing such a plant is at hand.

The promise of nuclear high-temperature process heat is enhanced by the results of economic studies of specially-designed, multi-purpose reactors for the production of electricity and desalting of sea water. These studies indicate definite advantages are gained by combining processes and increasing plant sizes. The same advantages should hold for a large reactor that produces process steam in addition to electricity. As large as the U. S. mineral industry is, there are still few, if any cases, where a single industry in any one location could economically utilize a nuclear plant solely for the production of process heat. Therefore, the combining of processes in a large plant is more or less obvious.

Since the cost of a reactor that produces all its energy at high temperature may well outweigh the increased thermodynamic efficiency at temperatures above 1800°F, the most attractive way of supplying this energy is

with a high-temperature loop within the reactor. Figure 6-1 is a simple schematic of a system that could serve a number of possible complexes. It features a reactor of conventional type, with a separate high-temperature section. The low-temperature process heat can be supplied by steam extracted from the turbine. In terms of long-range energy sources, this is the type of system that should be considered.

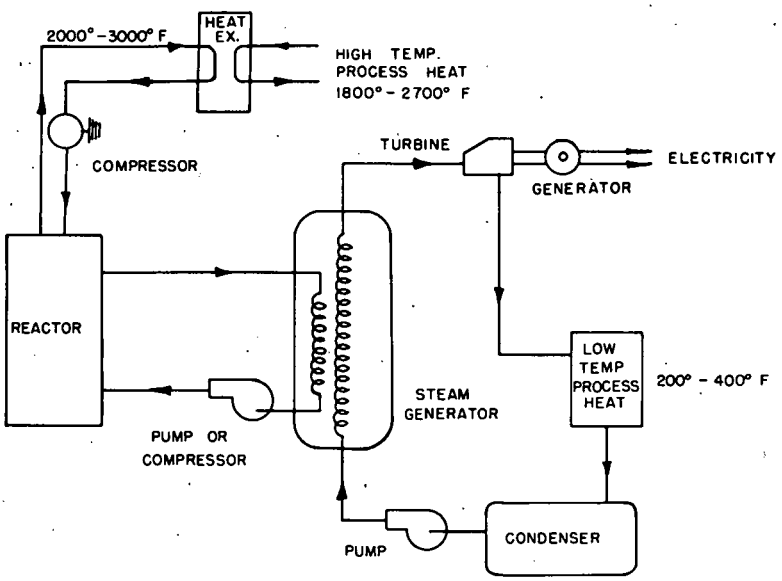

Fig. 6-1. Schematic of reactor system for dual production of electric power and high-temperature process heat

In the shorter term, assuming the technology exists to build such a system, the economics appear favorable. For example, studies of 3220-3500 MW(t) desalting plants indicate that heat costs for reactor steam will range from 19-26¢ per million Btu with state or federal financing, and 30-38¢ per million Btu with public-utility financing. These costs probably represent the lower limit associated with production of high-temperature heat from a loop in reactors of this size, since costs assignable to the high-temperature section will certainly be higher. Although the actual costs can only be determined by a detailed study, they might prove competitive for some applications.

There is no reason why such a system cannot be considered for almost any reactor type; however, the need for vessel penetrations to accommodate the high-temperature cycle favors a low-pressure reactor. From the standpoint of long-range fuel economy and latitude in material selection, a fast reactor would be preferred. If the desired fraction of high-temperature heat is not too large, then the high-temperature region could be confined to the blanket area. This would be desirable, since in a large, fast reactor the blanket structure should have less effect on the breeding ratio.

Technology being developed for both graphite and refractory-metal fuel elements as part of the rocket program, the high-temperature materials program, and the previously mentioned reactor programs gives every indication that a reactor core or blanket section could produce the high-temperature gas streams of interest.

A matter interrelated with the use of nuclear energy for high-temperature process heat is the development of high-temperature, corrosion-resistant, heat exchangers. For example, cement producing and ore pelletizing plants currently use direct-firing techniques. If these processes are to be carried out with nuclear-heated air, problems of product contamination will require a primary reactor loop and heat exchange to secondary air. The advent of very large heat exchangers to withstand corrosion by air at 2200 to 2700°F may entail considerable research and development. However, when the heat-exchange operation has been successfully accomplished, the high-temperature air can be routed to the process by standard techniques.

On the assumption that nuclear reactors ultimately will be able to produce gas streams at temperatures equivalent to direct firing of fossil fuels, it is unlikely that the transition will reflect significant changes in basic chemical or metallurgical processes. Nuclear reactors (like fossil fuels) are simply a source of heat, and the chemical and economic factors that determine the choice of processes should not be affected markedly by the source of heat. Even in the complete absence of hydrocarbon sources, electrolysis of water to produce hydrogen can supply a large portion of needed raw materials and chemical reducing agents. From there on, however, the basic processes will remain essentially unchanged.

REFERENCES

1. L. J. Gordon and J. F. Marchaterre, *A Preliminary Evaluation of the Use of High-Temperature Process Heat as Part of a Total Nuclear-Energy Source*, ANL-7035 (September, 1965).

Section 7

EDUCATION - RESEARCH ACTIVITIES

7.1 ANL-AMU Heat Transfer Program

The ANL-AMU Heat Transfer Program is one of many cooperative programs which permit university faculty and graduate students to participate in research projects at various AEC national laboratories. These projects are selected on the basis of their suitability for academic advancement and, more importantly, their potential contribution to the state of the art.

With respect to the ANL-AMU program, candidates for advanced degrees from Associated Midwest Universities are given research assignments designed to fill major technological gaps in the field of two-phase flow and heat transfer. The nature of these assignments is best illustrated by the following summaries of theses that were completed during fiscal 1965.

7.1.1 Frequency-Response Analysis of Steam Voids to Sinusoidal Power Modulation in a Thin-Walled Boiling Water Coolant Channel[1]

Knowledge of the transient behavior of volume steam fraction in a coolant channel during power transients is vital to the stable operation of boiling water reactors. Reactivity depends upon the vapor fraction in the channel, and the vapor fraction, in turn, depends upon the reactor power level. This constitutes a feedback loop which may lead to instability and, ultimately, to channel burnout.

The principal objective of this study was to measure the power-to-void transfer functions for a single rectangular flow channel at elevated pressures. The experimental loop consisted essentially of a heated section, steam separator, crossover, downcomer and return leg constructed mainly of 2-in. diameter Schedule 80 stainless steel pipe. This loop could be operated at pressures up to 2000 psia. The "out-of-pile" or boiling loop was operated in forced circulation for various fixed pressures, inlet flow rates and temperatures. The power was modulated sinusoidally around a steady-state level. Amplitude and phase of the void response were measured at various axial and transverse positions of the channel, employing a cross-correlation technique over the frequency range 0.01-5 cps. Through an analysis of this data, plotted in Bode diagram form, information was obtained on the propagation velocity of void perturbations, the range of linearity of the void response to power modulation, the shape of the axial variation of transient void amplitudes and break frequency of the transfer function.

Experimental measurements of power-to-void transfer functions were made in a vertical, rectangular, electrically heated test section in

which four main loop parameters were varied: pressure = 200-800 psia; inlet flow rates = 2.52-3.78 fps; heat fluxes = 2.28×10^4 - 9.12×10^4 Btu/(hr)(ft^2); and inlet subcoolings = 0.8-12.4°F. Data were obtained at three axial positions and at various transverse positions across the width of the channel for a fixed axial height.

All of the void amplitude data exhibited notches at frequencies ranging from 1.2 to 3.7 cps. The notch frequency was highest at axial positions nearest the test section inlet and decreased with increasing axial distance. Transverse measurements indicated a maximum value at the center of the channel; this value decreased as the wall was approached in downstream regions of the channel. Phase measurements also showed an undulation close to the notch frequency.

There was good agreement between the zero-frequency void amplitude response and the steady-state axial void distributions at various power levels. Increased inlet subcooling reflected an increase in the zero-frequency amplitude.

At pressures of 200, 300 and 400 psia, void response to power modulation was linear at amplitudes up to 20% of the average power level.

The axial variation in transient void amplitude was sinusoidal, being of the same form as the power-forcing function. As the modulation frequency increased, the period and amplitude of this sinusoidal function decreased until the test section length corresponded to one-half a wave length. Then a notch would appear in the void amplitude at the test section exit.

The cross-sectional average propagation velocities were intermediate between the mixture and vapor cross-sectional average velocities at all axial positions downstream of the concave-shaped transverse void distributions. Near the entrance of the test section, the propagation velocity decreased and became more closely related to the cross-sectional average liquid velocity.

At a fixed axial position, the local void propagation velocity was a function of the distance from the wall. In the downstream regions of the channel, the measured propagation velocity profiles exhibited a maximum at the center and decreased near the wall; this is consistent with the convex steady-state velocity profiles which are thought to exist in these regions.

From the Bode diagrams of the data, it was found that sharpness of the notch increased with increasing pressure and inlet temperature subcooling, but decreased with increasing axial length and increasing distance from the test section wall. By noting the analogous behavior of slip and the

sharpness of the notch, slip was believed to be of importance here in the determination of the break frequency of the power-to-void transfer function.

Steady-state axial and transverse void fraction distributions were obtained under loop operating conditions corresponding to those employed in the power-to-void transfer function measurements. The Marchaterre-Hoglund, Griffith, modified Bankoff and Neal models were all found to predict fairly closely the axial, steady-state, cross-sectional average void distributions.

Concave void distributions were found near the test section entrance. The degree of concavity and persistence of this profile with axial distance increased with increased inlet temperature subcooling. For all concave-shaped profiles, the calculated values of slip were less than or close to unity.

Theoretical models proposed by Zivi and Wright, Christensen, Solberg and Sanathanan were tested for their ability to predict the power-to-void transfer function data. A new model was constructed, similar to Solberg's "Kjeller Model," in that Bowring's physical model was employed in the subcooled boiling region. It differed, however, in that the heat capacity of the wall was accounted for in all three regions, the transitional bulk-boiling boundary effects were considered in every section of the subcooled boiling region, and the entire model was programmed for solution on a digital computer employing a step-by-step integration procedure.

Fairly close agreement between theory and data was found for the notch frequencies, phase lag and break frequencies. However, there were appreciable differences between model predictions and data for some of the zero-frequency amplitudes.

7.1.2 Heat Transfer Instabilities near the Thermodynamic Critical Point[2]

The purpose of this study was to determine the nature of severe pressure and flow oscillations which reportedly have occurred spontaneously during heat transfer to a fluid near its thermodynamic critical point. For example, pressure fluctuations of 380-psi amplitude (peak to peak) at frequencies of 1000-10,000 cps have been reported. In order to avoid operation at excessive pressures and temperatures, the experimental heat transfer loop was designed for either natural or forced circulation of Refrigerant 114 (symmetric dichlorotetrafluorethane; critical pressure = 473.18 psia; critical temperature = 294.26°F).

The data indicate that instabilities were strongly damped during forced convection operation at flow rates greater than would be attained by natural convection. During natural convection operation two types of

instabilities were encountered. The first, which occurred at bulk temperatures below the critical temperature, was of an acoustic nature, exhibiting harmonic pressure oscillations in the frequency range of 5-30 cps. It was shown that the fundamental wave length equals the length around the loop for the constant diameter construction employed in the tests. For a fixed wave length, the frequency varied with the sonic velocity. The second type of instability was characterized by a frequency which was two orders of magnitude less than for the sonic type. This type of oscillation was triggered and maintained by an abrupt improvement of the heat transfer coefficient as the bulk temperature approached the critical temperature. Improvement of the heat transfer coefficient was attributed to a "boiling like" behavior in the supercritical fluid.

An interesting anomaly was observed when the wall temperature exceeded 600°F-700°F. At this point, a chemical reaction apparently resulted in a "hot spot" on the heater wall. This phenomenon also has been observed during heat transfer to supercritical cryogenic fluids.

7.1.3 Flow Regimes and Transitions in Vertical Two-Phase Flow at Elevated Pressure[3]

The goals of this investigation were: (1) to identify the various flow patterns and their transitions in a fluid at relatively low temperatures and pressure; and (2) to establish a correlation between these flow regimes and similar phenomena which occur in water at elevated pressures.

The forced-circulation test loop was designed for operation with trichloromonofluoromethane (Refrigerant-11). It was constructed of all-welded stainless steel piping, with flanged connections to accommodate a heated test section, a transition section, and an unheated section. An enclosed centrifugal pump circulated the Refrigerant-11 with a head in excess of 50 psi for flows below 20 gpm.

Flow patterns in the unheated section were observed with the aid of a fluoroscope coupled to a closed-circuit television monitoring network. High-speed motion pictures were taken with a Fastex camera, augmented by directed beams of colored light, through optical windows in the test section. This technique of directing blue light from above, and red light from below the camera centerline provided a means of distinguishing vapor bubbles from liquid droplets through a color inversion. Pressure transducers were employed to obtain the local pressure drop in the unheated channel.

Two-phase mixtures were generated in the electrically-heated test section over a heat flux range of 4,000 to 74,000 Btu/(hr)(ft^2) for mass flow rates from 0.20×10^6 to 2.0×10^6 lb(hr)(ft^2). The orthobaric density

ratios ranged from 7 to 60. These ratios are equivalent to a saturation water pressure range from approximately 400 to 2000 psia. Mass qualities based upon thermodynamic equilibrium ranged to 90%; however, the majority of the data encompassed the segment from saturation to 50%.

A distinctive flow regime was observed at high mass flow rates in which ligaments of agglomerates of liquid travel in the vapor core. This regime has recently been termed "wispy annular." The phase transitions were separated into three segments: churn, annular, and wispy-annular flow. Plug flow was not observed at the elevated pressures under forced-flow conditions and net quality. Transition from wispy-annular to annular flow occurred at nearly constant superficial liquid velocity; this is in agreement with observations for water at elevated pressures.

Identical orthobaric density ratios were adjudged the best modeling parameter for comparison of the R-11 data with water; this is in contrast to the reduced temperature or reduced pressure form of presentation. Expressions were derived to correlate the transitions from churn to both annular and wispy-annular flow. These expressions incorporated the orthobaric density ratio and either the saturated vapor or liquid density. Transitions from annular to wispy-annular occurred over such a narrow band of superficial velocities that only a qualitative representation was obtained. It was found that the possible effects of surface tension and viscosity on the flow regime could not be separated from the expressions in terms of the saturation densities at identical orthobaric density ratios.

A gamma-ray traversing unit was used to determine local void fraction distributions for six sets of orthobaric density ratios. Average void fractions were compared to available void data for water and a refrigerant, R-22, at identical orthobaric density ratios. There was good agreement; however, none of the existing correlations could predict the results over the entire quality and mass flow rate range. A definite mass flow rate effect was observed, particularly at low mass flows. An empirical expression incorporating the mass velocity effect for low flow rates was obtained for a low-quality range. For low flow rates, the void fraction increased with increasing mass flow at constant quality. At high flow rates, the flow rate effect could not be ascertained. At identical orthobaric density ratios, the void fraction appeared to be identifiable among the fluids considered by employing the quality and mass flow rate at elevated pressures.

7.1.4 Propagation of Density Disturbances in Air-Water Flow[4]

As mentioned earlier, instability of a boiling water reactor can be promoted by the presence of a feedback loop consisting of the reactivity of the reactor, the vapor fraction in the coolant channel, and the power level of the reactor. In the past, investigations of these instabilities could not be

completed without making assumptions as to the behavior of variations or changes in the vapor fraction (void fraction). Recently, theoretical models have been suggested for predicting, from the steady-state characteristics, the propagation velocity and the decay (or dispersion) of variations (perturbations) in the void fraction. However, limited experimental data are available for verification of these theoretical predictions. Therefore, the principal objectives of this study were: (1) to investigate the behavior of density waves propagated vertically upward in a forced-circulation, atmospheric pressure air-water loop; and (2) to compare the results with theoretical predictions.

Two air-water mixers were used to effect primary air-water flow and the secondary perturbations. Upon attaining steady-state conditions, a regular sequence of low-frequency (~0.4 cps) density disturbances were generated by imposing a square-wave pattern on the solenoid valve which controlled the secondary air flow. Five improved electrical-resistivity probes were inserted in the clear plastic test section at different axial positions to facilitate radial traverse of the void perturbations as they propagated through the channel. In addition to measuring the local void fraction, these probes also provided information on bubble frequency and bubble-size distribution. Electrical signals from each probe were recorded on an FM tape recorder. These signals were sampled by an analog-to-digital converter for computer analysis. The results were then compared with theoretical predictions.

The computer output was in qualitative agreement with kinematic wave theory. However, at low-mixture velocities the experimental velocity was higher than the theoretical value, while for high-mixture velocities the reverse was true. Also, at low-mixture velocities, the propagation velocity was greater than the gas velocity, while at higher mixture velocities the correlation was reversed. The discrepancy between experiment and theory was rectified by modifying the basic continuity equations to include turbulent diffusion.

In general, the perturbation decay rate was considerably higher than predicted by kinematic wave theory. This disparity was also attributed to axial turbulent diffusion which is not considered by theory. A diffusion equation for two-phase flow was solved and diffusion coefficients were calculated from the experimental results. These coefficients tended to increase linearly with downstream void fraction and increasing mixture velocity. Also, the radial diffusivity profile decreased strongly near the wall.

7.1.5 Self-Sustained Hydrodynamic Oscillations in a Natural Circulation Two-Phase Flow Boiling Loop[5]

The objectives of this study were: (1) to obtain a consistent set of data over a wide range of pertinent operating variables: and (2) to use these

data in conjunction with available models in the hope of resolving the forces which promote oscillations in natural circulation boiling heat transfer systems.

More specifically, these parameters included:

Heat Flux, Btu/(hr)(ft^2):	0.2-3.1 x 10^5
Pressure, psia:	200-1500
Inlet Subcooling, °F:	0-62
Channel Geometry	
Length, in.:	48; 72; 96
I.D., in.:	0.364; 0.625; 0.8125
Riser	
Length, in.:	48; 60
I.D., in.:	0.3125; 0.625; 1.049

During the course of these tests, the frequencies of the oscillations varied from 0.24 to 0.76 cps and, in general, increased linearly with power. Periodic inlet flow reversals were observed at the higher frequencies. These reversals were more pronounced in the smaller test sections and risers during operation at low system pressures. Other parameters did not affect these phenomena in a distinct fashion.

Two theoretical models - one linear and the other nonlinear - were evaluated with respect to predicting the oscillation threshold and the frequency of the initial oscillations. The linear model due to Jones[6] predicted the threshold power within ±5% for over 60%, and within ±10% for over 80% of the test data.

On the other hand, the nonlinear model of Jahnberg[7] had to be modified to provide a satisfactory prediction of the steady inlet flow velocities. Moreover, neither the original model nor the modified version was able to predict the oscillation thresholds, frequencies, or the flow amplitudes. It is believed that the one-dimensional formulation fails to consider periodic vaporization of superheated liquid near the leading edge of the two-phase region. Introduction of such a periodic forcing function would facilitate computation of periodic bounded oscillations similar to those observed experimentally and, thus, provide a qualitative interpretation of the observed trends with parameter variation.

REFERENCES

1. C. C. St. Pierre, *Frequency-Response Analysis of Steam Voids to Sinusoidal Power Modulation in a Thin-Walled Boiling Water Coolant Channel*, ANL-7041 (May, 1965).
2. A. J. Cornelius, *An Investigation of Instabilities Encountered during Heat Transfer to a Supercritical Fluid*, ANL-7032 (April, 1965).
3. J. L. L. Baker, *Flow Regime Transitions in Vertical Two-Phase Flow at Elevated Pressures*, ANL-7093 (September, 1965).
4. G. P. Nassos, *Propagation of Density Disturbances in Air-Water Flow*, ANL-7053 (June, 1965).
5. K. C. Jain, *Self-Sustained Hydrodynamic Oscillations in a Natural Circulation Two-Phase Flow Boiling Loop*, ANL-7073 (August, 1965).
6. A. B. Jones, *Hydrodynamic Stability of a Boiling Channel*, KAPL-2170 (October, 1961).
7. S. Jahnberg, *A One-Dimensional Model for Calculation of Non-Steady Two-Phase Flow*, EAES Symposium, Studsvik, Sweden, October, 1963.

Section 8

PUBLICATIONS

8.1 Methods of Reporting

The status of various programmatic and basic research activities of the Reactor Engineering Division, and other Divisions at Argonne, is published in Laboratory Monthly Progress Reports. Ultimately, these chronologies are compiled to present a comprehensive description and evaluation of specific accomplishments in the form of ANL topical reports. These reports are distributed to all AEC sites and to pre-selected AEC-affiliated organizations and institutions which have an immediate interest in their contents.

In certain instances, the topicals are supplemented by abridged articles or papers. These are prepared for publication in trade journals, or for oral presentation to professional and educational organizations which maintain an interest in the state of the art.

Finally, and not too infrequently, Staff personnel are solicited or volunteer to publicize their expertise. The nature of these publications may range from brief critiques of journal articles, to editing or writing handbook chapters and monographs. These activities, the latter in particular, entail several man-months' effort on the part of the author. In most cases, the work is performed in addition to his regularly assigned tasks.

8.2 Recap of Publications

The following recapitulation represents the literary output by Division Staff personnel during the fiscal reporting period. In order to conserve space, the publications are indexed to the major sections which comprise this report.

REACTOR PROJECTS AND PROGRAMS

Experimental Breeder Reactor-II (EBR-II)

Ernest Hutter and G. D. Giorgis, *Design and Performance Characteristics of EBR-II Control Rod Drive Mechanisms*, ANL-6921 (August, 1964).

Ernest Hutter, *EBR-II Control Drives*, Proc. Meeting on Fast Reactor Control Mechanisms, Germantown, Md., September 16-17, 1964, WASH-1054, Pt. 1, pp. 36-70.

R. A. Jaross, *EBR-II System and Component Experience*, Proc. Sodium Components Information Meeting, Palo Alto, Calif., August 20-21, 1963, SAN-8002 (May, 1964), pp. 3-9.

L. J. Koch et al, *Sodium-Cooled Fast Breeder Reactors*, Paper No. 207, Third International Conference on the Peaceful Uses of Atomic Energy, Geneva, Switzerland, September, 1964.

L. J. Koch, *Fast Reactor Fuel Handling*, Proc. American Nuclear Society National Topical Meeting on Fast Reactor Technology, Detroit, Mich., April 26-28, 1965, ANS-100, pp. 333-347.

Fast Reactor Test Facility (FARET)

R. H. Armstrong and F. A. Smith, *FARET Fuel Assembly Flow Test Loop*, Trans. Am. Nucl. Soc., 8, No. 1, 149-150 (June, 1965).

M. M. Chen, *Structural Analysis of FARET Core Supports under Mechanical and Thermal Loadings*, ANL-6778 (September, 1964).

Ernest Hutter, *FARET Control Drives*, Proc. Meeting on Fast Reactor Control Mechanisms, Germantown, Md., September 16-17, 1964, WASH-1054, Pt. 1, pp. 72-86.

W. R. Simmons, P. J. Persiani and T. R. Bump, *Fast Reactor Test Facility (FARET) Initial Experimental Program*, Proc. American Nuclear Society National Topical Meeting on Fast Reactor Technology, Detroit, Mich., April 26-28, 1965, ANS-100, pp. 273-274.

Argonne Advanced Research Reactor (AARR)

L. W. Fromm et al, *Argonne Advanced Research Reactor - Preliminary Design Report*. Revised May 17, 1965; limited distribution for review and ultimate publication.

Experimental Boiling Water Reactor (EBWR)

EBWR Project Group, *EBWR Test Reports (100-MWt Operation)*, ANL-6703 (January, 1964).

N. Balai et al, *Inspection, Evaluation, and Operation of the EBWR Reactor Vessel*, ANL-7117 (November, 1965).

REACTOR PROJECTS AND PROGRAMS (Contd.)

B. J. Toppel, P. J. Vogelberger, Jr., and E. A. Wimunc, *Safety Analysis Associated with the Plutonium Recycle Experiment in EBWR*, ANL-6841 (to be published).

Nuclear Rocket Program

J. F. Marchaterre et al, *Refractory Metal Fast Reactors for Nuclear Rocket Propulsion.* Paper presented to the AIAA Propulsion Joint Specialist Conference, Colorado Springs, Colo., June 14-18, 1965.

W. H. Rettig and P. F. Fox, *Nuclear Rocket Preheater Concepts for the Graphite and Fast Reactors.* Paper presented to the AIAA Propulsion Joint Specialist Conference, Colorado Springs, Colo., June 14-18, 1965.

M. E. Stephenson, *Property Values of Parahydrogen*, ANL-7004 (March, 1965).

FAST REACTOR RESEARCH AND DEVELOPMENT

E. L. Kimont, *Engineering Development of a Practical 1200°F Sodium Vapor Trap*, Trans. Am. Nucl. Soc., 8, No. 1, 147 (June, 1965).

H. O. Monson et al, *Components for Sodium Reactors*, Paper No. 228, Third International Conference on the Peaceful Uses of Atomic Energy, Geneva, Switzerland, September, 1964.

HEAT TRANSFER AND FLUID FLOW

T. T. Anderson, Comments on: *Two-Phase Measurements Using a Resistive Probe*, AIChE Journal, 10, No. 5, 776 (September, 1964).

J. L. Baker and B. T. Chao, *An Experimental Investigation of Air Bubble Motion in a Turbulent Water Stream*, AIChE Journal, 11, No. 2, 268-273 (March, 1965).

T. R. Bump, *Fins in Series*, Communication to the Editor, AIChE Journal, 11, 174 (January, 1965).

H. K. Fauske et al, *Critical Flow Phenomena in Two-Phase Mixtures and Their Relationships to Nuclear Safety*, Paper No. 232, Third International Conference on the Peaceful Uses of Atomic Energy, Geneva, Switzerland, September, 1964.

H. K. Fauske, *Some Ideas about the Mechanism Causing Two-Phase Critical Flow*, Appl. Sci. Research, A13, 149-160 (1964).

HEAT TRANSFER AND FLUID FLOW (Contd.)

H. K. Fauske, *Two-Phase Critical Flow*, Notes for Special Summer Program in Two-Phase Gas-Liquid Flow, Massachusetts Institute of Technology, Cambridge, Mass., July 27-August 7, 1964.

H. K. Fauske, Comments on: *An Analysis of Burnout Conditions for Flow of Boiling Water in Vertical Round Ducts* by K. M. Becker, ASME Trans., J. Heat Transfer, Series C, 86, No. 4, 524 (November, 1964).

H. K. Fauske, Comments on: *Maximum Flow Rate of a Single Component, Two-Phase Mixture*, Paper No. 64-HT-35 by F. T. Moody, ASME Trans., J. Heat Transfer, Series C, 87, No. 1, 141 (February, 1965).

J. B. Heineman et al, Comments on: *New Theory of Thermal Stability in Boiling Systems*, by E. F. Adiutori, Nucleonics 22, No. 12, 6-7 (December, 1964).

R. E. Holtz, *Application of Electron-Bombardment Heating for Boiling Liquid Metals*, ANL-6869 (March, 1964).

R. E. Holtz, *A Study of the Initiation of Nucleate Boiling in Liquid Metals*, ANL-6980 (December, 1964).

R. E. Holtz, *Prediction of Liquid Superheats Required for Initiation of Nucleate Boiling in Liquid Metals*, ASME Paper No. 64-WA/HT31, 1964 Winter Annual Meeting.

John Johanns, *Development of a Fluoroscope for Studying Two-Phase Flow Patterns*, ANL-6958 (October, 1964).

A. A. Kudirka, *Two-Phase Heat Transfer with Gas Injection through a Porous Boundary Surface*, ANL-6862 (March, 1964).

P. A. Lottes et al, *Fluid Dynamics, Stability, and Vapor-Liquid Slip in Boiling Reactor Systems*, Paper No. 230-R-1 Third International Conference on the Peaceful Uses of Atomic Energy, Geneva, Switzerland, September, 1964.

P. A. Lottes, *Heat Transfer and Fluid Flow - Boiling Stability*, Proc. NASA-AEC Liquid-Metals Corrosion Meeting, Cleveland, Ohio, October, 1963, NASA-SP-41, Vol. 1 (June, 1964), pp. 257-271.

P. A. Lottes, *Fluid Flow: General Characteristics*, Reactor Handbook, Second Edition, Vol. IV: Engineering, (eds.) Stuart McLain and J. H. Martens (New York: Interscience Publishers, 1964), Ch. 1, Sec. 1.1, pp. 1-5.

P. A. Lottes and W. H. Cook, *Fluid Flow: Liquid-Vapor Systems*, Reactor Handbook, Ibid, Sec. 1.4, pp. 19-25.

P. A. Lottes, *Heat Transfer: Overall Heat Transfer Rates*, Reactor Handbook, Ibid, Ch. 2, Sec. 2.1, pp. 77-79.

R. P. Stein and P. A. Lottes, *Boiling "Burnout" for Reactor Design* Reactor Technology - Selected Reviews (ed.) L. E. Link, TID-8540 (1964), pp. 131-176.

HEAT TRANSFER AND FLUID FLOW (Contd.)

R. P. Stein, T. F. Irvine, Jr., and H. A. Simon, *The Influence of Radiation on Convection in a Flat Duct,* State University of New York, Stony Brook, N. Y., Report No. 18 (April, 1964).

R. P. Stein, *The Graetz Problem in Co-Current Flow, Double-Pipe, Heat Exchangers,* ANL-6889 (September, 1964).

R. P. Stein, *Heat Transfer Coefficients in Liquid-Metal Co-Current Flow, Double-Pipe, Heat Exchangers,* Proc. High-Temperature Liquid-Metal Heat Transfer Technology Meeting, Oak Ridge, Tenn., September 4-6, 1963, ORNL-3605, Vol. 1 (November, 1964), pp. 194-239.

R. P. Stein, *Radiation between Concentric Cylinders with Perforations,* ASME Trans., J. Heat Transfer, Series C, 87, No. 2, 316-317 (May, 1965).

Raymond Viskanta, *Heat Transfer with Laminar Flow in a Concentric Annulus with Prescribed Wall Temperatures,* Appl. Sci. Research, A12, No. 6, 463-476 (1964).

Raymond Viskanta, *Influence of Internal Thermal Radiation on Heat Transfer in UO_2 Fuel Elements,* Nucl. Sci. Eng., 21, 13-19 (January, 1965).

D. J. Wilhelm, *Condensation of Metal Vapors: Mercury and the Kinetic Theory of Condensation,* ANL-6948 (October, 1964).

MAGNETOHYDRODYNAMICS

J. R. Moszynski, *Electrical End Losses in an MHD Channel of Linearly Variable Cross Section,* ANL-6963 (March, 1965).

Michael Petrick and Kung-You Lee, *Performance Characteristics of a Liquid Metal MHD Generator,* ANL-6870 (July, 1964). See also Proc. ENEA International Symposium on MHD Electrical Power Generation, Paris, July 6-11, 1964, Vol. 2, pp. 953-970.

Michael Petrick, *Liquid-Metal Magnetohydrodynamics,* IEEE Spectrum 2, 137-151 (March, 1965).

R. M. Singer, *The Control of Condensation Heat Transfer Rates Using an Electromagnetic Field,* ANL-6861 (July, 1964).

R. M. Singer, *A Study of Unsteady Magnetohydrodynamic Flow and Heat Transfer,* ANL-6937 (November, 1964).

R. M. Singer, *Laminar Film Condensation in the Presence of an Electromagnetic Field,* ASME Paper No. 64-WA/HT47, 1964 Winter Annual Meeting.

E. S. Sowa, *The Liquid Metal Linear Generator,* Proc. AMU-ANL Conference on Direct Energy Conversion, November 4-5, 1963, ANL-6802 (December, 1963), pp. 181-185.

REACTOR SAFETY

D. W. Sparks, J. H. Tessier and J. C. Carter, *The Steady-State and Transient Kinetics of EBR-I, Mark III,* ANL-6851 (March, 1964).

D. W. Sparks, J. H. Tessier and J. C. Carter, *The Period Effect in Reactor Dynamics,* ANL-6852 (April, 1964).

W. C. Lipinski, J. M. Harrer and R. L. Ramp, *Control and Instrumentation,* Reactor Handbook, Second Edition, Vol. IV: Engineering, (eds.) Stuart McLain and J. H. Martens (New York: Interscience Publishers, 1964), Ch. 8, pp. 346-400.

C. F. Chen, E. F. Richards and Chun Hsu, *Constructing Liapunov Functions by Means of the Analog Computer,* IEEE Trans. E-7, Nos. 2 and 3, 63-66 (June - September, 1964).

E. S. Sowa et al, *Studies of Fast Reactor Fuel Element Behavior under Transient Heating to Failure. II: In-Pile Experiments on UO_2 Samples in the Absence of Coolant,* ANL-6845 (January, 1965).

Chun Hsu and W. C. Lipinski, *Statistical Error Estimation for the Transfer Function Measurements of a Noisy Reactor System,* Nucl. Sci. Eng., 21, No. 3, 407-408 (March, 1965).

Isaac Kliger and W. C. Lipinski, *The Z-Transform of a Product of Two Functions,* IEEE Trans., AC-9, No. 4, 582-583 (October, 1964).

Isaac Kliger, Comments on: *Closed Loop Optimal Control* by M. Sidar, IEEE Trans. AC-10, No. 2, 207 (April, 1965).

Isaac Kliger, *Optimal Control of a Space Dependent Nuclear Reactor,* Trans. Am. Nucl. Soc., 8, No. 1, 233-234 (June, 1965).

STUDIES AND EVALUATIONS

J. F. Marchaterre and L. J. Gordon, *A Preliminary Evaluation of the Use of High-Temperature Process Heat as Part of a Total Nuclear Energy Source,* ANL-7035 (September, 1965).

MISCELLANEOUS

Y. W. Chang, *Vibrations and Stability of Buckled Rectangular Plates,* University of Michigan Industry Program, Vol. IP-85 (November, 1964), pp. 1-78.

Gabriel Cinelli, *The Solution of Boundary Value Problems with Asymmetric Boundary Conditions by Means of Finite Fourier Transform,* IEEE International Convention Record, Part II, New York, March 23-26, 1964, pp. 235-244.

MISCELLANEOUS (Contd.)

L. W. Fromm, *Reactor Development Test Facilities*, Reactor Handbook, Second Edition, Vol. IV: Engineering, (eds.) Stuart McLain and J. H. Martens (New York: Interscience Publishers, 1964), Ch. 15, pp. 539-547.

E. E. Hamer et al, *Shielding*, Reactor Handbook, Second Edition, Vol. IV: Engineering, (eds.) Stuart McLain and J. H. Martens (New York: Interscience Publishers, 1964), Ch. 9, pp. 401-422.

A. H. Heineman, Member, Subcommittee No. 2 of Sectional Committee N6-ASA, *American Standard - Safety Standard for Design, Fabrication, and Maintenance of Steel Containment Structures for Stationary Nuclear Power Reactors*, ASA N6.2-1965, issued April 21, 1965.

M. J. Janicke and J. C. Carter, *A Repairable Nuclear Space Power Plant*, Trans. Am. Nucl. Soc., 7, No. 2, 533 (November, 1964).

M. J. Janicke, *Vapor Cycle Coolant Requirements for Nuclear Space Power Plants*, ANL-6857 (March, 1964).

A. H. Marchertas, S. H. Fistedis and R. O. Brittan, *Analytical and Experimental Investigation of a Nuclear Reactor Support Structure*, ANL-6781 (March, 1965).